THE EFFECT OF FATIGUE CRACKS ON FASTENER FLEXIBILITY, LOAD DISTRIBUTION, AND FATIGUE CRACK GROWTH

by
Zachary Layne Whitman

A dissertation submitted to the faculty of
The University of Utah
in partial fulfillment of the requirements for the degree of

Doctor of Philosophy

Department of Mechanical Engineering
The University of Utah
May 2012

Report Documentation Page

Form Approved
OMB No. 0704-0188

1. REPORT DATE	2. REPORT TYPE	3. DATES COVERED
01 DEC 2011	**N/A**	**-**

4. TITLE AND SUBTITLE	5a. CONTRACT NUMBER
The Effect of Fatigue Cracks on Fastener Flexibility Load Distribution and Fatigue Crack Growth	5b. GRANT NUMBER
	5c. PROGRAM ELEMENT NUMBER
6. AUTHOR(S)	5d. PROJECT NUMBER
Zachary Layne Whitman	5e. TASK NUMBER
	5f. WORK UNIT NUMBER
7. PERFORMING ORGANIZATION NAME(S) AND ADDRESS(ES)	8. PERFORMING ORGANIZATION REPORT NUMBER
Department of Mechanical Engineering, University of Utah A-10 Systems Program Office Hill AFB Utah	
9. SPONSORING/MONITORING AGENCY NAME(S) AND ADDRESS(ES)	10. SPONSOR/MONITOR'S ACRONYM(S)
	11. SPONSOR/MONITOR'S REPORT NUMBER(S)

12. DISTRIBUTION/AVAILABILITY STATEMENT
Approved for public release, distribution unlimited

13. SUPPLEMENTARY NOTES
The original document contains color images.

14. ABSTRACT

15. SUBJECT TERMS

16. SECURITY CLASSIFICATION OF:			17. LIMITATION OF ABSTRACT	18. NUMBER OF PAGES	19a. NAME OF RESPONSIBLE PERSON
a. REPORT	b. ABSTRACT	c. THIS PAGE			
unclassified	**unclassified**	**unclassified**	**UU**		

ABSTRACT

Fatigue cracks typically occur at stress risers such as geometry changes and holes. This type of failure has serious safety and economic repercussions affecting structures such as aircraft. The need to prevent catastrophic failure due to fatigue cracks and other discontinuities has led to durability and damage tolerant methodologies influencing the design of aircraft structures.

Holes in a plate or sheet filled with a fastener are common fatigue critical locations in aircraft structure requiring damage tolerance analysis (DTA). Often, the fastener is transferring load which leads to a loading condition involving both far-field stresses such as tension and bending, and localized bearing at the hole. The difference between the bearing stress and the tensile field at the hole is known as load transfer. The ratio of load transfer as well as the magnitude of the stresses plays a significant part in how quickly a crack will progress to failure.

Unfortunately, the determination of load transfer in a complex joint is far from trivial. Many methods exist in the open literature regarding the analysis of splices, doublers and attachment joints to determine individual fastener loads. These methods work well for static analyses but greater refinement is needed for crack growth analysis. The first fastener in a splice or joint is typically the most critical but different fastener flexibility equations will all give different results. The constraint of the fastener head and shop end, along with the type of fastener, affects the stiffness or flexibility of the fastener. This in turn will determine the load that the fastener will transfer within a given fastener pattern.

However, current methods do not account for the change in flexibility at a fastener as the crack develops. It is put forth that a crack does indeed reduce the stiffness of a fastener by changing its constraint, thus lessening the load transfer. A crack growth analysis utilizing reduced load transfer will result in a slower growing crack verses an analysis that ignores the effect.

ACKNOWLEDGEMENTS

I would like to thank my beautiful wife Kandace for her support while I pursued this work. She is a blessing to our family. Our precious daughters Lily and Briar also deserve great thanks for their patience during this endeavor. My hope is that they too grow up to appreciate the value in dedicating themselves to continual learning. This dissertation is devoted to them.

My appreciation is extended to members of my committee; whom without their advice this work would not have been completed. Many of my friends, co-workers, and extended family provided the emotional encouragement to complete my research. Thanks to Southwest Research Institute and many of the staff there for tuition support and encouragement during my studies, and for conducting the specimen manufacturing and testing. Finally, I would like to thank my Lord and Savior Jesus Christ for the clarity and peace required to complete everything good that I have ever accomplished in my life. To him goes all glory.

TABLE OF CONTENTS

Page

1.0 INTRODUCTION

The central focus of this dissertation is the study of joint analysis methods, specifically aircraft and how cracks affect the underlying analytical assumptions. Within this potentially broad spectrum there will be a focus on multiple fastener joints which transfer load via fasteners and the different layers they join. The coming sub-sections discuss fatigue in general and different paradigms used in aircraft over the years. The chapter following discusses fasteners, specifically those looked at in this dissertation. Chapter 3.0 contains discussion on the types of joints considered while Chapter 4.2 discusses fastener flexibility. These two chapters are critical since the type of joint affects the fastener flexibility and the fastener flexibility affects the amount of load transferred by each fastener. The more load transferred by a fastener, the more severe the crack growth. These methods all serve well for 'pristine' structure as designed, devoid of cracks or other discontinuities. However, once cracks start to form, the assumptions of these analysis methods can lose validity leading to less accuracy and precision than may be required. No prior method attempts to define load transfer for fasteners considering the presence of a crack and how it in turn affects the growth of the crack. Thus, as the effect of the crack starts to impact the load transfer of the joint there is a need to account for its presence to retain the accuracy of the analysis.

The study of these types of joints is not a new art. Civil engineers have used different methods to analyze the loads in fasteners for well over a hundred years as steel beam construction came into vogue. Similar considerations were made by the pioneers of aviation when analyzing the strength of details on aircraft. This early work involved mainly steels and non-isotropic materials; e.g. wood being bolted and glued together. In the most early of aircraft, fatigue was not a major design or operational consideration. More recently, fatigue became much more influential in the design and in the operation of aircraft. Thus the introduction splits the early background of the two topics separately, combining them as fatigue becomes a major factor considered in aviation. To avoid the need to bounce back and forth, Section 1.1 focuses on the background of joint analysis specifically as it relates to this topic in aircraft. Section 1.1 ends right about the time that fatigue starts to become part of the aviation world and breaks to Section 1.2 which discusses the evolution of the study of fatigue. Section 1.3 then picks up right about the time that fatigue becomes a crucial part of aviation. While the order is non-chronological, it should help keep the reader focused on each topic until their paths cross.

1.1 Aircraft in the Early Years

Aluminum in aircraft structures was relatively uncommon if not completely unheard of in the early 20th century. Wood was the primary structural material usually as compression and bending members with steel cables bracing the structure as tension members [1, 2]. Aircraft design tasks such as weight estimation were simplified by the commonality of many of the different wood/wire structures made during the period [3]. The benefit of

wood over contemporary metal alloys was its strength to weight ratio [4]. In addition, wood has the capability to survive stresses above the normal design strength for short periods of time so the structures ability to survive abrupt overloads during gusts and landings likely saved the life of many an early aviator [5].

In the seminal 1919 book on aircraft structural analysis, Pippard and Pritchard [6] wrote that, *"…the aeroplane designer is practically dependent upon two of these, timber and steel, and even with these his choice is limited to very few varieties."* The lack of aluminum in allied aircraft structures was reflected by Pomilio who stated that the only two uses for it are fuel tanks and engine cowls [7] which was a sentiment reflected in other contemporary writings as well [8-10]. Andrews and Benson discuss the four main materials of design in their 1920 book as being, timber, duralumin, steel and fabric [11]. However, the reign of wood as the principal material for aircraft construction was quickly coming to an end. As Judge wrote in 1921 [12]:

> *"The modern tendency in aeronautical practice is toward the elimination of such materials as wood, as the strength of this material depends upon its previous history and subsequent treatment, and is always an unreliable factor. For this purpose steel, and other metals, is replacing these non-homogeneous materials, and successful all-metal wings (and indeed complete machines have been built."*

This sentiment is echoed in many other contemporary writings. [13, 14] Exacerbating the variation in wood quality was the depletion of many forests of their prime timber.

Economic factors as well as engineering design led to a decline in wood as for structural members for aircraft [15, 16].

Metal as a primary structural material and covering was pioneered by Dr. Hugo Junkers who developed the first all metal monoplane, the J 1 [17]. Its first flight occurred on 12 December 1915. The Junkers F 13, first flown on 25 June 1919, was the first all metal commercial aircraft featuring a single low wing with internal wing bracing and full with a metal covering of corrugated duralumin. It was a development of the similarly constructed CL 1 aircraft which was a two seat ground-attack aircraft of WWI. This, when the common aeronautical structure was a wing with wooden spars and ribs, fabric covering and external bracing using struts and cables. However, butt joints with splice plates and fasteners is not peculiar to metals alone; considerable research in these types of joints were done using plywood as well [18, 19]. In fact, many common metal aircraft details were common in wooden structure long before metal aircraft were flying.

Metal was increasingly used in aircraft structure during the 1920s though typically in the form of steel tubing and steel strip but fastened joints were still not common in these structures since the steel was easily welded. Aircraft were commonly built in this time period with steel tube truss structure with fabric covering [20]. Steel strip structure was well developed in Britain at Boulton and Paul, Vickers, as well as others manufacturers but often the design was such that it was merely steel shapes substituting wood in spar and rib designs over 20 years old [21-25]. Aluminum alloys of the early 1920s were still rather weak and were not used commonly outside of cast engine parts, propellers and other non-structural applications [26]. The one exception is in the wing structure where

the smaller depth due to the airfoil and necessary moment of inertia due to a lack of external bracing meant an increase in the use of metal, particularly aluminums [27, 28]. Flying boats and seaplanes were some of the first types of aircraft to see widespread use of aluminum alloy coverings due to the improvement of strength to weight in service over wood which is hygroscopic. By the end of the 1920s, aluminum alloys played a large role in the structure of new aircraft thanks to improved alloy strength by newly developed heat treatment and working methods as well as improved structural design techniques [29-36]. The early problems with corrosion also were addressed by the new development of aluminum clad sheets [37]. The 1920s also marked the start of serious treatment of the fatigue of aluminum and other non-ferrous alloys and the beginning of material fatigue for aircraft [38, 39].

Development of pin and bolted connections for wood also progressed greatly in the 1920s and 1930s with work done by Grenoble [40, 41], Trayer [42-44], and others. Due to the very large difference in stiffness of wood relative to the common steel bolt, connections often are made with a bolt with a length to diameter ratio much greater than that used in metallic joints. This causes significant bending in the bolt and as the ratio of L/D increases, the bolt becomes less efficient without causing permanent set. This is particularly true when the bolt is used in a single shear joint causing a proportional limit in the joint of only one fourth of a joint were the bolt is loaded symmetrically [45].

As stressed skin metal coverings came into vogue, monocoque construction was increasingly employed [46-48]. Monocoque construction is unique in that the skin is stressed instead of an internal frame. The original use of monocoque construction in

aircraft were the Deperdussin racers that first revolutionized the method using wood and were the first aircraft to exceed 100 miles per hour. Wooden semi-monocoque construction was later put into use by the Albatross and Pfalz aircraft of World War I which employs stressed skin with some internal stiffening [49]. These wooden aircraft were laboriously assembled by overlying thin plies of thin wood which were glued and pinned.

Metal semi-monocoque construction, on the other hand, usually results in thousands of rivets joining the sheets to each other and to the substructure which stiffens it. The 1930s were flooded with new methods for joining ranging from welding and adhesives, to rivets and other mechanical joints [50-55]. These innovations required improvements in the analytical methods to develop new structural designs as well as understand their modes of failure. Many allowables and design guidelines were developed during this time through elasticity and empirical methods [56, 57]. Wooden monocoque construction also made a small comeback in the 1930s with the development of Duramold which was plastic impregnated, formed plywood [58]. In general however, with the exception of the DeHavilland Mosquito, all high performance aircraft were exclusively of metal construction in the airframe by World War II [59, 60].

Through the early years of aviation, aircraft design changed rapidly. As a result few aircraft saw a service life of more than a decade. Yet in the 1940s, aircraft design stabilized somewhat and combined with the pressures of war; commercial aircraft were used for increasingly long periods of time [61]. Single load path structure was common in this period. Fatigue started to become more of a problem for aircraft as speeds of

aircraft increased, service lives became longer, wing loading increased and load factors decreased [62]. But fatigue effects were often not in the forefront of aircraft design [63, 64].

Little was published in aviation literature regarding fatigue and the factors that affect performance prior to a series of two articles by Johnson [65, 66]. His articles are significant as they addressed various factors such as corrosion, smoothness of surfaces, and notches. Prior publications regarding aeronautical fatigue were mostly metallurgical studies in other trade publications [67]. But beyond this point, fatigue becomes a much greater concern.

1.2 Fatigue the Early Years

The nature of fatigue life is one susceptible to a myriad of variables. Microstructure of the material, residual stresses, surface finish, and assembly quality are but some of the variables that will affect fatigue performance of the material prior to the first load cycle. The type of design also will influence fatigue as certain details will result in greater stress concentrations or pre-load parts during the assembly phase. Once in service, the design will be affected by usage factors ranging from the intensity of the load and the frequency of application, to the environment, length of time in service and combinations thereof.

As such, fatigue information ranging from S-N diagrams to da/dn versus ΔK are typically shown on log scales as the variation easily can be an order of magnitude or greater. In the lower end of the crack length spectrum, microstructure dominates fatigue crack nucleation, damage progression, and short crack life. However, the effect being studied

here is on a macro-scale by comparison where a fatigue crack is in place and is growing within the regime of Linear Elastic Fracture Mechanics (LEFM) assumptions during its long-crack phase and into its ultimate fracture. It is specifically the understanding of fastened joints that will be further explored. The other reason to concentrate in the long-crack regime is that damage tolerance methodologies are necessarily focused on cracks of detectable length by Non-Destructive Inspection (NDI) which, excepting for certain laboratory situations, is exclusively in the long-crack regime.

The difficulty in understanding fatigue and applying the results of coupon tests to the analysis of the fatigue life of structure is well documented in many places. Early aerospace methods were typically safe life/finite life or safe life/infinite life if fatigue was considered at all. Safe life/infinite life attempts to keep operating stresses below the fatigue limit (sometimes referred to as the ‘endurance limit’) and thus eliminating fatigue from design because, by the definition of fatigue limit, a fatigue crack cannot nucleate and propagate. This was met with varying levels of success given the materials of the day. One of the problems with this design paradigm is that aluminum alloy structure does not exhibit a fatigue limit at all, particularly the high strength aerospace alloys. Other factors such as corrosion and other time-based mechanisms can effectively reduce or eliminate the fatigue limit leading to failure thought otherwise impossible under this paradigm. This and other issues helped usher in the concept of safe life/finite life in some parts of the aviation industry.

Methods of predicting fatigue life have grown considerably over the years but they all require basic data regarding fatigue. Of the first, Basquin proposed the power law for S-

N curves during the 1910 congress of ASTM whereby the cycles to failure could be described by the equation [68]:

$$S=CR^n$$

Equation 1-1 Basquin Power "Law" for S-N Cruves

where S is the applied stress and R is the repetitions to rupture. C and n are found by regression over data points at different stresses.

In the late 1920s a method was published whereby fatigue limits developed from fully reversed stress could be modified to other stress ratios via the formula [69]:

$$(FL)' = \frac{3(FL)_{-1}}{2-r}$$

Equation 1-2 Fatigue Limit for Fully Reversed Stress

where $(FL)_{-1}$ is the fatigue limit, fully reversed and r is the ratio of minimum stress to maximum stress.

This formula was corroborated for riveted joints in later work by Wilson and Thomas [70]. These are, however, civil engineering methods as the fatigue strength is defined at 2,000,000 cycles which corresponds to the assumed number of maximum stress cycles seen during the desired life of a railroad bridge [71].

The vast majority of fatigue tests during this period were of the rotating bending type [72, 73]. In these tests a specimen is turned by a motor and bent simultaneously such that the cycles seen on a single outer fiber of the specimen goes from tension to bending in a completely reversed fashion. The main advantage in this type of test is that cycles can be applied quickly. The disadvantage is that fatigue has cyclical frequency dependence in

the large hertz range. Other disadvantages are that rotating bending is not equivalent to fully reversed bending and that the only stress ratio that can be tested is -1, (stress ratio is the minimum stress of the cycle divided by the maximum stress). Later flexural, axial, torsional and combined stress fatigue tests were developed. Up through the 1920s and 1930s many different types of machines existed with little if any standardization between them with many machines being built to test specific configurations or unique problems [74-76]. For a more complete treatise of the history of fatigue one is referred to Walter Schütz's paper, "A History of Fatigue" [77].

Some early aircraft lifing strategies that were proposed were on the basis of calendar years in service. This may well serve modes of degradation such as corrosion but is inadequate for fatigue. One aircraft might be a passenger plane used regularly and another might be a personal aircraft or a hanger queen[1] which would see far less service. Pugsley [78] recommended a more appropriate lifing strategy whereby the hours in service are considered instead. The post-war period saw much advancement in fatigue evaluation, not the least of which is the recognition that fatigue is indeed a serious problem [79-83]. Fatigue analysis during this time was hampered by both a lack of data as well as methods to forecast life in this fledgling science [84, 85].

[1] A hangar queen is an aircraft that has a problematic maintenance history that keeps it in the hangar for repair far more often than other aircraft.

1.3 Aircraft and Fatigue

In the search for stronger and stronger alloys designers were unwittingly building aircraft with less and less residual strength in the presence of a crack. The ratio of fracture toughness and fatigue strength to yield strength decreases as the strength of the aluminum increases [86, 87]. New alloys such as 7075 and 7079 had higher rates of crack propagation than did the 2XXX series alloys. They also proved more susceptible to Stress Corrosion Cracking (SCC) which also affected the structural life of aircraft considerably. The late 1940s and 1950s saw a rapid shift in the thinking within the aeronautical community leading to increased focus on fatigue [88-90].

In the early 1950s a series of accidents involving the de Havilland *Comet I* highlighted fatigue as a serious problem with a crash in May 1953 [91] and two more aircraft crashing into the sea in early 1954 [92]. A fatigue crack, which had nucleated at the window opening in the fuselage, grew to the point where explosive decompression and loss of the aircraft [93] with the failure mode being recreated through extensive testing following the accident [94]. The Comet was the first commercial jet passenger aircraft used on regular airline routes. An outcome of this event was increased focus on stress concentrations and sharp reentrant corners in structure by the aeronautical community. Another contributing factor was the practice of using the ultimate strength article as the fatigue test article as well. Following ultimate load conditions the regions which fatigued were plastically stretched and put into residual compression which improved its fatigue properties [95-98].

Full scale testing of aircraft structure started full swing in the 1950s [99, 100]. New commercial aircraft such as the Comet IV [101], Armstrong Whitworth Argosy [102, 103], Douglas DC-8 [104], SE-210 Caravelle [105-107], BAC Britannia [108], Fokker Friendship [109], as well as military aircraft like the Jet Provost T.Mk.3 [110], Fiat G 91 [111], and P-16 [112]. Existing, mature aircraft were also the subject of considerable testing such as the North American P-51 Mustang, de Havilland Mosquito [113], de Havilland DH 104 Dove [114, 115], C-46 Commando [116]. This also produced an early report showing what would later be known as Multiple Site Damage (MSD) and Multiple Element Damage (MED) which documented the progression of cracking from the wing skin into different stringer and spar elements [117]. The surplus of airframes available following World War II made a wide range of research possible.

As aeronautical designers became more aware of the fatigue problem, redundant structure became more common. This type of structure required new forms of analysis including matrix solutions to determine loads. The concept that fatigue can damage one structural member but catastrophic failure does not occur due to redundancy is known as fail-safety. This design feature was common for many aircraft of the period [118]. On 13 March, 1958, two B-47s were lost following in-flight structural failure. Within a month three more B-47s experienced structural failure in flight. This led to the grounding of the mid-range nuclear bomber fleet in the middle of the Cold War. In less than one year, the USAF initiated three fatigue tests, verified the cause of failure, and verified a repair to increase the service life of the aircraft. The fleet was modified in two locations thus getting them back in the air.

The other tool in the structural toolbox to fight fatigue was improvements in design through taper-pins, interference fits, tapered and stepped straps [119], scarf joints, and combinations thereof [120, 121]. Yet with all these improvements fatigue failures continue to occur. These fatigue improvements do not represent a paradigm shift due to a true understanding of the problem but rather one of comparative improvement. Most of these features were incorporated with the belief that fatigue could be eliminated as a concern by taking certain steps. These same design features would be combined with a better understanding of structure later to vastly improve the fatigue resilience of structure. At the time, aircraft were not bought with an intended life for the structure, nor was fatigue life considered analytically or through test. When the B-47 was first procured it was believed that it was a 7 year solution but that afterwards, a new weapon system would be needed. However, increases in the gross weight and thrust of the aircraft, combined with a change in the usage from high-altitude flight to a low-level approach with pop-up bombing, greatly increased both the frequency and magnitude of stresses on the airframe. The Aircraft Structural Integrity Program (ASIP) grew out of this challenge being first called for in 1958. ASIP also was required of all weapon systems operated by the USAF.

Early USAF fatigue certification procedures included full-scale and component testing of aircraft to validate their service life. These early tests did not account for spectrum loading but typically were cycled from 1g to limit or maximum flight load and then correlated to measured usage using Miner's Rule [122]. This method, though crude by today's standards was used until the establishment of the ASIP following the crash of

several B-47 aircraft. Early aircraft to follow new procedures established by ASIP include: RF/F-101, F-104, F-105, F-106, B-47, B-52, B-58, T-37, T-38, C-130, C-133, and C/KC-135 [123]. It will be noted that both the C-141 and F-111 also were being procured under these new requirements, noting later the significance of the F-111. Key under the new requirements was full-scale fatigue testing under varying load levels which would later be correlated to measured VGH data in use. This translates into an ongoing fatigue certification program whereby the service life of the aircraft evolved to account for changes in mission related to load or force spectra; a marked improvement over the earlier methods.

Many tests of the time exhibited significant scatter from what was predicted up to a factor of 16 [124]. Early USAF regulations tended toward a scatter factor for fatigue tests of 2 to 4 in Lowndes's response to a question from W. Schütz [125] while the US Navy uses a factor of 2 [126]. This factor simply aligns the tested fatigue life with the median life seen in service. An additional factor is required to act as a 'safety factor' which will reduce the probability of failure due to fatigue to an acceptable level. Indeed in the mid-1950s some authors used scatter factor and safety factor interchangeably with regard to fatigue. Specific discussion to this effect can be found following Turner's paper entitled "Fatigue Design of Aircraft Structures" [127]. Freudenthal suggested that a statistically based safety factor be used to prevent a single failure which accounted for the total number of aircraft in a given fleet [128].

As the study of fatigue increased so did the proposed methods to include fatigue in design. Shanley recommended in 1953 against prediction of the [actual] fatigue life of

aircraft but rather check the suitability against a ‘sufficiently high’ factor of safety [129]. Different formulas to equate life with miles or speed were studied [130]. Williams showed that based on cumulative damage that total passenger miles for a given fatigue life varied greatly with altitude due to gust frequency; distance being chosen as opposed to time to eliminate the variable aircraft velocity though this was put forth much earlier by engineers in Germany [131-133]. Others advocated a statistically based scatter factor to be used in the determination of fatigue life based on the likelihood of a failure in some number of hours [134].

One of the keys to the discrepancy in fleet usage to constant amplitude tests is the interaction of different stress levels. Schive’s work showed that significant variation from unity that can be expected when applying Miner’s Rule to complex structure [135, 136] and is well illustrated with both effects and potential pitfalls in ESDU 69024 [137]. In addition, differences in failure location may be exhibited when testing is done to a spectrum not used in service [138-141].

The recording of flights for the determination of fatigue loads increased greatly in the 1950s. Many recording programs were initiated in an attempt understand the different sources of loading. On a single aircraft, different structure may be susceptible to any combination of ground buffeting, turbulence, landing loads, pressurizations, g-loads, ground handling and taxiing, etc [142-148]. Eventually aeronautical structural design progressed toward durability type structure. Full-scale testing continued to be important in the certification of these new structure types. In fact, so many articles of older

structure had been tested that S-N curves were developed for entire wing structures [149-153].

Fail-safety and designs that were optimized for prevention of fatigue crack development were prevalent throughout the 1960s, even through today. Fail-safety was a new concept whereby a progressive failure was designed into the structure to prevent complete catastrophic failure [154-160]. Redundancy, 'crack-stoppers', and tear straps were all means of providing fail-safety in aircraft structure. In 1969 however, two USAF events forever changed the way aircraft structure was managed.

On 22 December, 1969, an F-111 with 107 flight hours, suffered an in-flight separation of its wing due to a crack at the wing pivot that was rather small relative to the capability of inspection methods at the time. This crack nucleated at a forging lap and quickly grew to critical size in the low-fracture toughness D6AC steel. The F-111 had a test demonstrated durability life of 4,000 hours and survived 16,000 hours of cyclic testing. In a separate incident, an F-5 with about 1,900 of its 4,000 hour life expended failed catastrophically due to a fatigue crack in the lower wing skin [161]. These two events brought on a new paradigm known as damage tolerance.

It became apparent that it was not enough to simply try to prevent cracks from forming but it also was necessary to prevent a crack from growing undetected to failure. Work on durability methods continued [162, 163] but by the mid-1970s, a large amount of research was shifting to the aspect of propagating a fatigue crack and not necessarily on the development of a fatigue crack [164, 165]. Others supported a mix of methods to predict fatigue life by capturing the "initiation" phase (crack initiation defined as the

existence of a crack 0.01” in length in this case) and the crack growth phase [166]. USAF requirements however, kept the propagation phase of a “rogue flaw” and the “initiation” phase of the crack separate [167-176]; although full-scale testing may actually combine these two phenomena [177].

Fatigue life is actually comprised of four regions [178]. The first is the period of crack formation or nucleation. The second is the ‘short’ crack regime where crack propagation is dependent on the local material structure. The ‘long’ crack regime is where the crack propagates generally under the principles of Linear Elastic Fracture Mechanics (LEFM), Elastic Plastic Fracture Mechanics (EPFM), or Fully Plastic Fracture Mechanics (FPFM). The last portion of the crack growth life is the unstable portion of the crack life.

The core of crack growth analysis during this time is LEFM. The fundamental basis for LEFM is attributed to Griffith and his early work studying glass as a model material as early as 1921 [179, 180]. The Griffith criterion equates the change in elastic energy due to the crack growth amount (elastic energy release rate signified by the capital letter G) as equal to the change in the energy required for that same amount of crack growth. Griffith equated the elastic energy release rate as the change in surface energy in the crack itself since glass is almost perfectly elastic at room temperature and experiences negligible plastic deformation [181].

Principles of fracture mechanics were first applied to metals by Irwin in the late 1940s. He recognized the need to include the work done in plastic deformation to be applicable to metals which are more ductile and that the surface tension, critical to Griffith, was not as significant [182]. A similar effort was undertaken by Orowan around the same time as

Irwin's work. These principles were successfully applied to the failure of high strength steel missile cases by Irwin in late 1950s [183]. It was Irwin's development of the stress intensity approach that injected the needed boost in this type of analysis. The stress intensity factor is represented by a capital letter 'K' and has units of pressure multiplied by the square root of a length such as ksi√in [184].

Stress intensity has three main types of loading as shown in Figure 1-1. Mode I is the opening mode designated by K_I and is the primary driver of most cracks. Mode II is the shearing mode and is designated by K_{II}. Mode III is the tearing mode and is designated by K_{III}. Modes II and III do not occur on their own as a pure form but rather in combination with Mode I as mixed mode loading such as I-II, I-III, or I-II-III [185]. Later analysis done as part of this research considers Mode I only.

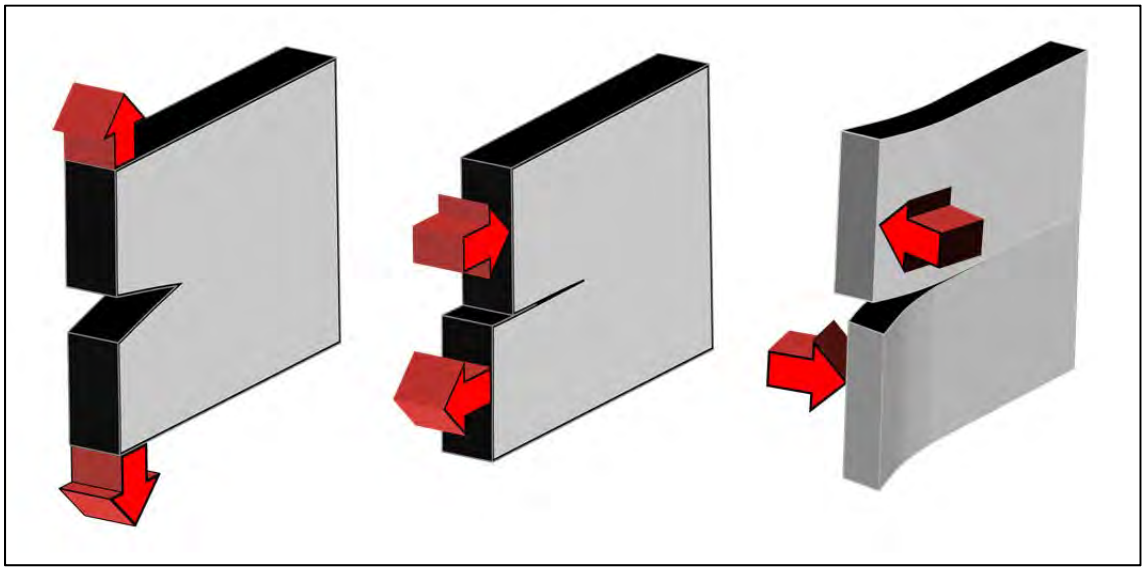

Figure 1-1 The Three Modes of Loading: Opening, Mode I on Left; Shearing, Mode II in Center; and Tearing, Mode III on Right

Stress intensity solutions for different configurations grew greatly in the decade following. Work by Paris, Sih, Bowie, etc. produced many new solutions common in handbooks today [186, 187].

The concept of stress intensity then can be used to predict crack growth. Material data is typically presented as a terms of da/dN versus ΔK where 'da' is the change in crack length, 'dN' is the change in cycle count, and ΔK is the change in stress intensity from the minimum to the maximum in a cycle which is a function of crack length and stress. The cyclical stresses can then be applied to these material curves to calculate crack growth through integration.

These material curves can be represented by raw tabular data or by a crack growth equation. One of the first was the Paris, Gomez, and Anderson equation which accounts for the 'linear' region only [188]. Linear is in quotes since some materials do not have a truly linear region but may exhibit a 'knee' in the data. Other common equations include Forman [189], Walker [190], and NASGRO [191] equation however a multitude of others exist [192]. Different methods to handle crack growth retardation and crack closure due to spectrum loading effects also received considerable treatment in the literature [193-199].

The USAF decision to require damage tolerance for their non-commercial derivative aircraft led to many new full-aircraft analysis programs. Each weapon system was required to identify critical locations and prove their damage tolerance or implement any inspections, modifications, or replacements necessary to prevent catastrophic failure. This is one of the primary responsibilities of each ASIP office. The damage considered

by damage tolerance per Reference [200] is not limited to cracks but includes corrosion as well as 'accidental damage' and 'discrete source damage'; but still, most of the focus is on fatigue[2]. This is not necessarily without reason though since fatigue or the interaction of fatigue with other degradation mechanisms has been the most likely cause in catastrophic failures of USAF aircraft [201]. Perhaps USAF leadership experienced scale aversion causing fatigue to receive so much attention even to the expense of other failure mechanisms such as corrosion and fretting.

The standard ASIP requirement was that a "rogue flaw" could not progress to failure under representative spectrum loading without one inspection at a point half of the total time. The USAF requires at least a factor of two to be applied (i.e., one half the total crack growth interval) but larger factors can be used. Following this 'initial inspection' the interval is based on the growth of a crack from a reliably detectable size to failure. The reliably detectable size is theoretically based on a 90% Probability of Detection (POD) at 95% confidence. Early on however, these Non-Destructive Inspection (NDI) inspection crack sizes ($a_{90/95}$, or a_{NDI}) were just as likely based upon 'analysis by committee' than by actual inspection reliability data though much work has been accomplished characterizing POD since. Subsequent recurring inspections are based on a fraction of the interval of time required to grow from $a_{90/95}$ to failure. Figure 1-2 depicts

[2] 'Accidental' and 'discrete source' damage is mentioned in MIL-STD-1530C only in the definition of damage tolerance. No definition of 'accidental' or 'discrete source' is given nor are they mentioned again in the document; however, fatigue and corrosion are mentioned frequently elsewhere.

the preceeding graphically using a factor of two to subdivide the crack growth lives to obtain the inspection intervals.

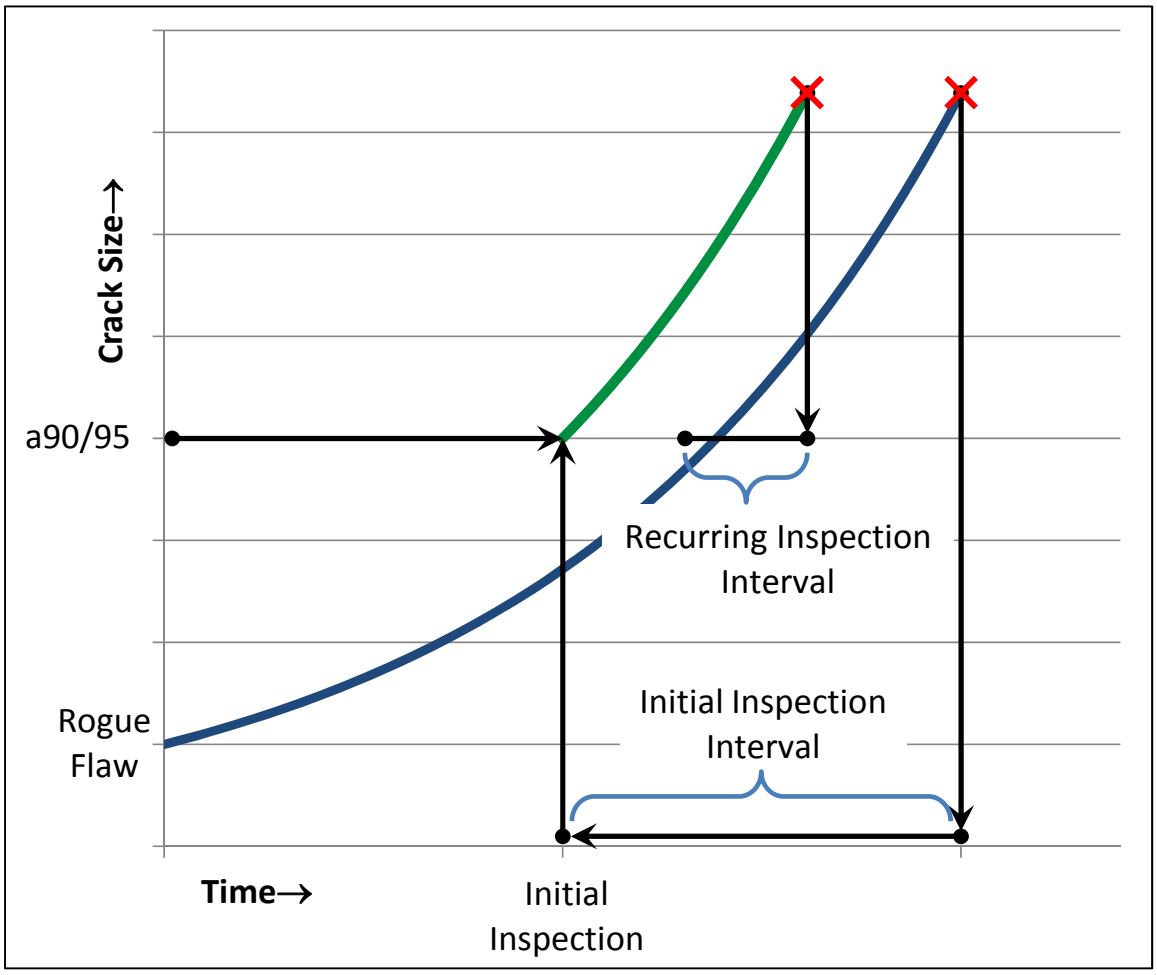

Figure 1-2 Depiction of the USAF Inspection Interval Methodology

These requirements increase the importance of capturing as much of the phenomena that affect crack growth as possible since the shape of the crack growth curve can greatly affect the required maintenance intervals. Simply knowing how long it will take to grow from a rogue flaw to failure is insufficient. The more 'bent' the crack growth curve, the less time the crack will spend in a detectable region as illustrated in Figure 1-3.

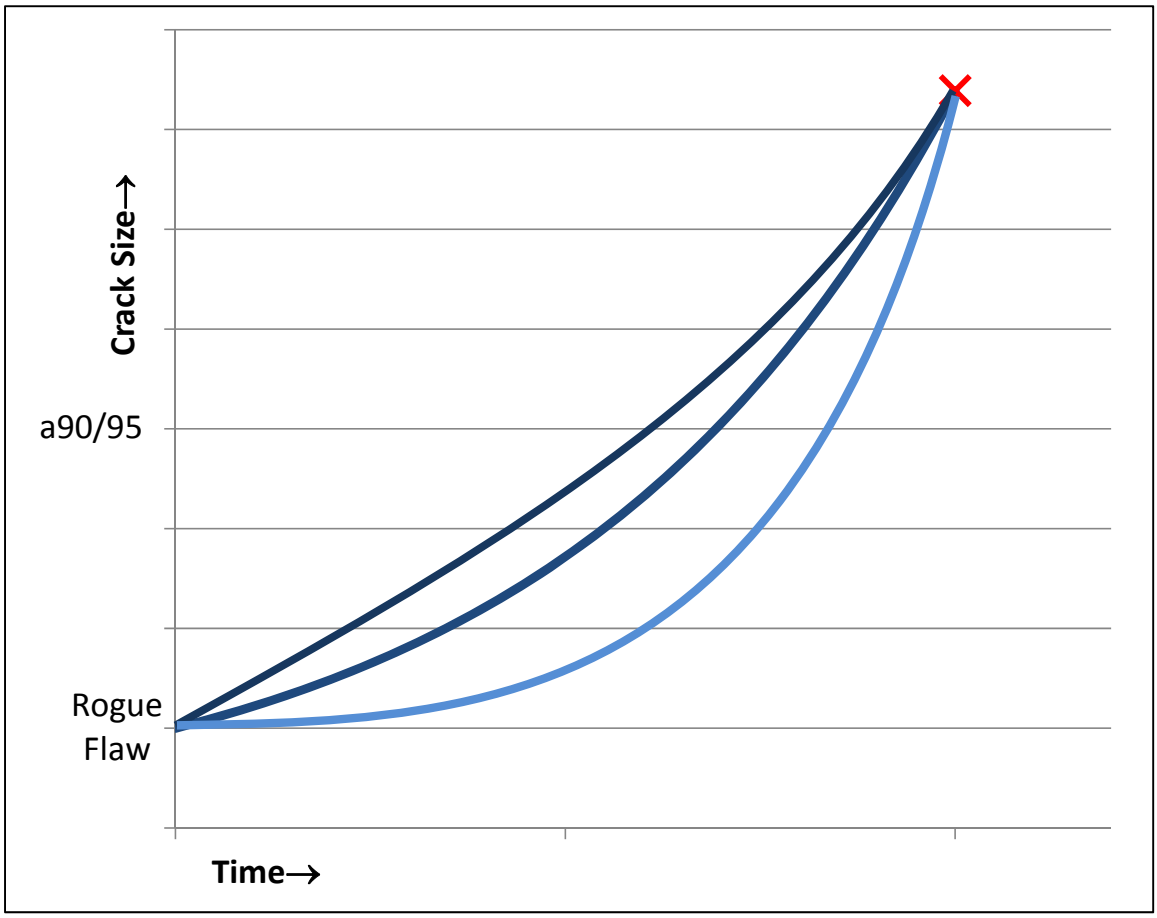

Figure 1-3 Depiction of the Effect of Different Crack Growth Curve Shapes

This leads now to the simple problem at hand, fastener flexibility is necessary to determine the load of each fastener in each joint. From the standpoint of an analysis at limit load or ultimate load a certain fastener load transfer distribution will be common to each or at least calculated for one and then converted to the other by a ratio of the limit and ultimate load. Often this is in error given the material non-linearity of the joint as the bulk material approaches ultimate. Further, load transfer in load levels below limit are often inaccurate due to the assumptions of the analysis. For the sake of expedience fastener flexibility often is assumed to be a linear relationship between force and

displacement. A common way to determine the fastener flexibility is through test where by the highly non-linear force vs. displacement response of the fastener is reduced by determining a secant line up to limit or some other point in the data. Since the load displacement is actually non-linear then for any given load flowing into a joint a different fastener load distribution should be expected as shown in many different fastener joint strength tests [70, 202-207]. Much of the recent work from Europe focusing on this topic have had a focus on composites and other laminated materials [208, 209]. Other non-linear or piece-wise linear approximations exist to handle fastener response [210, 211].

When a DTA is performed the current methods define a constant relationship between the bearing load and the bypass stress. If the force vs. displacement response of the fastener joint being analyzed was truly linear then this assumption would be safe but in truth it is not. Further corrupting the analysis is the fact that the load transfer used in the DTA is often taken from a limit or ultimate analysis of the joint for which loads are usually generated. This is the point where most of the fasteners will be fully effective and any nonlinear load-deflection response will produce an error if linearly scaled to a lower load for the joint. This is important because in spectrum loading the vast majority of the spectrum is far below. A typical fighter-type spectrum will have maybe 1 to 5 occurrences of limit load over 1000 hours but 10,000 occurrences of a load of maybe half limit. Thus the ratio between the bearing and tensile stress solutions is correct for only $1/10{,}000^{th}$ or less of the entire spectrum being analyzed.

The solution is a correlated analysis that combines the intertwined effects of load transfer between components and load redistribution as a function of both load and crack length.

The first step in this process is validation and verification of the process by analysis by one variable at a time. Specimens presented in Section 6-1 do this by applying load cycles in a constant amplitude spectrum. With the maximum load end point the effect of any fastener displacement hysteresis is minimized leaving the only variable to handle being the variation in load distribution with crack length. It will be shown that this is indeed a significant variable which requires some finesse in handling analytically above and beyond the current USAF methods. Future work should focus on variable amplitude loading or block loading to further explore the effects of load level on load distribution and fatigue crack growth.

1.4 Dissertation Hypothesis and Constraints

The hypothesis of this dissertation is:

Cracks that develop at fastener holes in a multiple fastener, aluminum alloy joint in structural load bearing applications, will change the constraint on the fastener. Quantification by more accurate modeling of the load redistribution to other fasteners due to fastener flexibility changes in the joint system will result in a more accurate fatigue crack growth prediction for the joint system.

Since this topic could be quite open-ended, a number of constraints will be applied to the research. These include:

- Consideration of joints at room temperature only

- Composite materials will not be considered to include fiber reinforced composites, metal matrix composites, and metal/fiber materials such as Glare®, ARALL, etcetera
- The only metals that will be considered are those used in the Fuselage Station (F.S.) 284 joint structure; aluminum alloy 7075 plate in two different tempers: -T651, and –T7351
- Omit the detrimental effects of fretting and corrosion on the joints and their interaction with fatigue
- Use test examples where the effect of friction load transfer between layers of a tightly clamped fastener system can be ignored
- Vibration/dynamic effects are ignored (static load only)
- Joints will be considered where the loads are transferred by fasteners in shear only

This dissertation will address:

- Different types of fasteners specifically, those that are pertinent to the hypothesis
- Different types of joints common to aircraft structures.
- Joint load analysis
- Joint stress analysis
- Joint fatigue and fracture mechanics analysis to include testing and analysis which tests the hypothesis
- Conclusions regarding the hypothesis
- Recommendations for current analysis and for future work

2.0 TYPES OF FASTENERS

> *"The question of structural materials and methods of construction are among the most vital of all that the aeronautical engineer has to face. Every matter of safety and success depends directly upon the quality and reliability of the materials of which the machines are built, and the ways in which these materials are put together."* V. Lougheed [212]

Only six years after the Wright brothers' first powered flight, Victor Lougheed wrote these words and they still ring true 100 years later.

There are many types of fasteners made of many different materials. The purpose of this paper is to develop methods for fatigue crack growth analysis specifically for aircraft, thus aerospace fasteners will be the type further discussed. This category will be further dissected into types pertinent to this study. Some types of aerospace fasteners such as Dzus fasteners, rivnuts and machine screws generally serve the purpose of securing a removable panel only. These panels are not primary structure and these fasteners are not optimized for shear load transfer. Screws retained by nuts or nutplates may transfer load when used in a neat fit application but these are generally only for simple panel attachment and often include a single fastener row only.

Fasteners also are employed to secure hydraulic lines, wiring harness, and other aircraft equipment. These items are important to consider during initial design but the loads in

these situations are usually much lower than the fastener's allowable load. Additionally though there may be some the change in fastener flexibility due to fatigue cracks, it is less of a concern since most are retained by one or two fasteners at most in a specific given location.

Methods considered in this dissertation are applicable to a wide range of fasteners. Common fasteners that would be considered are rivets and bolts to include blind versions of each type as well. These can be made of various materials and have either a loose fit, neat fit or interference fit. A loose fit means the diameter of the hole is greater than that of the fastener's shank. A neat fit means that for the diameters are the essentially the same. An interference fit is one where the fastener's shank has a diameter greater than that of the hole. These fasteners can have different heads: extending above the material, countersunk flush with the material or recessed in a counterbore. Since the focus of this study is multiple fastener joints, the permutation of a fastener in a counterbored hole will not be considered since it is not commonly used for load transfer when the load is perpendicular to the fastener's axis as is the case in a shear application.

Many of the fasteners have different heads and collars or nuts depending on whether the fastener is to carry loads in tension or shear. Tension fasteners have larger heads and bearing surfaces on the collar or nut to increase the amount of bearing surface to react the load. These types of fasteners are sometimes used in shear applications if it is possible for tension loads to develop due to load path eccentricities or serve some other purpose such as equipment attachment. Since one of the bounds on this work is joints where the

fasteners are in shear, it is assumed that the detrimental effect of fatigue on the thread roots and under the head of the fasteners can be ignored.

There are numerous publications that deal directly with different types of aerospace fasteners. Included are maintenance reference guides or handbooks [213-215], technical orders (TO) or standards [216, 217], and other specialized publications to include manufacturer's proprietary data. General figures throughout this document will feature a generic rivet to represent a fastener. Other fastener types will be shown to represent specific types as specific tests or studies were performed.

3.0 TYPES OF JOINTS

3.1 Joint Configurations and Fastener Patterns

Three types of joints are discussed in this paper; those being lap joints, butt joints, and doublers. These joints will have one or more rows of fasteners with each row containing one or more fasteners each.

A lap joint is one where pieces are connected by overlapping and fastening through their thickness, Figure 3-1. Load is transferred from one sheet to another through the fasteners connecting them. A single shear lap is so called since there is but one shear plane in the fastener, Figure 3-2. Even if one of the sheets is joggled outside of the fastened region, there is some eccentricity to this joint, Figure 3-3. The primary issue with this type of joint is the inherent eccentricity that results in bending of the plate or sheets due to the mis-aligned load path as illustrated in Figure 3-4.

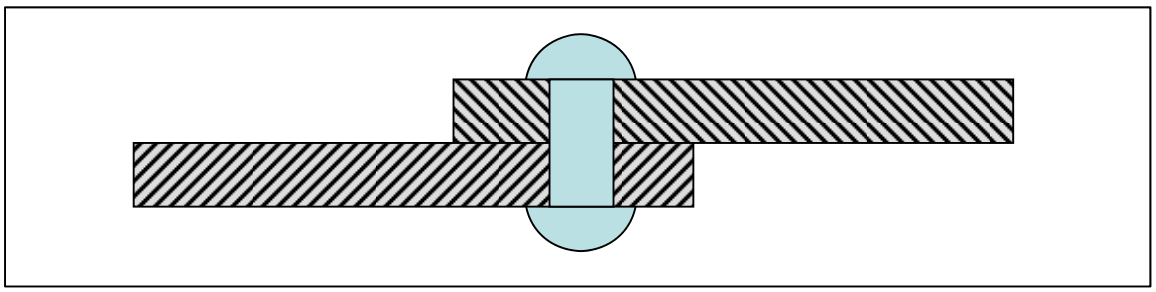

Figure 3-1 Depiction of a Lap Joint

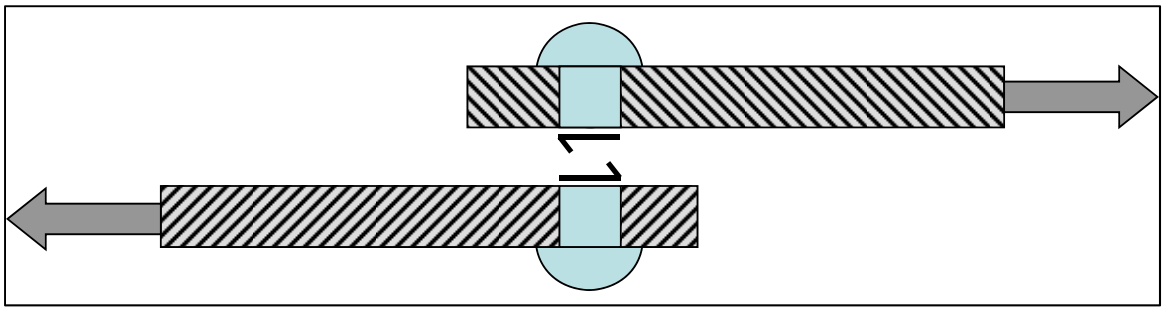

Figure 3-2 Typical Applied Loading and Resulting Fastener Shear

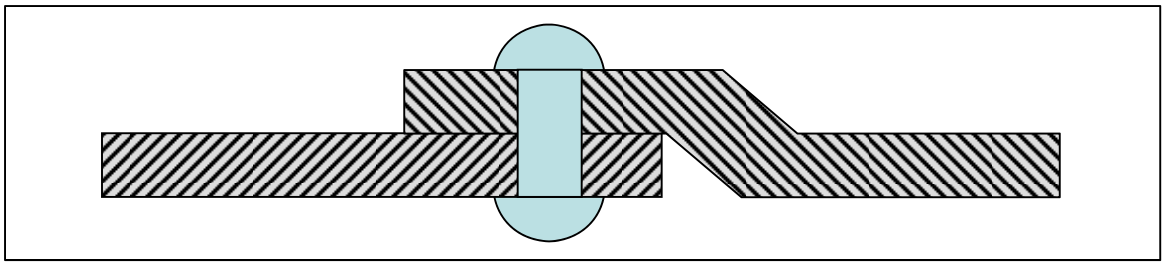

Figure 3-3 Depiction of a Joggled Single Lap Joint

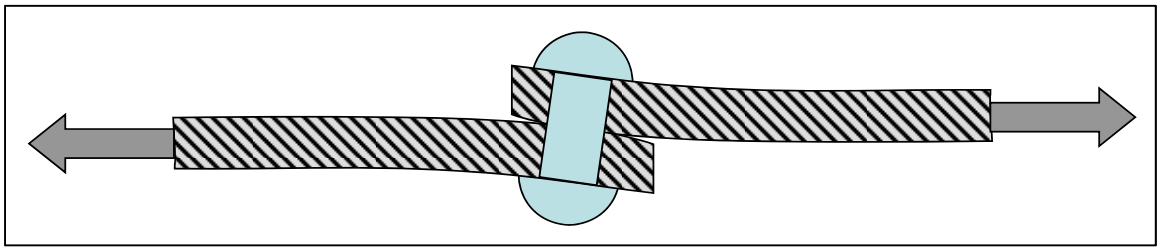

Figure 3-4 Out of Plane Bending in a Lap Joint

A butt joint is where two pieces of structure are joined by one or more other pieces of material which overlap both sides. The load is transferred from one component, through the strap or straps, into the other component. The two types considered here are single and double shear joints. In both instances the common nomenclature for the joint is that the two abutted pieces are referred to as ‘plates’ while the connecting piece of material is the strap. A single strap joint is essentially two adjacent single shear lap joints, typically

symmetric about the mid-plane of the strap (Figure 3-5). A double shear has straps on either side of the plate (Figure 3-6) thus each fastener has two shear planes. The internal loads can be seen in Figure 3-7, by taking a cut at the end of the left plate through both straps. Of these two joints, the single strap will always have a non-symmetrical load path resulting in bending similar to the lap joint as depicted in Figure 3-8.

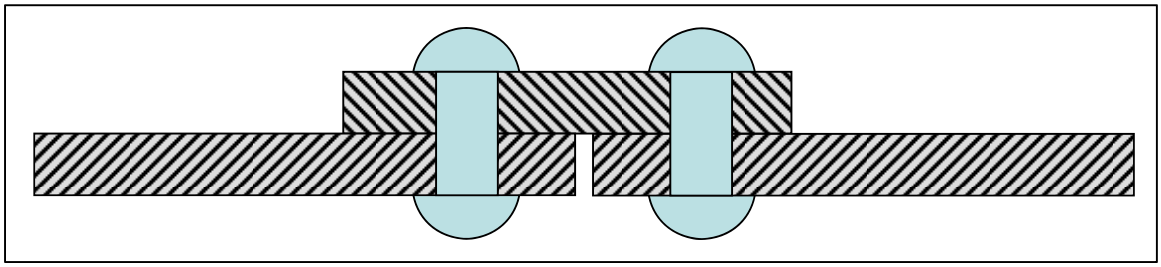

Figure 3-5 Depiction of a Single Strap Butt Joint

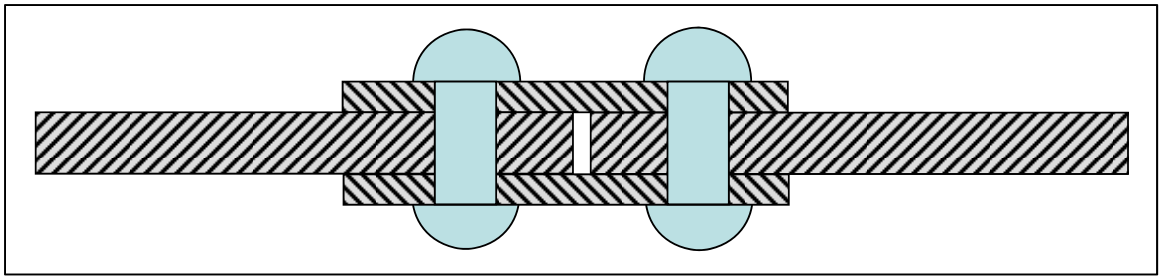

Figure 3-6 Depiction of a Double Strap Butt Joint

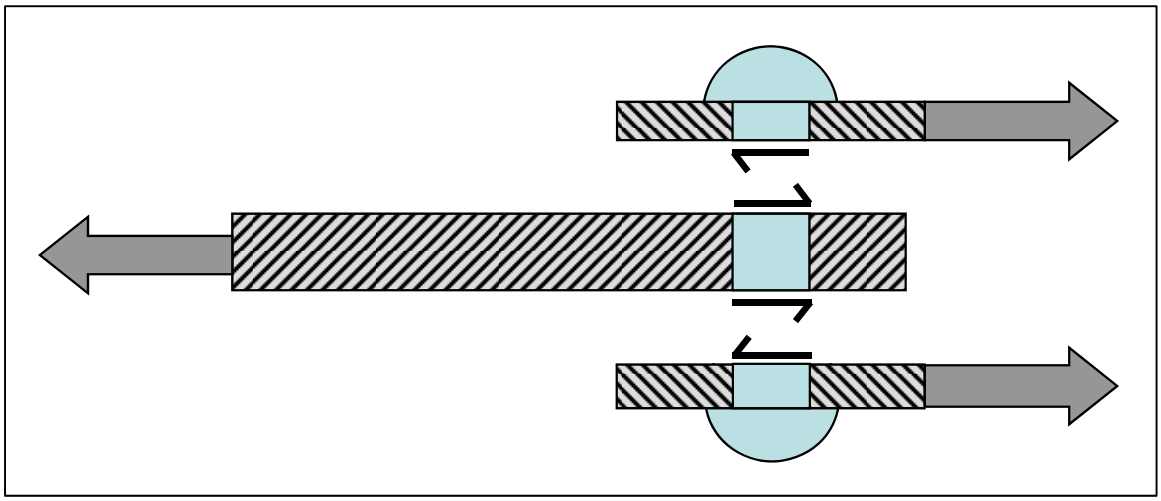

Figure 3-7 Typical Applied Loading and Resulting Fastener Shear

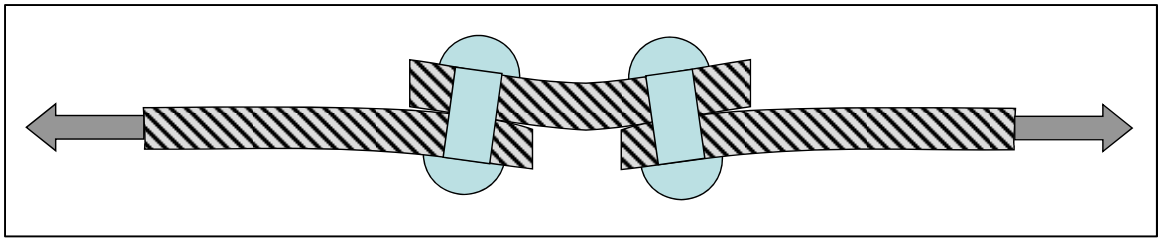

Figure 3-8 Out of Plane Bending in a Single Strap Joints

In the case of a double shear strap joint the straps are usually thinner, thus the parts they connect are commonly referred to as plates. The same terminology will be used here for convenience even when the thickness is less than 0.125” which is a common breakpoint for the qualitative terms of sheet and plate. It also is important to note that the straps need not to be symmetrical about the mid-plane of the plate as shown in Figure 3-9 where the fasteners of the first row are single shear and the second row are double shear.

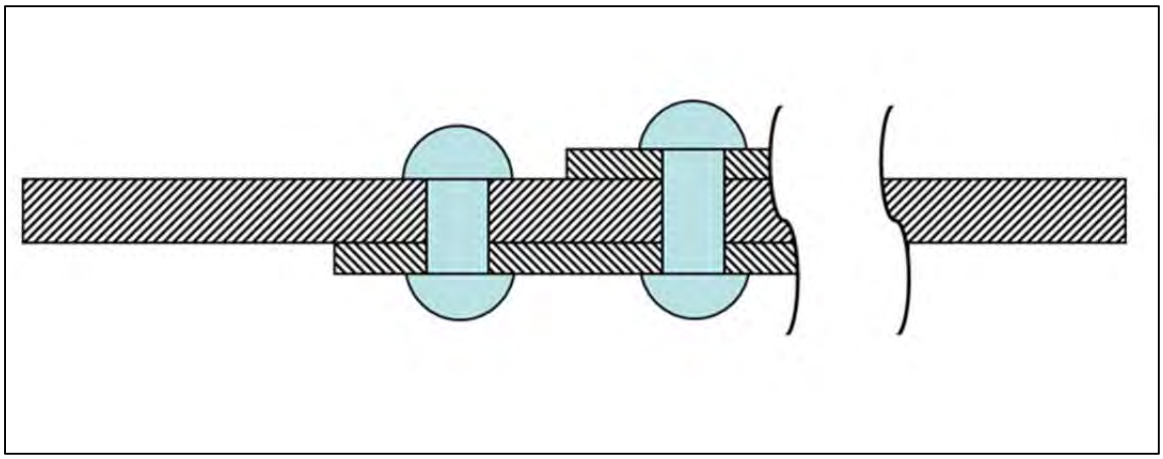

Figure 3-9 Strap Arrangement, Non-Symmetrical about the Mid-Plane of the Plate

The straps and plates also might comprise more than one layer resulting in a wedding cake arrangement and shown in Figure 3-10. This type of joint is common in many regions of aircraft structure particularly where localized reinforcement is needed near a point of load introduction, e.g., pylons, production break joints, wing attach fittings, etc. They are less common on newer aircraft since there are problems with inspectability on the hidden layers. The benefits of monolithic and localized thickened regions over built-up structure in fatigue, damage tolerance/ and inspectability have also led to a decrease in this type of arrangement. In addition, there is the question about what the proper spring constant is for these types of joints. The lack of symmetry means that the stiffness of a fastener as represented analytically on one side of the plate may be greater than on the other side.

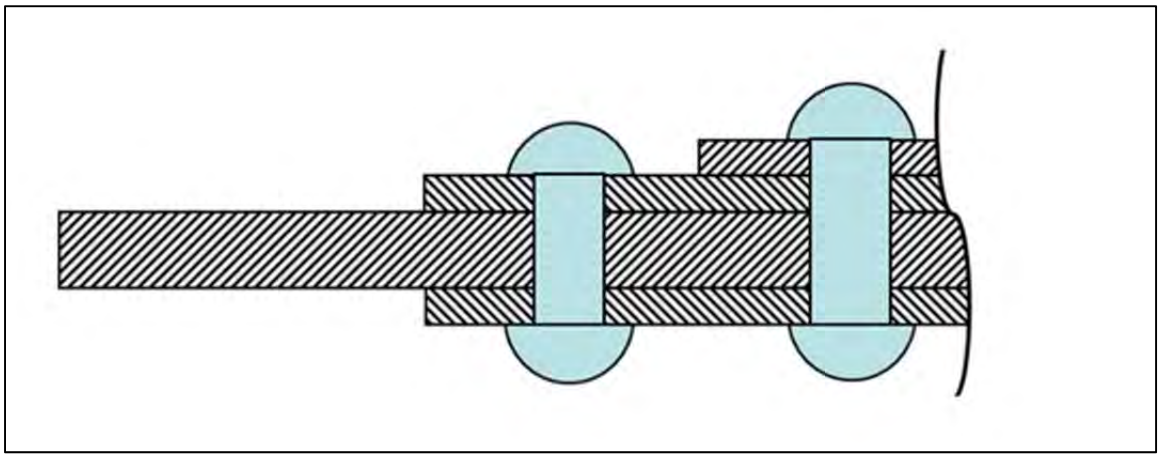

Figure 3-10 Example of a Wedding Cake Joint

The previous figures show the load being transferred solely through shear of the fastener. In reality, the load often is transferred through friction between faying surfaces due to clamp-up from the fastener. Some joints are even designed to transfer load solely on the basis of friction [239]. The downside is that the clamping action of these joints tend to decrease over time and that the nucleus of the fatigue crack may change to one of fretting [240, 241].

A doubler is not a joint per se since there is no break in the primary structure. The doubler's purpose is to increase local strength or stiffness either restoring such due to a cutout in the material or in an area of load introduction. However, for the doubler to be effective it must carry load, and to do so there must be load transfer through the fasteners. Therefore it is possible to analyze them in much the same way as splices are analyzed [242].

Beyond the previously shown combinations of rows, plates and splices there are different patterns for the rows themselves. A simple lap joint such as shown in Figure 3-1 or Figure 3-3 may appear similar to Figure 3-11 when viewed looking down the diameter of

the fasteners. All the fasteners are in a single line joining the two sheets. Also common is a staggered pitch as shown in Figure 3-12 (staggered is referred to as ‘reeled’ in some publications [243]). Staggered patterns are common in areas where the required number of fasteners exceeds that available in a single row due to minimum pitch requirements but lacks room for a second row. This is common at angles and flanges in some designs.

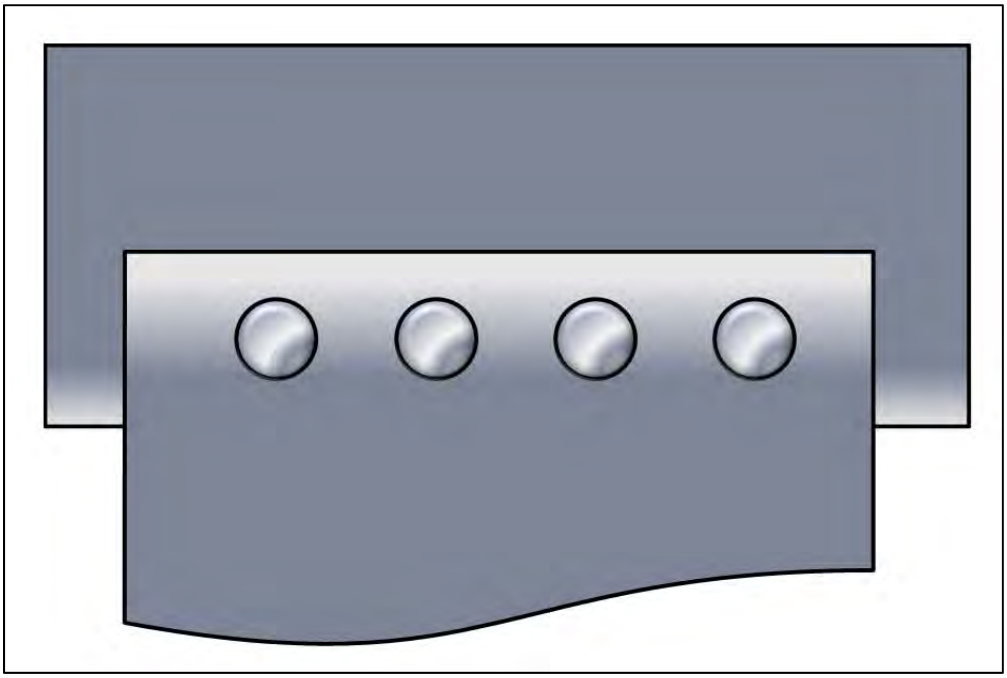

Figure 3-11 Example of a Single Row of Fasteners

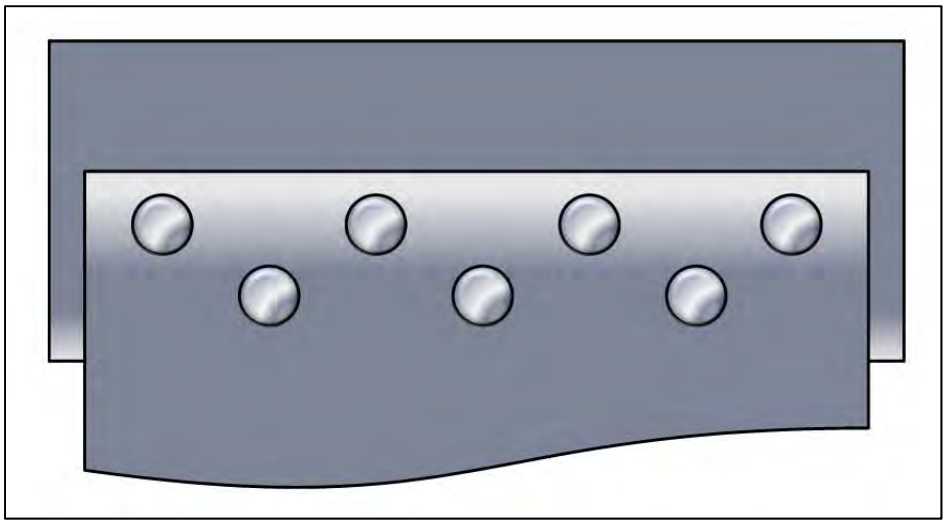

Figure 3-12 Example of a Staggered Row of Fasteners

When multiple rows are used often times the first row of fasteners will have a skip pattern to reduce the load transfer at the first row as shown in Figure 3-13. The most complex but most inspectable of fastener patterns is a permutation of a multiple row joint where the exposed plate or sheet is ‘fingered’ or cut such that each fastener appears to take the position of the fingernail on a hand such as in Figure 3-14. One of the chief advantages is the reduction in stiffness between rows which reduces the load transferred at the first row with the added bonus of inspectability of the typically covered sheet between the fingers. Other types of joints would be doublers and attachment joints such as those given in Figure 3-15.

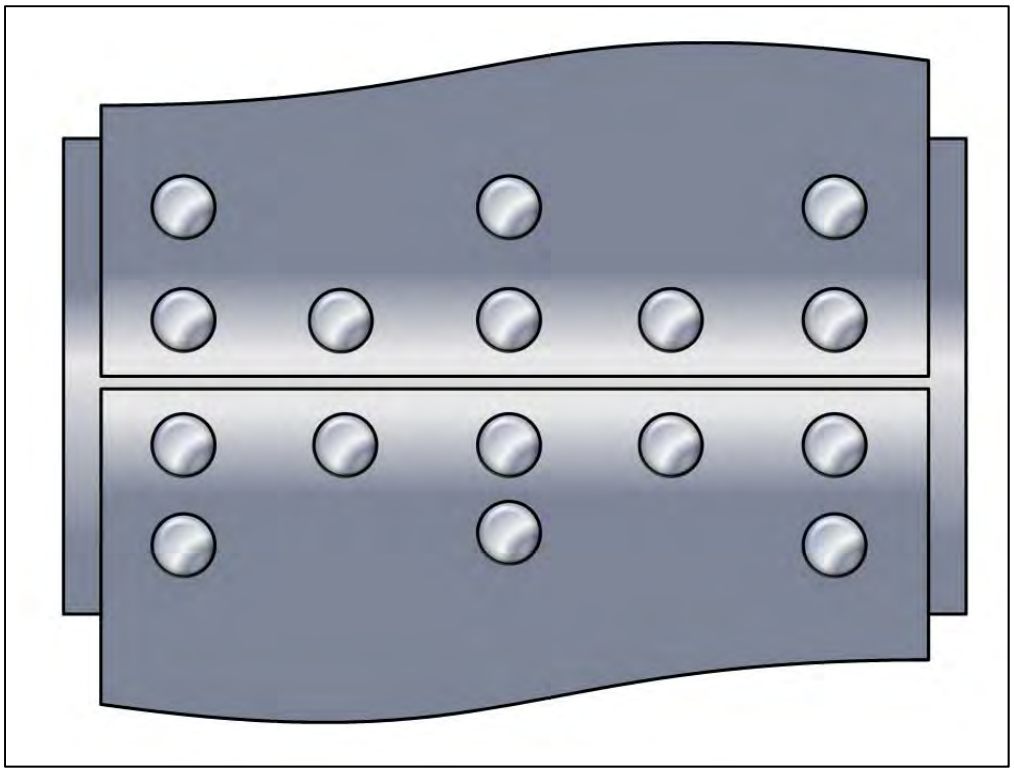

Figure 3-13 Example of a Butt Splice with a Different Fastener Spacing in the First Row

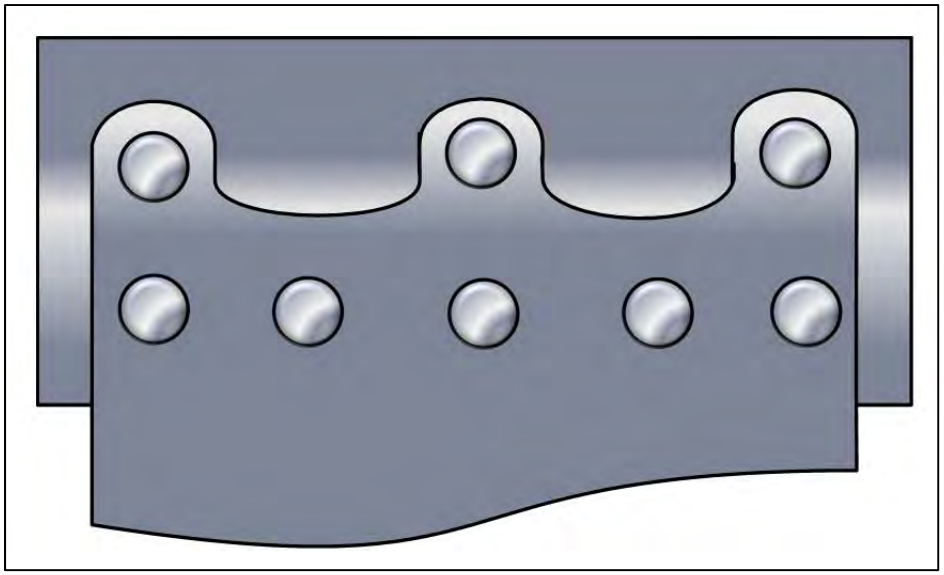

Figure 3-14 Example of a ‘Fingered’ Splice

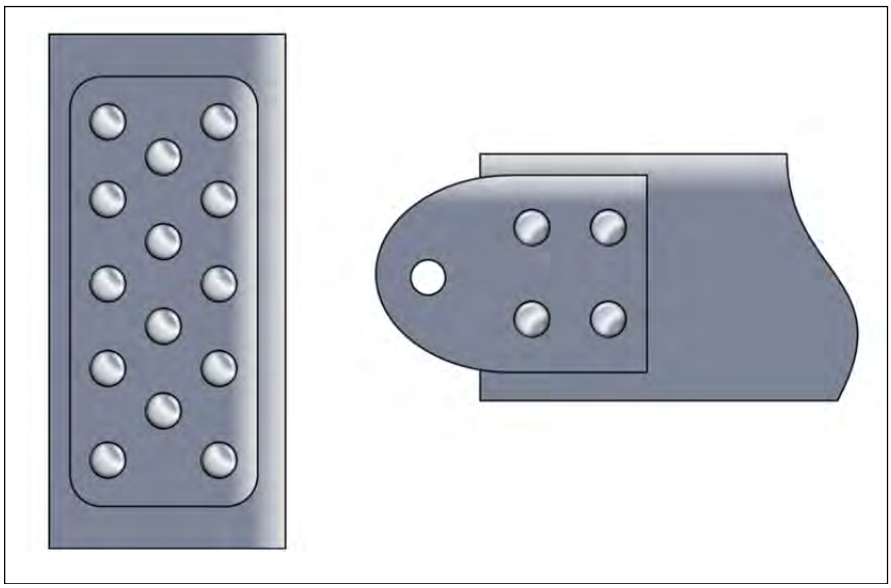

Figure 3-15 Example of Doubler on Left and an Multiple Fastener Attachment Joint on the Right

4.0 JOINT LOAD ANALYSIS

There are many classic aircraft structural analysis texts that discuss the analysis of fastened joints from a static strength approach [27, 226, 244-252]. Of those, the text by Mangurian and Johnston is probably the best illustrated and methodical in its address of the topic. As such, it is the primary reference for the static strength method of joint analysis that is further developed in the following pages.

The static strength approach of analyzing joints makes the assumption of non-flexible sheets such that all fasteners are all loaded to their maximum capability. A bolt's individual load is thus the ratio of the total joint load divided by the total of all the joint's bolt's strength multiplied by the individual bolt's strength. The load in each bolt is therefore:

$$P_{bolt} = \frac{P_{joint} * S_{bolt}}{\sum_{i=1}^{n} S_{bolt}(i)}$$

Equation 4-1 Static Strength Approach to Individual Bolt Load

where:

P_{joint} is the total load in the joint

S_{bolt} is the shear allowable for the bolt

Equation 4-1 is generally applicable where the load of the joint passes through the centroid of the fastener group. In instances where the load does not the load develops a load at each fastener in its own direction and magnitude as determined previously but also an added load due to the moment of the load about the centroid. The centroid of the group is determined in a method like section areas but instead the allowable bolt loads are used.

$$\bar{y} = \frac{\sum_{i=1}^{n} P_{Bi} y_i}{\sum_{i=1}^{n} P_{Bi}}$$

Equation 4-2 Location of the Centroid on the Y-Axis

$$\bar{x} = \frac{\sum_{i=1}^{n} P_{Bi} x_i}{\sum_{i=1}^{n} P_{Bi}}$$

Equation 4-3 Location of the Centroid on the X-Axis

where:

P_{Bi} is the allowable load in the bolt

y_i is the bolts location in the y-axis

x_i is the bolts location in the x-axis

$$I_p = \sum_{i=1}^{n} P_{Bi} * r_i^2$$

Equation 4-4 Polar Moment of Inertia of the Fastener Group

where:

r_i is the radial distance of the fastener from the centroid

$$P_{Mi} = \frac{M * P_{Bi} * r_i}{I_p}$$

Equation 4-5 Bolt Load due to Moment in the Joint

where:

M is the moment of the total joint load about the centroid

The final load in each fastener is thus:

$$P_{BoltTotal} = P_{bolt} + P_M$$

Equation 4-6 Total Bolt Load due to Eccentric Load

This process is shown graphically in Figure 4-1. For fastener groups where the load is concentric, only Equation 4-1 is needed.

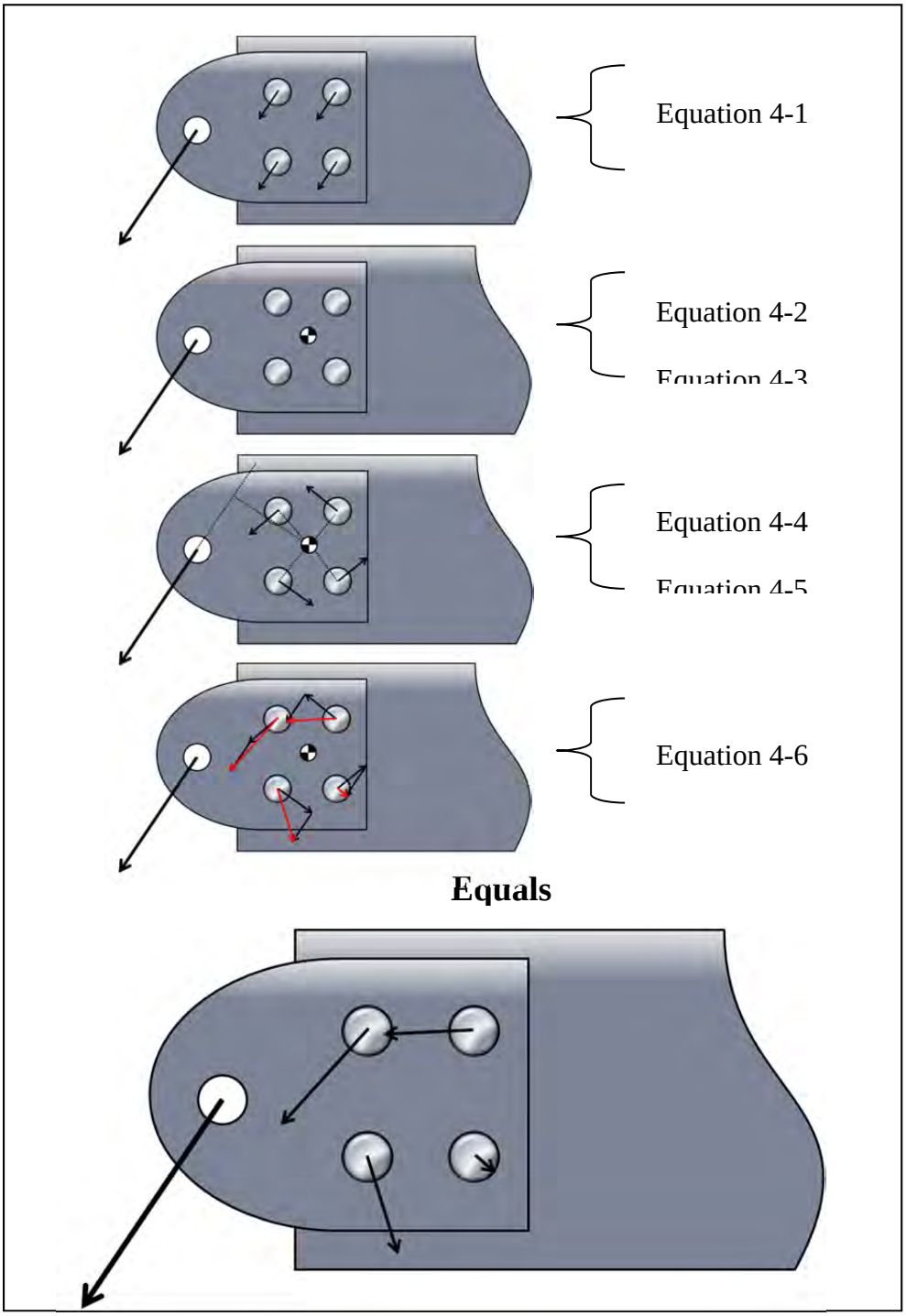

Figure 4-1 Graphical Representation of the Calculation of Fastener Loads due to Eccentric Loading

In situations where the fastener group do not all connect the same structural items the method shown in Figure 4-1 would not apply. This would include gussets where the fastener pattern defines the line of force such as the tubes connected by gussets shown in Figure 4-2.

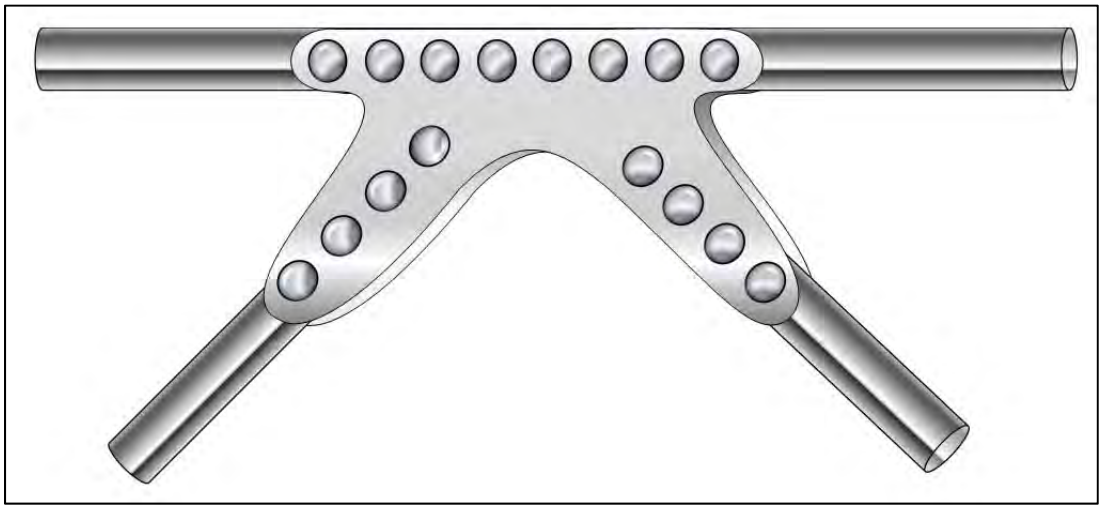

Figure 4-2 Tubular Joint Made with Sheet Gussets

4.1 Wooden Joints

As mentioned in the introduction, this work is focused on the analysis of metallic joints. However, some of the original groundwork in fastener joint loads was spawned from the complexities of the wooden aircraft joint and the efforts of early aeronautical engineers; thus it does bear some mention here. Wooden aircraft structure is not common in new aircraft outside of smaller homebuilt aircraft and rebuilt older aircraft [253]. The one exception to this being Bellanca aircraft which were of wood construction and were produced up through the 1980s [254]. As the wood was superseded by metal in aircraft design in the early 20th century the art of wooden construction has progressed little. New

manufacturing techniques were needed to utilize the shorter lengths of spruce and other woods that available after the virgin strands of timber were logged. Original aircraft, particularly those used during World War I required long, near flawless lengths of straight grained wood to use for fuselage longerons and wing spars. Of hundreds of board feet of spruce logged only a few could be used for aircraft production.

Wood also has physical properties different from metals that both benefit and hinder their use in aircraft structure. Wood is subject to much more variability in strength parameters than metals due to differences in grain, growing conditions, and natural discontinuities like knots [255, 256]. The strength properties also have a unique strength behavior due to the cellular nature of this material. Wood can support more load in short duration than it can over a greater period of time. Standard wood strength tests have a duration roughly 5 minutes but if the load is applied for only a second or so the wood can potentially sustain 15% more stress [257-261]. For long term duration loadings such as building columns and beams the allowable working stress and modulus of elasticity [262] might be half of that measured in the test. For complex structure such as aircraft components like wings and tailplanes, the increase in strength for short duration loads is less than small component tests; more in the 7% range [263]. These traits combined with wood's natural ability to absorb shock and dampen vibration made it the ideal material for the pioneers of aviation.

Difficulty in attachment in wood is a difficult problem. Grain orientation can greatly affect the strength capabilities of the joints as well as different manufacturing qualities such as effects of clean holes and material preparation for gluing [264, 265]. Neat fit holes are especially important to prevent splitting along the grain. When loads are out of

alignment with the grain or not perpendicular to the grain the Hankinson formula is use to determine the allowable load [266]:

$$n = \frac{pq}{p\sin^2\theta + q\cos^2\theta}$$

Equation 4-7 Hankinson Formula for Off-Angle Bolt Loads in Wood

where ‘n’ is the load at angle θ from the direction of grain; ‘p’ is the bolt compression parallel with the grain and ‘q’ is the bolt compression allowable perpendicular with the grain.

As mentioned earlier, the much higher length to diameter ratio of the typical wooden bolted joint can lead to excessive set in the joint and exceed the proportional limit of the joint at far less load than a conventional joint analysis might indicate [267]. This is due to bending of the fastener and the consequence that the load is being borne unevenly through the cross-section. Thus early design sought to produce hollow fasteners which maximize the bending stiffness to shear strength ratio such that the available strength of the thicker wooden beams could be fully utilized through standard fastened connections [41]. This same concept will be shown later to be in effect in much smaller thicknesses in metallic joints. This is critical since it requires an understanding of the basic phenomena in not just two dimensions but in all three.

4.2 Fastener Flexibility

Fastener flexibility methods are another way to calculate the fastener load distribution. As discussed in Section 1.0 in the elastic region a multi-fastener joint is an indeterminate

problem and the loads carried by individual fasteners are not necessarily equal. These methods are essentially solving a system of equations where different components are modeled as springs. The springs can be linear or non-linear and can include any number of complicating assumptions to try and provide a more accurate solution. Fastener flexibility, denoted by the lowercase letter (f) is the inverse of the fastener spring constant given as the lowercase letter (k). The displacement of the fastener is given by:

$$\delta = Pf = \frac{P}{k}$$

Equation 4-8 Relationship between Fastener Flexibility, Load, and Deflection

where P is the load and δ is the displacement. In almost all cases, fastener flexibility is linear. Some piece-wise linear approximations do exist and will also be discussed. The non-linearity previously mentioned is a geometric non-linearity and is commonly introduced for lap splices that exhibit rotation due to the unaligned load paths.

Use of fastener flexibility methods are most common in the analysis of aircraft structure where the need for light weight leads to lower margins of safety than those used in buildings and bridges. As such fastener flexibility methods of determining load distribution are uncommon outside of aeronautical research. Civil engineering calculations for the most part use ultimate strength type analyses where all fasteners take an equal portion of the load. This is evidenced by the methods taught in textbooks on the subject [268-271], though many give the caveat that it is a first order approximation of the actual load distribution. However, credit is due to the civil and mechanical engineering communities and their pioneering work on the variation of load transferred in

joints [272-276]. Later work by Lantos [277] and furthered by Zahn [278] develop methods to handle unequal load sharing for wooden connections.

4.3 Fastener Flexibility Equations

As stated in the abstract, many different methods exist in literature to determine fastener flexibility. A review of the different methods is presented in this section.

The Swift method is an empirical equation for rivets in single shear which accounts for fastener material type, skin and doubler thickness and modulus of elasticity of the skin and doubler [219]. Note that the modulus must be the same for both the skin and doubler.

$$f = \frac{\left[A + B\left(\frac{D}{t_1} + \frac{D}{t_2} \right) \right]}{ED}$$

Equation 4-9 Swift Equation for Fastener Flexibility

where: E = Modulus of Elasticity for the skin and doubler

D = Fastener diameter

t_1 = Skin thickness

t_2 = Doubler thickness

A = 5 for aluminum fasteners, 1.667 for steel fasteners

B = 0.8 for aluminum fasteners, 0.86 for steel fasteners

A revised form for the rivets at crack stoppers is given by [219]:

$$f = \frac{\left[A + B\left(\frac{D}{t_1} + \frac{D}{t_2}\frac{E_a}{E_{cs}} \right) \right]}{E_a D}$$

Equation 4-10 Swift Equation for Fastener Flexibility at Crack Stoppers

where: variables are the same as above except for

E_a = Modulus of Elasticity for the skin

E_{cs} = Modulus of Elasticity of the crack stopper

t_2 = Crack stopper thickness

The empirical method for fastener flexibility for a double shear arrangement, presented by Tate and Rosenfeld in Reference [220, 221], is seen in many different forms. The base equation they present is made up of five terms, the shear in the fastener, the bending in the fastener, the bearing in the fastener, the bearing in the straps and the bearing in the plate constituting, in order, the five terms summed in the equation below.

$$f = \frac{2t_s + t_p}{3G_b A_b} + \frac{8t_s^3 + 16t_s^2 t_p + 8t_s t_p^2 + t_p^3}{192E_{bb} I_b} + \frac{2t_s + t_p}{t_s t_p E_{bbr}} + \frac{1}{t_s E_{sbr}} + \frac{2}{t_p E_{pbr}}$$

Equation 4-11 Tate and Rosenfeld Fastener Flexibility Equation

where: t_s = thickness of the strap

t_p = thickness of the plate

G_b = Shear modulus of the bolt or $E_{bb} / 2 * (1 + \nu_b)$

ν_b = Poisson's ratio for the bolt

A_b = area of the bolt cross-section or π * bolt diameter^2 / 4

E_{bb} = Young's modulus of the bolt

I_b = moment of inertia of the bolt cross-section or π * bolt diameter^4 / 64

E_{bbr} = bearing modulus of the bolt

E_{sbr} = bearing modulus of the strap

E_{pbr} = bearing modulus of the plate

The pivotal work done by Tate and Rosenfeld was the genesis for many different versions of their base equation. This basic form for the Tate and Rosenfeld in double shear is presented in a reduced form for a single shear in de Rijck [222]:

$$f = \frac{1}{E_f t_1} + \frac{1}{E_f t_2} + \frac{1}{E_1 t_1} + \frac{1}{E_2 t_2} + \frac{32(1+\upsilon_f)(t_1+t_2)}{9E_f \pi d^2} + \frac{8}{5E_f \pi d^4}\left(t_1^3 + 5t_1^2 t_2 + 5t_1 t_2^2 + t_2^3\right)$$

Equation 4-12 Tate and Rosenfeld Fastener Flexibility Equation for Single Shear

where:

E_f = Young's modulus of the fastener

t_1 = thickness of plate 1

t_2 = thickness of plate 2

E_1 = Young's modulus of plate 1

E_2 = Young's modulus of plate 2

ν_f = Poisson's ratio for the fastener

d = diameter of the bolt

Tate and Rosenfeld also presented a simplified form based on the assumption that $t_p = t_s / 2$ and four constants defined as:

$k_1 = E_{bb} / G_b$

$k_2 = E_{bb} / E_{bbr}$

$k_3 = E_{bb} / E_{sbr}$

$k_4 = E_{bb} / E_{pbr}$

such that:

$$f = \frac{2}{t_p E_{bb}} \left\{ \frac{4}{3\pi} \left(\frac{t_p}{D} \right)^2 \left[k_1 + \frac{5}{4} \left(\frac{t_p}{D} \right)^2 \right] + 2k_2 + k_3 + k_4 \right\}$$

Equation 4-13 Tate and Rosenfeld Fastener Flexibility Simplified for Balanced Joints

where: t_p = thickness of the plate

E_{bb} = Young's Modulus of the bolt

D = diameter of the bolt

$k_{1\text{-}4}$ = as defined above

Tate and Rosenfeld arrive at five different equations (Cases) by substituting the different moduli for the different combinations of steel and aluminum fasteners, straps and plates. They are as follows:

Case I consists of aluminum fasteners, straps and plate

Case II consists of steel fasteners, straps and plate.

Case III consists of steel fasteners with aluminum straps and plate

Case IV consists of steel fasteners and straps with aluminum plate

Case V consists of aluminum fasteners and plate with steel straps

Michael Niu presents a reduced form of above also given by Tate and Rosenfeld in reference [226]. In this simplification, the substitution of t_{ave} is made for t_p and t_s where $t_{ave} = (2t_s + t_p) / 2$. Also given are two additional cases considering titanium where:

Case VI consists of titanium fasteners and aluminum straps and plate

Case VII consists of titanium fasteners and straps with aluminum plate

These equations agree exactly with that determined by Tate and Rosenfeld for the case where $t_{ave} = t_p$.

The approximation made by Niu is accurate within a few percent for Cases I, II, III, IV, and V. Consider the situation where the plate thickness and fastener diameter are 0.25 inch. The strap thickness varies ±20% from $t_s = t_p / 2$, or from 0.100 to 0.150 inch thick.

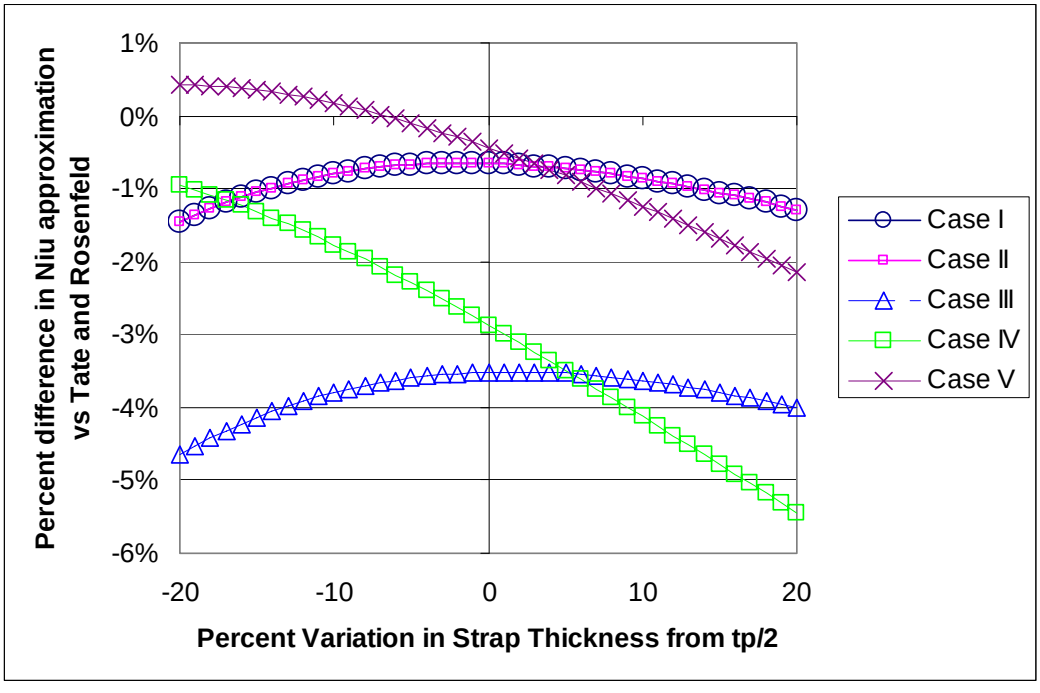

Figure 4-3 Total Error in Fastener Flexibility Given the Use of the t_{ave} Assumption

As shown in Figure 4-3 above, the percent variation for Cases I and II are less than 2% and identical and all are less than 6% off from base equation. Note that in all but part of Case V, the use of the t_{ave} approximation results in a slightly less flexible fastener value. Vogt also used the Tate and Rosenfeld equation for the limiting case where "the bolt is very large" [227]:

$$f_1 = \left(\frac{P}{Ed}\right)\frac{\left(9t_1^3 + 15t_1^2t_2 + 10t_1t_2^2 + 2t_2^3\right)}{11.78d^3} + \left(\frac{P}{Ed}\right)\frac{\left(2t_1 + t_2\right)}{d}$$

Equation 4-14 Vogt's Simplification to the Tate and Rosenfeld Fastener Flexibility Equation

Vogt also noted that if $t_1 = 0.5t_2$:

$$f_1 = \left(\frac{P}{E}\right)\left\{0.6\left(\frac{t_2}{d}\right) + \left(\frac{t_2}{d}\right)^3\right\}$$

Equation 4-15 Vogt's Simplification for Balanced Joints

or if $t_1 = t_2$:

$$f_1 = \left(\frac{P}{E}\right)\left\{0.9\left(\frac{t_2}{d}\right) + 3.0\left(\frac{t_2}{d}\right)^3\right\}$$

Equation 4-16 Vogt's Simplification for Equal Plate Thicknesses

Huth's equation was incorrectly translated in his ASTM paper [223] but is given in corrected form [224]:

$$f_1 = \left(\frac{t_1 + t_2}{2d}\right)^a \times \frac{b}{n}\left(\frac{1}{t_1E_1} + \frac{1}{nt_2E_2} + \frac{1}{2t_1E_3} + \frac{1}{2nt_2E_3}\right)$$

Equation 4-17 Huth Fastener Flexibility Equation

where: t_1 = thickness of the plate

t_2 = thickness of the straps

E_1 = Young's modulus of the plate

E_2 = Young's modulus of the straps

E_3 = Young's modulus of the bolt

a = 2/3 for bolted metallic joints and bolted graphite/epoxy joints; 2/5 for riveted metallic joints

b = 3.0 for bolted metallic joints; 4.2 for bolted graphite/epoxy joints; 2.2 for riveted metallic joint

From Gunbring, the earlier Boeing equation was [209]:

$$f = \frac{4\left(t_s + t_p\right)}{5G_b A_b} + \frac{t_s^3 + 5t_s^2 t_p + 5t_s t_p^2 + t_p^3}{40E_{bb} I_b} + \frac{t_s + t_p}{t_s t_p E_{bbr}} + \frac{1}{t_s E_{sbr}} + \frac{1}{t_p E_{pbr}}$$

Equation 4-18 Boeing Fastener Flexibility Equation from Reference [209]

The Grumman Equation [237]:

$$f_1 = \frac{\left(t_1 + t_2\right)^2}{E_f d^3} + 3.7\left(\frac{1}{t_1 E_1} + \frac{1}{t_2 E_2}\right)$$

Equation 4-19 Grumman Fastener Flexibility Equation

where: t_1 = thickness of the plate

t_2 = thickness of the straps

d = diameter of the fastener

E_1 = Young's modulus of the plate

E_2 = Young's modulus of the straps

E_f = Young's modulus of the bolt

Single Shear Boeing formula from Reference [224]:

$$f = \frac{2^{\left(\frac{t_1}{d}\right)^{0.85}}}{t_1}\left(\frac{1}{E_1}+\frac{3}{8E_f}\right)+\frac{2^{\left(\frac{t_2}{d}\right)^{0.85}}}{t_2}\left(\frac{1}{E_2}+\frac{3}{8E_f}\right)$$

Equation 4-20 Boeing Single Shear Fastener Flexibility Equation

Boeing from Reference [224]:

$$f = \frac{1.25^{\left(\frac{t_1}{d}\right)}}{t_1}\left(\frac{1}{E_1}+\frac{3}{8E_f}\right)+\frac{1.25^{\left(\frac{t_2}{d}\right)}}{t_2}\left(\frac{1}{E_2}+\frac{3}{8E_f}\right)$$

Equation 4-21 Boeing Fastener Flexibility Equation

Morris also studied various fastener flexibility equations and derived his own for single shear [225]:

$$f = \left(\left(\frac{2845}{E_1 t_1}+\frac{2845}{E_2 t_2}\right)+c_f\left(\left(\frac{500}{E_f t_1}+\frac{1000}{E_{ST_1} t_1}\right)\left(\frac{t_1}{d}\right)^2+\left(\frac{500}{E_f t_2}+\frac{1000}{E_{ST_2} t_2}\right)\left(\frac{t_2}{d}\right)^2\right)\right)$$
$$*\left(\frac{d_{head}}{d}\right)^{-0.34} * \left(\frac{s}{d}\right)^{-0.5} * \left(\frac{p}{d}\right)^{0.34} * e^{0.3r}$$

Equation 4-22 Morris Fastener Flexibility Equation for Single Shear

where:

$E_{1,2}$ is the Modulus of Elasticity for the Strap and Plate respectively

$E_{ST1,2}$ is the Modulus of Elasticity in the thickness direction for the Strap and Plate respectively

E_f Modulus of Elasticity of fastener

D is the hole diameter

D_{head} is the diameter of the deformed fastener head

P is the row pitch

R is the number of rows

S is the fastener pitch

$T_{1,2}$ is the sheet thickness

C_f is equal to 1 for aluminum rivets, 8.2 for countersunk aluminum rivets, 13.1 for titanium Hi-Loks

Vought from Reference [225]:

$$f = 56\left(e\left(\frac{t_1}{d}\right)\frac{1}{t_1} + e\left(\frac{t_2}{d}\right)\frac{1}{t_2}\right)$$

Equation 4-23 Vought Fastener Flexibility Equation

Where:

E = 1 for t / d ≤ 0.65 and e = 1.29 * t / d for t / d ≥ 0.9 with a smooth transition for aluminum sheets joined by steel fasteners

Many other fastener flexibility forms exist but are difficult to compare here since they use charts or nomographs to determine fitting parameters for the equations. Therefore, they will not be discussed in this dissertation.

4.4 Solution Methods Using Fastener Flexibility

The method developed by Tate and Rosenfeld was essentially a system of equations starting at the first fastener row and building into each successive row a ratio in terms of total load.

$$P_{i+1} = \frac{f_i}{f_{i+1}} P_i + \frac{2K_p + K_s}{f_{i+1}} P_i - \frac{2K_p}{f_{i+1}} P_{Total} + \frac{2K_p + K_s}{f_{i+1}} \sum_{1}^{i-1} P$$

Equation 4-24 Relationship between Loads for Symmetrical Double Shear Joints

and:

$$K = \frac{p}{btE}$$

Equation 4-25 Plate Spring Constant

where:

P is the load in the bolt

P_{Total} is the total joint load

p is the fastener pitch

b is the width

t is the thickness

E is the Young's Modulus

working through one reaches the end with all P_x in terms of P_1 and P. Since P_{Total} equals the sum of all P_x terms this gives the second equation to solve for the two unknowns.

$$P_{Total} = \sum P_i$$

Equation 4-26 Total Joint Load

Another solution method often described as the 'ladder' method involves idealization of the joint into springs with the plate and strap sections forming the 'side pieces' and the fasteners idealized as springs as the 'rungs'. For example, Figure 4-4 gives a

hypothetical six row riveted lap splice and Figure 4-5 shows the spring equivalent problem as the ‘ladder’.

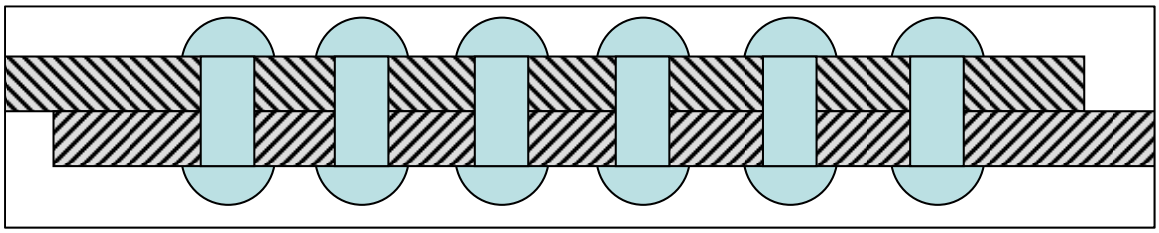

Figure 4-4 Example Six Row Riveted Lap Splice

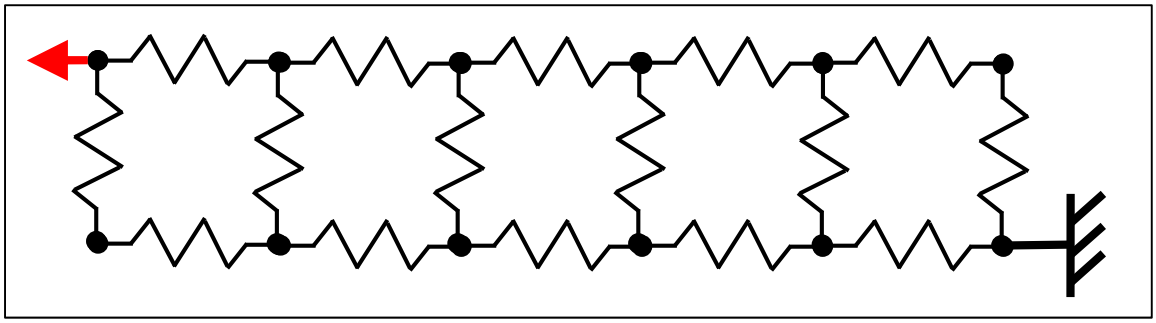

Figure 4-5 Ladder Spring Analogy for the Six Row Riveted Lap Splice

The different fastener and plate stiffnesses then are put into a matrix and the deflections are then computed.

Many other methods exist to solve this problem. Some of the more unique approaches were the electrical analogy method of Ross which equated electrical resistance to stiffness to solve the system [228] and the rubber analog of Demarkles which used a foam rubber joint with embedded metal particles to record displacements via x-ray [229]. Another approach is the ‘ladder’ method where a series of springs are solved. Parameters are very similar using the same fastener flexibilities derived previously.

Vogt also expanded the method put forth by Tate and Rosenfeld to calculate loads above the proportional limit [227, 230]. Even more complex methods were put forth later to handle the displacements above the proportional limit including certain joint simplification methods to combine lines of fasteners and different rows to make computation more expedient [231, 232]. In 1978, Barrois proposed a matrix solution to capture other non-planar effects such as rotation and variation of bearing pressure through the thickness [233].

4.5 Finite Element Modeling of Fasteners

New analytical methods are available today following the development of matrix methods leading to Finite Element Modeling (FEM) and Finite Element Analysis (FEA). Different techniques are available to the current analyst to evaluate fasteners and joints for loads and strength using FEM [234-236].

Considerable work has been done over the years modeling fasteners using FEA. Harris, et al. worked on the problem in 1970 [232] while considerable recent work has come from Europe on the topic of fastener load transfer in composites and fiber reinforced metal laminates [208, 209, 222].

5.0 JOINT ANALYSIS METHODS

Joint analysis may be done to determine the distribution of loads or for the overall suitability of the different components and details of the joint. The suitability comes in many different forms but the most basic is static strength. If the joint can survive the maximum load then different criteria can be checked such as durability, damage tolerance, fail safety, etc. These analyses can be done as part of the initial design and certification or occur later as part of sustainment but the important idea is that all of the methods are applicable regardless of the life-cycle phase of the aircraft.

5.1 Material Data

Different types of material data are required for different types of analysis. Firstly elastic and plastic response is needed for the different materials as a non-linear FEM analysis of the joint is required. Data needed includes items such as Young's Modulus, the yield strength, ultimate strength, Poisson's Ratio, shear modulus, etcetera. For this analysis the plastic region is of importance so a representative stress-strain curve also is required. For DTA, properties such as plane strain fracture toughness (K_{Ic}), da/dn vs. ΔK data and retardation parameters must be known.

The following additional considerations for material properties are made:

- It is reasonable to assume that material processing has evolved to “improve” material properties (noted in 7050-T7451 in [279] and by [280-282]). As such, all reasonable effort is made to get material properties that match those of the materials used in the experiments.
- It is known that many material properties are not normally distributed. If they were then the mean, median and mode would all be the same value. However, when multiple material tests are considered, distributions of parameters such as yield and ultimate strength can reveal considerable skewedness and kurtosis. [283]. Therefore properties specific to the plate used would be ideal.
- Since the goal of this research is to obtain a more accurate load redistribution in a complex joint, the median value of a material property would be preferred in the material models used in the FEM. The more conservative A-basis is used to calculate margins of safety but would be in error to use in the model as only 1% of the material produced would behave so.

5.2 Static Strength Methods

The overall static strength of a joint is dependent on the failure mode which occurs at the lowest load. Joints can and are designed specifically to prevent certain modes of failure and to ensure that other modes will occur first. Failures can occur in either the fastener or the different layers being fastened. From a static strength perspective, three main types of failure are checked for each (see Figure 5-1): shear, tension, and bearing. Static strength is typically reported in a margin of safety (M.S.) format which is the allowable

load or stress divided by the actual load or stress minus one. Often, M.S. are set greater than zero (or fitting factors greater than 1) to ensure safety of structure that is critical, has an ambiguous load path, or made of a material with a 'large' variation in strength [284-286]. For example, a standard minimum M.S. for joints and fittings is 15%.

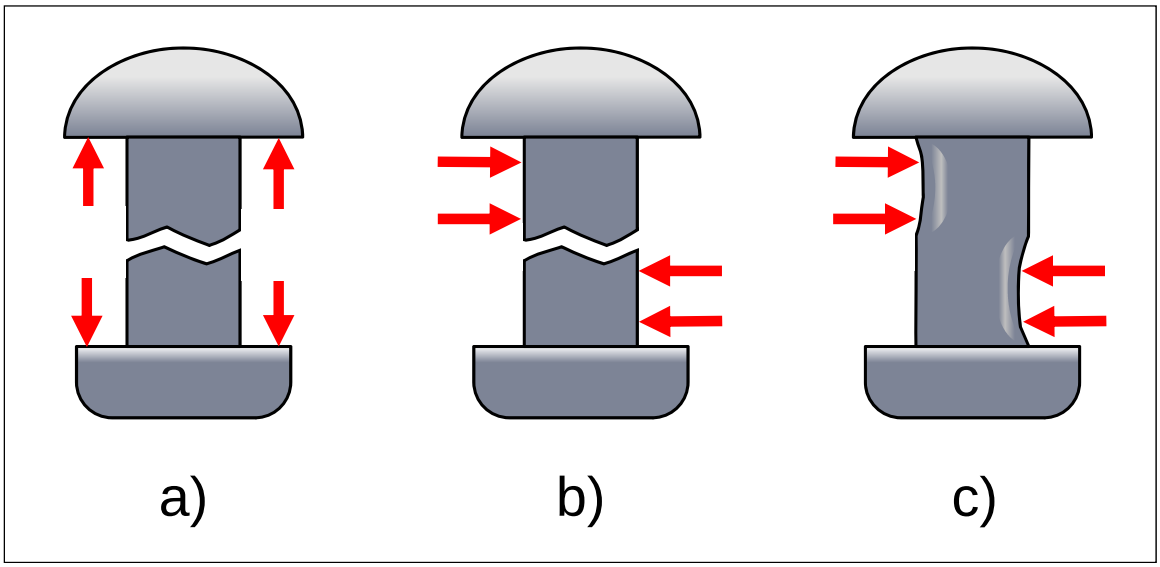

Figure 5-1 Three Primary Failure Modes of Fasteners: a) Tension, b) Shear, c) Bearing

Tension failure of a fastener is typically calculated as the strength across a minimum section along the length of the fastener. Shear joints as discussed here in this paper; tend to keep tension in the fastener to a minimum. In practice, fastener tension due to rotation in an asymmetrical joint (such as a single shear joint) is ignored in the calculation of margins of safety thus:

$$M.S.(tension) = \frac{F_{tu}\left(\frac{\pi(D_{\min})^2}{4}\right)}{ActualTensionLoad} - 1$$

Equation 5-1 Fastener Tension Margin of Safety

where:

D_{min} is the diameter at minimum section of the fastener

F_{tu} is the ultimate strength of the fastener material

Shear failure of a fastener is a function of the cross-sectional area of the fastener as well as the fastener arrangement. As discussed previously, a single shear fastener joint puts only a single cross-sectional slice of the fastener in shear while a pure double shear arrangement puts twice the cross-section of the fastener in shear. Wedding cake and other complex arrangements add a commensurate amount of complexity to the shear calculation.

$$M.S.(shear) = \frac{F_{su}\left(\frac{\pi(D)^2}{4}\right)}{ActualShearLoad} - 1$$

Equation 5-2 Fastener Single Shear Margin of Safety

or for double shear

$$M.S.(shear) = \frac{F_{su}\left(\frac{\pi(D)^2}{2}\right)}{ActualShearLoad} - 1$$

Equation 5-3 Fastener Double Shear Margin of Safety

where:

D is the diameter of the fastener

F_{su} is the shear ultimate strength of the fastener material

Bearing failure of a fastener is a function of the frontal area of the fastener to the load applied by that particular layer. If the fastener is stronger than the parent material then this calculation is unnecessary as the plate material will fail first. An exception to this rule is when a bushing is used as the two diameters used for the bearing calculation are unequal. In addition, different minimum M.S. may be required as well.

$$M.S.(bearing) = \frac{F_{br}(Dt)}{ActualBearingLoad} - 1$$

Equation 5-4 Fastener Bearing Margin of Safety

where:

D is the diameter of the fastener

t is the thickness of the plate at the layer being analyzed

F_{br} is the bearing ultimate strength of the fastener

The three main types of failure modes in the parent material include: tension failure, shear tear-out and bearing failure. These failure modes are shown in Figure 5-2 and while they are shown in the context of the last fastener or a lug, the same failure modes can occur in a line of fasteners such as shear tear-out of the material between fastener holes in the direction of the load if the spacing between fasteners is insufficient (see Figure 5-3). Note that this is only an issue for tensile loads, compressive loads will not affect fastener rows the same way unless the fit of the fasteners is exceptionally loose.

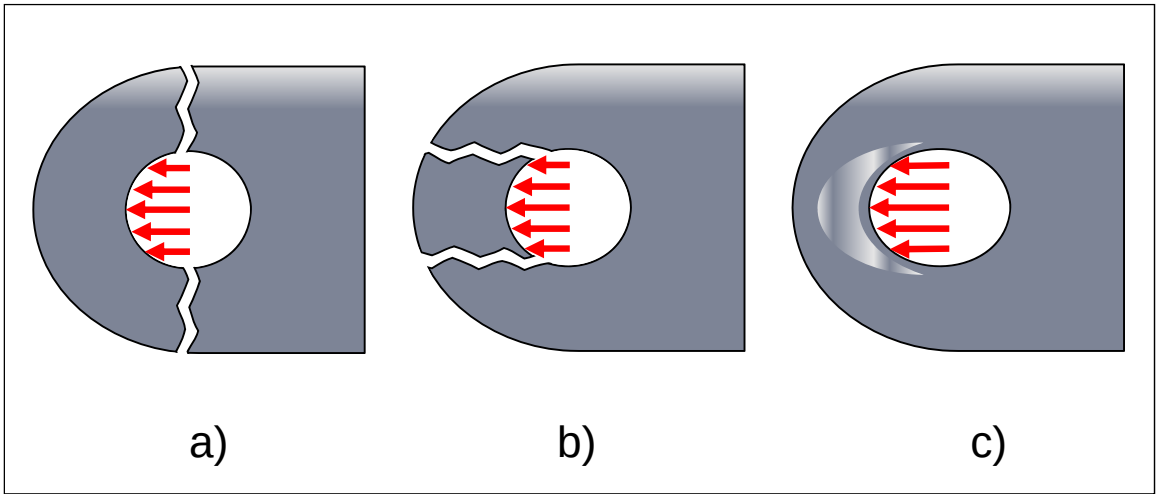

Figure 5-2 Three Primary Failure Modes of the Parent Material: a) Tension, b) Shear Tear-out, c) Bearing

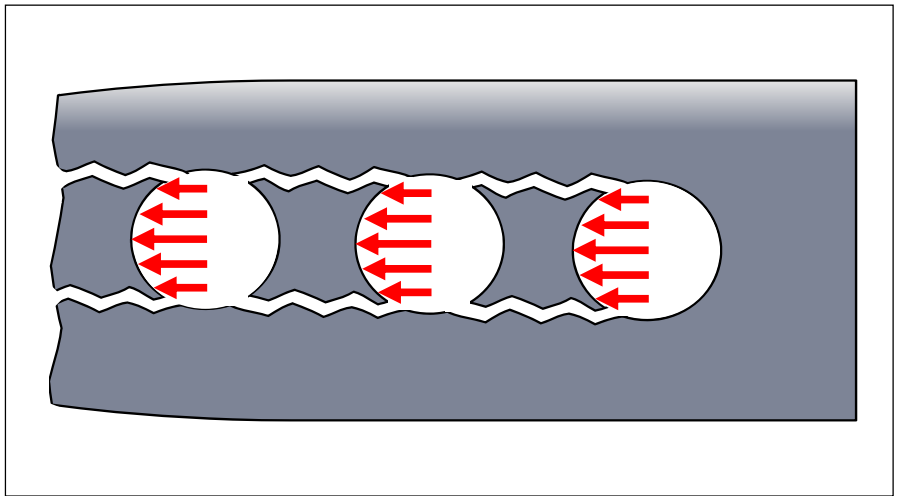

Figure 5-3 Shear Tear-out Between Closely Spaced Fasteners

$$M.S.(tension) = \frac{F_{tu}\left((W - D)t\right)}{ActualBearingLoad} - 1$$

Equation 5-5 Plate Tension Margin of Safety

$$M.S.(bearing) = \frac{F_{br}\left(Dt\right)}{ActualBearingLoad} - 1$$

Equation 5-6 Plate Bearing Margin of Safety

For shear tear-out the custom is to consider the length (a) as being the line along which shear will take place which is the length from a point 40° from the load vector at the edge of the hole, in the direction of the load vector toward the free edge (see Figure 5-4). For rounded end lugs (a) is almost the same length as (a'). For shear tear-out between fasteners, (a') is the minimum ligament length between fasteners. This makes it an easy parameter to define minimum hole spacing between lines of fasteners.

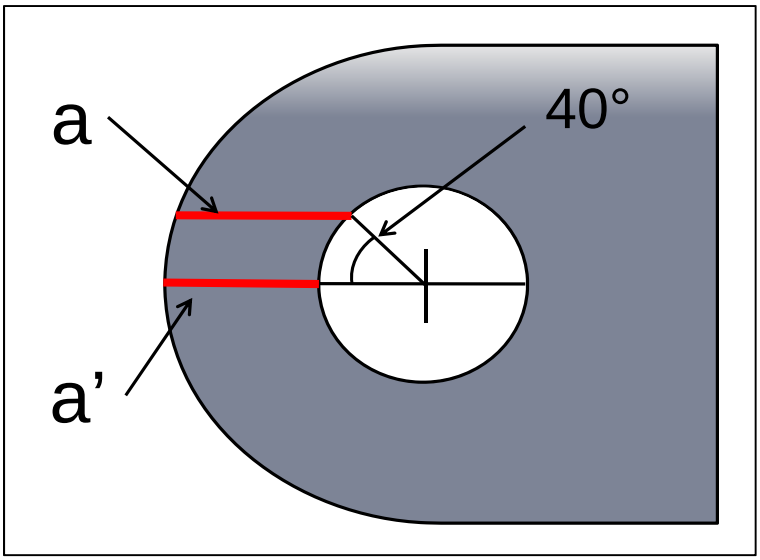

Figure 5-4 Dimension "a" for Shear Tear-Out Calculations

This gives the following two margins of safety for shear tear-out of a single fastener and for a series of fasteners tearing between fastener holes.

$$M.S.(shear) = \frac{F_{su}(2at)}{ActualBearingLoad} - 1$$

Equation 5-7 Plate Shear Tear-Out Margin of Safety

$$M.S.(shear) = \frac{F_{su}\left(2t\sum a'\right)}{\sum ActualBearingLoad} - 1$$

Equation 5-8 Plate Shear Tear-Out between Fasteners Margin of Safety

It is important to realize that Equation 5-1 through Equation 5-8 are all based on constant thickness. These equations change for tapering thickness and the shear tear-out equation changes as well if a step exists between fastener rows.

Sheet splices are treated differently. The preceding set of margin calculations were for a series of fasteners in the direction of the load; i.e., multiple rows of fasteners with a single fastener in each line. In a sheet splice, the number of fasteners in a line is much greater than the number of rows. Sheet tension stresses are usually given as a running load (units of lbs/inch) while fastener allowables for sheet are usually given in handbook tables as an allowable load per fastener. To convert the fastener allowable (P_a) to units of load/length multiply by the number of fastener rows divided by the fastener pitch in the line. Thus the margin of safety for fastener shear and tensile failure of the remaining net section through the line of fasteners are:

$$M.S.(Shear) = \frac{P_a * n}{RunningLoad * s} - 1$$

Equation 5-9 Sheet Splice Fastener Shear Margin of Safety

$$M.S.(Tensile) = \frac{RunningLoad}{n(s-d)t} - 1$$

Equation 5-10 Sheet Splice Tensile Margin of Safety

where:

P_a = allowable rivet load

n = number of rows of fasteners

s = actual rivet spacing

Other margins that were calculated previously are not necessarily required since the fastener shear allowables are used for design as long as the general edge distance spacing used in testing is enforced. For all fastener rows with a shear tear-out distance (a) of at least 2*D will be safe automatically since the shear allowable for the rivet will occur first. One caveat to the proceeding methods is that they assume that the fastener remains parallel to its unloaded position; i.e., no bending. This is of course an assumption but one that has been shown to work fairly well in practical aerospace structures. In books of allowable fastener loads, most tables are caveated with minimum diameter/thickness ratios. Also, methods exist in material strength handbooks such as ANC-5, MIL-HDBK-5 and MMPDS that combine the effects of tension and shear to compare against the tension and shear allowables.

One notable exception is bolted joints in wood. Wooden joints typically include thick members and fasteners with a much larger length to diameter ratio than metal-to-metal

joints. As such, bending of the fastener can play a prominent role in the strength of the joint. Good sources for details regarding calculations of bolted wooden joints include: Bearing Strength of Bolts in Wood [287], Airplane Structures [27, 288], and ANC-18 [45].

5.3 Durability Methods

Classical durability analysis methods focus essentially on correlation of empirical data to a set detail through transfer functions. The empirical data can either be data points or curves that equate a certain number of events to a given stress level, of a certain type. Commonly, the data are cyclical stress versus number of cycles or cyclical strain versus a number of reversals. Analyses using these data types are commonly referred to as stress-life (σ-N) and strain-life (ε-N) respectively.

Stress-life is the older of the two approaches. Beyond being just material specific, the data are usually specific to a set stress concentration (K_t); type of loading such as fully reversed, rotating bending, bending, etc.; and particular surface condition, such as etched, machined, shot-peened, and so on. Sometimes, the stress ratio, R, (which is the minimum stress divided by the maximum stress) is an additional factor for the curves. This myriad of options forces the analyst to seek out data that are as close to the detail being analyzed as possible. In addition, how the data are used can vary as well.

Constant amplitude fatigue data was commonly presented as stress level versus number of cycles to failure (S-N). Curves from these data then can be used in analysis. These curves are sensitive to a number of factors and exhibit considerable scatter. Freudenthal,

Weibull, and others contributed much toward the statistical understanding of fatigue and the S-N curve [289-293]. A compounding variable is that different methods have been used over time to fit the curves to the empirical data; typically done by the trained eye of an analyst. Finney and Mann pointed out the potential error from this effect along can be quite significant [294].

Fatigue experiments typically focused on cycles to failure for different conditions; many were specific to certain manufacturing methods [295-297]. Where full S-N curves are not utilized such as for design methods a fatigue life ratio will be used which compares an increase in fatigue life to a nominal configuration [298, 299]. Knock-down factors are determined experimentally to magnify the stress due to certain details for comparison to nominal S-N curves or to a 'fatigue limit'. S-N curves can be problematic since different bases exist to define failure. Most data available is total life from the start of test, through crack nucleation and propagation until final failure. Other tests attempt to develop curves for the "initiation" portion only assuming that once the fatigue crack nucleates and propagates a certain size, such as 0.01 inch, then the failure criterion has been met.

Many different methods exist to combine spectrum data with S-N curves to calculate expected life. The first and still one of the most common is Miner's rule. Miner postulated that the once the total damage from individual cycles summed to one, the fatigue life was reached [122]. Still, this is only one of many cumulative damage theories. The vast number of methods will not be repeated here with the excellent discussions provided by Kaechele, Schijve, and Hoeppner regarding the different theories [300-302]. The spectrum then needs to be counted to determine the number of cycles at a

given stress range. Different procedures for doing so exist including level crossing, peak counting and rainflow counting [303, 304].

There are many other ways to display S-N data, common forms being the Goodman and Modified Goodman diagrams. Goodman, Gerber, Soderberg, and others proposed different strategies to plot lines of constant life as it relates to the maximum and mean stresses in a constant amplitude spectrum [305-307]. A Modified Goodman diagram is the more common method of presenting fatigue data which was commonly used in earlier editions of the MIL-HDBK-5 series of handbooks [308].

Empirical methods also exist such as coupon, detail, component, and full-scale tests. It has been customary since the 1950s to take at least one full aircraft and subject it to repeated loadings to test the structures durability. The nature of the load being applied as well as the testing methods themselves have evolved greatly over time. Also, even as the methods have evolved so have the ways that fielded aircraft have been used. This drives further testing on all levels from coupon to full-scale as part of partial or full-recertification efforts.

Strain-life methods operate under the principles of true stress and true strain and strain control. Material data required includes a cyclical stress-strain curve and a description of ε-N. The cyclical stress strain curve is typically generated by testing under strain controlled conditions resulting in a series of hysteresis loops. The locus of the tips of each reversal then defines the points on the cyclical stress-strain curve [309]. This curve is for smooth specimens thus a fatigue notch factor is required to calculate the actual stress at the location of interest. This is typically modified by the Neuber notch factor to account for a material's notch sensitivity.

The ε-N curve is the material's resistance to strain cycling. Total resistance is the summation of the elastic and plastic strain cycling resistance. Different forms of the equation exist with some taking a more complex description to capture the nuances in the transition from the plastic to elastic region [310]. This curve represents a fully-reversed cycle, R = -1, thus additional methods are required to account for non-zero mean stress cycles. Different equations exist to handle mean stress effects and each has its supporters and detractors depending on its usage. Qualitative discussion about the applicability of different equations can be found in Reference [311].

Many different approaches have been used to determine the stress concentration at holes for the purpose of durability analysis of joints. For holes with a fastener load, different sources include closed form analytical methods, photoelastic techniques [312, 313], empirical methods, handbooks [314], and numerical methods such as FEM. Stress concentration methods were the primary focus of many analysts since, at the time, detail design was one factor they had more control over when compared to the uncertainty of structural loadings [315].

5.4 Damage Tolerance Analysis Methods

Damage tolerance methods for analyzing holes have been in place for over four decades. Nearly all the methods used to analyze aircraft structure utilize linear elastic fracture mechanics. Four of the fundamental building blocks for these analyses are: a crack growth model for the material, an idea of where the cracks will form, a model that

represents the geometric detail, and a cyclical loading spectrum. Variation in any of these inputs becomes magnified in the result.

Considerable variation is possible in the interpretation of a fatigue crack growth test based on the frequency of crack size measurements and other lab practices [316]. Combined with the natural scatter in the material response there can be significant variation between da/dN versus ΔK data. Different results can be obtained depending on the regression method thus the way crack growth equations are fit can affect the results of the analysis [317, 318].

Important to any analysis is where to consider cracks for analysis. Much work has been done on the expected location of cracks that occur around fasteners. Some cracks nucleate at the side of the hole while others nucleate at an off angle propagating to the side. Fretting of the fastener against the plate or between plate layers also can cause cracks that occur outside the hole and do not propagate through the hole at all. Studies have shown that the level of applied load can make a difference in the location of cracking. For the purposes of USAF certification, cracks are assumed in place at the side of the holes. One ‘rogue’ crack is placed at the most critical location and other ‘continuing damage’ cracks are considered at the critical locations of all other holes and grow concurrently.

Significant contributions to the literature have taken place with respect to stress intensity solutions for loaded holes that is relative to this dissertation. Newman, Raju, Fawaz, and Andersson have developed solutions for open holes subjected to tensile, bending, and bearing loads that are used in crack growth codes [319-321]. Shaw presented solutions for through and part through cracks at a neat filled hole [322]. Isida, Harter, and others

have expanded the applicability of the solutions by developing correction factors (denoted by a capital ‘F’) to account for finite width panels, offset holes and other geometric factors [323, 324]. Ways to calculate stress intensity are as diverse as those used to develop stress concentration including closed form solutions, finite and boundary element methods, even photoelastic techniques [325]. These correction factors are dimensionless and are combined with the basic equation for stress intensity by compounding such as given below.

$$K_{I,II,or\ III} = \sigma\sqrt{\pi a}F_1F_2 \ldots F_n$$

Equation 5-11 Stress Intensity Determined by Multiple Correction Factors

Different stress intensity solutions can be combined using superposition to build more complex solutions. Figure 5-5 presents an example of how a stress intensity solution for a plate with a loaded pin and remote tension can be built from two separate solutions. Note the nomenclature used such that the far-field stress is the summation of the stress in the plate due to pin loads as well as the bypass stress. Bypass stress is non-zero for most locations in a joint except for the end fastener which behaves more like a lug.

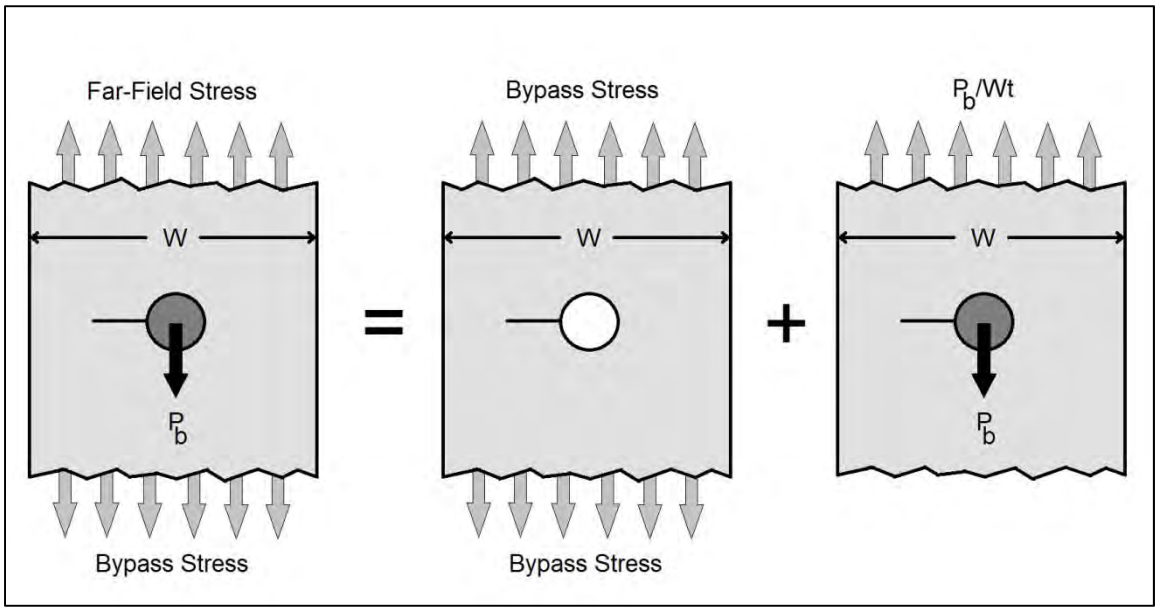

Figure 5-5 Example of Superposition for Stress Intensity Factors

Loading spectra is an incredibly complex topic both in what the loads are and how they affect the material. The current trend for aircraft is to record flight parameters for each aircraft and to analyze each critical location on every aircraft [326]. This means a multitude of data and complex analyses. However spectrum effects have to be accounted for which usually means a crack closure model or crack growth retardation model. These are unnecessary if the spectrum is constant amplitude.

6.0 T-38 F.S. 284 SPLICE JOINT

Specimens representative of a portion of the Fuselage Station (F.S.) 284 splice joint repair were built and cyclically tested to better understand this critical region. This part contains a number of Fatigue Critical Locations (FCL) and is an important load carrying member of the aircraft fuselage. Its primary purpose is to transmit longitudinal loads along the upper portion of the fuselage structure.

6.1 F.S. 284 Splice Joint Mechanical Testing

The splice itself is a repair of a T-shaped longeron where the upper crossbar of the T repair part is in single shear common to the original upper crossbar of the T from the original longeron. The downward leg of the original longeron was cut away and is replaced by the downward leg of the splice repair piece. The two downward legs butt up against one another and are connected by two straps with an alternating stagger fastener pattern of Hi-Loks®[3] in a symmetrical double shear joint (see Figure 6-1). The tests only replicate the down leg of the 'T' shape and the splice straps as shown in the dimensioned drawing in Figure 6-2.

---

[3] "Hi-Lok and "HL" are internationally registered trademarks of the Hi-Shear Corporation

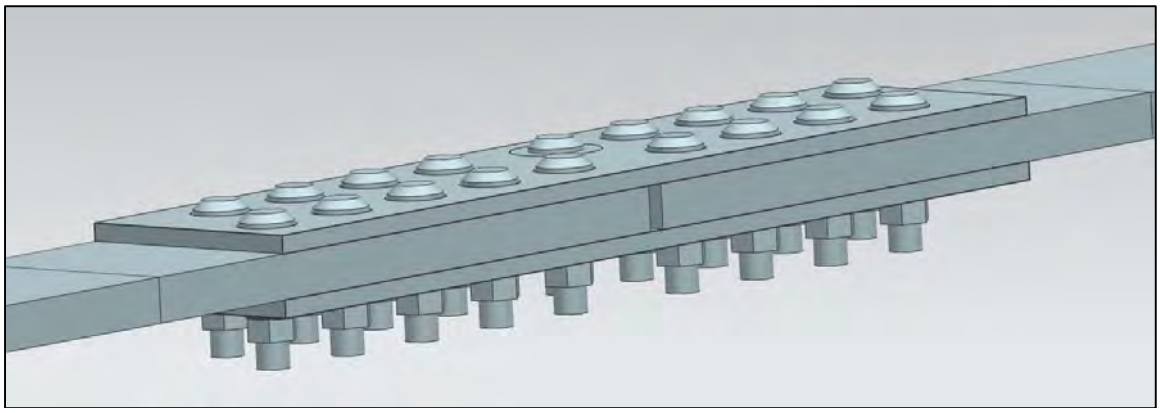

Figure 6-1 Oblique View of a Solid Model of the Splice Joint Specimen

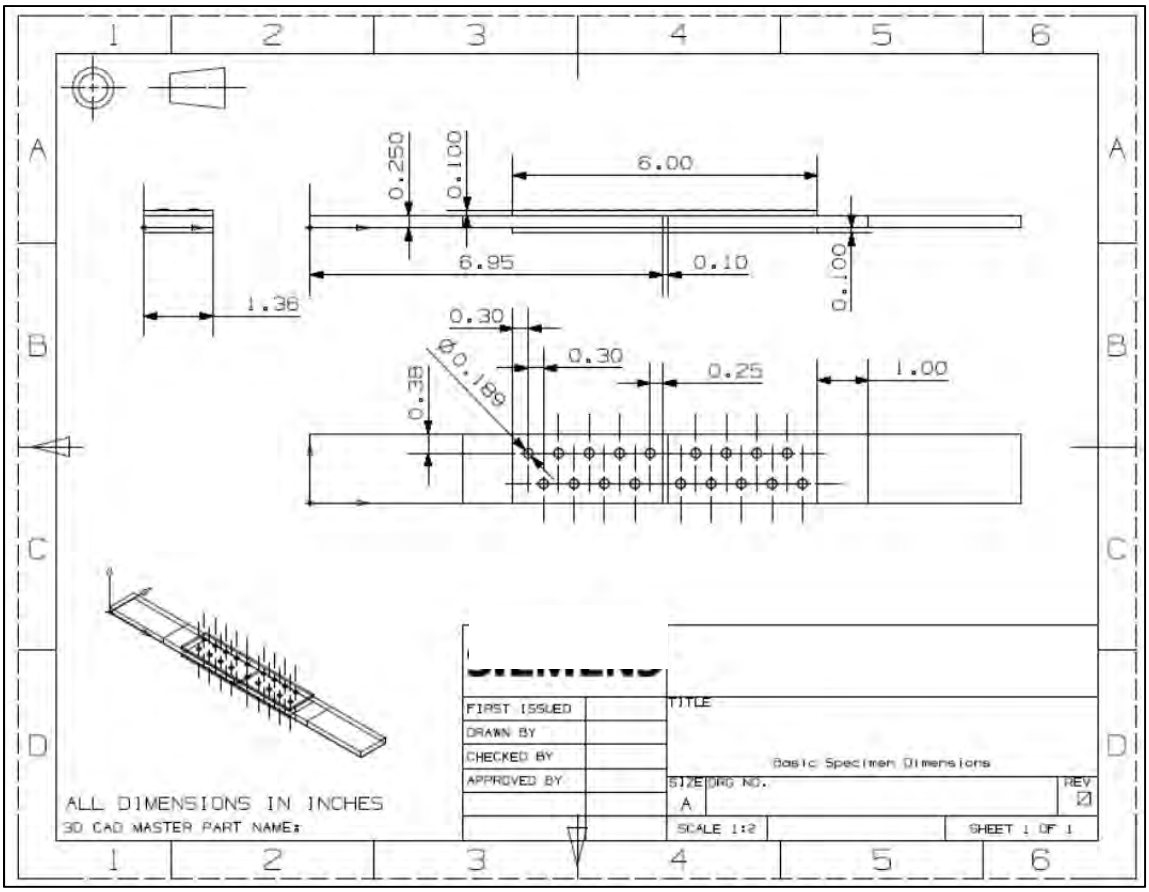

Figure 6-2 Dimensions of the Splice Test Joint

To facilitate inspection of the holes, the specimens were assembled with Hi-Lok pins (HL18-6) with MS21042 ‘jet-nuts’ being used instead of the HL70-6 collars that are used in the actual repair. This also introduces a certain uncertainty about the actual preload in the fastener. This was exacerbated by the fabrication of the joints which neglected to put a slight countersink on the head side to allow for the radius in the shank to head transition of the Hi-Lok to seat leaving the head clear of the surface of the upper plate [327, 328]. Actual gaps were measured after testing with a feeler gauge and are given in Table A-1. The nuts were torqued to the break-away torque of the HL70 collar which is used on the actual repair.

The Hi-Lok collar wrenching features are designed to shear at a given torque corresponding to a set minimum bolt pre-load. For the HL18-6 pin, that preload happens to be 700 lbs. [329] when a shear collar such as the HL70 is used. The MS21042 nut also includes a self-locking feature [330] but the overall pre-load to applied torque ratio is unclear. The nut’s self-locking feature is described in Reference [331] but the torque to preload ratio is not available from that source either, likely since it is a function of the fastener/nut system. Figure 6-3 shows general differences between a HL70 collar and the MS21042 nut. Not readily visible is that the nut has a slightly larger bearing surface against the plate and is made of steel versus the aluminum of the Hi-Lok collar. Also not readily apparent is the counter-bore relief on the HL70 collar on the shank side which allows it to thread onto the HL18 pin further allowing for a range of thicknesses to be used with a single pin-collar combination

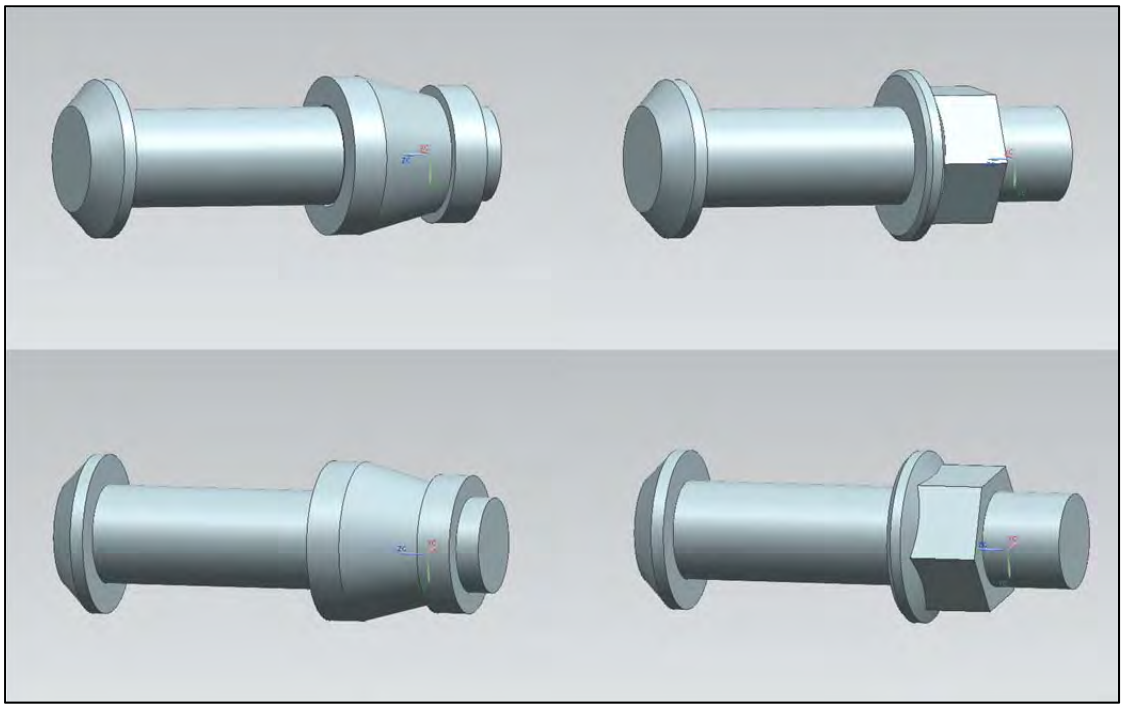

Figure 6-3 Depiction of Differences in a HL70 Collar on Left versus a MS21042 Nut on Right when Assembled to a HL18 Pin

The specimens and laboratory time were paid for by USAFA Contract FA7000-09-D-0021 0003. The requirements and funding were such that four specimens could be tested given a trade-off between even more complex yet more representative structure and number of replicates. The goal was to represent the general dimensions, materials, joint type, and fastener pattern of the critical location and to evaluate two slightly different configurations to try and better understand the effects of faying surface friction on load transfer. Specimens one and two had Teflon® between the parts to prevent frictional transfer of load between the plates. Specimen three and four did not have the Teflon inserts. Paint and other coatings on the actual structure were not simulated and the specimens were assembled bare. Specimens one and three had strain gages placed on them, three on the back plate, two on the bottom main plate and one on the side of the

main plate. All four specimens had a speckle pattern sprayed on them to allow the use of a Digital Image Correlation (DIC) system to develop the complex strain gradients that appear on the plate in the presence of the crack. The fastener hole numbering pattern is given in Figure 6-4 and also indicates the direction and hole (number nine) where the 0.020" Electro-Discharge Machining (EDM) notch was placed to start a crack.

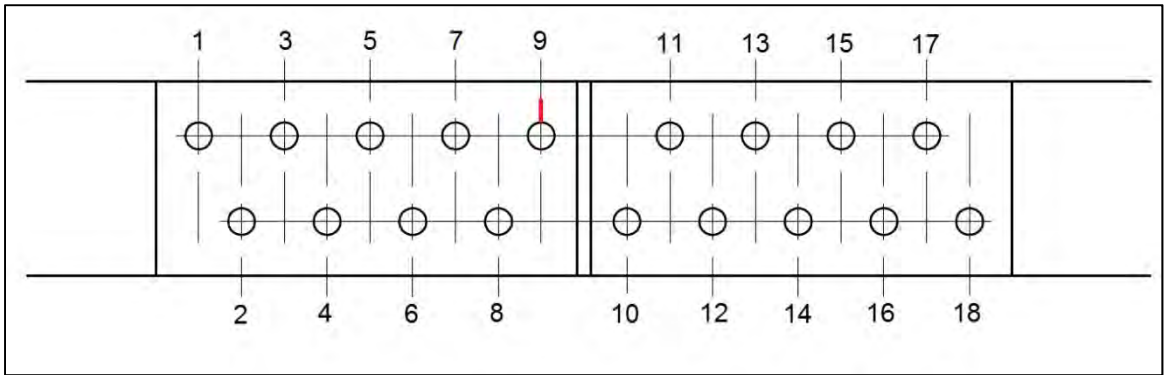

Figure 6-4 Fastener Hole Numbering Pattern with Primary Crack Direction Indicated at Hole #9

Specimen manufacture and testing was performed by Southwest Research Institute (SwRI) in San Antonio, Texas. The author was involved in the project from an analytical standpoint at the SwRI location at Hill AFB, Utah; but was not part of the specimen building or testing process. Based on the project workload division, the assembly practice and the instrumentation plan was beyond his control and it is unknown what the instrumentation plan was originally. However, it is clear that between the two strain gaged specimens there were some differences. It appears that one splice plate was rotated 180° in-plane and installed with the gages on the opposite side of the main plate break relative to the other. Retaining the numbering scheme that the crack occurs at hole number nine, it is clear from pictures that on specimens two and three that were installed

such that the crosshead was near to fastener one while the actuator side was near fastener eighteen. The reverse is true for specimens one and four. Figure 6-5 through Figure 6-8 show specimens one through four respectively in the same orientation. Note the difference in the position of the crack. Also, since strain gages were installed in the same locations relative to the specimen installed in the load frame. This caused the position of the strain gages to be on an opposite side of specimen one than on specimen three.

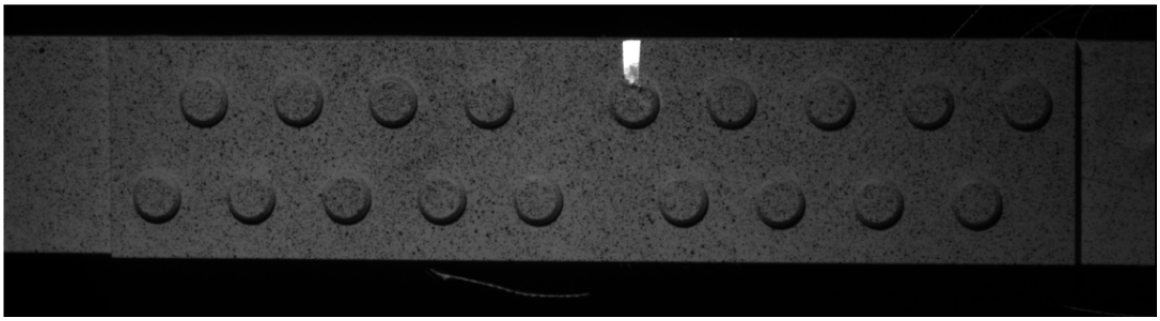

Figure 6-5 DIC Image of Specimen 1

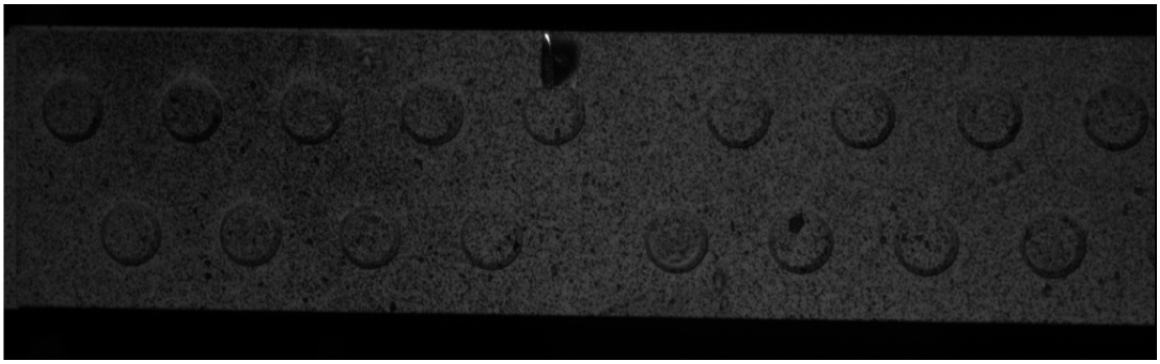

Figure 6-6 DIC Image of Specimen 2

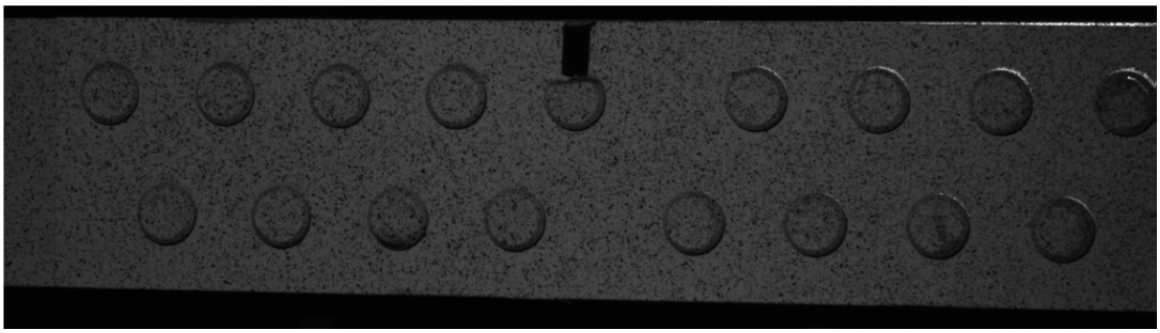

Figure 6-7 DIC Image of Specimen 3

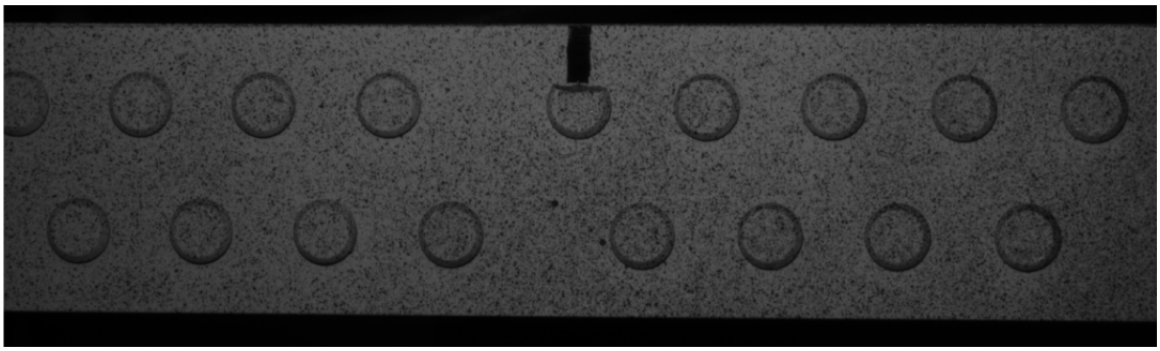

Figure 6-8 DIC Image of Specimen 4

Some general comments can be made about the disassembly of the different specimens. It was attempted to measure the break-away torque of the jet-nut from the Hi-Lok but the resolution of the available torque wrench at the time of disassembly was not accurate enough in the lower torque regime to be of general academic interest. There was some permanent set on the bottom plates; i.e., they were bowed such that the assembled specimens were concave on the bottom. The permanent set was clearly visible in the assembled specimen when viewed along the length down the side. The concavity was measured on the plate after disassembly with a nominally 0.51” wide feeler gauge set.

- Specimen One
    - Breakaway torque seemed lower than install torque by at least 10 lbs.

  - All fasteners fell out or were removable with light finger pressure indicating a neat fit
  - Permanent set on the bottom splice plate was 0.006”
- Specimen Two
  - Breakaway torque was higher than in the first specimen
  - Most fasteners fell out or only required light finger pressure except for fasteners three and five which required firm pressing to pop them free
  - Permanent set on the bottom splice plate was less than 0.0015” (thinnest feeler gauge available)
- Specimen Three
  - Breakaway torque was somewhere between specimens one and two
  - All fasteners fell out easily
  - Permanent set on the bottom splice plate was 0.004”
- Specimen Four
  - Breakaway torque was about the same as specimen three
  - Several of the fasteners (including the set of thirteen, fifteen, and seventeen) required firm pressing to pop them out. Seemed to be binding or racking between the layers preventing their removal
  - Permanent set on the bottom splice plate was 0.0015”

Specific details regarding measurements of the disassembled parts are presented in APPENDIX A. Average offsets for the different layers and specimens are given in Table 6-1 and the standard deviation, maximum and minimum of the offsets are given in Table 6-2 through Table 6-4 respectively.

Table 6-1 Average Hole Offsets in Different Specimens and Assembly Layers

Layer	Specimen 1	Specimen 2	Specimen 3	Specimen 4	Total
Top Plate	0.382	0.381	0.382	0.381	0.381
Main Plates	0.382	0.381	0.381	0.381	0.381
Bottom Plate	0.381	0.382	0.382	0.381	0.382
Total	0.382	0.381	0.382	0.381	0.381

Table 6-2 Standard Deviation of Hole Offsets in Different Specimens and Assembly Layers

Layer	Specimen 1	Specimen 2	Specimen 3	Specimen 4	Total
Top Plate	0.0067	0.0072	0.0074	0.0078	0.0073
Main Plates	0.0034	0.0034	0.0035	0.0030	0.0034
Bottom Plate	0.0069	0.0072	0.0075	0.0071	0.0072
Total	0.0059	0.0062	0.0064	0.0064	0.0062

Table 6-3 Maximum Hole Offsets in Different Specimens and Assembly Layers

Layer	Specimen 1	Specimen 2	Specimen 3	Specimen 4	Total
Top Plate	0.392	0.392	0.394	0.393	0.394
Main Plates	0.390	0.386	0.386	0.386	0.390
Bottom Plate	0.393	0.394	0.395	0.392	0.395
Total	0.393	0.394	0.395	0.393	0.395

Table 6-4 Minimum Hole Offsets in Different Specimens and Assembly Layers

Layer	Specimen 1	Specimen 2	Specimen 3	Specimen 4	Total
Top Plate	0.369	0.369	0.370	0.367	0.367
Main Plates	0.375	0.373	0.375	0.376	0.373
Bottom Plate	0.370	0.370	0.371	0.368	0.368
Total	0.369	0.369	0.370	0.367	0.367

The crack growth was measured and tabulated in terms of cycles from test start. Note that the starting crack was actually a 0.02 inch EDM notch. Crack growth data, a-N, are presented for the four specimens in Figure 6-9. Since it takes some time for the fatigue portion to nucleate at the stress concentration and start growing via fatigue, the curves are adjusted to a starting size of 0.034 inch which is the largest first increment of crack

length for any of the four specimens. This ensures that the interpolation does not include any of the crack nucleation portion of the curve. For specimens two, three, and four, the starting point is thus an interpolated value. This a-N chart is presented in Figure 6-10. Tabular data for these two charts can be found in the appendix in Table A-6 and Table A-7.

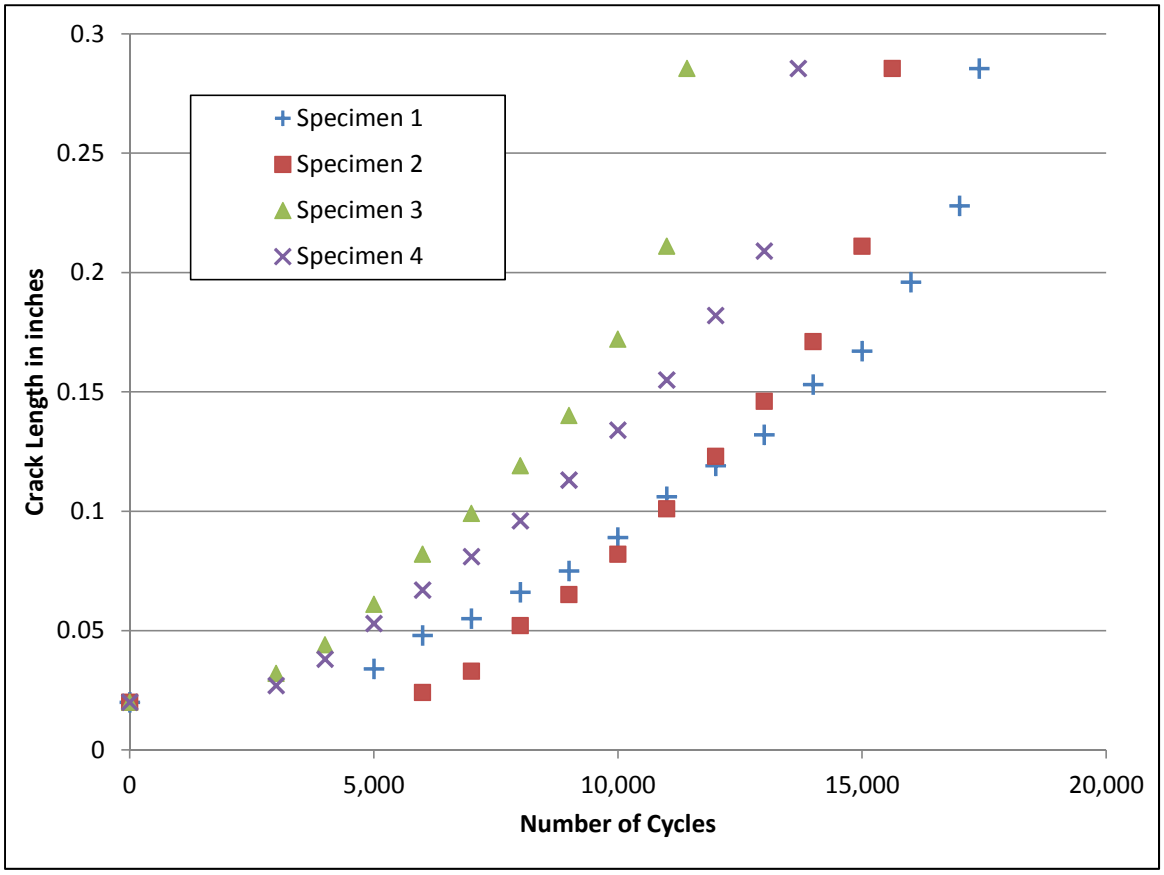

Figure 6-9 Crack Growth Curves for the Four Specimens

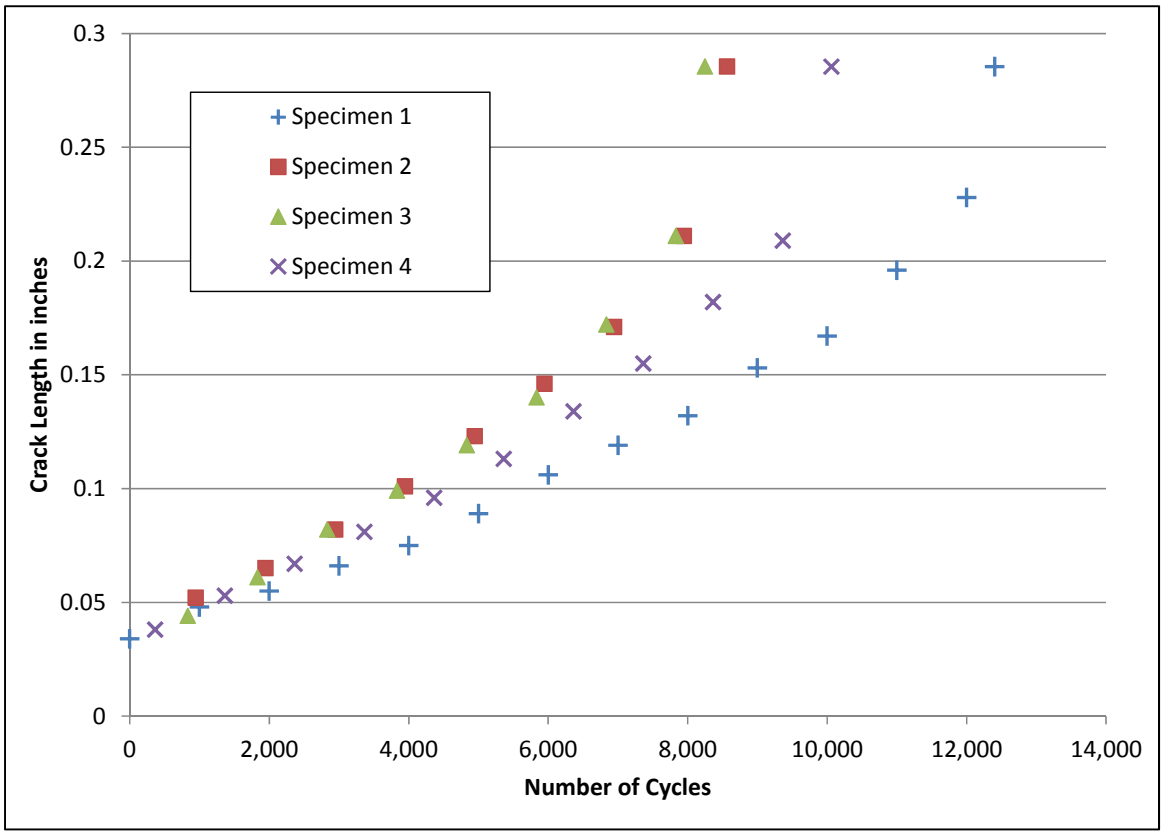

Figure 6-10 Crack Growth Curves for the Four Specimens Adjusted to a 0.032" Starting Size

The a-N curves shifted to a start of 0.034 inch will be used for all comparisons to the FEM because the focus of this dissertation is the crack growth. This does not trivialize the important problem of crack nucleation but to consider crack nucleation in a bolted joint hole in the presence of an EDM notch is beyond the scope of this work. The very nature of the EDM notch being through the thickness eliminates the interesting short crack portion where the crack is semi-elliptical and not yet completely through the thickness.

The final aspect of the specimens to report is the strain information taken during the periodic strain surveys throughout the test. Strain information from the six strain gages at different strain surveys is presented in appendix Section A.6. Additionally, strain maps

using the DIC images are also given in appendix Section A.7. What will be discussed is the existence of considerable evidence of slip in the strain readings at cycle zero.

Figure 6-11 contains a series of nine plots from strain data for specimen three. Three different strain gages are represented, from top down: two, four, and five. Across are the readings from these three gages at the first cycle, the 3,000th cycle and the 9,000th cycle where the crack was nearing its final length. Recall that gage two was opposite the crack so it would be expected to change its load response as a function of crack length more than others. What is noticeable is that with the exception of gage two, that the difference in response between 3,000 and 9,000 cycles the hysteresis is more or less the same, yet is quite different than the first cycle. Also, gage number two does not change too much following the first initial slip.

Figure 6-12 presents similar data for specimen one. However, the intervals are 5,000 and 11,000 instead of 3,000 and 9,000. These were chosen since 5,000 was the first interval with recorded crack growth and thus was the first strain survey available after cycle one. The 11,000th cycle was chosen since the difference between it and the first strain survey of crack growth were the same as for specimen three (i.e., the time delta between 9,000 and 3,000 is 6,000 cycles). Recall that the configuration of specimen one had Teflon between the different faying surfaces of the plates. This causes any most if not all slip to be due to some fasteners taking load prior to others becoming effective due to differences in their placement or hole clearance. Notice that after the first cycle that the loading and unloading cycles lie on top of one another substantiating the presumption that there is not friction between the surfaces. This is in contrast with the hysteresis exhibited in the same gage readings from specimen three.

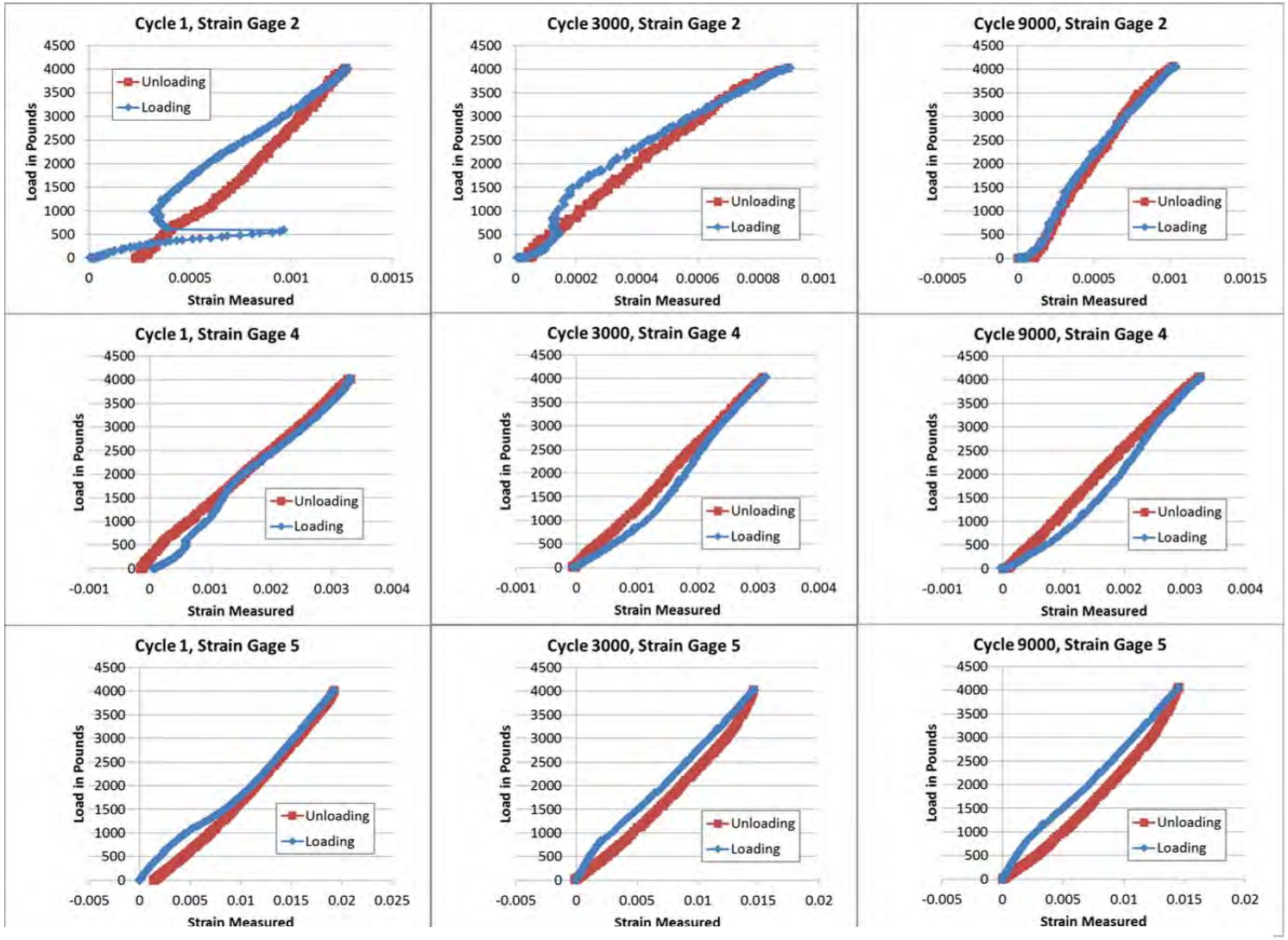

Figure 6-11 Example of Slip from Strain Gage Readings from Specimen Three

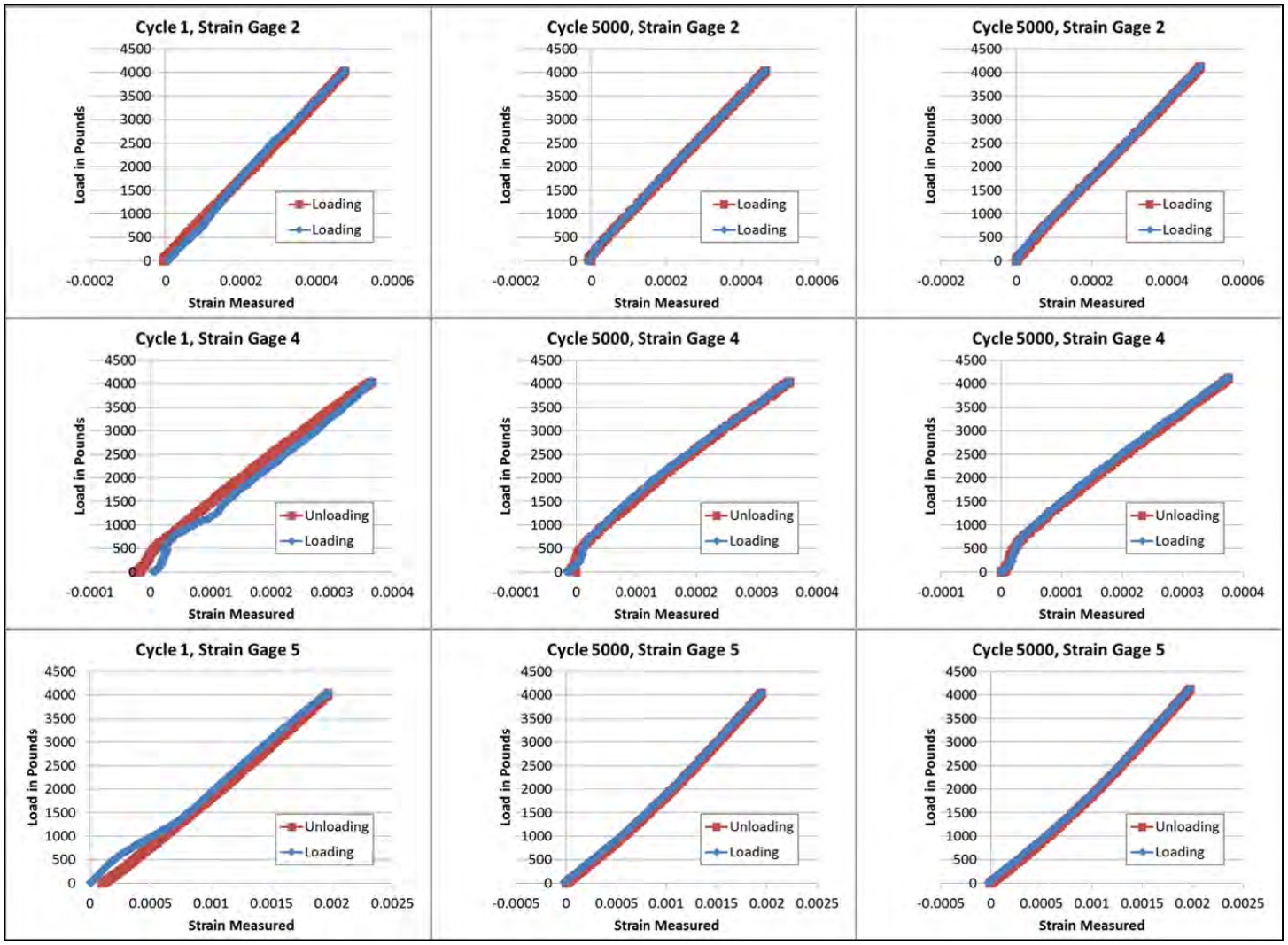

Figure 6-12 Example of Slip from Strain Gage Readings from Specimen One

6.2 F.S. 284 Splice Joint Finite Element Modeling and Load Analysis

The joint was modeled using NX [332] to build the solid model. This model was to be fully part separated with fasteners modeled in three dimensions with contact surfaces for all faying surfaces. Fastener rotation and other higher order effects can play a substantial role in the overall crack growth that is not necessarily captured in a two dimensional model. This level of refinement was sought to better understand the complex interaction between the joints, any eccentricity due to dissimilarities between the head and nut side, and to capture the through the thickness effects at the fasteners. Automatic meshing was used with localized refinement in regions that would be in contact to reduce the required Degrees of Freedom (DOF). The models were solved using NX Nastran [333].

The basic model of the joint has 163,729 tetrahedral 10-node elements and is shown in Figure 6-13. The region within the grips on one side is fully constrained and the opposite side is constrained to translate in the x-direction only. The load is applied as to put the entire joint in tension. The only connectivity between the separate main plates are the fasteners and side plates and the contact surfaces between them. Local surfaces were put onto the top and bottom of the side plates to give a region of increased mesh density (0.04 inch) to increase the resolution in these portions as shown in Figure 6-14. Mesh density was reduced to 0.08 inch outside of the hole bores, fastener bearing and faying surfaces, and bolt contact regions of the side plate was to reduce run time (see Figure 6-15). Similarly, the regions held by the test grips had a further reduced mesh density (0.25 inch) to further reduce the DOF of the model.

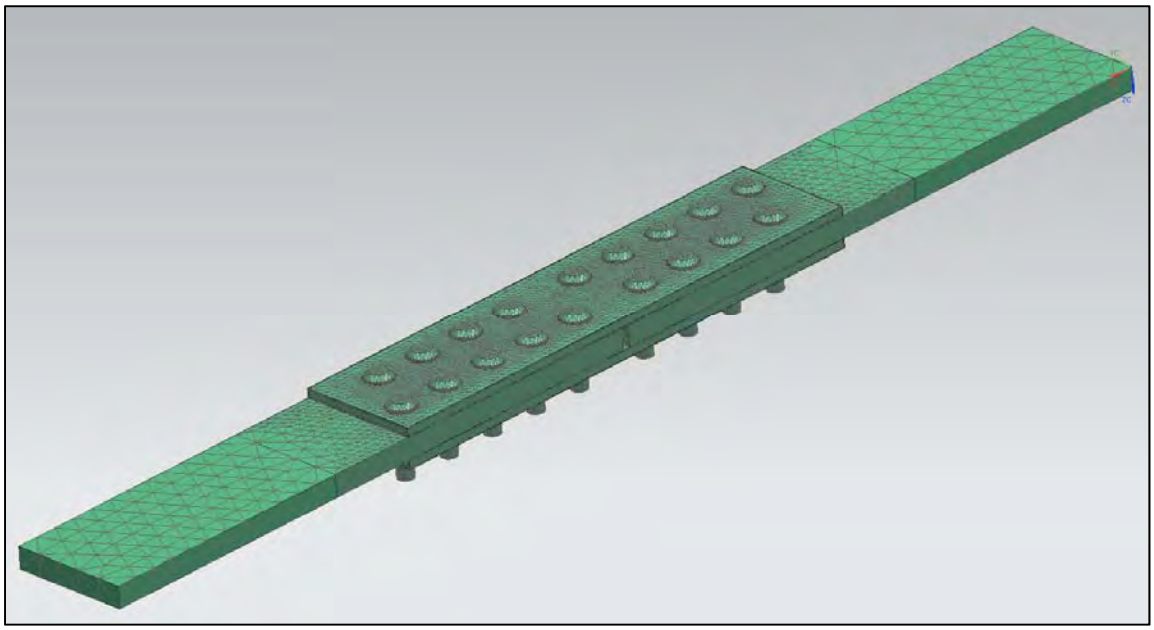

Figure 6-13 Oblique View of Overall Model

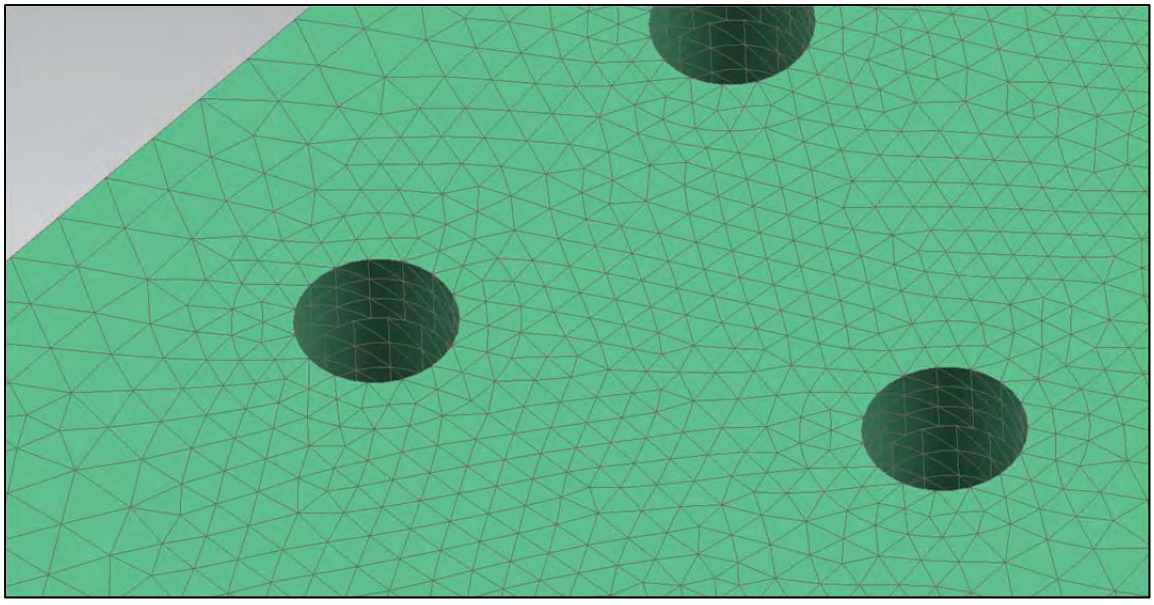

Figure 6-14 Close-Up of Mesh Refinement at Fastener Holes

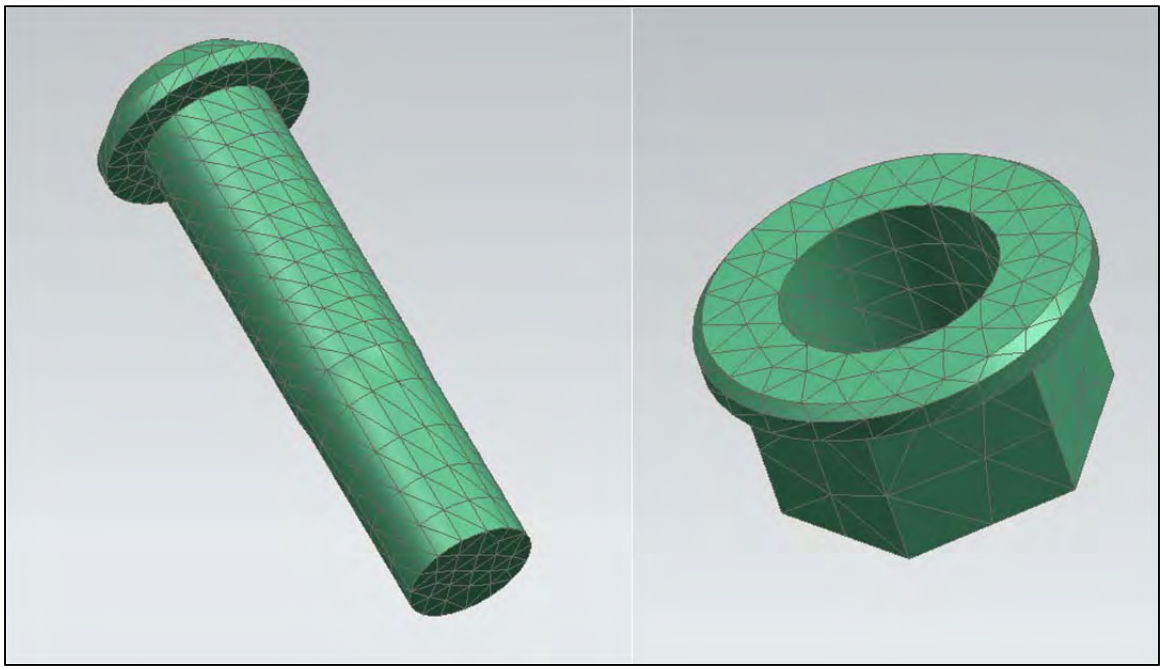

Figure 6-15 Close-Up of Fastener and Nut Meshes

Fasteners were constrained on one side by contact between the bottom side of the head and the top plate. The other side was held in place by 'attachment' of the nut by using a 'glue' boundary condition and the faying side of the nut was in contact with the bottom plate. The advantage of the glue boundary condition is that equivalence nodes are not needed. All contact conditions assumed zero friction between surfaces including those between the splice plates and the main plates. The shank of the fastener was in contact through the bore of the hole against all three layers. To assist with node selection for strain gage correlation, surfaces were created to represent the location and size of the strain gages. This forces the mesh to define boundaries of elements to simplify selection of nodes to compute average strain over the exact region of the strain gage.

The aluminum alloys were modeled as non-linear elastic with a von Mises yield function criterion. The material was considered linear up to one half their yield stress for both

aluminum materials which was taken as their proportional limit. Beyond that, the material conformed to a tabular input Ramberg-Osgood material model [334]. Equations describing the Ramberg-Osgood material model are below.

From Reference [335]:

$$\varepsilon_{total} = \frac{f}{E} + \varepsilon_p$$

Equation 6-1 Total Strain

and,

$$\varepsilon_p = 0.002\left(\frac{f}{f_{0.2ys}}\right)^n$$

Equation 6-2 Plastic Strain

where:

f = stress

$f_{0.2ys}$ = 0.2% yield stress

n = Ramberg-Osgood parameter

More importantly, these parameters are published in handbooks used for design such as MIL-HDBK-5J or the new series of Metallic Materials Properties Development and Standardization (MMPDS). Table 6-5 contains the material model parameters used in the FEM. Note however that the non-linear elastic material models were input as a data table and not as raw parameters and since the stresses in the Hi-Lok were below the elastic limit the fasteners and nut were modeled with a linear elastic material model. The tabular material models extended from the proportional limit up to the ultimate stress using the

Ramberg-Osgood equation to define the strain at those points. The resulting curves are shown in Figure 6-16.

Table 6-5 Material Model Parameters for the FEM

Parameter	Top/Bottom Plate	Main Plate	Fastener	MS21042
Material	7075-T651	7075-T7351	HiLok Material	Nut Material
Young's Modulus Tension (psi)	1.03E+07	1.03E+07	2.90E+07	2.90E+07
Young's Modulus Compression (psi)	1.06E+07	1.03E+07	2.90E+07	2.90E+07
Poisson's Ratio	0.33	0.33	0.32	0.32
Yield Strength Tension (psi)	69,000	57,000	152,500	152,500
Yield Strength Compression (psi)	69,000	57,000	152,500	152,500
Ultimate Strength Tension (psi)	77,000	68,000	170,000	170,000
Ultimate Strength Compression (psi)	77,000	68,000	170,000	170,000
Proportional Limit Tension (psi)	34,500	28,500	N/A	N/A
Proportional Limit Compression (psi)	34,500	28,500	N/A	N/A
R-O Tension Exp	32	32	N/A	N/A
R-O Compression Exp	16	16	N/A	N/A

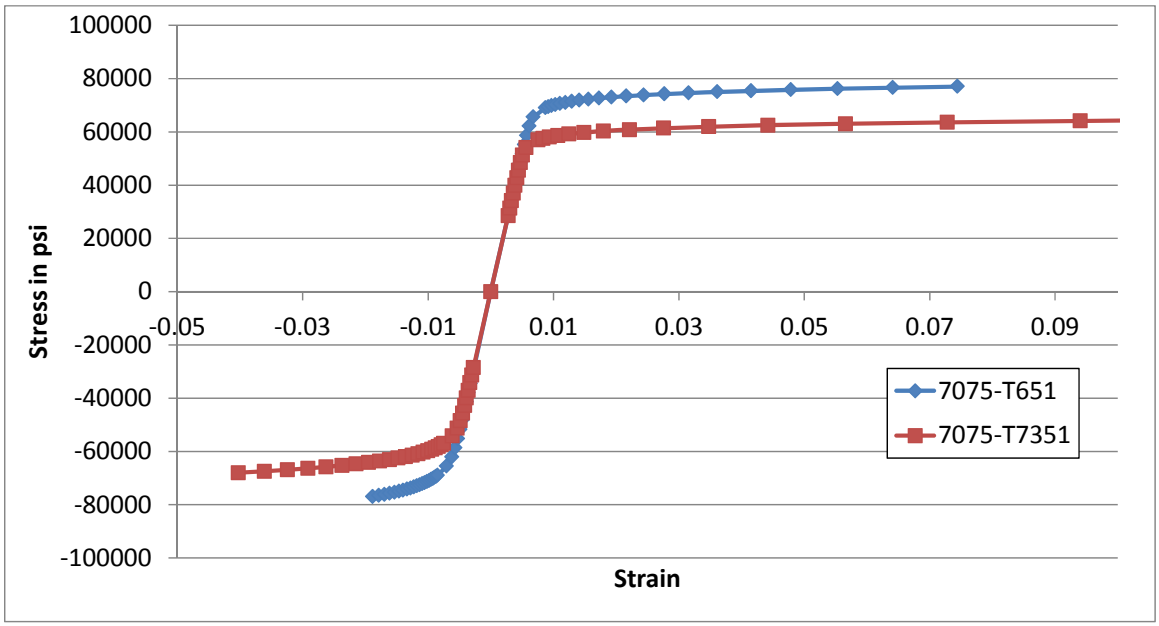

Figure 6-16 Plot of Stress-Strain Curves Used in the FEM

6.2.1 Modeling Results

The calculated load transfer for each fastener as a function of crack length are presented in pounds in Table 6-6 through Table 6-8 for the top strap, middle plates and bottom strap respectively.

Table 6-6 Top Strap Fastener Loads

Fastener	No Crack	0.02	0.04	0.06	0.08	0.1	0.12	0.14	0.16	0.18	0.2	0.22
#1	283	283	283	283	282	282	281	281	280	279	279	277
#2	275	275	275	275	276	276	276	277	277	277	278	278
#3	154	154	153	153	153	153	153	152	152	151	150	150
#4	148	148	148	148	148	149	149	149	150	150	150	151
#5	118	118	118	118	117	117	117	117	116	116	115	114
#6	164	165	165	166	166	166	167	167	168	169	169	170
#7	178	178	179	179	178	178	178	177	176	176	174	173
#8	333	334	335	336	337	338	340	341	343	344	346	348
#9	334	334	330	326	327	324	320	318	315	313	311	309
#10	340	341	341	342	342	343	343	344	344	345	347	348

Fastener	No Crack	0.02	0.04	0.06	0.08	0.1	0.12	0.14	0.16	0.18	0.2	0.22
#11	330	330	329	328	327	326	325	323	322	320	318	315
#12	177	177	177	178	178	178	178	178	179	179	179	180
#13	161	161	161	161	160	160	159	159	158	157	156	156
#14	117	117	117	117	117	117	117	117	118	118	118	118
#15	150	150	150	150	149	149	149	149	148	148	147	147
#16	155	155	155	155	155	155	155	155	155	155	155	155
#17	273	273	273	272	272	272	271	271	270	269	269	268
#18	283	283	283	283	283	283	283	283	283	283	283	283

Table 6-7 Middle Plates Fastener Loads

Fastener	No Crack	0.02	0.04	0.06	0.08	0.1	0.12	0.14	0.16	0.18	0.2	0.22
#1	576	576	576	576	575	575	575	574	574	573	572	571
#2	557	557	557	558	558	558	559	559	560	560	561	562
#3	302	302	302	302	302	302	302	302	302	301	301	301
#4	294	294	294	294	294	294	294	295	295	295	295	295
#5	232	232	232	232	232	232	233	233	233	233	233	232
#6	326	327	327	327	327	327	328	328	328	328	328	328
#7	356	356	357	358	357	357	358	358	358	358	358	358
#8	679	680	681	682	682	683	684	685	686	687	688	689
#9	689	687	684	680	682	680	678	676	675	674	674	674
#10	698	698	698	699	699	700	701	702	702	703	705	706
#11	677	677	677	676	676	675	675	674	674	673	672	671
#12	352	352	352	352	352	352	352	352	352	352	353	353
#13	323	323	323	323	322	322	322	322	322	321	321	320
#14	228	228	228	228	228	228	228	228	228	228	228	228
#15	298	298	298	298	298	297	297	297	297	297	296	296
#16	304	304	304	304	305	305	305	305	305	305	305	306
#17	553	553	552	552	552	551	551	550	549	549	548	547
#18	577	578	578	578	578	579	579	580	581	581	582	583

Table 6-8 Bottom Strap Fastener Loads

Fastener	No Crack	0.02	0.04	0.06	0.08	0.1	0.12	0.14	0.16	0.18	0.2	0.22
#1	293	293	293	293	293	293	293	293	293	294	294	294
#2	282	282	282	282	282	282	283	283	283	283	283	284
#3	148	148	149	149	149	149	149	150	150	150	151	151
#4	146	146	146	146	146	146	145	145	145	145	144	144
#5	114	114	114	115	115	115	116	116	117	117	118	119

Fastener	No Crack	0.02	0.04	0.06	0.08	0.1	0.12	0.14	0.16	0.18	0.2	0.22
#6	162	162	162	162	162	161	161	160	160	159	159	158
#7	177	178	178	179	179	179	180	181	182	182	184	185
#8	346	346	346	346	345	345	344	344	343	342	341	340
#9	355	353	353	354	355	356	358	359	360	362	363	366
#10	357	357	357	357	357	357	357	358	358	358	358	358
#11	347	347	348	348	349	349	350	351	352	353	354	356
#12	174	174	174	174	174	174	174	174	174	173	173	173
#13	161	162	162	162	162	162	163	163	163	164	164	165
#14	111	111	111	111	111	111	111	111	111	111	110	110
#15	148	148	148	148	148	148	148	149	149	149	149	149
#16	149	149	149	149	150	150	150	150	150	150	150	150
#17	279	279	279	279	279	279	279	279	279	279	279	279
#18	295	295	295	295	295	296	296	297	297	298	299	300

The change in loads as a function of crack length is shown graphically for the top strap in Figure 6-17 which places sparklines next to the fastener numbers to show the variation in load transfer. The same information is presented for the bottom strap in Figure 6-18. The sparklines feature the same y-axis relative scale so that the delta change is comparative. Note that as the load drops at fastener nine that it also does not flow across as much to fastener eleven. Fasteners eight and ten then have to pick up the extra load that has now shifted to the other side. Also of interest is that as the load drops in the upper strap the load gets picked up more in the bottom plate.

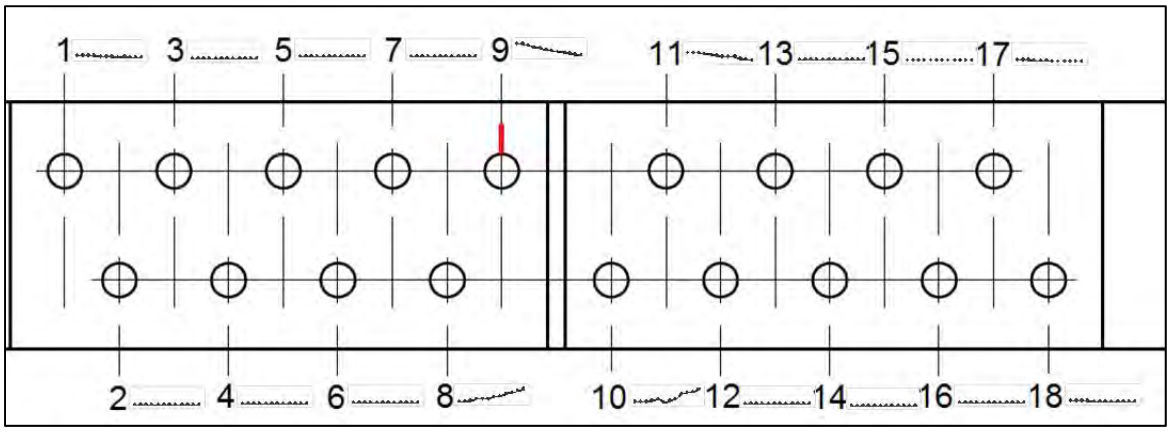

Figure 6-17 Hole Layout with Sparklines Showing Change in Load Transfer with Crack Growth, Top Strap

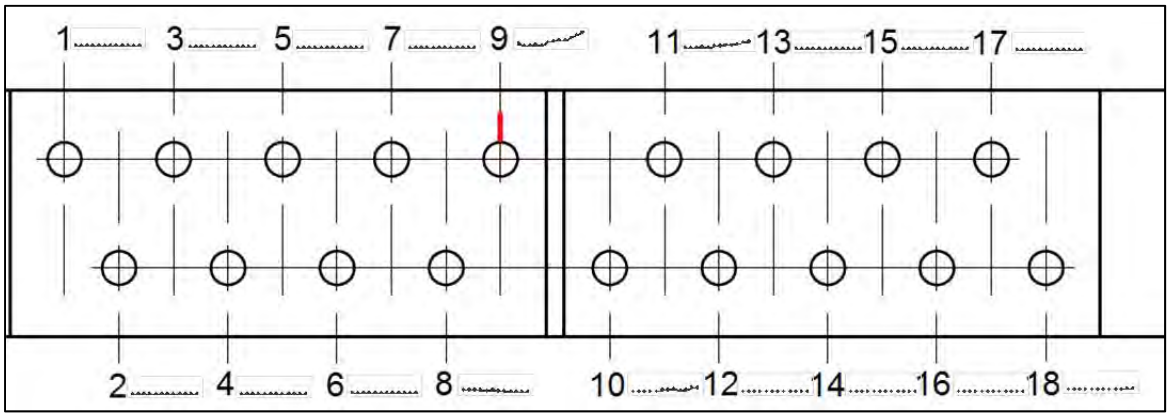

Figure 6-18 Hole Layout with Sparklines Showing Change in Load Transfer with Crack Growth, Bottom Strap

6.2.2 Finite Element Model Verification and Validation

The model previously described was built using NASTRAN. Other simplified modeling methods of calculating load transfer are explored later using the software StressCheck®. Each of these software programs was evaluated using single element tests and it was verified that material response was the same as it is defined in the software manuals. The various single element tests are located in Appendix C.

Other convergence tests and verification tests were performed including tests of an open hole to verify the stress intensities as well as correlation photoelasticity contact case of a clearance “rivet” bearing on a plate [336]. All tests showed convergence to the closed form solutions and matched results within the error of the solutions themselves.

Validation of the FEM was done by comparison to the four 284 Joint specimens. Strain gages were located in various locations on the experiments as indicated in Section A.3 of Appendix A. Correlation information is presented in Section A.6 of Appendix A. Additionally, each specimen had a speckle pattern applied to the upper plate with the crack. This data was analyzed and a series of “faux gages” were developed to compare the FEM with the four specimens with locations shown in Figure 6-19. The comparisons are presented in Section A.7 of Appendix A.

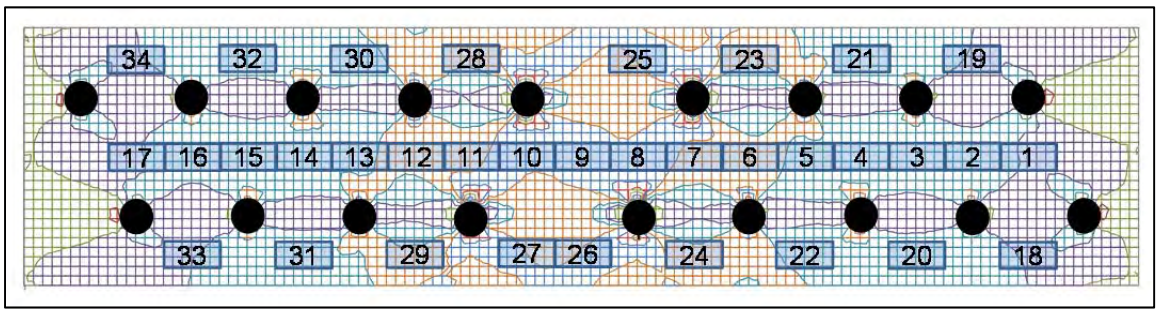

Figure 6-19 Location of Faux Gages for 3-D FEM Correlation

In all cases some variation was seen between the FEM and the tests. However, in almost all cases the FEM results fell within the spread of the joint specimen data. The most important faux gage locations are 7, 8, 9, 24, 26, and 27 that surround the crack location.

Even if other gages indicate that the joint load distribution is somewhat off, if these gage correlations are close, then the stress intensities that are calculated can be relied upon.

One interesting point is that the DIC results for joint specimen 4 show appear to be very different than the other specimens. It is unknown why this variation exists and since there were not strain gages on the specimen, an estimate of the top plate loads based on the bottom plate load distribution is not possible.

6.3 F.S. 284 Splice Joint Stress Intensity and Crack Growth Analysis

One issue with current crack growth analysis methods is that the way the beta corrections are developed may not match reality well. Models are typically used to generate stress intensities which then can be converted to betas for crack growth analysis. The problem is that the way the model is constrained can have a profound effect on the overall solution [337]. A common boundary condition for models used for generation of beta solutions is a symmetry condition on the far side of the crack and at one end opposite of an even stress profile at the other end [338]. In these flat plate models, the crack opening is somewhat constrained by the far edge which may or may not reflect the actual structure. In actual structure, the ‘flat plate’ often is constrained by longerons, stiffeners, ribs and bulkheads. If a crack develops at a hole common to one of these structures there is often an entire line of constraining fasteners in the loading direction reducing the crack opening compared with the symmetry condition used to develop geometry betas. These other structural pieces provide a ‘load bridge’ or a clamping effect reducing the crack opening not unlike the stringers investigated by Poe [339].

As an example, take Figure 6-20 where the top model has the back side unconstrained versus the bottom model where the backside is reacted with a symmetry condition indicated by the line of circles. Here, when the far-field load is applied, the upper model will experience increased in-plane bending which increases the crack opening displacement and thus the stress intensity at the crack tip.

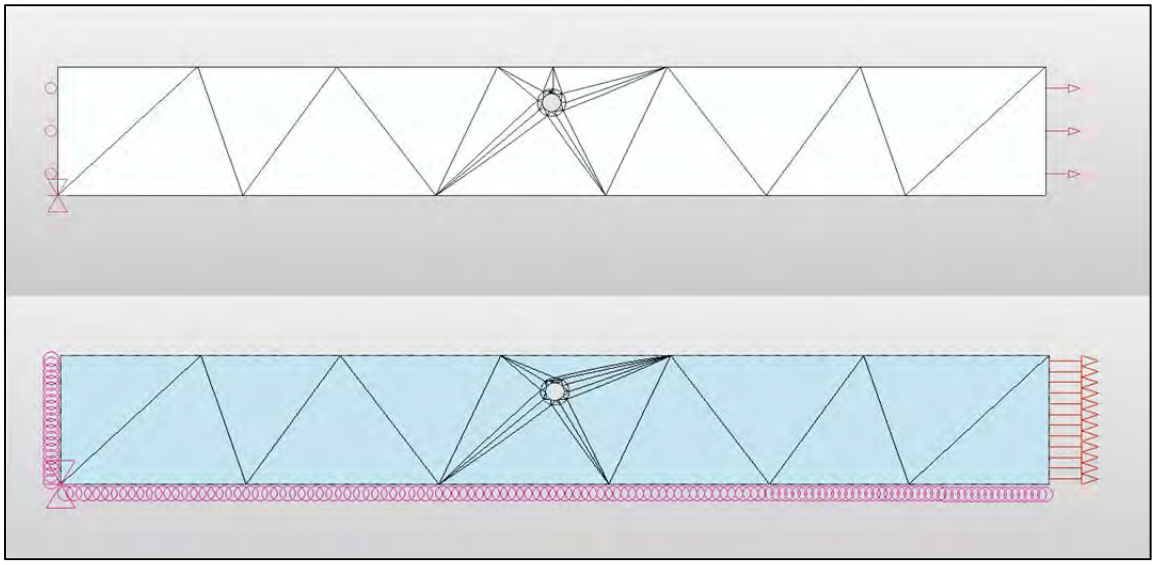

Figure 6-20 Depiction of Two Different Boundary Conditions Which Affect the Calculated Stress Intensity

The finite element software StressCheck® [340] was used to calculate stress intensities for the different crack sizes. StressCheck uses a p-element formulation where the error of estimation can be controlled by adjusting the polynomial level (p) of the elements [341]. It should be noted the StressCheck uses a slightly different formulation of the Ramberg-Osgood equations where (from Reference [341]) :

$$\varepsilon = \frac{\sigma}{E} + \frac{3}{7}\frac{S_{70E}}{E}\left(\frac{\sigma}{S_{70E}}\right)^{n}$$

Equation 6-3 Ramberg-Osgood Model from StressCheck

such that:

$$S_{70E} = \left[\frac{f_{0.2ys}}{\left(\frac{0.014}{3}E\right)^{\frac{1}{n}}}\right]^{\frac{n}{n-1}}$$

Equation 6-4 Calculation of the S_{70E} Parameter for StressCheck

These two different models were run with two different sizes of cracks: 0.02 inch, and 0.22 inch. Table 6-9 contains the beta correction factors calculated from the models for the different crack lengths. Note that by leaving the back side unconstrained a higher beta correction is calculated and that the relative difference increases with crack length. Figure 6-21 contains images of the deformed models one over the other for the shorter 0.02 inch crack length. Note little visible difference between the two plots. Figure 6-22 contains the same plots for the longer crack and there is a very discernible difference between the two results.

Table 6-9 Comparison of Different Beta Factors Depending on Constraint and Crack Size

Crack Size	Back Side Constrained	Back Side Unconstrained	Ratio
0.02 Inch	2.32	2.50	1.08
0.22 Inch	1.18	1.35	1.15

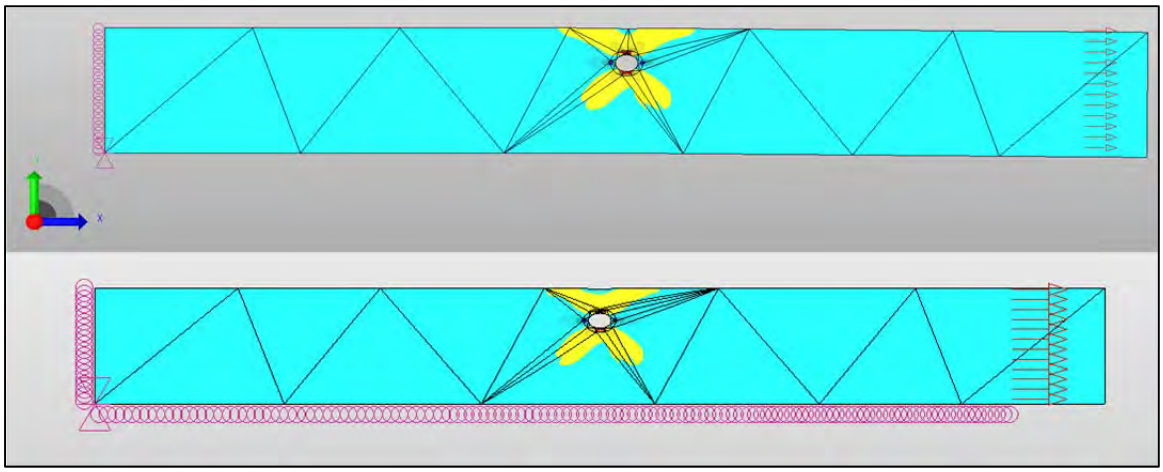

Figure 6-21 Deformed Plots of the Two Differently Constrained Models with a 0.02 Inch Crack

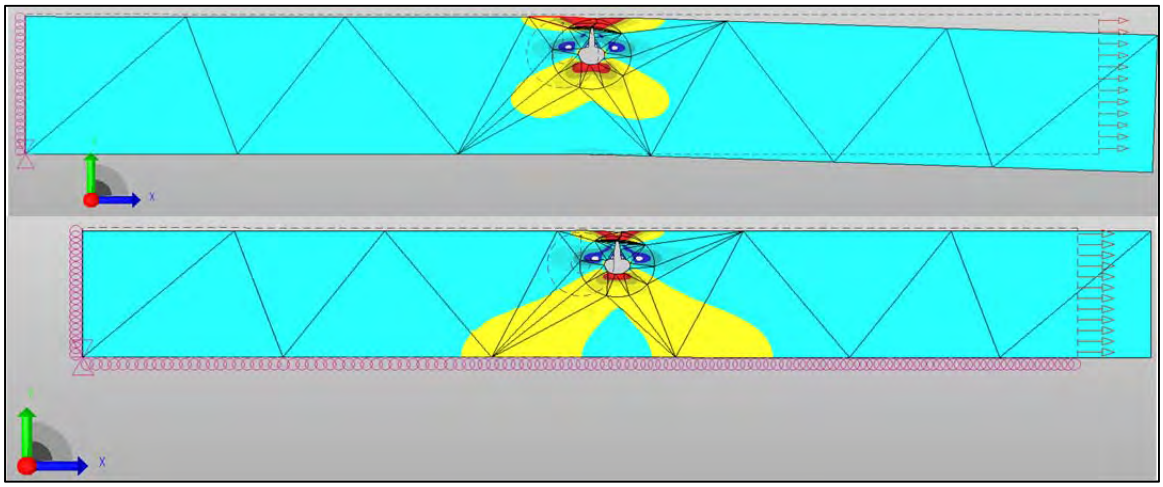

Figure 6-22 Deformed Plots of the Two Differently Constrained Models with a 0.22 Inch Crack

There is also an additional factor which cannot be ignored and that is hole fill. The preceding examples were for an unfilled hole which tends to collapse around the edges in the presence of load. In the case of many actual structural parts and, more importantly, in the case of the specimens tested, the hole is neatly filled meaning the fastener props open the hole which changes the stress intensity [322]. For the sake of accuracy, all these effects need to be addressed because they can have a significant impact on the stress

intensity solution that will be put into AFGROW for crack growth analysis [342]. Integrating StressCheck solutions with the crack growth software AFGROW has a history of successes [343].

To ensure that the constraint about the fastener is as accurate as possible a model representative of the splice plate was generated in StressCheck. Each fastener other than that with the crack was filled with a fastener element which automatically wagon wheels a center node to the surrounding plate representing the fastener filling the hole. The fastener element cannot be used at the cracked hole since the wagon wheel helps 'pull' the hole closed resisting the crack opening displacement. The fastener with a crack is modeled by a filled 'plug' of elements with contact on the surrounding surfaces. Figure 6-23 shows a view of the overall model and Figure 6-24 shows a close-up of the mesh region at the crack specifically highlighting the circles around the tip to refine the mesh to improve stress intensity convergence. Also shown in Figure 6-24 are the spring connection symbols of the contact condition and the pinned nodes that resist translation. To prevent rotation of the plate, fastener five is pinned in the Y-direction which only had two or three pound loads for all crack lengths. Note that all other fasteners shown have applied loads equal to that determined in the three dimensional FEM. Appendix C contains discussion of the various element types used and the effects of each as well as meshing techniques and convergence. Table 6-10 presents the target and actual loads for constrained fasteners five and nine; all loads were within four pounds in the y-direction and within one pound in the x-direction which is the primary loading direction.

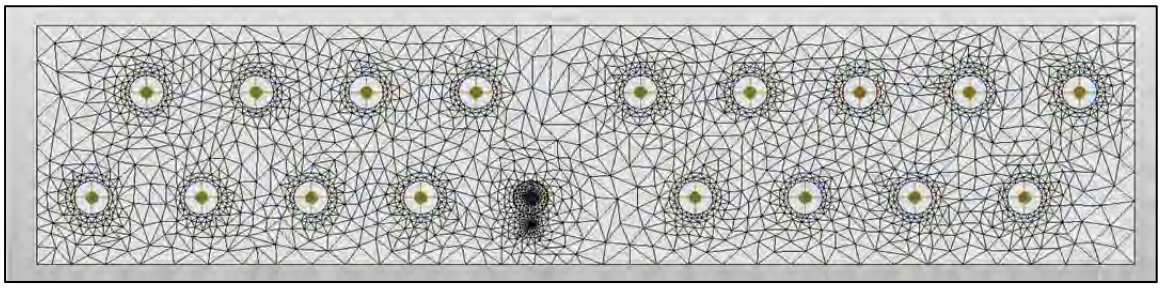

Figure 6-23 View of the 284 Splice Stress Intensity Model

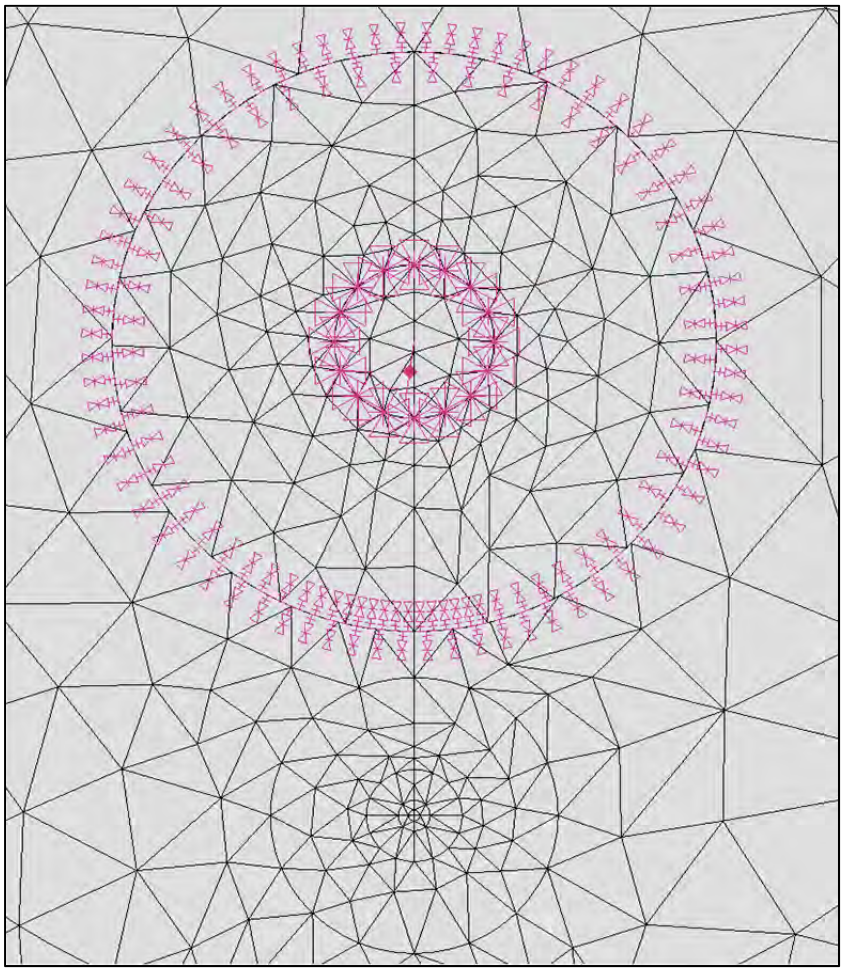

Figure 6-24 Close-Up of the Crack Mesh Region of the 284 Splice Stress Intensity Model with a 0.12 Inch Crack

Table 6-10 Target Loads and Actual Reaction Loads at the Constrained Fasteners

Crack Length	Fastener 5 (lbs)		Fastener 9 (lbs)			
	Target Y-Direction Load, 3-D FEM	Actual Y-Direction Load	Target X-Direction Load, 3-D FEM	Actual X-Direction Load	Target Y-Direction Load, 3-D FEM	Actual Y-Direction Load
0.02	-2.02	-5.29	333.7	333.8	-9.26	-5.84
0.04	-2.07	-5.26	330.2	329.8	-9.84	-6.39
0.06	-2.22	-5.46	326.3	325.7	-8.74	-5.21
0.08	-2.48	-5.57	326.9	327	-5.56	-2.11
0.1	-2.69	-5.76	323.5	323.1	-3.67	-0.20
0.12	-3.00	-6.17	320.1	321.1	-0.86	2.45
0.14	-3.35	-6.46	317.5	317.1	2.58	5.89
0.16	-3.77	-6.96	315.3	314.7	5.71	8.97
0.18	-4.24	-7.43	312.5	311.8	9.30	11.82
0.2	-4.72	-7.73	310.6	310.1	14.85	17.59
0.22	-5.49	-8.55	308.6	309	20.52	22.96

Finite element models were made for each crack length and the stress intensities are extracted. The stress intensity models was set up to include gap between the fastener and the splice strap for a neat fit pin, and diametrical gaps of 0.001 and 0.002 inch to evaluate the effect of pin fit. These stress intensities were analyzed using the 'User Defined' through crack model in AFGROW. The User Defined models require the user to prescribe all stress intensity corrections for finite width, hole offset, and etcetera. However, by modeling the complete splice, additional correction factors are not needed. The correction factors to enter into the User Defined model are generated by taking the stress intensity and dividing by $\sqrt{\pi a}$ to obtain an overall correction including stress. Crack growth data properties are given in units of ksi so the correction factors are divided by one-thousand and the combination of the stress and correction factors which are presented in Table 6-11. This means that the spectrum to be applied has a maximum

stress of unity (ksi) with a stress ratio of 0.1 as was used in the joint experiments. Even though the model is displayed within AFGROW as a through crack at the edge of a finite width plate, no additional factors are being used to influence crack growth. The net cross-sectional area was not used to calculate failure because of the amount of constraint provided by redundant structure in the actual joint which is not accounted for in the AFGROW model. The only failure criteria used was the end of stable crack growth in the short ligament which represents the data available from the four joint experiments. Width and thickness for the model is set to 1.171 inches and 0.1 inch respectively to account for the net section with the hole subtracted.

Table 6-11 User Defined Stress Intensity Correction Factors

Crack Length (inch)	User Defined Stress Intensity Factor		
	Neat Fit	0.001 inch Gap	0.002 inch Gap
0.02	36.23	39.10	41.29
0.04	28.79	30.73	32.11
0.06	24.61	25.90	26.85
0.08	22.06	22.95	23.64
0.10	20.34	20.97	21.51
0.12	19.23	19.66	20.09
0.14	18.49	18.81	19.15
0.16	18.10	18.32	18.60
0.18	18.03	18.15	18.36
0.20	18.29	18.31	18.45
0.22	18.98	18.89	18.95

Crack growth rate data in the form of da/dN versus ΔK data is needed for crack growth analysis. Exact pedigree of the materials used is unknown but what is known is that they were left over from a previous project. The material specifications are known and match those of Pilarczyk whose coupons were manufactured in 2008 [344]. Pilarczyk conducted two ASTM E647 [345] tests with the 7075-T651 material to validate his test

setup against Harter-T and NASGRO material curves with reasonable agreement between the datasets (Figure 6-25) [346]. A tabular look-up material file for AFGROW was produced using the information from the two ASTM E647 tests and is shown in Figure 6-26.

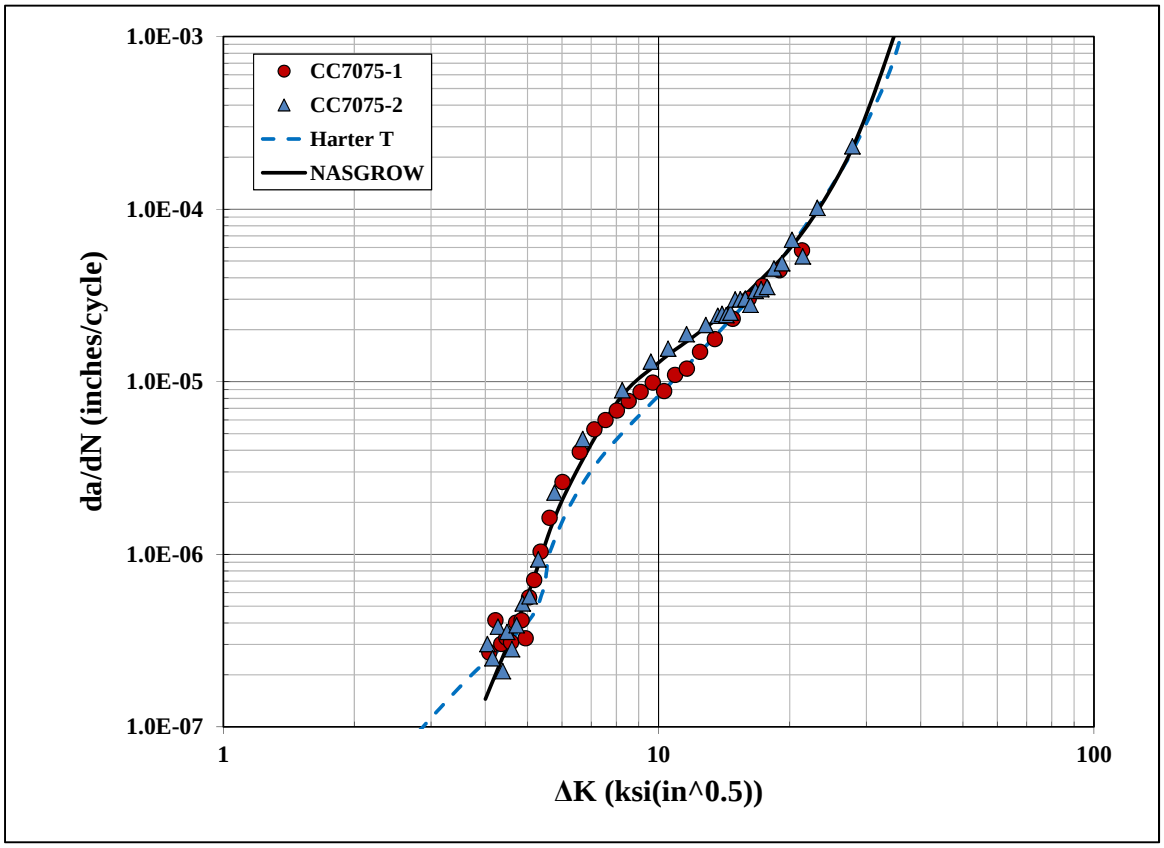

Figure 6-25 Crack Growth Data from Pilarczyk [346]

The complete material model input data are presented in Table 6-12. Note that the shaded data are only used in the composite patch repair analysis so those values are not important to the crack growth analysis. Also, some of the inputs are not optimized since only a constant amplitude spectrum with a stress ratio of 0.1 was used thus controls on R-shift are not necessary. The starting crack size is assumed to be the size of the EDM

notch of the specimens. Given the starting crack size, applied loading spectrum and geometry of the splice, only ΔK values of approximately 8ksi√in and higher will be needed.

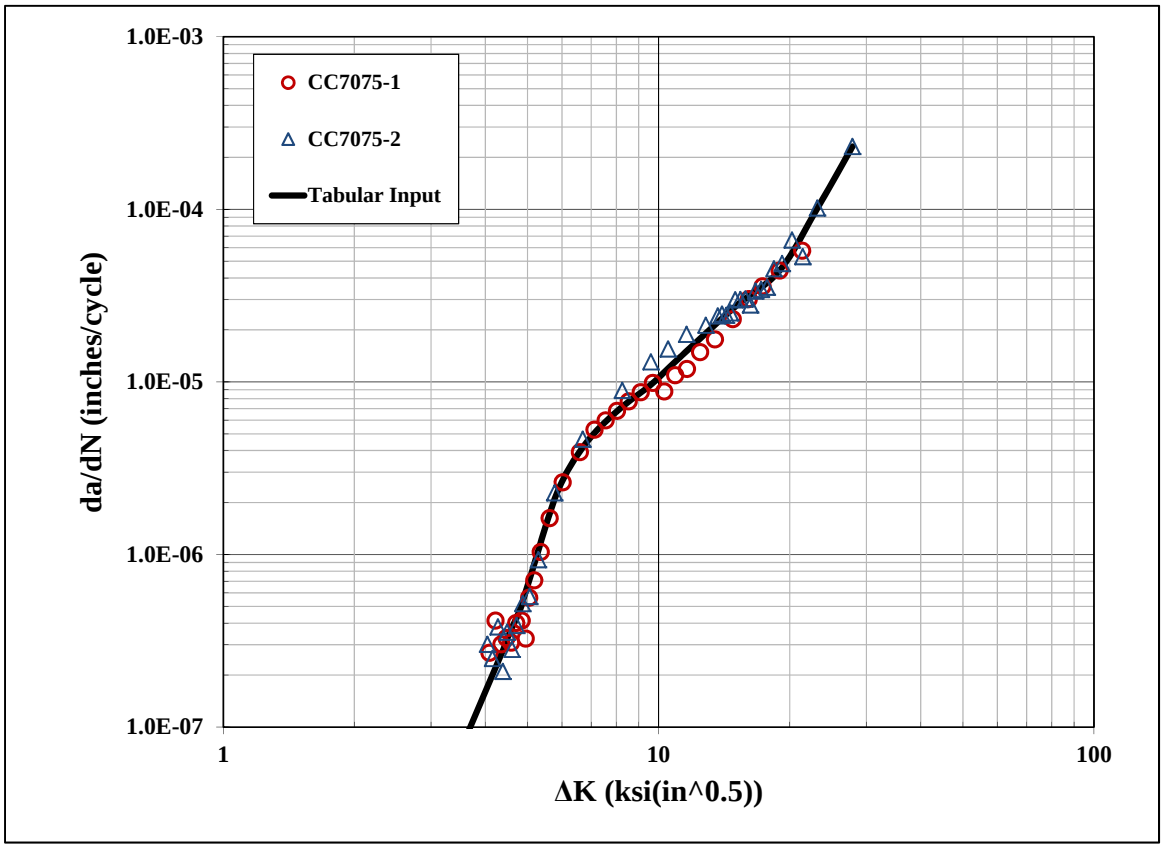

Figure 6-26 Tabular Input Material Model Compared with Data

Table 6-12 Tabular Input Information Used in AFGROW

da/dN	ΔK	Parameter	Value	Units
1.00E-08	2.500	Stress Ratio, R	0.1	--
2.81E-07	4.396	Ultimate Strength	77	ksi
3.09E-07	4.449	Yield Strength	69	ksi
4.97E-07	4.832	E	10,300	ksi
5.65E-07	4.904	Poisson's Ratio	0.33	--
6.44E-07	4.985	Coefficient of Thermal Expansion*	1.31E-05	/°K
1.03E-06	5.276	DADNHI	0.01	in/cycle
1.29E-06	5.419	DADNLO	1.00E-08	in/cycle

da/dN	ΔK	Parameter	Value	Units
1.71E-06	5.612	KC*	64	ksi√in
2.22E-06	5.817	KIC*	32	ksi√in
2.79E-06	6.061	Threshold	2.5	ΔK
3.42E-06	6.344	Lower R Shift	-0.3	--
4.14E-06	6.678	Upper R Shift	0.63	--
4.90E-06	7.042			
5.70E-06	7.458			
7.10E-06	8.201			
7.75E-06	8.577			
9.97E-06	9.757			
1.17E-05	10.423			
1.28E-05	10.820			
2.70E-05	14.924			
4.42E-05	18.967			
1.02E-04	23.165			
2.31E-04	27.879			

Shaded cells are values not used in the crack growth analysis
* Asterisk items have values taken from the NASGRO 7075-T651 L-T material model

The resulting crack growth curve from AFGROW is presented in Figure 6-27 along with the four joint specimens. The specimens had their holes for the fasteners drilled with a number 12 drill with a nominal diameter of 0.189 inch but can routinely go oversize by 0.002 inch if not drilled underside and reamed to final diameter. Check-gage data prior to testing is unavailable thus the actual finished diameter of the specimens are unknown. Yet looking at the hysteresis and nonlinearity at low load levels in the strain gage response in Figure 6-11 and Figure 6-12 it is apparent that some fasteners became engaged at much lower loads, or displacements, than others. Thus it is possible that the gap between fastener and plate was greater or misalignment of holes caused some fasteners to be more effective than others.

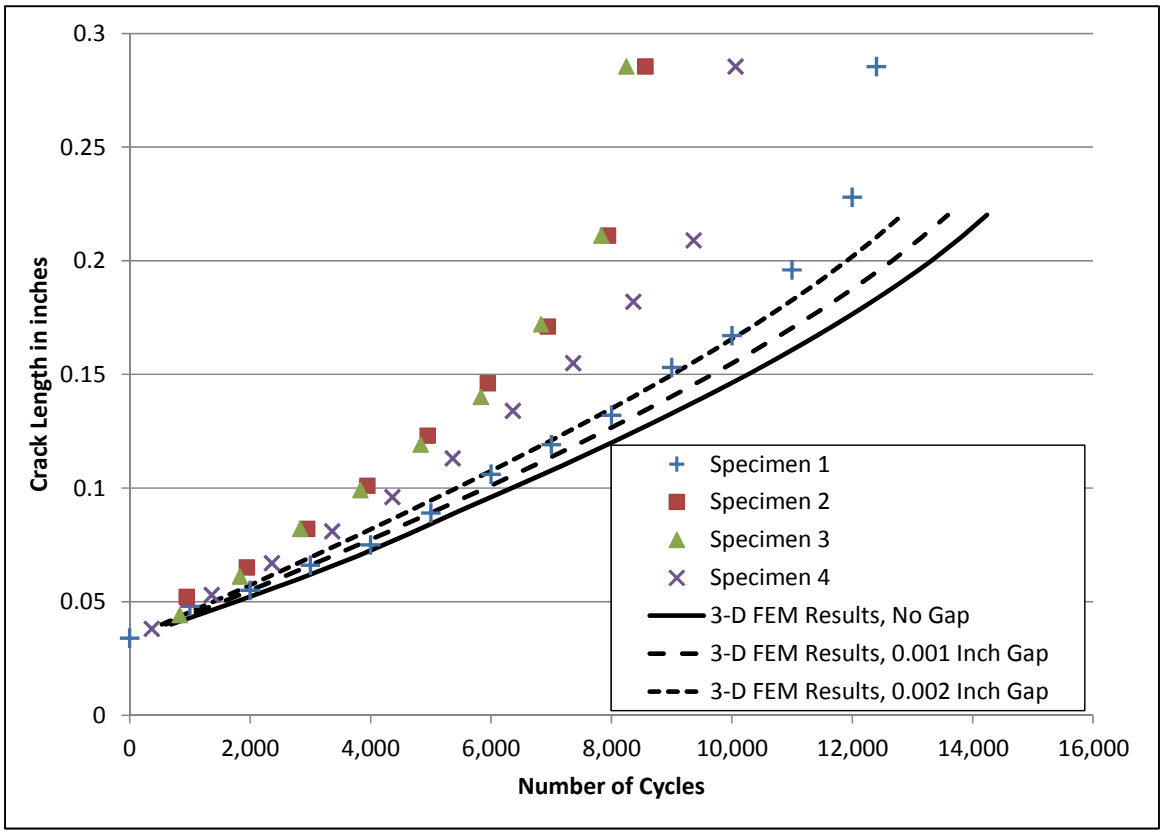

Figure 6-27 Analytical Crack Growth Curve Compared to the Four Joint Specimens

6.4 Comparison of Different Load Analysis Methods

The different load analysis methods that were presented previously were used to calculate the fastener load transfer for the 284 Splice. The static strength approach for the eccentric fastener pattern was evaluated and the calculations are presented in Appendix Section B.2. Fastener flexibility methods also shown previously were evaluated and are presented in Appendix Section B.3. Two dimensional planar models which are commonly used for fastener load transfer calculations were built using StressCheck and are presented in Sections B.4 and B.5. The total load transferred by each fastener using

these different methods are shown in Table 6-13 along with the percent difference from that calculated by the FEM discussed in Section 6.2.

6.4.1 The Static Strength Load Distribution Method

Presented in this section is a comparison of the static strength method outlined in Figure 4-1. Each fastener takes a portion of the total load based on a number of factors. In the 284 Splice, all fasteners are the same size so the 4,000 lbs would be considered distributed evenly across all the fasteners in the direction of loading. An additional load is applied to each fastener based on the eccentricity of the load to the centroid of the fastener pattern. Table 6-13 presents P_{total} from the static strength analysis compared with P_{total} from the 3-D FEM. Directions of the P_{total} vectors are not given.

Table 6-13 Bolt Loads from the Static Strength Method and its Percent Variation from the 3-D FEM Results

Fastener	P_{total} from a Static Strength Eccentricity Model		P_{total} from the 3-D FEM
1	471	-18%	576
2	465	-16%	557
3	459	52%	302
4	454	55%	294
5	450	94%	232
6	454	39%	326
7	459	29%	356
8	465	-31%	679
9	471	-32%	689
10	471	-33%	698
11	465	-31%	677
12	459	30%	352
13	454	41%	323
14	450	97%	228

Fastener	P_{total} from a Static Strength Eccentricity Model		P_{total} from the 3-D FEM
15	454	52%	298
16	459	51%	304
17	465	-16%	553
18	471	-18%	577
Sum and Average Error Magnitude	8295	41%	8020

The static strength method using eccentricity was the least accurate of the methods evaluated. This would be expected however since the fundamental assumption is that the load is evenly spread across the fasteners because they are taking their maximum load and the joint is becoming fully plastically deformed.

6.4.2 Fastener Flexibility Load Distribution Methods

One aspect of the 284 Splice that makes a traditional fastener flexibility method difficult is the double line of staggered fasteners. A method is required to reduce the pattern into straight rows. Two different approaches were explored.

The first approach splits the pattern into two separate lines, one with five fastener rows and another with four. The total load carried by each row is a ratio of the number of fasteners divided by the total number of fasteners in the pattern prior to splitting. This approach is depicted in Figure 6-28. The second approach combines fasteners in pairs starting from both ends leaving the middle row with a single fastener as depicted in Figure 6-29.

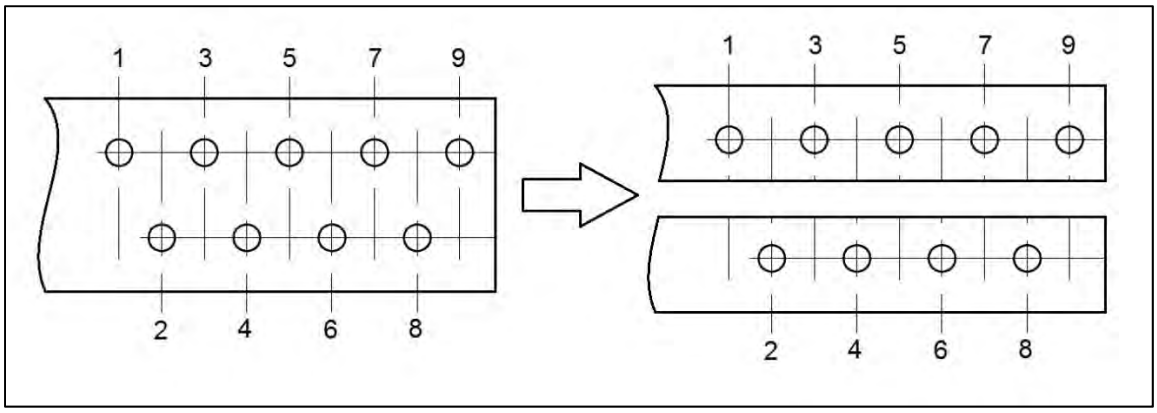

Figure 6-28 Fastener Flexibility Simplification by Splitting Lines of Fasteners

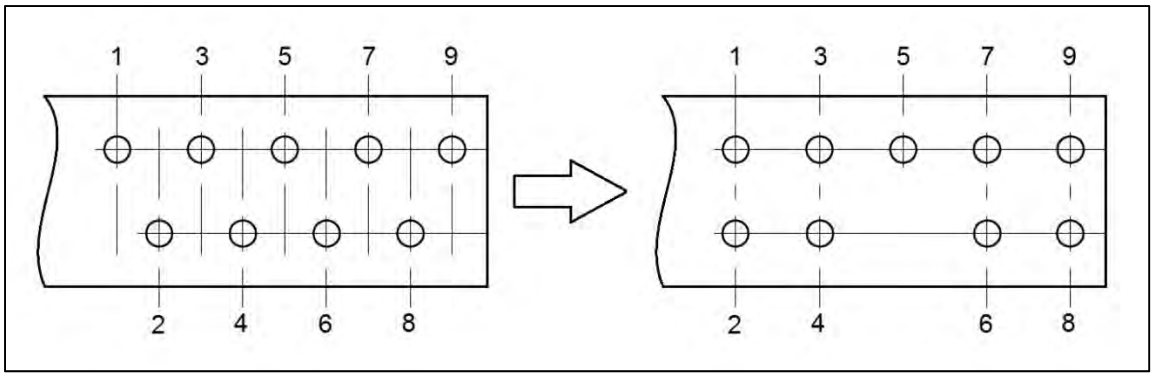

Figure 6-29 Fastener Flexibility Simplification by Combining Rows of Pairs

Each of these approaches was exercised using both the Tate and Rosenfeld equation as well as the Huth equation. The results are shown in Table 6-13 versus P_X from the 3-D FEM.

Table 6-14 Bolt Loads from Different Fastener Flexibility Methods and their Percent Variation from the 3-D FEM Results

Fastener	P from a T & R Model, Split Rows		P from a T & R Model, Paired Rows		P from a Huth Model, Split Rows		P from a Huth Model, Paired Rows		P_X from the 3-D FEM
1	551	-4%	517	-10%	645	13%	613	7%	573
2	492	-11%	517	-6%	544	-1%	613	11%	552
3	340	13%	337	12%	276	-8%	248	-18%	301
4	348	17%	337	14%	278	-6%	248	-16%	297

Fastener	P from a T & R Model, Split Rows		P from a T & R Model, Paired Rows		P from a Huth Model, Split Rows		P from a Huth Model, Paired Rows		P_X from the 3-D FEM
5	291	26%	318	37%	196	-15%	203	-12%	231
6	370	12%	375	14%	305	-8%	289	-12%	330
7	382	7%	375	5%	321	-10%	289	-19%	357
8	569	-15%	612	-8%	651	-3%	749	12%	668
9	657	-5%	612	-11%	783	13%	749	9%	690
10	657	-5%	612	-12%	783	13%	749	8%	692
11	569	-15%	612	-8%	651	-3%	749	12%	668
12	382	6%	375	4%	321	-11%	289	-19%	359
13	370	13%	375	15%	305	-7%	289	-11%	326
14	291	26%	318	37%	196	-15%	203	-12%	231
15	348	16%	337	12%	278	-8%	248	-18%	301
16	340	13%	337	12%	276	-9%	248	-18%	302
17	492	-10%	517	-5%	544	0%	613	12%	547
18	551	-4%	517	-10%	645	12%	613	7%	574
Sum and Average Magnitude	8000	12%	8000	13%	7998	9%	8002	13%	8000

Of the two fastener flexibility methods evaluated the Huth equation resulted in the most accurate total fastener loads when they are taken as being in series. One shortfall of this method is that the simplifications needed to divide the load between the different sides ignores the connectivity of the plate down the middle. The Huth equation predicts a stiffness of 6.87E+5 which is 2.19 times more stiff than the Tate and Rosenfeld equation stiffness of 3.13E+5. Looking at the load distribution, in all cases the Tate and Rosenfeld methods under predict the first two and last two fasteners loads and overpredicts in the middle. The Huth equation exhibits an opposite trend being more severe at the first and last fasteners and somewhat underpredicting through the middle. The stiffer the fastener connection, the less that load will by-pass the fastener to later fastener rows.

This raises the question that if the most correct fastener stiffness was somehow chosen a priori, how accurate would be the resulting fastener loads? A new solution was made for each reduction assumption that minimized the average magnitude of the error by solving for the optimum fastener stiffness; approximately 5.15E+5 for the split rows and 5.12E+5 for the paired rows. The other question was if the relative fastener flexibility from the 3-D FEM was used what would be the resulting fastener loads? The answer to the second question was found by consulting the 3-D FEM with no crack and extracting the equivalent fastener flexibility by dividing the fastener load in the main plate by the relative deflection. The relative deflection in this case is the deflection in the sides of the holes (direction of loading being the front); and is the difference between the average displacement between the middle plate and top and bottom plates. Based on the locations indicated in Figure 6-30, the deflection would be the average of B-A, B-C, B'-A', and B'-C'. Note that each 'location' is actually an extraction through the thickness since such large differences can be seen as a function of depth through the layer. The calculated fastener stiffnesses are presented in Table 6-15.

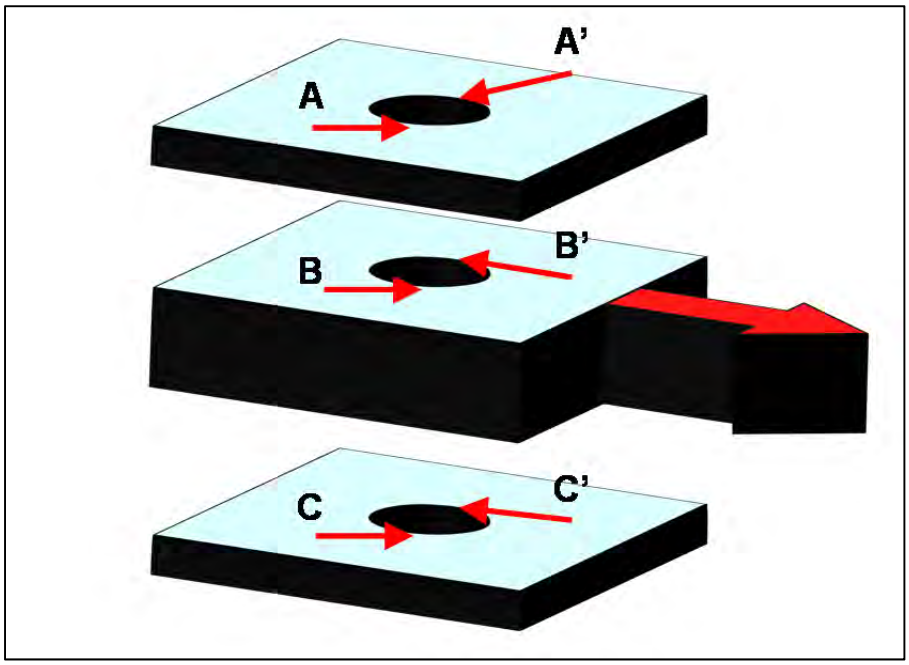

Figure 6-30 Extraction Locations for FEM Fastener Stiffness

Table 6-15 Fastener Stiffness from the 3-D FEM

Fastener	Stiffness
1	7.27E+5
2	7.18E+5
3	5.72E+5
4	5.48E+5
5	5.02E+5
6	5.55E+5
7	5.83E+5
8	7.27E+5
9	6.96E+5
Average	6.25E+5

Answers to both the preceding questions are presented in Table 6-16 with the optimized flexibility giving an average error of 3.5% while the average 3-D FEM based stiffness of 6.25E+5 gives an average error of 6.6%. The solutions for these two scenarios are presented in Appendix Section B.3.

Table 6-16 Bolt Loads from Different Optimized Fastener Flexibilities and their Percent Variation from the 3-D FEM Results

Fastener	P from an Optimized Flexibility Model, Split Rows		P from an Optimized Flexibility Model, Paired Rows		P from a 3-D FEM based Flexibility Model, Split Rows		P_X from the 3-D FEM
1	607	6%	560	-2%	633	10%	573
2	522	-5%	560	1%	537	-3%	552
3	301	0%	296	-2%	284	-6%	301
4	306	3%	296	0%	288	-3%	297
5	232	1%	265	15%	208	-10%	231
6	331	0%	337	2%	314	-5%	330
7	346	-3%	337	-6%	330	-7%	357
8	618	-8%	674	1%	639	-4%	668
9	734	6%	674	-2%	768	11%	690
10	734	6%	674	-3%	768	11%	692
11	618	-8%	674	1%	639	-4%	668
12	346	-4%	337	-6%	330	-8%	359
13	331	2%	337	3%	314	-4%	326
14	232	1%	265	15%	208	-10%	231
15	306	2%	296	-2%	288	-4%	301
16	301	0%	296	-2%	284	-6%	302
17	522	-5%	560	2%	537	-2%	547
18	607	6%	560	-3%	633	10%	574
Sum and Average Magnitude	8000	3.5%	7998	3.7%	8000	6.6%	8000

To understand why the fastener flexibilities are so different consider the conditions under which the equations were developed. Tate and Rosenfeld used standard aircraft bolts and nuts and used a ‘collar’ (thickness of several washers) to take up the extra length of un-threaded bolt. The fasteners were installed with a ‘wring fit’ which not a slip or interference but tight enough to require twisting of the fastener to install. Extra-long bolts were used to prevent any bearing taking place on threads. The nuts were tightened to tighten the joint then the nuts were backed off to a ‘finger tight’ condition to minimize

the load transfer by friction between layers. Huth used standard NAS and Hi-Lok bolts for his set of tests with interference fits and 'normal clamping forces'. It appears from this comparison that the interference fit and normal clamping process built into aerospace hardware makes a much more stiff connection. These specimens with Hi-Loks, a neat fit hole, and clamp-up with a slightly proud head due to lack of countersink falls somewhere in between.

The problem still remains that these comparisons are of loads in the main plates. The FEM and testing showed that great differences exist between the top and bottom straps that is not captured in these types of analyses. These same problems are evident in any 2-D modeling approach.

6.4.3 Finite Element Load Distribution Methods

This section explores the accuracy of other FEM methods and how accurately they can depict the differences in loads in the parts. One aspect of these models is that they can capture the loads both in the axis aligned with the direction of loading as well as the axis that is transverse. Still, the 2-D models presented here cannot capture the variation between the top and bottom straps.

Two different approaches were used. The first is a split model of only nine fasteners with cuts in the middle of the straps and symmetry conditions applied (see Figure 6-31). The full piece was modeled as similarly to the 3-D FEM as possible and is shown in Figure 6-32. Section B.4 and B.5 of Appendix B contain details of these two models. Comparisons of P_{total} extracted from these models are presented in Table 6-17 for both

the linear and the non-linear results. Note that for both of these models that the part separation is provided only for the sake of clarity. Mathematically, they are all in the same plane and the 'link' that connects them is a spring with a stiffness to account for deflection due to fastener bending and shear.

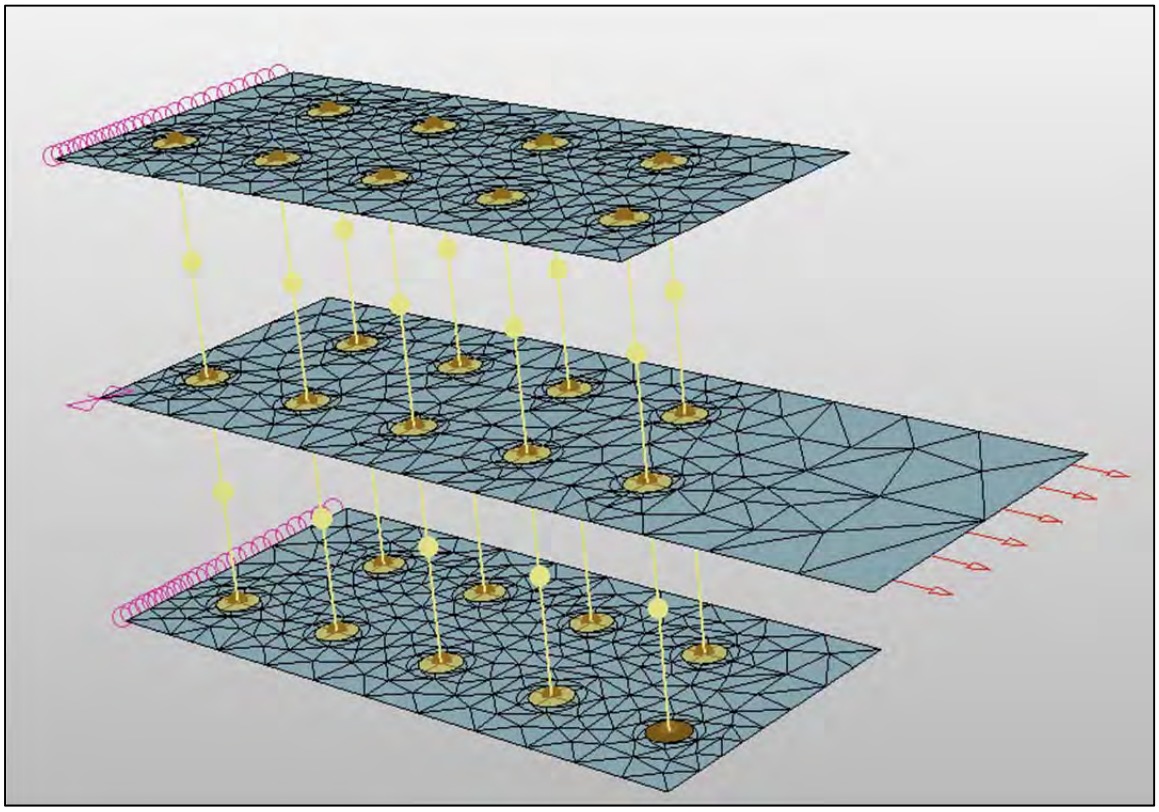

Figure 6-31 Planar Half FEM of the 284 Joint

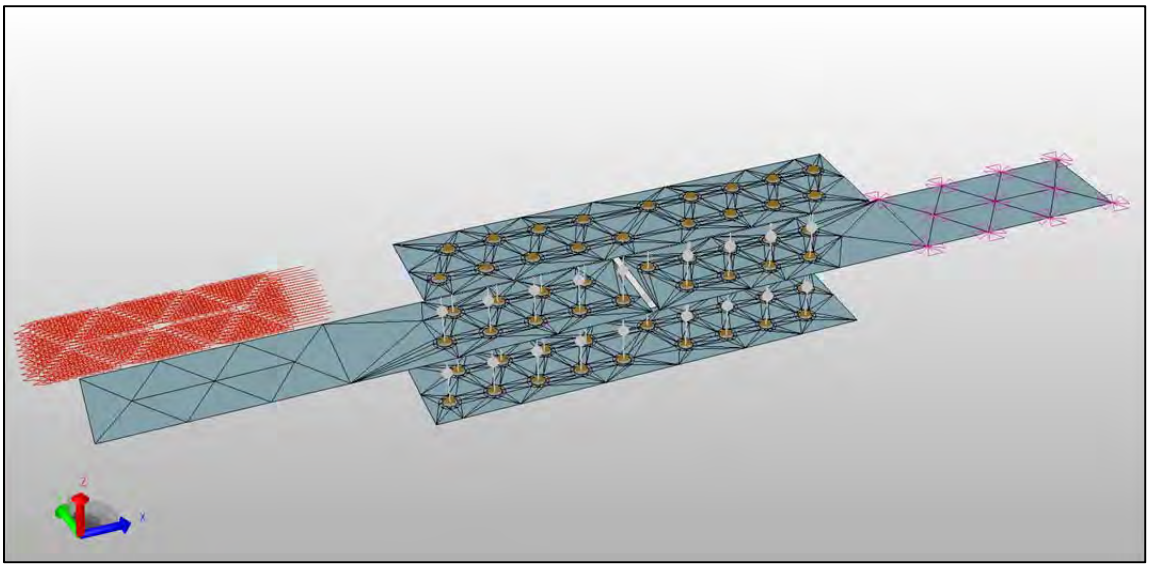

Figure 6-32 Planar Full FEM of the 284 Joint

Table 6-17 Bolt Loads from Different Types of Computer Calculation Methods and their Percent Variation from the 3-D FEM Results

Fastener	P_{total} from an Elastic 2-D Half Model		P_{total} from a Non-Linear Elastic 2-D Half Model		P_{total} from an Elastic 2-D Model		P_{total} from a Non-Linear Elastic 2-D Model		P_{total} from the 3-D FEM
1	608	6%	565	-2%	615	7%	566	-2%	576
2	572	3%	546	-2%	566	2%	548	-2%	557
3	280	-7%	312	3%	283	-6%	314	4%	302
4	283	-4%	311	6%	281	-4%	311	6%	294
5	207	-11%	247	7%	209	-10%	248	7%	232
6	310	-5%	337	3%	310	-5%	338	3%	326
7	324	-9%	361	2%	327	-8%	362	2%	356
8	689	2%	648	-5%	690	2%	652	-4%	679
9	742	8%	672	-3%	736	7%	672	-3%	689
10	742	6%	672	-4%	739	6%	675	-3%	698
11	689	2%	648	-4%	688	2%	651	-4%	677
12	324	-8%	361	3%	327	-7%	361	3%	352
13	310	-4%	337	4%	309	-4%	337	4%	323
14	207	-9%	247	8%	209	-8%	248	9%	228
15	283	-5%	311	4%	280	-6%	311	4%	298
16	280	-8%	312	2%	284	-7%	314	3%	304
17	572	4%	546	-1%	564	2%	547	-1%	553
18	608	5%	565	-2%	617	7%	567	-2%	577
Sum and	8030	6%	7998	4%	8034	6%	8022	4%	8020

Fastener	P_{total} from an Elastic 2-D Half Model		P_{total} from a Non-Linear Elastic 2-D Half Model		P_{total} from an Elastic 2-D Model		P_{total} from a Non-Linear Elastic 2-D Model		P_{total} from the 3-D FEM
Average Magnitude									

It is interesting that little if any increase in accuracy comes from increasing the detail and modeling the full joint. Slight differences however can be seen between similar fasteners, e.g., 1 and 18 or 9 and 10, can be seen in both the full 2-D FEM and the 3-D FEM and the general trends of which carries more load are the same. Also of interest is that the non-linear results are more accurate than the linear elastic results. Thus both the 2-D and 3-D models indicated that some non-linearity is softening the more highly loaded end fasteners causing an increase in by-pass load over the linear results. This non-linear effect is something else that would not be possible to capture using standard fastener flexibility methods. Complete results for P_X and P_Y are presented in Table 6-18 and Table 6-19 for the half model and full model respectively.

Table 6-18 Bolt Loads for the 2-D Half Model and their Percent Variation from the 3-D FEM Results

Fastener	P_X from a Non-Linear Elastic 2-D Half Model		P_Y from a Non-Linear Elastic 2-D Half Model		P_X from the 3-D FEM	P_Y from the 3-D FEM
1	565	-1%	-4.0	-49%	573	-7.9
2	546	-1%	63.7	-3%	552	65.9
3	312	4%	-11.8	-8%	301	-12.9
4	311	5%	2.8	-6%	297	3.0
5	247	7%	2.8	10%	231	2.6
6	337	2%	-1.8	-208%	330	1.7
7	361	1%	16.6	-8%	357	18.1
8	648	-3%	-77.0	-4%	668	-80.1
9	672	-3%	10.8	-37%	690	17.0

Fastener	P_X from a Non-Linear Elastic 2-D Half Model		P_Y from a Non-Linear Elastic 2-D Half Model		P_X from the 3-D FEM	P_Y from the 3-D FEM
10	-672	-3%	-10.8	-37%	692	-17.2
11	-648	-3%	77.0	-3%	668	79.0
12	-361	1%	-16.6	-7%	359	-17.8
13	-337	3%	1.8	-181%	326	-2.3
14	-247	7%	-2.8	-6%	231	-3.0
15	-311	3%	-2.8	82%	301	-1.6
16	-312	3%	11.8	-12%	302	13.4
17	-546	0%	-63.7	-5%	547	-67.3
18	-565	-2%	4.0	-58%	574	9.5
Sum 1-9 and Average Magnitude	3999	3%	2.2	37%	4000	7.3
Sum 10-18 and Average Magnitude	-3999	3%	-2.2	43%	-4000	-7.3

Table 6-19 Bolt Loads for the 2-D Full Model and their Percent Variation from the 3-D FEM Results

Fastener	P_X from a Non-Linear Elastic 2-D Full Model		P_Y from a Non-Linear Elastic 2-D Full Model		P_X from the 3-D FEM	P_Y from the 3-D FEM
1	566	-1%	-5.6	-29%	573	-7.9
2	544	-1%	64.4	-2%	552	65.9
3	314	4%	-11.6	-11%	301	-12.9
4	311	5%	3.5	15%	297	3.0
5	248	7%	3.5	36%	231	2.6
6	338	2%	-1.2	-172%	330	1.7
7	362	1%	17.4	-4%	357	18.1
8	647	-3%	-76.2	-5%	668	-80.1
9	672	-3%	12.0	-30%	690	17.0
10	-675	-2%	-12.3	-28%	-692	-17.2
11	-646	-3%	75.9	-4%	-668	79.0
12	-361	0%	-17.4	-3%	-359	-17.8
13	-337	3%	1.1	-147%	-326	-2.3

Fastener	P_X from a Non-Linear Elastic 2-D Full Model		P_Y from a Non-Linear Elastic 2-D Full Model		P_X from the 3-D FEM	P_Y from the 3-D FEM
14	-248	7%	-3.7	23%	-231	-3.0
15	-311	3%	-3.7	135%	-301	-1.6
16	-314	4%	11.2	-16%	-302	13.4
17	-543	-1%	-63.8	-5%	-547	-67.3
18	-567	-1%	4.7	-51%	-574	9.5
Sum 1-9 and Average Magnitude	4000	3%	6.1	34%	4000	7.3
Sum 10-18 and Average Magnitude	-4001	3%	-7.9	46%	-4000	-7.3

Both 2-D planar models exhibit less overall difference between the 3-D FEM versus the optimized fastener flexibility methods. This is especially significant since the fastener flexibility methods could not be optimized without knowing the target distribution a priori. The 2-D models in this instance represent a minimal compromise in accuracy over the much more computationally expensive and time intensive 3-D models.

6.5 Comparison of Different Damage Tolerance Analysis Methods

This section explores the accuracy and applicability of different stress intensity factor solutions and compares the resulting crack growth predictions against test. Classical solutions are developed and analyzed using a user defined model in the AFGROW software. Built-in models in AFGROW are also compared using the different inputs from the different load analyses.

6.5.1 Classical Solutions for Damage Tolerance Analysis

This section discusses various classic solutions and their implementation for damage tolerance analysis. All of these get combined by superposition in a manner identical to that shown in Figure 5-5. The stress intensity is assumed to be mode I and corrections for finite width and offset holes are needed for both solutions. The overall stress intensity is thus:

$$K_{I,total} = \sigma_{bypass}\sqrt{\pi a}F_{Through\ Crack}F_W F_{Offset} + \frac{L}{2Rt}\sqrt{\pi a}F_{Through\ Crack}F_W F_{Offset}$$

Equation 6-5 Total Stress Intensity Equation Based on Superposition

where:

a is the crack length

L is the fastener load

R is the hole radius

t is the thickness

Note the $F_{Through\ Crack}$, F_W, and F_{Offset} are not necessarily the same for the remote tension case and pin loaded case. For the splice plate geometry, it was given previously that the width, W, is 1.36 inches; thickness, t, is 0.1 inch; diameter, D, is 0.189 inch; and the hole offset, B, is 0.38 inch. The crack is assumed to be a through crack as was tested thus the number of solutions is reduced to a great extent since corner crack stress intensity solutions are not needed. Loads from the 3-D FEM are used to minimize variation from the previously calculated stress intensity solutions and those presented here. Summing fasteners one through eight and dividing by the area gives a bypass stress of 12.12 ksi.

The load transferred in the un-cracked state by fastener number nine is 334.1 pounds thus the bearing stress is 17.68 ksi. These values are used in the following comparisons

Superposition also can be used to develop stress intensity factors for a pin loaded hole modeling the method used in Reference [347] as shown in Figure 6-33. This expands the somewhat limited field of pin loaded hole stress intensity factor solutions a recommended approach in many older textbooks on the subject. Additionally, two crack solutions can be transformed to a single crack solution using a single crack correction factor, $F_{1/2}$.

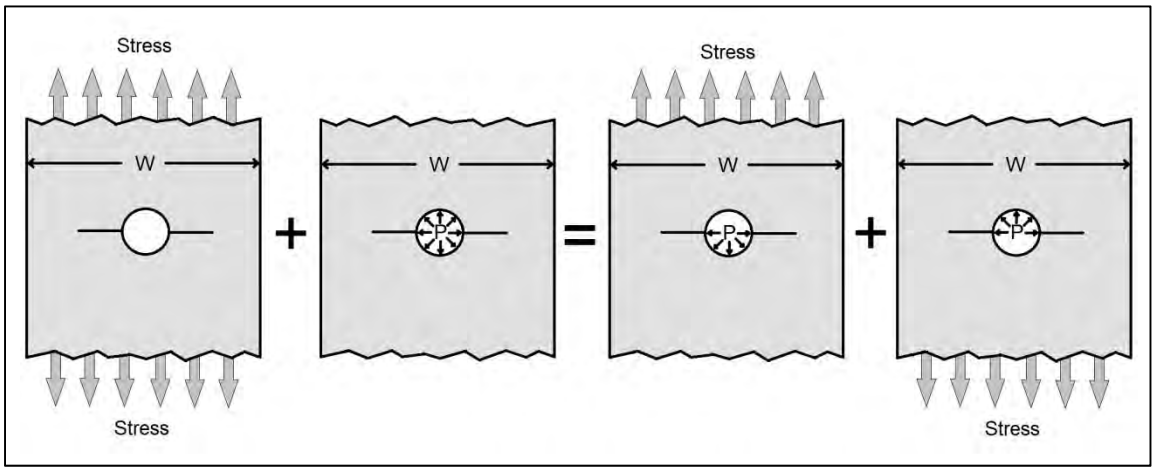

Figure 6-33 Method of Determining Pin Loaded Hole Stress Intensities by Superposition

Bowie's seminal solution from 1956 for one or two cracks at a circular hole in an infinite sheet subjected to bi-axial stress is given by the following equation and Table 6-20 [348]:

$$K_I = \sigma\sqrt{\pi a}F\left(\frac{L}{r}\right)$$

Equation 6-6 Bowie's Stress Intensity Equation for One or Two Cracks at a Hole in an Infinite Sheet under Uniaxial or Biaxial Stress

Table 6-20 Correction Factors for Equation 6-6

L/R	F(L/r), One Crack	F(L/R), Two Cracks

	Uniaxial Stress	Biaxial Stress	Uniaxial Stress	Biaxial Stress
0.0	3.39	2.26	3.39	2.26
0.1	2.73	1.98	2.73	1.98
0.2	2.30	1.82	2.41	1.83
0.3	2.04	1.67	2.15	1.70
0.4	1.86	1.58	1.96	1.61
0.5	1.73	1.49	1.83	1.57
0.6	1.64	1.42	1.71	1.52
0.8	1.47	1.32	1.58	1.43
1.0	1.37	1.22	1.45	1.38
1.5	1.18	1.06	1.29	1.26
2.0	1.06	1.01	1.21	1.20
3.0	0.94	0.93	1.14	1.13
5.0	0.81	0.81	1.07	1.06
10.0	0.75	0.75	1.03	1.03
∞	0.707	0.707	1.00	1.00

Newman presents solutions for biaxial stress intensity solutions for double symmetrical cracks at a hole both under remote tension and with a pressurized hole [349]. Note in Reference [349] that the headings in the biaxial part of the remote stress solution are mislabeled. The columns of solutions are in the order of λ equals -1, 0, and 1 respectively. Also, crack length a is defined in the basic equation as being from the center of the hole to the crack tip thus the values in Table 6-21 are converted to match the definition for crack length used in this dissertation.

Table 6-21 Correction Factors for Two Symmetrical Cracks at a Hole for Two Different Types of Loading from Reference [349]

a/R	Remote Tension	Hole Subjected to Internal Pressure
0.01	3.272	1.093
0.02	3.224	1.034
0.04	3.101	1.041
0.06	2.986	1.004

0.08	2.882	0.971
0.10	2.786	0.940
0.15	2.581	0.872
0.20	2.413	0.814
0.25	2.274	0.763
0.30	2.156	0.719
0.40	1.971	0.645
0.50	1.833	0.586
0.60	1.726	0.537
0.80	1.574	0.460
1.0	1.472	0.403
1.2	1.400	0.359
1.5	1.324	0.308
2.0	1.244	0.249
3.0	1.164	0.179

Broek, in References [181] and [350] discusses an engineering approximation approach whereby the single crack is assumed to be equivalent to the crack length plus the diameter. This is explained by the equation below where $2a_{eff} = D + a$ as well as depicted in Figure 6-34. As pointed out in Reference [350], the solution is slightly unconservative when compared with other, more accurate methods.

$$K = \sigma\sqrt{\pi a_{eff}} = \sigma\sqrt{\pi a}\sqrt{\frac{D}{2a} + \frac{1}{2}} = \sigma\sqrt{\pi a} f\left(\frac{a}{D}\right)$$

Equation 6-7 Broek Engineering Approximation for a Single Crack at a Hole in an Infinite Plate Subjected to Remote Tension

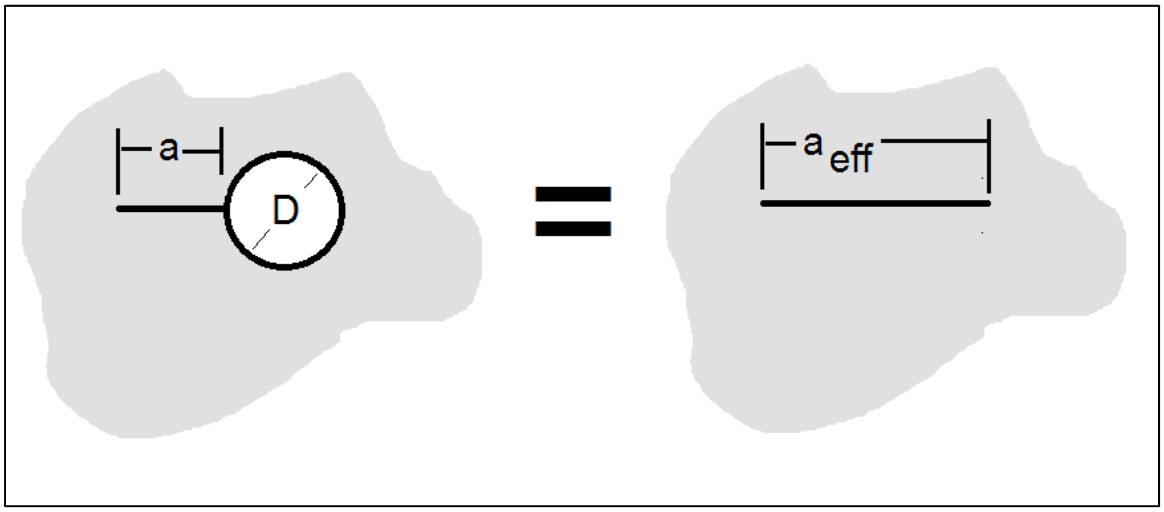

Figure 6-34 Broek Engineering Approximation for a Single Through Crack at a Hole

Tweed and Rooke used a Mellin transform technique to determine an integral equation for the stress intensity factor and the crack formation energy for a through crack at a circular hole in an infinite plate [351]. The results are presented as a table of a/R values.

Table 6-22 Correction Factors for a Single Through Crack at a Circular Hole Subjected to Remote Tension from Reference [351]

a/R	F_I	a/R	F_I
0.01	3.291	0.3	2.092
0.02	3.223	0.4	1.884
0.04	3.095	0.5	1.727
0.06	2.978	0.75	1.464
0.08	2.87	1	1.306
0.1	2.771	1.5	1.127
0.12	2.679	2	1.03
0.14	2.594	3	0.93

a/R	F_I	a/R	F_I
0.16	2.515	4	0.877
0.18	2.442	5	0.845
0.2	2.373	7	0.808
0.25	2.221	9	0.787

Shah states that for the case of filled holes subjected to remote tension that the stress distribution between filled and unfilled holes is less than three percent if the crack length is greater than 30% of the hole radius [322]. Below this, the effect is much greater for some extreme cases but does point out that in real structures it may not be as severe. Shah also points out that simple superposition of the loaded filled hole without remote tension solution and the unloaded filled hole subjected to remote tension solution will not be accurately combined since the contact solution is non-linear. However, it is common to do so anyway since the error diminishes as the crack grows further from the hole. This solution is for an infinite plate so finite plate and offset corrections are needed for comparison.

$$K_{IPin} = \sigma_B \sqrt{\pi a} F_1$$

Equation 6-8 Stress Intensity for a Single Crack at a Hole Loaded by a Neat Fit Pin

where:

σ_B is the load applied at the hole divided by the cross-section to which it is applied (equal to P / (2*Radius*t))

a = crack length

F_1, is the solution for one crack converted from the two crack solution using the following equation:

$$F_{1/2} = \sqrt{\frac{2R + L}{2R + 2L}} F_2$$

Equation 6-9 Correction Factor for the Two Crack Solution for a Single Crack

And the two crack solution, F_2 is given as:

$$F_2 = A_0 + \frac{2}{\pi}\left(A_2(R^2 I_2) + A_4(R^4 I_4) + A_6(R^6 I_6)\right)$$

Equation 6-10 Two Crack Correction Factor

where $A_0 = 0.04374$, $A_2 = 0.71304$, $A_4 = -0.66404$, and $A_6 = 0.91998$.

Shah's solution for stress intensity for crack under biaxial stress at an open hole is:

$$K_I = \sigma\sqrt{\pi a}\left\{1 + \frac{1}{\pi}[(1 + \lambda)R^2 I_2 + 3(1 - \lambda)R^4 I_4]\right\}$$

where:

σ = the tension stress

a = crack length

λ = the factor multiplied to the biaxial stress that is applied in the direction of cracking (λ = 0) for uniaxial tension

and:

$$R^6 I_6 = \frac{1}{5(1 - \xi^2)}[-\xi + 9R^5 I_5 - 4R^4 I_4]$$

$$R^5 I_5 = \frac{1}{4(1 - \xi^2)}[-\xi + 7R^4 I_4 - 3R^3 I_3]$$

$$R^4 I_4 = \frac{1}{3(1 - \xi^2)}\left[-\xi + \frac{\xi(\xi^2 - 16)}{2(1 - \xi^2)^2} + \frac{(6 + 9\xi^2)}{2(1 - \xi^2)^2} R I_1\right]$$

$$R^3 I_3 = \frac{1}{2(1-\xi^2)}\left[\frac{-\xi(4-\xi^2)}{1-\xi^2} + \frac{2+\xi^2}{1-\xi^2} RI_1\right]$$

$$R^2 I_2 = \frac{1}{1-\xi^2}[-\xi + RI_1]$$

$$for\ \xi \neq 1$$

and:

$$RI_1 = \frac{2}{\sqrt{1-\xi^2}} \tan^{-1} \sqrt{\frac{1-\xi}{1+\xi}}\ for\ \xi < 1$$

$$RI_1 = 1\ for\ \xi = 1$$

$$RI_1 = \frac{1}{\sqrt{\xi^2-1}} \log \frac{\sqrt{\xi+1}+\sqrt{\xi-1}}{\sqrt{\xi+1}-\sqrt{\xi-1}}\ for\ \xi > 1$$

Equation 6-11 Inputs for Two Crack Solution Given in Equation 6-10

where:

ξ = a/R

Schijve in Reference [352] presents a stress intensity solution for a single through crack at a hole subjected to remote tension. The first bracketed term is a correction for a single crack and the second bracketed term is an equation fit of two crack data from Newman [349]. The single crack correction comes from a fit of the Newman [349], Tweed-Rooke [351] solution ratio. Schijve's correction is an improvement over Shah's near the hole at shorter crack lengths.

$$K = \sigma\sqrt{\pi a}\left[\sqrt{\frac{2+\xi}{2+2\xi}} \times \left(1 + \frac{0.2\xi}{(1+\xi)^3}\right)\right] \times \left[1 + \frac{1}{2\xi^2 + 1.93\xi + 0.539} + \frac{1}{2(\xi+1)}\right]$$

Equation 6-12 Schijve Stress Intensity for a Single Through Crack at a Hole in an Infinite Plate Subjected to Remote Tension

where:

ξ = a/R

Two different methods of arriving at the remote tension solution are possible using the book, *The Stress Analysis of Cracks Handbook* by Tada, Paris, and Irwin [353]. The first equation below is for a single crack at a hole in an infinite width plate and the second is a double crack at a hole that can be reduced to a single crack using a $F_{1/2}$ term. Note that Reference [354] presents the single crack solution as being for a finite width plate yet there is not a 'W' term in the equation. The solution for symmetric double cracks at a hole in an infinite plate with internal pressure at a hole along with the basic remote tension solution needed to develop the pin loaded solution through superposition are also given below.

$$K = \sigma\sqrt{\pi a}[1 + 0.2(1 - s) + -0.3 * (1 - s)^6] \times [2.243 - 2.64s + 1.352s^2 - 0.248s^3]$$

Equation 6-13 Stress Intensity for a Single Crack at a Hole in an Infinite Plate Subjected to Remote Tension

$$K = \sigma\sqrt{\pi a}\frac{3 - s}{2}[1 + 1.243(1 - s)^3]$$

Equation 6-14 Stress Intensity for Two Symmetric Cracks at a Hole in an Infinite Plate Subjected to Remote Tension

$$K = P\sqrt{\pi a}(1 - s)[0.637 + 0.485(1 - s)^2 + 0.4s^2(1 - s)^2]$$

Equation 6-15 Stress Intensity for Two Symmetric Cracks at a Hole in an Infinite Plate Subjected to Internal Pressure at the Hole

where $s = \frac{a}{R+a}$

There are additional solutions from Reference [353] for cracked holes in a finite width plate but the correction factors have to be determined by interpolating between lines in a graph. These will not be used in a comparison here due to the potential inaccuracy caused by the manual look-up process. For the sake of comparison of the preceding equations that have been discussed, the stress intensity solutions need to be converted to the state of a single crack at an offset hole in a finite width plate. Schijve's method, given in the equation below is contrasted with Shah's given in Equation 6-9.

$$F_{1/2} = \left[\sqrt{\frac{2+\xi}{2+2\xi}} \times \left(1 + \frac{0.2\xi}{(1+\xi)^3}\right)\right]$$

Equation 6-16 Correction Factor for a Single Crack from a Symmetrical Two Crack Solution from Reference [352]

Both Bowie and Tada et al., present both a single and double symmetric crack solution. The double symmetric crack solutions are converted to a single crack solution using both the Schijve and Shaw methods. The differences between these are illustrated by Figure 6-35 and the difference values are given in Table 6-23.

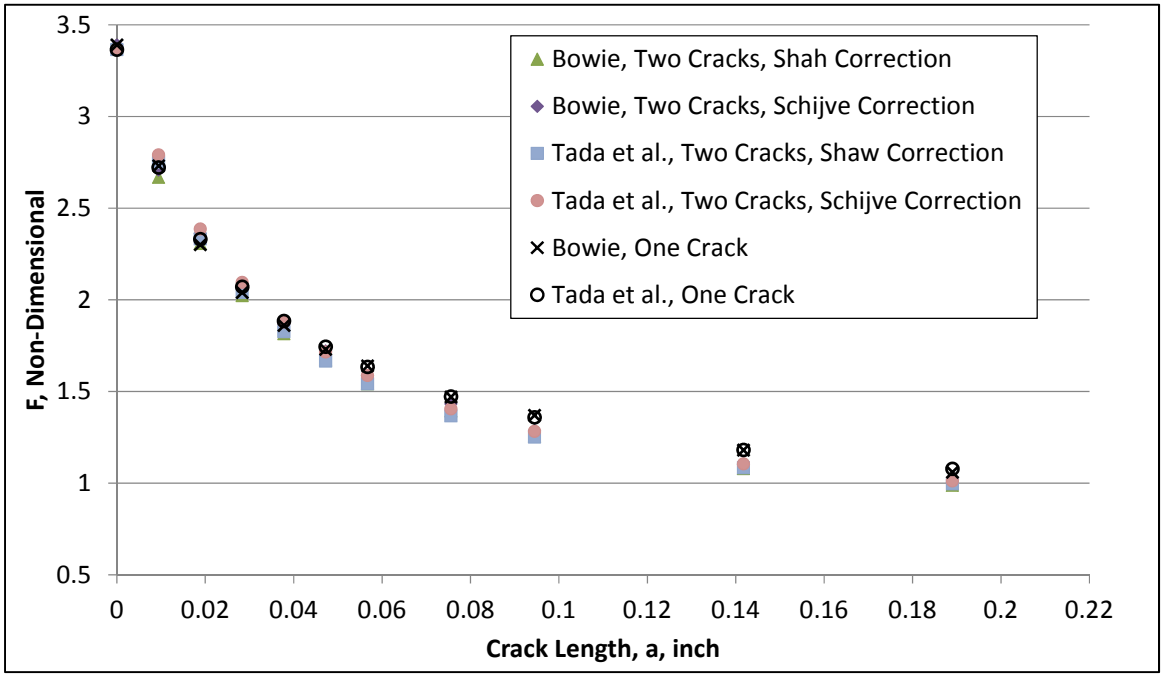

Figure 6-35 Plot of Single Crack Solutions and Double Crack Solutions modified by $F_{1/2}$

Table 6-23 Error between the Single Crack Solution and the Converted Two Crack Solution

Crack Size, a, inch	Bowie, Two Cracks, Shah Correction	Bowie, Two Cracks, Schijve Correction	Tada et al., Two Cracks, Shaw Correction	Tada et al., Two Cracks, Schijve Correction
0.000	0.0%	0.0%	0.0%	0.0%
0.009	-2.3%	-0.8%	1.0%	2.5%
0.019	0.3%	2.6%	0.1%	2.4%
0.028	-0.9%	1.8%	-1.5%	1.2%
0.038	-2.4%	0.4%	-3.1%	-0.3%
0.047	-3.4%	-0.6%	-4.5%	-1.7%
0.057	-6.0%	-3.3%	-5.6%	-2.9%
0.076	-5.2%	-2.6%	-7.2%	-4.6%
0.095	-8.3%	-6.0%	-8.0%	-5.6%
0.142	-8.5%	-6.8%	-8.2%	-6.5%
0.189	-6.8%	-5.4%	-7.6%	-6.2%
0.284	-4.1%	-3.2%	-6.0%	-5.2%
0.473	0.9%	1.4%	-3.9%	-3.5%
0.945	1.4%	1.6%	-1.9%	-1.8%

Schijve's correction factor has the lowest difference overall but is slightly greater at the shorter crack lengths. Thus Schijve's solution is used to correct symmetric two crack solutions to a single crack even though this somewhat trivializes the comparison between Newman and the Tweed and Rooke solutions since it was developed from a ratio of the two. Finite width and offset hole corrections for a part-through or through crack at a single hole in a plate are available from numerous sources including those following from Reference [323]:

$$F_w = \sqrt{\sec\left(\frac{\pi}{2}\sqrt{\frac{a}{t}}\left(\frac{D+c}{2B-c}\right)\right)\sec\left(\frac{\pi D}{4B}\right)}$$

Equation 6-17 Finite Width Correction Factor from Reference [323]

$$F_{offset} = \sqrt{\frac{\sin\gamma}{\gamma}}\ where: \gamma = \frac{D}{t} - \frac{2D}{W}$$

Equation 6-18 Offset Hole Correction Factor from Reference [323]

However, later work by Harter developed a different solution of the offset hole correction factor [324].

$$F_{offset} = \frac{\sin\left(\sqrt{\frac{a}{t}}\left(\frac{D+c}{B-c/2}\right)\left(\frac{W-2B}{W}\right)\right)}{\sqrt{\frac{a}{t}}\left(\frac{D+c}{B-c/2}\right)\left(\frac{W-2B}{W}\right)}\left(1-\left(\frac{c}{B-D/2}\right)^{12}\right)^{\frac{D}{2B}}$$

Equation 6-19 Offset Correction Factor from Reference [324]

The offset and width corrections presented above are for both through and corner cracks. For through cracks as considered in this thesis the a/t term is equal to unity. For the crack growth comparisons, the following correction factors will be used: F_W from Reference [323] in Equation 6-17, F_{offset} from Reference [324] and Equation 6-19, and if needed, $F_{1/2}$ from Reference [352] in Equation 6-16. The bullets below list the total combinations and the resulting stress intensity factors for the bypass stress portion is presented in Figure 6-36.

- Bowie Single Crack*F_W*F_{offset}
- Newman Double Crack*$F_{1/2}$*F_W*F_{offset}

- Broek Single Crack Engineering Approximation*F_W*F_{offset}
- Tweed and Rooke Single Crack*F_W*F_{offset}
- Shaw Double Crack*$F_{1/2}$*F_W*F_{offset}
- Schijve Double Crack*$F_{1/2}$*F_W*F_{offset}
- Tada, Paris, and Irwin Single Crack,*F_W*F_{offset}

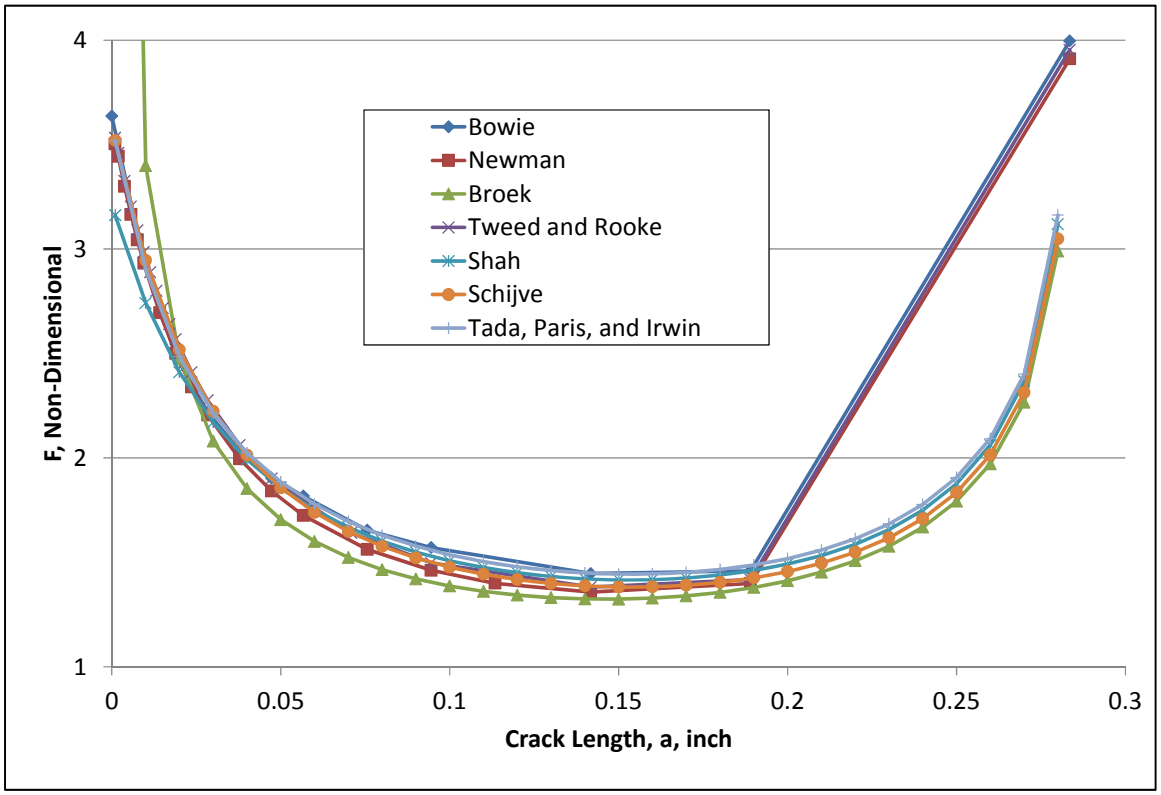

Figure 6-36 Stress Intensity Factors for the Bypass Stress Portion of the Total Stress Intensity Equation

$$P = \frac{L}{2Rt} \; and \; \sigma_{Remote-Tension} = \frac{2RP}{W}$$

Equation 6-20 Relationship between Remote Tension Stress, Hole Internal Pressure, and Fastener Load

where:

P is the internal pressure at the hole

L is the load on the fastener

W is the plate width

R is the hole radius

t is the plate thickness

This relationship can be used to combine remote tension solutions and hole with internal pressure solutions to approximate a pin loaded solution as outlined in Figure 6-33. Combinations of this principle come from Newman and Tada, Paris, and Irwin [349, 353]. Assuming that F_W and F_{offset} are applicable to both solutions, the final pin load solution is:

$$K = \frac{L}{2Rt}\sqrt{\pi a}\frac{\left(F_{IP} + \frac{2R}{W}F_{RT}\right)}{2}F_{1/2}F_W F_{offset}$$

Equation 6-21 Stress Intensity Solution for a Pin Loaded Hole by Superposition

where:

F_{IP} is the correction factor for a hole with internal pressure

F_{RT} is the correction factor for a hole subjected to remote tension

Naturally there is some error since F_{offset} is not the same for both solutions. Both the Newman solutions and the solutions from Tada, Paris, and Irwin were combined using superposition and the two crack pin loaded solution from Shah are compared. The resulting pin load correction factors are presented in Figure 6-37. Note that the approximate method using superposition compares well with the equation developed by Shah.

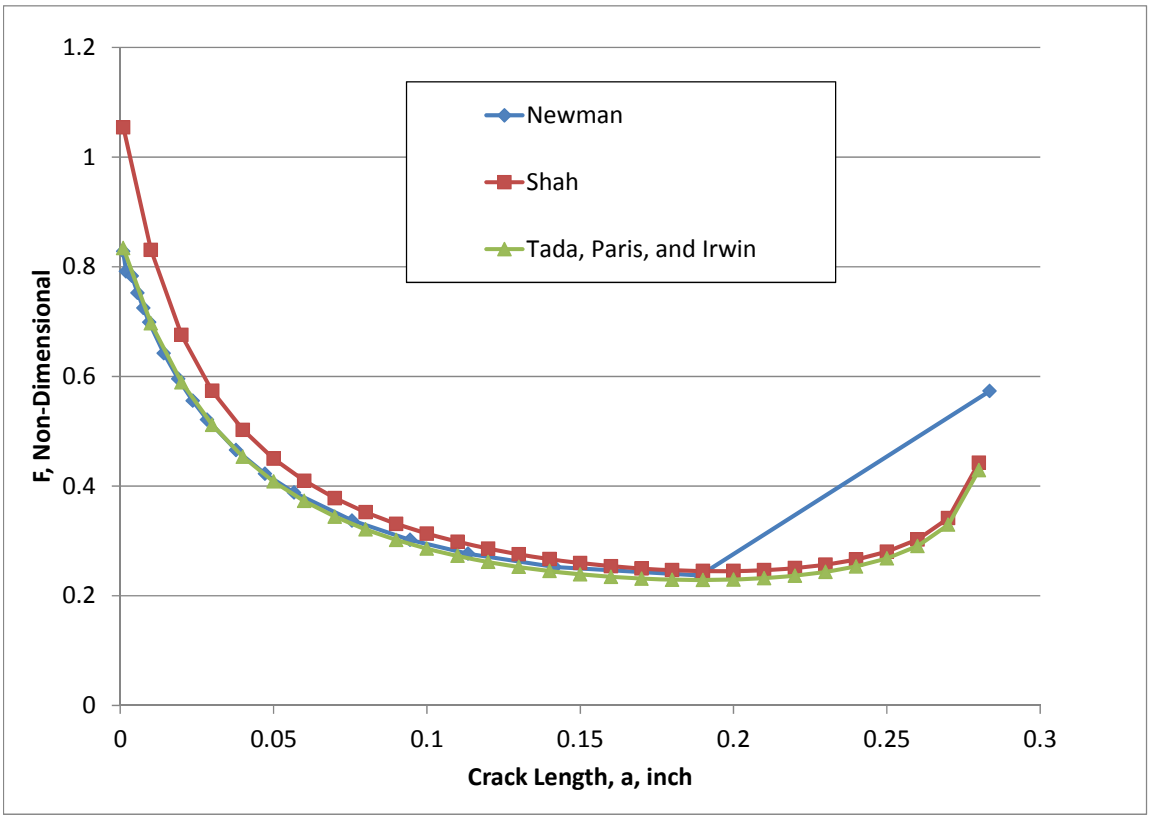

Figure 6-37 Stress Intensity Factors for the Pin Load Portion of the Total Stress Intensity Equation

For crack growth analysis the Newman and Shaw portions are combined together while the other bypass stress solutions are combined with the Tada, Paris, and Irwin stress intensity solution for the pin load. The units of pressure for the material crack growth model is ksi so total stress intensity equation is presented in ksi as well. Data for the total load and the fastener load transfer are available from the 3-D FEM in steps of 0.02 inch from 0 to 0.22 inch. The points are interpolated for discrete solutions such as Bowie, Newman, and Tweed and Rooke as well as for the other solutions at the 0.01 inch midpoints. By developing a total correction factor including the stress the spectrum used for analysis can be set to unity with a stress ratio, R, of 0.1. Bearing stress and far-field stress values for the analysis are presented in Table 6-24 along with the fastener number

nine load, L, and the ‘far-field load’ which is the load summation of fasteners one through eight.

Table 6-24 Stresses as a Function of Crack Length

Crack Length	L, lbs	L/2Rt in ksi	Far-Field Load, lbs	Far-Field Stress, ksi
0	334.1	17.68	1648.6	12.12
0.02	333.7	17.66	1649.2	12.13
0.04	330.2	17.47	1651.5	12.14
0.06	326.3	17.26	1654	12.16
0.08	326.9	17.30	1652.7	12.15
0.1	323.5	17.12	1654.4	12.16
0.12	320.1	16.94	1655.8	12.18
0.14	317.5	16.80	1656.6	12.18
0.16	315.3	16.68	1656.8	12.18
0.18	312.5	16.53	1657.2	12.19
0.2	310.6	16.43	1657	12.18
0.22	308.6	16.33	1656.2	12.18

The User Defined through crack model was used in AFGROW to perform the crack growth analyses. AFGROW uses tables of correction factors called β’s to do the analysis. The β-tables were generated such that all corrections were included as was the stresses for the pin loading and remote tension cases. Thus β in this case equaled:

$$\beta = \sigma_{Bypass} F_{Bypass\ Stress} + \sigma_{Bearing} F_{Pin\ Load}$$

Equation 6-22 Beta Factors for AFGROW

The resulting crack growth curves for the seven different classical solutions are presented in Figure 6-38. Note that the discrete points of the Bowie, Newman, and Tweed and Rooke solutions are not dense enough to prevent large swings in growth due to interpolation. All three feature a large step from 0.189 inch to 0.2835 inch which is very

near the end of the ligament. This causes through interpolation a much higher stress intensity and thus much higher crack growth rate than would otherwise be expected. An interpolation method could have been used to smooth the region approaching the edge but this was useful to demonstrate the effect of uneven steps or gaps in the table of Beta factors used in analysis. Note that all the curves lie in the same general region between specimens one and four except for Broek which was a slightly unconservative approximation as mentioned previously.

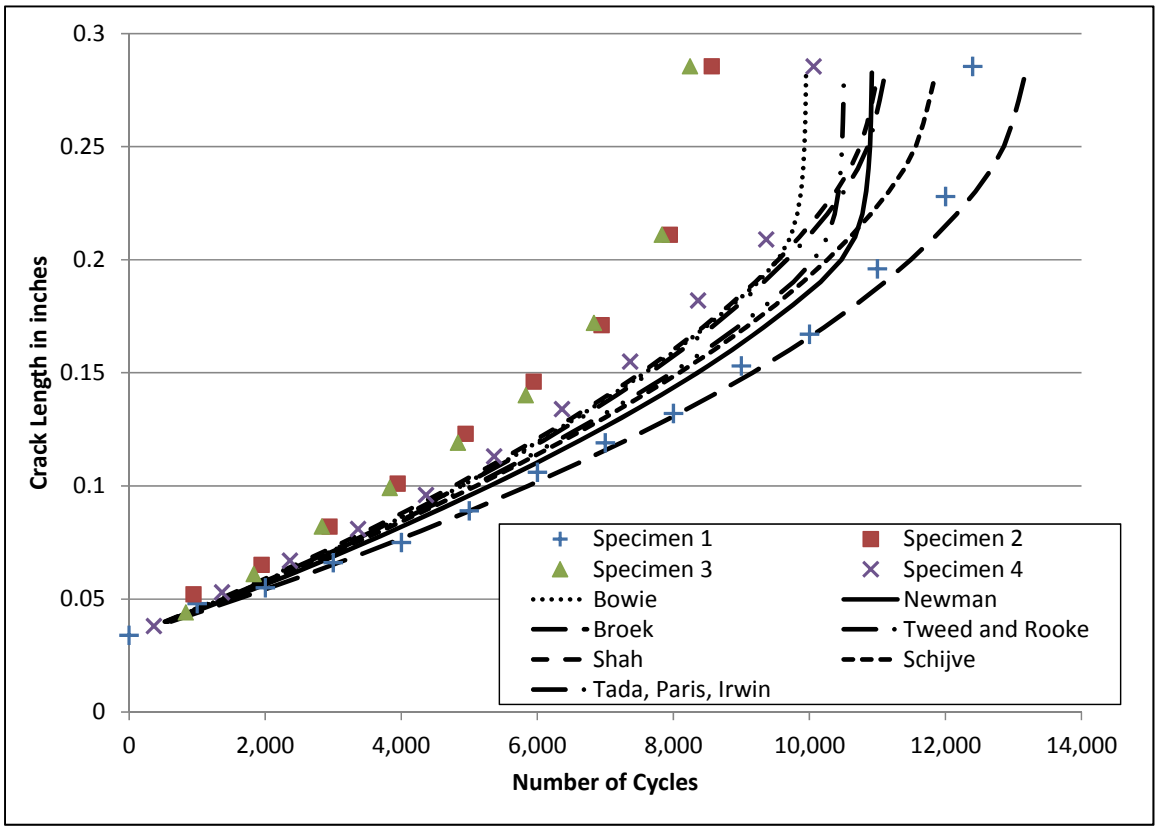

Figure 6-38 Comparison of Different Classical Solutions with the Fatigue Crack Growth Data

6.5.2 Comparison of Joint Specimens with Built-In AFGROW Models

The previous comparison reviewed the variation possible by using different stress intensity solutions with the same applied loads. This section uses a single stress intensity solution and compares different methods of determining the loads. For the sake of comparison, a conventional crack growth model was built in AFGROW using the built-in classic model of an offset hole in a plate with a through crack and the current modeling practice [355]. The geometry of the model is shown in Figure 6-39 and input values are given in Table 6-25. The previously developed material file was used in the analysis to reduce outside variation. The effective width concept considers the region affected by the bearing load. For the case presented in Figure 6-39, the effective width is generally assumed to be twice the offset. This is because much of the wider ligament is relatively unaffected by the localized effects of the bearing stress given the way the load disperses from the hole.

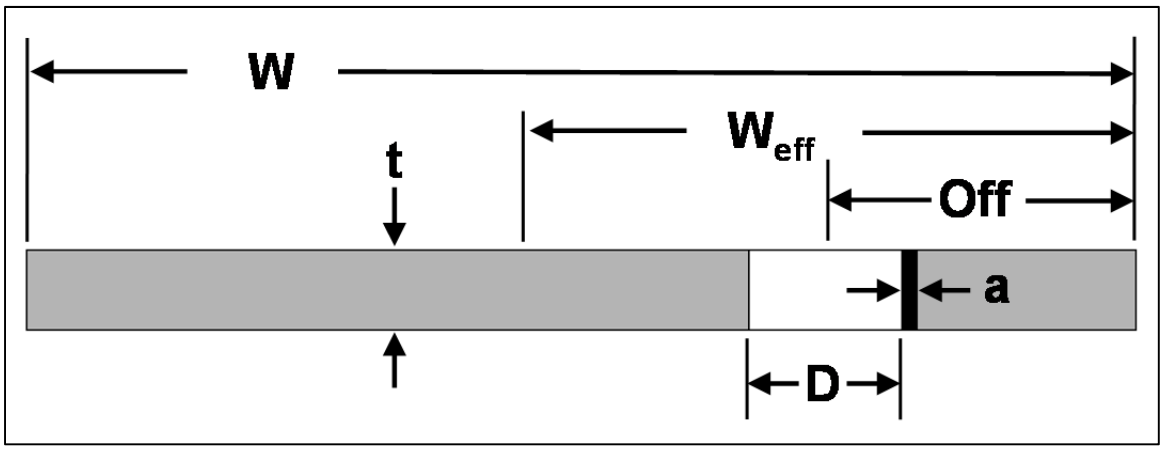

Figure 6-39 Depiction of the Basic Model Used for Crack Growth Comparisons

Table 6-25 Basic Model Geometry

Dimension	Value
Width, W	1.36 inches
Effective Width, W_{eff}	0.76 inch
Hole Offset, Off	0.38 inch
Initial Crack Length, a	0.02 inch
Hole Diameter, D	0.189 inch
Thickness, t	0.1 inch

Beyond the geometric inputs needed for analysis there are inputs to handle the tensile and bearing components. The through stress is the tensile portion and that transferred into the strap from the main plate at fastener nine comprises the bearing portion. Within AFGROW this is handled by entering a tension stress fraction which is the bypass portion of the load and a bearing stress fraction. The 'far-field' stress is used as the spectrum stress. This means that due to load transfer the tensile stress fraction will be less than one. Conversely, the bypass stress could be used as the spectrum stress and the tension stress fraction would be one. The bearing stress fraction would have to be modified as well. It is not necessary for the bearing stress fraction and the tension stress fraction to be equal to one since they simply act as modifiers to the spectrum stress to calculate stress intensities. Note that in these analyses, the bending stress fraction is zero for all cases.

Four different analyses were generated using the basic model as presented. Two of the analyses use the results of the fastener flexibility analyses; Tate and Rosenfeld, and Huth. The maximum spectrum stresses are the same but with a different load calculated at fastener nine there is a difference in the tension and bearing stress fractions. Two other analyses were done using loads from the StressCheck full splice model and the 3-D FEM. It is interesting to note that even though the Huth had the closest load distribution overall

with respect to the 3-D FEM, the Tate and Rosenfeld method had the closest load calculated at fastener nine. Inputs for the four comparisons are presented in Table 6-26. Crack growth results are presented in Figure 6-40 along with the four joint specimens.

Table 6-26 Load Properties Used in Analysis

Load Properties	3-D FEM	StressCheck Full Splice Model	Tate and Rosenfeld Equation Results	Huth Equation Results
Total Load (pounds)	1983	2000	2000	2000
Maximum Spectrum Stress (ksi)	14.6	14.7	14.7	14.7
B-9 Fastener Load (pounds)	334	336	329	392
Tension Stress Fraction	0.831	0.832	0.836	0.804
Bending Stress Fraction	0	0	0	0
Bearing Stress Fraction	0.678	0.676	0.660	0.787

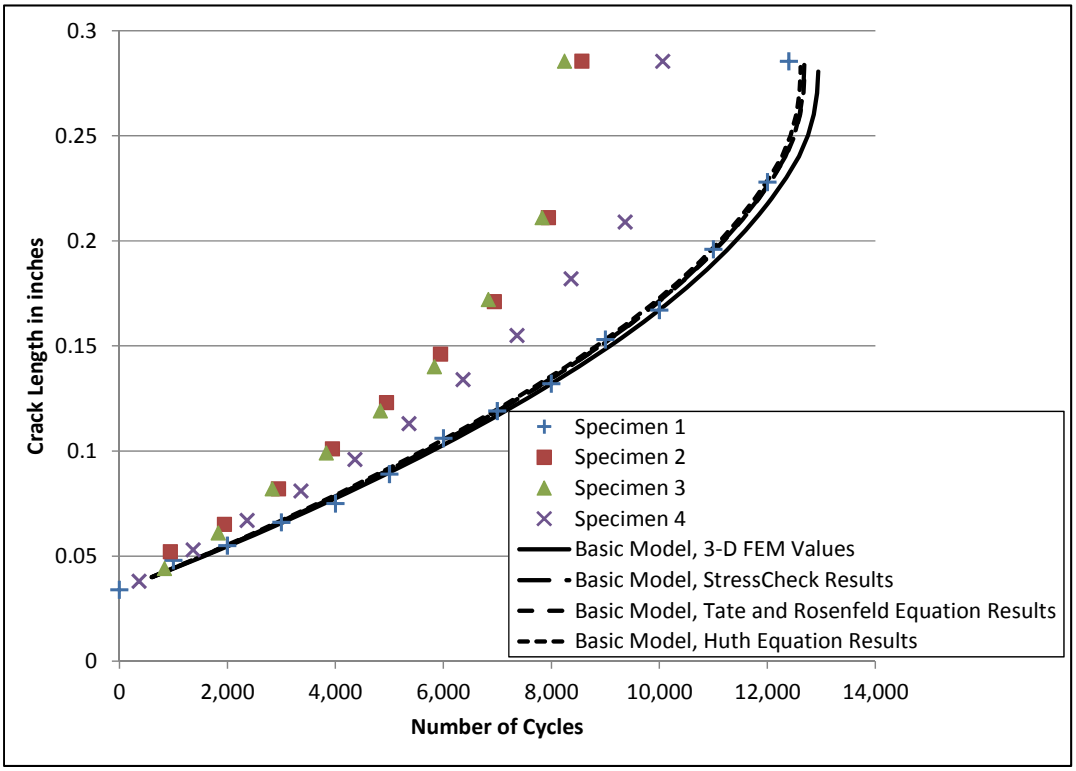

Figure 6-40 Comparison of Different Crack Growth Analyses to the Four Experiments

Overall there is very less than 3% variation in the results since the only parameters that change are the maximum spectrum stresses and what the distribution of that stress is between remote tension and pin loading. With the lower overall stress, the 3-D FEM does predict a slightly longer life than the other three comparisons but only by two percent.

The other issue is that hole fill can make a large difference in crack growth rates but the effect is greatest local to the hole. Table 6-27 presents the difference in the stress intensity correction factor calculated and presented in Table 6-11. This highlights the importance of maintenance methods to ensure hole fill or the analyst should take the more conservative approach and use stress intensities for a loaded hole with no hole propping. Solutions normal used in AFGROW include a cosine distributed force which sufficiently approximates the load distribution being transferred into the hole but does not prop the hole.

Table 6-27 Variation in Stress Intensity Correction Factor by Crack Length and Gap Size

Crack Size	0.001 inch Gap	0.002 inch Gap
0.02	7.93%	13.96%
0.04	6.74%	11.52%
0.06	5.23%	9.12%
0.08	3.58%	4.30%
0.1	3.08%	5.73%
0.12	2.39%	4.58%
0.14	1.71%	3.42%
0.16	1.18%	2.72%
0.18	1.00%	1.90%
0.2	0.50%	1.10%
0.22	-0.49%	-0.16%

7.0 CONCLUSIONS

Different methods were explored to calculate the load distribution in the fastener group and all of these methods were evaluated for a non-cracked situation. None of the fastener flexibility methods have a currently defined method to calculate the reduction of stiffness due to the presence of the crack. It was shown that the more stiff the fastener connection in terms of fastener flexibility, the less that load will by-pass the fastener to later fastener rows.

Different classical 'hand analysis' techniques were explored such as the static strength approach and the fastener flexibility approach. Both are applied in different situations with the static strength approach usually only being used in ultimate load margin calculations. However, if these loads are used for limit load calculations or are used to develop load transfer ratios for fatigue loads then considerable error might be introduced.

Also evaluated were 2-D planar methods using the StressCheck software. Both the half and full models were able to develop fastener loads within 3% of the 3-D FEM on average. One negative of these models is that the fastener element makes a wagon wheel of springs connecting to the main plate around the hole. This causes a bridging action if a crack is inserted to the hole resulting in incorrect displacements and would thus skew the fastener load distribution. This is why a contact plug was required in the 2-D StressCheck models that were used to calculate the stress intensity solution. However, if

the problem sought to evaluate a crack growing from the outside of the plate inward toward the hole then the 2-D StressCheck model using the fastener element might be more successful.

Boundary conditions used to develop stress intensity factors need to be carefully considered. Many of the 'textbook' solutions may have conditions that make their applicability to the analysis of complex details suspect. It was shown that using different classical solutions that some variability was indeed possible. More importantly, the shapes of the curves generated varied which has a profound effect on the timing of inspections using these crack growth curves. In all instances, the different solutions showed less scatter than the crack growth specimens themselves.

A second comparison was made using a single stress intensity solution but with different applied loads determined using the different methods reviewed in Section 6.5.2. The variation exhibited in this comparison was much less than that caused by using different stress intensity factors. It appears that in this situation, the variation in loads is much less than the variation due to the method of calculating stress intensities. This is highlighted by the differences between the Tate and Rosenfeld and the Huth fastener flexibilities.

The Huth equation predicted a flexibility that was 219% as stiff, a fastener load transfer at fastener nine that was almost 20% greater, but a total fatigue crack growth life of only 0.7% less. The simple fact is that each has the same far-field stress and it has to go somewhere. If it does not contribute to the stress intensity from the pin loading then it contributes through the bypass stress; and in this case, it was a fairly even trade off. Whether this is always the case or not could be determined a priori by comparing the different loading correction factors for the overall contribution of each. Even though the

analytical crack growth shows very little difference, it is important establish the intermediate data as accurately as possible because fastener loads are required for static analysis as well.

The four test specimens were of different configuration and exhibited more scatter than the different methods used to calculate fatigue crack growth. Two of the specimens almost perfectly replicated each other even though their configuration was different in that one had Teflon between the faying surfaces and the other did not. However, since the fasteners were not fully seated, it is probable that all of the specimens did not have excessive load being transferred through friction at the faying surfaces.

The stress intensities calculated based on loads from the three dimensional FEM represent a ‘best case’ where alignment is perfect and holes are fully round which may not accurately represent actual structure being to ideal. The results show that the AFGROW calculated curves’ variation between predicted crack growth and the experiments retained the best shape suggesting that little if any hole propping action occurred in the specimens.

Finally, the three dimensional FEM represents the most refined analytical load calculation method which was able to capture the out of plane behavior that was noted in the strain gage results. Some interesting aspects from the three dimensional FEM include:

- The overall difference in maximum load between the upper and lower straps from the three dimensional FEM grew from 1.7% when the crack was short to 3.6% by the time the crack was 0.22 inches in length.

- The load transferred into the cracked strap by the fastener with the crack reduced a total of 7.6% over the same change in crack length.
- The load transferred into the bottom plate by the fastener at the crack increased 2.8% over the same change in crack length.
    - The above to items might be causal in MED where additional elements nucleate cracks at locations common to cracks in adjacent structure. While additional cracks did not nucleate during this series of experiments, evidence of this was seen at this joint in actual T-38 structure during full scale fatigue testing of the fuselage.

It was shown that changes in loads do have an effect on crack growth, however limited. Therefore the hypothesis is correct and fatigue cracks do affect fastener constraint and load transferred in a multiple fastener joint which, in turn, affects the fatigue crack growth.

8.0 RECOMMENDATIONS

Ultimate load calculations usually begin with a check of the ratio of ultimate strength to yield strength. If the ratio is less than 1.5 then only an ultimate margin will be calculated since 1.5 is the magnification factor applied to limit loads to determine ultimate loads any margin safe by ultimate analysis would also be safe. However, the difference between the static strength approach to fastener loads and that of fastener flexibility call that into question. The static strength approach underpredicted the end fastener loads to an extent that would have given a false sense of security regarding a limit load margin against local yielding. Even at limit loads it may be possible for an end fastener to be approaching ultimate strength even though the average fastener load in the joint is well below the proportional limit for certain joint designs. It is recommended that in all cases of fastener joints that both a static strength ultimate load margin, and a fastener flexibility based limit load margin be calculated to ensure safety.

Two different fastener flexibility reduction assumptions were explored for the staggered rows. In all cases, the method that split the rows provided the closer approximation to the three dimensional FEM loads. The end fastener loads also were higher using the split fastener rows which provides a more conservative margin which is important to ensure safety which is, after all, the whole point of calculating a margin in the first place.

Two different fastener flexibility equations were evaluated and each gave different results. While the Huth method was the more accurate of the two overall, the end fastener loads were further off of that predicted by the three dimensional FEM. This suggests that the analyst should carefully consider that similarity of the tests that led to each empirical equation to determine its suitability. This is much more important for single shear joints where a greater variety of fastener flexibility equations exist.

For increased accuracy over a fastener flexibility method, the two dimensional planar FEM analysis is recommended since both produced more accurate results than even the optimized fastener flexibility solutions. Care should still be exercised because most would assume the experiments conducted here were pure double shear joints, symmetrical about the main plate's mid-thickness. However, it was shown this was not entirely correct thus two dimensional planar FEM results must be treated with caution for obviously non-symmetrical joints. In addition, joints with out-of-plane loads, out-of plane-fixation such as where a fuselage skin laps meet a former, highly eccentric fastener patterns and other complicating factors should be treated with care due to the possibility of out-of-plane bending and twist that might not be properly captured.

The processes used in manufacturing of specimens are sources of potential variability. The specimens were manufactured by personnel not intimately familiar with aerospace manufacturing methods and as a result, the installation of the fasteners was not truly representative of actual aircraft structure.

Verification and validation testing highlighted the differences in stress intensity solutions depending on the constraint of the model and gage length where the 'far-field' stress is applied. This also is illustrated by classic stress intensity solutions for finite width which

varied depending on the ratio of the plate's finite width to finite length. Care should always be taken to ensure that representative models are used in damage tolerance analyses especially considering the complexity of aerospace structural details. It is preferable to build a model specific to the location when possible to maximize accuracy. Automation of the software is possible so new sets of 'handbook' solutions specific the standard details for a specific aircraft would be possible.

Based on the comparisons made here and the stress intensities that were calculated for various levels of hole fill, there is a crack growth rate benefit from neat hole fill. Maintenance and manufacturing processes should be specified to produce the highest level of fill possible in critical locations. However, if the hole fill quality cannot be guaranteed, the analysis, maintenance scheduling, and inspection intervals should be based on a un-propped hole.

Some potential areas for follow on work using the groundwork of this dissertation are listed below.

- Any further testing should use a design of experiments process to develop a test plan
- A closed form modification to current fastener flexibility equations to account for the presence of a crack
- The applicability and validity of a two dimensional planar model using the StressCheck fastener element to evaluate load transfer and stress intensity with a crack growing from the edge of the plate or mid-plate toward the hole where the wagon wheel will not induce artificial crack closure effects

- An upgraded fastener element in the finite element code that was designed to only push on the side of the hole and was not allowed to pull on it as well creating a contact boundary condition between the element and the surrounding material
- Investigation of modeling techniques and variation load transfer for a standardized coupon with varying levels of fastener clamping. This may provide valuable insight into the potential decay of fastener clamping force with increased cycles.
- Further investigation of single shear fastener configurations or complex wedding cake configurations using the processes set forth in this dissertation.
- Additional testing of specimens with identical geometry as presented here with fully seated fasteners to provide a baseline for comparison to these results to establish the effect of joint manufacture quality.

9.0 REFERENCES

1. Petit, R., *How to Build an Aeroplane*, D. Van Nostrand Company, 1910

2. Fage, A., *The Aeroplane. A Concise Scientific Study*, Charles Griffin & Company, Limited, 1915

3. Barnwell, F. S., *Aeroplane Design*, McBride, Nast & Co., 1917

4. Klemin, A., Aeronautical Engineering and Airplane Design, Gardner-Moffat Co., Inc., 1918

5. Wood, L. W., "Relation of Strength to Wood to Duration of Load", Report No. 1916, Forest Products Laboratory, December 1951

6. Pippard, A. J. S., Pritchard, J. L., *Aeroplane Structures*, Longmans, Green and Co., 1919

7. Pomilio, O., *Airplane Design and Construction*, McGraw-Hill Book Co., Inc., 1919

8. Rathbun, J. B., *Aeroplane Construction and Operation*, Stanton and Van Vliet Co. Publishers, 1919

9. Hanby, W., *Metals in Aircraft Construction*, The Standard Air Press LTD., 1920

10. Swinton, A. J., *The Aeroplane Handbook*, The Aeroplane and General Publishing Company, Limited, 1920

11. Andrews, S. T. G., Benson, S. F., *The Theory & Practice of Aeroplane Design*, E. P. Dutton & Company, 1920

12. Judge, A. W., *Elementary Principles of Aeroplane Design and Construction*, Sir Isaac Pitman & Sons, Ltd., 1921

13. Royer, E. "Commercial Airplanes and Seaplanes," from "Premier Congres International de la Navigation Aerienne," Paris, November, 1921, Vol. II; translated to English and republished as NACA-TM-85, 1922

14. Woodward, R. W., "Recent Developments in Light Alloys", NACA TM-3, 1920

15. Camm, S., Aeroplane Construction, Crosby Lockwood and Son, 1919

16. Knappen, T. M. Wings of War: An Account of the Important Contribution of the United States to Aircraft Invention, Engineering, Development and Production during the World War, G. P. Putnam's Sons, 1920

17. Taylor, M. J. H., Jane's Encyclopedia of Aviation, Crescent Books, 1993

18. Anon, Wood in Aircraft Construction, Aircraft Design Data Note No. 12, U.S. Department of Agriculture, Forest Products Laboratory, 1920

19. Elmendorf, A., "Data on the Design of Plywood for Aircraft," NACA Report-84, 1920

20. Klemin, A., Airplane Stress Analysis, Ronald Press, 1929

21. Sayers, W. H., "Steel Strip Construction", "Aircraft Engineering and Aerospace Technology", Volume 3, Number 5, May 1931

22. Pollard, H. J., "Metal Construction Development, Part I, Strip Metal Construction – Fuselage", NACA TM-526, 1929

23. Pollard, H. J., "Metal Construction Development, Part II, Strip Metal Construction – Wing Spars", NACA-TM-527, 1929

24. Pollard, H. J., "Metal Construction Development, Part III, Workshop Practice, Strip Metal Construction – Wing Ribs", NACA-TM-528, 1929

25. Pollard, H. J., "Metal Construction Development, Part IV, Moments of Inertia of Thin Corrugated Sections, NACA TM-529, 1929

26. Daniels, S., Sisco, F. T., Metallurgy in Aircraft Construction, Engineering Division, U.S. Army Air Service, 1925

27. Niles, A. S., Newell, J. S., Airplane Structures, John Wiley & Sons, Inc., 1929

28. Swickard, A. E., "Metal-Truss Wing Spars", NACA TN-383, 1931

29. Anon, "Metal Aircraft Construction at Vickers", NACA-TM-440, 1927

30. Mayo, R. H. Major, "Aircraft Design Tendencies", "Aircraft Engineering and Aerospace Technology", Volume 1, Number 9, September 1929

31. Mortimer, G., "Wrought Alloys of Aluminum in Aircraft", "Aircraft Engineering and Aerospace Technology", Volume 1, Number 9, September 1929

32. Hanson, D., "Non-Ferrous Metals for Aircraft", "Aircraft Engineering and Aerospace Technology", Volume 2, Number 11, November 1930

33. Hanson, D., “Non-Ferrous Metals for Aircraft”, “Aircraft Engineering and Aerospace Technology”, Volume 2, Number 12 December 1930

34. Sutton, H., “The Corrosion of Metals”, “Aircraft Engineering and Aerospace Technology”, Volume 2, Number 8, August 1930

35. Mathar, J., “Metal Covering of Airplanes”, NACA-TM-592, 1930

36. Wagner, H., “Structures of Thin Sheet Metal, Their Design and Construction”, NACA-TM-490, 1928

37. Dix, E. H. Jr., “Alclad, A New Corrosion Resistant Aluminum Product”, NACA-TN-259, 1927

38. Aitchison, L., “Materials in Aircraft Construction”, Flight, 24 January 1924

39. Moore, H. F., Jasper, T. M., “An Investigation of the Fatigue of Metals”, Illinois Bulletin No. 152, Engineering Experiment Station, November 23, 1925

40. Grenoble, H. S., “Bearing Strength of Bolts in Wood, The Line of Force not Parallel to the Grain of the Wood”, FPL Serial TM-7, 6 June 1923

41. Grenoble, H. S., “Bearing Strength of Hollow Bolts in Wood”, Forest Products Laboratory Serial TM-1, 1925

42. Trayer, G. W., “Some Factors Influencing Fitting Design with Special Reference to the Bearing Strength of Wood under Steel Bolts”, FPL Serial TM-9 1927

43. Trayer, G. W., “Bearing Strength of Wood under Steel Aircraft Bolts and Washers”, NACA TN-296, 1928

44. Trayer, G. W., The Bearing Strength of Wood under Bolts”, USDA Technical Bulletin No. 332, 1932

45. Anon, “Design of Wood Aircraft Structures”, ANC-18, Munitions Board, Aircraft Committee,

46. Sechler, E., E., “Problems Relating to the Use of Sheet Metal in Airplane Construction”, Thesis from the California Institute of Technology, 1930

47. Mossman, R. W., Robinson, R. G., “Bending Tests of Metal Monocoque Fuselage Construction”, NACA-TN-357, 1930

48. Kahn, L. L., “Stressed Coverings in Naval and Aeronautic Construction”, NACA-TM-447

49. Hallion, R. P., “Wooden Aircraft and the Great War”, “Journal of Forest History”, Volume 22, Number 4, October 1978

50. Nelson, W., Seaplane Design, McGraw-Hill Book Company, Inc. 1934

51. The Royal Aeronautical Society, Handbook of Aeronautics; Volume I – A Compendium of the Modern Practice of Aeronautical Engineering, Sir Isaac Pitman & Sons, LTD., 1934

52. Nye, W. L., Metal Aircraft; Design and Construction, A Cadet Series Publication, Aviation Press, 1935

53. Younger, J. E., Structural Design of Metal Airplanes, McGraw-Hill Book Company, Inc. 1935

54. Langley, M., Metal Aircraft Construction, Sir Isaac Pitman & Sons, LTD., 1941

55. Loudy, F. E. Maj. Metal Airplane Structures, Norman W. Henley Publishing Company, 1938

56. Hilbes, W., “Riveted Joints in Thin Plates”, NACA TM-590, National Advisory Committee for Aeronautics, November 1930

57. Pleines, W., “Riveting in Metal Airplane Construction. Part III, Strength of Riveted Joints in Duralumin”, NACA TM-598, National Advisory Committee for Aeronautics, December 1930

58. Brimm, D. J. Jr., Boggess, H. E., Aircraft Maintenance, Pitman Publishing Corp, 1940

59. Anon, “The Use of Wood for Aircraft in the United Kingdom”, U.S. Department of Agriculture, Forest Products Laboratory Report No. 1541, June 1944

60. Garratt, G. A., “Wood in War and Peace”, U.S. Department of Agriculture, Forest Products Laboratory Report No. R1541, October 1944

61. Schuler, W. T., “Fatigue Problems in Transport Aircraft”, Aeronautical Engineering Review, Volume 10, Number 6, June 1951

62. Bland, R. B., Sandorff, P. E., “The Control of Life Expectancy in Airplane Structures”, Aeronautical Engineering Review, Vol 2, No 8, August 1943

63. Boyvey, H. O., “Fatigue – The Forgotten Member of the Design Family, Aero Digest, Volume 44, Number 1, January 1944

64. Owen, J. B. B., “Service Failures in Aircraft Structures Associated with Fatigue, Repeated or Dynamic Loads”, ARC RM-2688, August 1946

65. Johnson, J. B., “Fatigue of aircraft parts, The first of two articles on its various characteristics”, Aviation, Volume 30, Issue 8, August 1931

66. Johnson, J. B., “Fatigue of aircraft parts, The second of two articles”, Aviation, Volume 30, Issue 9, September 1931

67. Johnson, J. B., Daniels, S., “Study of some failures in aircraft plane and engine parts”, Transactions of the American Society of Steel Treatment, Volume 2, Issue 12, September 1922

68. Basquin, O. H., “The Exponential Law of Endurance Tests”, Proceedings of the Thirteenth Annual Meeting, American Society for Testing Materials, 1910

69. Moore, H. F., Text-Book of the Materials of Engineering, 4th Edition, McGraw-Hill Book Company, Inc., 1930

70. Wilson, W. M., Thomas, F. P., “Fatigue Tests of Riveted Joints”, Bulletin No 302, The Engineering Experiment Station, University of Illinois, 1938

71. Jones, J., “Fatigue Provisions in Riveted Joints”, Civil Engineering, Vol. 10, No. 6, June 1940

72. Moore, H. F., Kommers, J. B., “An Investigation of the Fatigue of Metals”, Bulletin No. 124, Engineering Experiment Station, University of Illinois, October 1921

73. Mann, J. Y., *Fatigue of Materials; An Introductory Text*, Melbourne University Press, 1967

74. Gough, H. J., *The Fatigue of Metals*, Ernest Benn Limited, 1926

75. Moore, H. F., Kommers, J. B., *The Fatigue of Metals; With Chapters on the Fatigue of Wood and of Concrete*, McGraw-Hill Book Company, Inc., 1927

76. Templin, R. L., “Fatigue Machines for Testing Structural Units”, Proceedings ASTM, Volume 39, 1939

77. Schütz, W., “A History of Fatigue”, Engineering Fracture Mechanics, Volume 52, No. 2, 1996

78. Pugsley, A. G., “Repeated Loading on Structures”, *The Failure of Metals by Fatigue*, Melbourne University Press, 1947

79. Davis, D. M., “Fatigue Failure of Aircraft Parts – Their Cause and Cure”, Automotive and Aviation Industries, Volume 92, Issue 9, May 1945

80. Wills, H. A., “The Life of Aircraft Structures”, *Second International Aeronautical Conference, New York May 24-27, 1949*, Berneice H. Jarck, ed., Institute of the Aeronautical Sciences, Inc., 1949

81. Arnstein, K., “Fatigue Failures in Aircraft”, Proceedings of the Society for Experimental Stress Analysis, Volume 2, Issue 2, 1946

82. Lundberg, B., “Bear-Up Requirements for Aircraft”, Aero Digest, Volume 55, No. 6, December 1947

83. Sutton. H., “Fatigue Problems Associated with Aircraft Materials”, *The Failure of Metals by Fatigue*, Melbourne University Press, 1947

84. Jewett, F. D., Gordon, S. A., “Repeated Load Test – Some Experimental Investigations on Aircraft Components”, Proceedings of the Society of Experimental Stress Analysis, Volume 3, Issue 1, 1945

85. Jacobson, J. M., “Problems of Aircraft Life Evaluation”, SAE Quarterly Transactions, Volume 3, No. 4, 1949

86. Piper, T. E., Finlay, K. F., Binsacca, A. P., “Fatigue Characteristics of Aircraft Materials and Fastenings”, Bulletin American Society for Testing Materials, Volume 166, May 1950

87. Munier, A. E., “Fatigue of Combat Aircraft”, Aero Digest, Volume 70, No 4, April 1955

88. Anon., “Airframe Fatigue”, Flight, Volume 67, No. 2408, 18 March 1955

89. Giddings, H., “Aircraft Fatigue”, Journal of the Royal Aeronautical Society, Volume 60, Issue 545, May 1956

90. Anon., “More Thoughts on Fatigue”, The Aeroplane, Volume 88, Issue 2278, March 1955

91. Anon, “Comet Court of Inquiry”, The Engineer, Volume 189, Issue 5153, October 1954

92. Anon, “Comet: Fatigue Caused Jet Crashes”, Iron Age, Vol 174, October 1954

93. Atkinson, R. J., Winkworth, W. J., Norris, G. M., “Behaviour of Skin Fatigue Cracks at the Corners of Windows in a Comet I Fuselage”, ARC RM-3248, 1962

94. Anon, “The Comet Investigations at Farnborough”, Engineering London, Vol 178, Issue 4631, October 1954

95. Anon, “Comet Crash Inquiry Aids Future Aircraft Design”, Product Engineering, Volume 26, Issue 1, January 1955

96. Duncan, W. J., “The Comet and Design Against Fatigue”, Engineering London, Volume 179, Issue 4647, February 1955

97. Bishop, T., “Fatigue and the Comet Disasters”, Metal Progress, Volume 67, Issue 5, May 1955

98. Walker, P. B., “The Experimental Approach to Aircraft Structural Research”, Aircraft Engineering, Volume 24, No. 3, March 1952

99. Anon, “Aircraft Fatigue Tests at Farnborough”, Engineering London, Volume 177, Issue 4592, January 1954

100. Tye, W., “The Outlook on Airframe Fatigue”, Journal of the Royal Aeronautical Society, Volume 59, Issue 533, May 1955

101. Bishop, T., “Designed to Fly…High”, Metal Progress, Volume 75, Issue 3, March 1959

102. Anon, “Argosy, First of a Family of Transport Aircraft”, Engineering London, Volume 187, Issue 4845, January 1959

103. Winkworth, W. J., “The Fatigue Testing of Aircraft Structures”, Full-Scale Fatigue Testing of Aircraft Structures, F. J. Plantema and J. Schijve, ed., Pergamon Press, 1961

104. Anon, “Fatigue Life and Safety Stressed in DC-8 Design”, Machine Design, Volume 31, Issue 18, September 1959

105. Vallat, P., “Caravelle Structure Designed for Good Fatigue Strength”, Aviation Age, Volume 27, Issue 5, May 1957

106. Larré, R., “Installation Developed for Full-Scale Fatigue Testing of the SE-210 Caravelle Aircraft”, Full-Scale Fatigue Testing of Aircraft Structures, F. J. Plantema and J. Schijve, ed., Pergamon Press, 1961

107. Vallat, P, “Caravelle, Complete Structure Fatigue Tests Development and Analysis”, Full-Scale Fatigue Testing of Aircraft Structures, F. J. Plantema and J. Schijve, ed., Pergamon Press, 1961

108. Atkinson, R. J., “Fatigue Testing in Relation to Transport Aircraft”, Fatigue in Aircraft Structures, A. M. Freudenthal ed., Academic Press Inc., 1956

109. Van Beek, I. E., “Full-Scale Fatigue Tests on the Fokker Friendship”, Full-Scale Fatigue Testing of Aircraft Structures, F. J. Plantema and J. Schijve, ed., Pergamon Press, 1961

110. Samson, D. R., "The Fatigue Testing of the Jet Provost", Full-Scale Fatigue Testing of Aircraft Structures, F. J. Plantema and J. Schijve, ed., Pergamon Press, 1961

111. Locati, L., Sarzotti, G., "Fatigue Ratio as Design Evaluation of Aircraft Structures", Full-Scale Fatigue Testing of Aircraft Structures, F. J. Plantema and J. Schijve, ed., Pergamon Press, 1961

112. Nicole, W., "Some Results of Fatigue Tests with Parts of Vital Importance of the Ground-Attacker P-16", Full-Scale Fatigue Testing of Aircraft Structures, F. J. Plantema and J. Schijve, ed., Pergamon Press, 1961

113. Johnstone, W. W., Payne, A. O., "Aircraft Structural Fatigue Research in Australia", Fatigue in Aircraft Structures, A. M. Freudenthal ed., Academic Press Inc., 1956

114. Payne, A. O., "Determination of the Fatigue Resistance of Aircraft Wings by Full-Scale Testing", Full-Scale Fatigue Testing of Aircraft Structures, F. J. Plantema and J. Schijve, ed., Pergamon Press, 1961

115. Hooke, F. H., Langford, P. S., "Australian Work on Aircraft Fatigue and Life Evaluation", Aircraft Engineering, Volume 28, Number 12, December 1956

116. Huston, W. B., "Comparison of Constant-Level and Randomized-Step Tests of Full-Scale Structures as Indicators of Fatigue-Critical Components", Full-Scale Fatigue Testing of Aircraft Structures, F. J. Plantema and J. Schijve, ed., Pergamon Press, 1961

117. Whaley, R. E., McGuigan, M. J., Bryan, D. F., "Fatigue-Crack-Propatation and Residual-Static-Strength Results on Full-Scale Transport-Airplane Wings", NACA TN-3847, National Advisory Committee for Aeronautics, December 1956

118. Stambler, I., "Boeing Designs 707 Structure for Long Fatigue Life", Aviation Age, Volume 28, Issue 2, August 1957

119. Goran, L. A., "Fatigue Strength of Structures Having Bolted Connections", Proceedings of the American Helicopter Society's Annual National Forum, May 1956

120. Stephenson, B. E., "Fatigue in Aircraft Design", Journal of the Royal Aeronautical Society, Volume 57, Issue 513, September 1953

121. Heywood, R. B., *Designing Against Fatigue of Metals*, Reinhold Publishing Corporation, 1962

122. Miner, M. A., "Cumulative Damage in Fatigue", Journal of Applied Mechanics, American Society of Mechanical Engineers, September 1945

123. Bachman, R. W., Wells, H. M. Jr., "Detail Requirements and Status Air Force Structural Integrity Program", Aeronautical Systems Division (ASD) TN-61-142, Structures and Air Environment Division, September 1961

124. Raithby, K. D., "A Comparison of Predicted and Achieved Fatigue Lives of Aircraft Structures", *Fatigue of Aircraft Structures*, Pergamon Press,1963

125. Lowndes, H. B. Jr., Miller, W. B., "The U.S. Air Force Weapon Systems Fatigue Certification Program", *Fatigue Design Procedures*, E. Gassner and W. Schütz, ed., Pergamon Press, 1969

126. Rosenfeld, M. S., "Predictive Testing of Aircraft Structures", *Testing for Prediction of Material Performance in Structures and Components, ASTM STP 515*, American Society for Testing and Materials, 1972

127. Turner, F., "Aspects of Fatigue Design of Aircraft Structures", *Fatigue in Aircraft Structures*, A. M. Freudenthal ed., Academic Press Inc., 1956

128. Freudenthal, A. M., "The Expected Time to First Failure", AFML-TR-66-37, Air Force Materials Laboratory, February 1966

129. Shanley, F. R., "Fatigue Analysis of Aircraft Structures", RM-1127, Rand Corporation, 1953

130. Walker, P. B., "Estimation of the Fatigue Life of a Transport Aircraft", Journal of the Royal Aeronautical Society, Volume 57, Issue 514, October 1953.

131. Nissen, O., "Fatigue in Aeroplane Structures, A German Appreciation of the Relationship of Recurrent Stresses and Structural Failure", Aircraft Engineering, Volumen 12, Issue 140, October 1940

132. Williams, K., Fatigue Life of Wing Components for Civil Aircraft, Journal of the Royal Aeronautical Society, Volume 56, Issue 503, November 1952

133. Walker, P. B., "Design Criterion for Fatigue of Wings", Journal of the Royal Aeronautical Society, Volume 57, Issue 505, January 1953

134. Kennedy, A. P., "A Method for Determining the "Safe" Life of an Aircraft Wing from Fatigue Test Results", Journal of the Royal Aeronautical Society, Volume 58, Issue 521, May 1954.

135. Schijve, J., "The Endurance under Program-Fatigue Testing", Full-Scale Fatigue Testing of Aircraft Structures, Proceedings of the Symposium held in Amsterdam, 5th – 11th June 1959, Pergamon Press, 1961

136. Schijve, J., "Estimation of Fatigue Performance of Aircraft Structures", Symposium on Fatigue Tests of Aircraft Structures: Low-Cycle, Full-Scale, and Helicopters, ASTM STP 338, ASTM, 1963

137. ESDU, "The Cumulative Damage of Aluminum Alloy Specimens Under Variable Amplitude Fatigue Loading", ESDU 69024, October 1969

138. Wills, H. A., "Structural Fatigue", Aircraft, Volume 28, Issue 8, May 1950

139. Harpur, N. F., Discussion of "Fatigue Evaluation of Aircraft Structures", Full-Scale Fatigue Testing of Aircraft Structures, Proceedings of the Symposium held in Amsterdam, 5th – 11th June 1959, Pergamon Press, 1961

140. Locati, L., Sarzotti, G., "Fatigue Ratio as Design Evaluation", Full-Scale Fatigue Testing of Aircraft Structures, Proceedings of the Symposium held in Amsterdam, 5th – 11th June 1959, Pergamon Press, 1961

141. Kirkby, W. T., Edwards, P. R., "Constant Amplitude or Variable Amplitude Tests as a Basis for Design Studies", Fatigue Design Procedures, E. Gassner and W. Schütz, ed., Pergamon Press, 1969

142. Burns, A., "Fatigue Loadings in Flight: Loads in the Tailplane and Fin of a Varsity", ARC CP-245, 1956

143. Burns, A., "Fatigue Loadings in Flight: Loads in the Wing of a Varsity", ARC CP-285, 1956

144. Wells, E. W., "Fatigue Loadings in Flight Loads in the Fuselage and Nose Undercarriage of a Varsity", ARC CP-287, 1956

145. Burns, A., "Fatigue Loadings in Flight: Loads in the Tailplane of a Comet I", ARC CP-363, 1957

146. Burns, A, "Fatigue Loadings in Flight: Loads in the Tailplane and fin of a Jet Provost", ARC CP-440, 1959

147. Burns, A., "Fatigue Loadings in Flight: Loads in the Tailplane of a Devon", ARC CP-472, 1960

148. Wells, E. W., "Fatigue Loadings in Flight: Loads in the Nose Undercarriage and Wing of a Valiant", ARC CP-521, 1960

149. McGuigan, M. J., Bryan, D. F., Whaley, R. E., "Fatigue Investigation of Full-Scale Transport-Airplane Wings: Summary of Constant-Amplitude Tests Through 1953", NACA TN-3190, National Advisory Committee for Aeronautics, March 1954

150. Raithby, K. R., Longson, J., “Some Fatigue Characteristics of a Two Spar Light Alloy Structure (Meteor 4 Tailplane)”, ARC CP-258, 1956

151. Parish, H. E., “Fatigue Test Results and Analysis of 42 Piston Provost Wings”, ARC RM-3474, 1967

152. Molent, L., “The History of Structural Fatigue Testing at Fishermans Bend Australia”, Defence Science and Technology Organization, DSTO-TR-1773, October 2005

153. Kepert, J. L., Payne, A. O., “Interim Report on Fatigue Characteristics of a Typical Metal Wing”, NACA TM-1397, National Advisory Committee for Aeronautics, March 1956

154. McBrearty, J. F., “Airframe Design”, SAE Transactions, Volume 64, 1956

155. Anon., “Fail-Safe Airframe Design”, Flight, Volume 69, Issue 2463, 6 April 1956

156. McBrearty, J. F., To Prevent Catastrophic Failure due to Fatigue Aircraft Structures Must be Fail Safe, SAE Transactions, Vol 64, Issue 6, June 1956

157. Hardrath, H. F., Whaley, R. E., “Fatigue-Crack Propagation and Residual Static Strength of Built-Up Structures”, National Advisory Committee for Aeronautics, TN-4012, May 1957

158. Kuhn, P., Peters, R. W., “Some Aspects of Fail-Safe Design of Pressurized Fuselages”, National Advisory Committee for Aeronautics, TN-4011, June 1957

159. Anon., “Fail-Safe Aircraft Pressure Cabins – Hoop Reinforcement Limits Cracking”, Engineering London, Volume 184, Issue 4787, 6 December 1957

160. Harpur, N. F., “Fail-Safe Structural Design”, Journal of the Royal Aeronautical Society, Volume 62, Issue 569, May 1958

161. Lincoln, J. W., “Damage Tolerance – USAF Experience”, *Durability and Damage Tolerance in Aircraft Design*, EMAS, 1985

162. Various, *Manual on Low Cycle Fatigue Testing, ASTM STP 465*, American Society for Testing and Materials, 1969

163. Various, *Cyclic Stress-Strain Behavior – Analysis, Experimentation, and Failure Prediction, ASTM STP 519*, American Society for Testing and Materials, 1973

164. Various, *Mechanics of Crack Growth, ASTM STP 590*, American Society for Testing and Materials

165. Various, *Fatigue Crack Growth Under Spectrum Loads, ASTM STP 595,* American Society for Testing and Materials, 1976

166. Rich, D. L., Impellizzeri, L. F., "Fatigue Analysis of Cold-Worked and Interference Fit Fastener Holes", *Cyclic Stress-Strain and Plastic Deformation Aspects of Fatigue Crack Growth, ASTM STP 637,* American Society for Testing and Materials, 1977

167. Rudd, J. L., Yang, J. N., Manning, S. D., Garver, W. R., "Durability Design Requirements and Analysis for Metallic Airframes", *Design of Fatigue and Fracture Resistant Structures, ASTM STP 761,* American Society for Testing and Materials, 1982

168. Manning, S. D., Garver, W. R., Henslee, S. P., Norris, J. W., Pendley, B. J., Speaker, S. M., Smith, V. D., Yee, B. G. W., "Durability Methods Development, Volume I, Phase I Summary", AFFDL-TR-79-3118, September 1979

169. Manning, S. D., Flanders, M. A., Garver, W. R., Kim, Y. H., "Durability Methods Development, Volume II, Durability Analysis: State-of-the-Art Assessment", AFFDL-TR-79-3118, September 1979

170. Pendley, B. J., Henslee, Manning, S. D., "Durability Methods Development, Volume III, Structural Durability Survey: State-of-the-Art Assessment", AFFDL-TR-79-3118, September 1979

171. Shinozuka, M, "Durability Methods Development, Volume IV, Initial Quality Representation", AFFDL-TR-79-3118, September 1979

172. Yang, J. N, Manning, S. D., Garver, W. R., "Durability Methods Development, Volume V, Durability Analysis Methodology Development", AFFDL-TR-79-3118, September 1979

173. DoD, "Aircraft Structural Integrity Program, Airplane Requirements", MIL-STD-1530A, Air Force Aeronautical Systems Division, December 1975

174. DoD, "Airplane Damage Tolerance Requirements", MIL-A-83444, Air Force Systems Division, July 1974

175. Wood, H. A., Engle, R. M., "USAF Damage Tolerance Design Handbook: Guidelines for the Analysis and Design of Damage Tolerant Aircraft", AFFDL-TR-79-3021, March 1979

176. Rudd, J. L., Brussat, T. R., Chiu, S. T., Creager, M., "Experimental Evaluation of Initial Flaw Criticality and Analysis Methods for Damage Tolerant Air Force Aircraft", *Design of Fatigue and Fracture Resistant Structures, ASTM STP 761,* American Society for Testing and Materials, 1982

177. DOD, Airplane Strength and Rigidity, Ground Tests", MIL-A-8867B, Air Force Aeronautical Systems Division, August 1975

178. Hoeppner, D. W., "Parameters that Input to Application of Damage Tolerance Concepts to Critical Engine Components", "Damage Tolerance Concepts for Critical Engine Components, AGARD-CP 393", NATO-AGARD, August 1985

179. Griffith, A. A., "The Phenomena of Rupture and Flow in Solids", Philosophical Transactions, Royal Society of London, Series A, Volume 221, 1921

180. Griffith, A. A., "The Theory of Rupture", Proceedings of the First International Congress of Applied Mechanics, 1924

181. Broek, D., *Elementary Engineering Fracture Mechanics, 4th Edition*, Martinus Nijhoff Publishers, 1986

182. Irwin, G., "Fracture Dynamics", *Fracturing of Metals*, American Society for Metals, 1948

183. Cambell, J. E., Gerberich, W. W., Underwood, J. H., *Application of Fracture Mechanics for Selection of Metallic Structural Materials*, American Society for Metals, 1982

184. Janssen, M., Zuidema, J., Wanhill, R. J. H., *Fracture Mechanics, 2nd Edition*, Delft University Press, 2002

185. Broek, D., *The Practical Use of Fracture Mechanics*, Kulwer Academic Publishers, 1989

186. Paris, P. C., Sih, G. C., "Stress Analysis of Cracks", *Fracture Toughness Testing and its Applications, ASTM STP 381,* American Society for Testing and Materials, 1965

187. Bowie, O. L., "Rectangular Tensile Sheet with Symmetric Edge Cracks", Journal of Applied Mechanics, Series E, Volume 31, Number 2, American Society of Mechanical Engineers, June 1964

188. Paris, P. C., Erdogan, F., "A Critical Analysis of Crack Propagation Laws", Journal of Basic Engineering, Transactions of the ASME, Volume 85, December 1963

189. Forman, R. G., Hearney, V. E., Engle, R. M., "Numerical Analysis of Crack Propagation in Cyclic-Loaded Structure", Journal of Basic Engineering, Transactions of the ASME, Volume 89, 1967

190. Walker, K., "The Effect of Stress Ratio During Crack Propagation and Fatigue for 2024-T3 and 7075-T6 Aluminum", *Effects of Environment and Complex Load History on Fatigue Life, ASTM STP 462,* American Society for Testing and Materials, 1970

191. Forman, R. G., Mettu, S. R., "Behavior of Surface and Corner Cracks Subjected to Tensile and Bending Loads in Ti-6Al-4V Alloy", *Fracture Mechanics: Twenty-second Symposium, Volume I, ASTM STP 1131*, American Society for Testing and Materials, 1992

192. McEvily, A. J., "On the Quantitative Analysis of Fatigue Crack Growth Propagation", *Fatigue Mechanisms: Advances in Quantitative Measurement of Physical Damage, ASTM STP 811*, American Society for Testing and Materials, 1983

193. Elber, W., "The Significance of Fatigue Crack Closure", Damage Tolerance in Aircraft Structures, ASTM STP 486, American Society for Testing and Materials, 1971

194. Willenborg, J., Engle, R. M., Wood, H. A., "A Crack Growth Retardation Model Using an Effective Stress Concept", AFFDL, TM-71-1-FBR, January 1971

195. Wheeler, O. E., "Spectrum Loading and Crack Growth", Journal of Basic Engineering, Series D, Volume 94, Number 1, Transactions of the American Society of Mechanical Engineers, March 1972

196. Gallagher, J. P., "A Generalized Development of Yield Zone Models", AFFDL-TM-FBR-74-28, January 1974

197. Newman, J. C., "Prediction of Fatigue Crack Growth under Variable-Amplitude and Spectrum Loading using a Closure Model", Design of Fatigue and Fracture Resistant Structures, ASTM STP 761, American Society for Testing and Materials, 1982

198. Kathiresan, K., Hsu, T. M., Brussat, T. R., "Advanced Life Analysis Methods – Crack Growth Analysis Methods for Attachment Lugs, Volume II", AFWAL-TR-84-3080, September 1984

199. Deiters, T. W., "Hsu Model", AFRL-RB-WP-TR-2008-3, 2008

200. Department of Defense, "Aircraft Structural Integrity Program (ASIP)", MIL-STD-1530C, 1 November 2005

201. Department of Defense, "Aircraft Structures", JSSG-2006, 30 October 1998

202. Gottlieb, R., "Test Data on the Shear Strength of Machine Countersunk-Riveted Joints Assembled by an NACA Flush-Riveting Procedure", NACA WR-L-523, 1942

203. Mandel, M. W., Schuette, E. H., "Test Data on the Shear Strength of Joints Assembled with Round-Head and Brazier-Head Rivets", NACA WR-L-519, 1943

204. Carter, J. W, Lenzen, K. H., Wyly, L. T., "Fatigue in Riveted and Bolted Single Lap Joints", Proceedings American Society of Civil Engineers Volume 80, Separate No. 469, August 1954

205. Baron, F. M., Larson, E. W. Jr., "Comparative Behavior of Bolted and Riveted Joints", Proceedings American Society of Civil Engineers Volume 80, Separate No. 470, August 1954

206. Hechtman, R. A., Chin, A. G., Savikko, E. K., "Slip of Joints Under Static Loads", Proceedings American Society of Civil Engineers Volume 80, Separate No. 484, September 1954

207. Ramkumar, R. L., Tossavainen, E., "Bolted Joints in Composite Structures: Design, Analysis and Verification; Task II Test Results –Multifastener Joints", AFWAL-TR-85-3065, August 1985

208. Ekh, J., "Multi-Fastener Single-Lap Joints in Composite Structures", Doctoral Thesis, Royal Institute of Technology, Stockholm, Sweden, May 2006

209. Gunbring, F., "Prediction and Modelling of Fastener Flexibility Using FE", LIU-IEI-TEK-A—08/00368—SE, Masters Thesis, Linköping University Institute of Technology, 2008

210. Hart-Smith, L. J., "Design Methodology for Bonded-Bolted Composite Joints, Vol. 1, Analysis Derivations and Illustrative Solutions", AFWAL-TR-81-3154, February 1982

211. Ramkumar, R. L., "Strength Analysis of Composite and Metallic Plates Bolted Together by a Single Fastener", AFWAL-TR-85-3064, August 1985

212. Lougheed, V. Vehicles of the Air: A Popular Exposition of Modern Aeronautics with Working Drawings, The Reilly and Britton Co., Chicago, 1909

213. Reithmaier, L., *Standard Aircraft Handbook for Mechanics and Technicians, 6th Edition*, McGraw-Hill, 1999

214. Crane, D., *Aviation Mechanic Handbook*, 3rd Edition, ASA-M-HB3, Aviation Supplies and Academics, Inc., 2002

215. Barrett, R. T., "Fastener Design Manual", NASA Reference Publication 1228, National Aeronautics and Space Administration, 1990

216. USAF, "Technical Manual, Engineering Manual Series, Aircraft and Missile Repair, Structural Hardware", TO 1-1A-8, 15 May 2003

217. Aerospace Industries Association, "Fastener Code", National Aerospace Standard NAS 523 Revision 28, 8 February 1993

218. Swift, T., "Repairs to Damage Tolerant Aircraft", Presented to International Symposium on Structural Integrity of Aging Airplanes, Atlanta, GA., March 20-22, 1990

219. Swift, T., "Development of Fail-Safe Design Features of the DC-10", *Damage Tolerance in Aircraft Structures, ASTM STP 486,* American Society for Testing and Materials, 1971

220. Tate, M. B., Rosenfeld, S. J., "Preliminary Investigation on Loads Carried by Individual Bolts in Bolted Joints," NACA TN-1051, National Advisory Committee for Aeronautics, Washington, DC, 1946

221. Rosenfeld, S. J., "Analytical and Experimental Investigation of Bolted Joints", NACA TN-1458, National Advisory Committee for Aeronautics, October 1947

222. de Rijck, J. J. M., "Stress Analysis of Fatigue Cracks in Mechanically Fastened Joints", Ph.D. Dissertation, Technical University Delft, 2005

223. Huth, H., "Influence of Fastener Flexibility on the Prediction of Load Transfer and Fatigue Life for Multiple-Row Joints", *Fatigue in Mechanically Fastened Composite and Metallic Joints, ASTM STP 927,* American Society for Testing and Materials, 1986

224. Huth, H., Zum Einfluß der Nietnachgiebigkeit mehrriehiger Nietverbindungen auf die Lastübertragungs- und Lebensdauervorhersage", LBF Report No. FB-172, Dissertation, Technische Universität Munchen, Munich, Germany, 1984

225. Morris, G., Defining a Standard Formula and Test-Method for Fastener Flexibility in Lap-Joints, Dissertation, Technical University Delft, 2004

226. Niu, M., *Airframe Stress Analysis and Sizing*, 2nd Edition, Conmilit Press Ltd., 2001

227. Vogt, F., "The Load Distribution in Bolted or Riveted Joints in Light Alloy Structures," NACA TM-1135, National Advisory Committee for Aeronautics, Washington, DC, 1947

228. Ross, R. D., "An Electrical Computer for the Solution of Shear-Lag and Bolted-Joint Problems," NACA TN-1281, National Advisory Committee for Aeronautics, May 1947

229. Demarkles, L. R., "Investigation of the Use of a Rubber Analog in the Study of Stress Distribution in Riveted and Cemented Joints", NACA TN-3413, National Advisory Committee for Aeronautics, November 1955

230. Vogt, F., "The Distribution of Loads on Rivets Connecting a Plate to a Beam Under Transverse Loads", NACA TM-1134, National Advisory Committee for Aeronautics, April 1947

231. McCombs, W. F., McQueen, J. C., Perry, J. L., "Analytical Design Method for Aircraft Structural Joints", AFFDL-TR-67-184, Air Force Flight Dynamics Laboratory, January 1968

232. Harris, H. G., Ojalvo, I. U., Hooson, R. E., “Stress and Deflection Analysis of Mechanically Fastened Joints”, AFFDL-TR-70-49, Air Force Flight Dynamics Laboratory, May 1970

233. Barrois, W. “Stresses and Displacements Due to Load Transfer by Fasteners in Structural Assemblies”, Engineering Fracture Mechanics, Volume 10, 1978

234. Iyer, K., Bastias, P. C., Rubin, C. A., Hahn, G. T., “Local Stresses and Distortions of a Three-dimensional, Riveted Lap Joint”, WL-TR-96-4093 Proceedings of the 1995 USAF Structural Integrity Program Conference, August 1996

235. Actis, R. L., Szabo, B. A., “Modeling Fastened Structural Connections Using Finite Elements”, AFRL ML-WL-TR-1988-4134 Proceedings of the 1997 USAF Aircraft Structural Integrity Program Conference, Volume II, August 1998

236. Hahn, G. T., Iyer, K. A., Rubin, C. A., *Structural Shear Joints; Analyses, Properties and Design for Repeat Loading*, ASME Press, 2005

237. De Rijck, J. J. M., “Stress Analysis of Fatigue Cracks in Mechanically Fastened Joints”, Technical University Delft, 2005

238. Hartmann, E. C., Holt, M., Eaton, I. D., “Additional Static and Fatigue Tests of High-Strength Aluminum-Alloy Bolted Joints,” NACA TN-3269, National Advisory Committee for Aeronautics, Washington, DC, 1954

239. Higgins, T. R., “Bolted Joints Found Better Under Fatigue”, Engineering-News Record, Volume 147, Issue 5, August 1951

240. Baron, F., Larson, E. W., “Comparative Behavior of Bolted and Riveted Joints”, Proceedings of the American Society of Civil Engineers, Volume 80 , Issue 470, Aug 1954

241. Fisher, W. A. P., Winkworth, W. J., “The Effect of Tight Clamping on the Fatigue Strength of Joints”, Aeronautical Research Council, Reports and Memoranda No. 2873, February 1952

242. Swift, T., “Repairs to Damage Tolerant Aircraft”, Presented at the International Symposium on Structural Integrity of Aging Airplanes, Atlanta, Georgia, 20-22 March, 1990

243. Langley, M., “On Solid Rivets”, Flight, May 29, 1931

244. Shanley, F. R., Basic Structures, John Wiley & Sons, Inc., 1944

245. Mangurian, G. N., Johnston, N. M., Aircraft Structural Analysis, Prentice-Hall, Inc., 1947

246. Sechler, E. E., Dunn, L. G., Airplane Structural Analysis and Design, John Wiley & Sons, Inc., 1942

247. Barton, M. V., Fundamentals of Aircraft Structures, Prentice-Hall, Inc, 1948

248. Bruhn, E. F., Analysis and Design of Airplane Structures, Tri-State Offset Company, 1949

249. Peery, D. J., Aircraft Structures, McGraw-Hill Book Company, Inc., 1950

250. Maddux, G. E., Vorst, L. A., Giessler, F. J., Moritz, T., "Stress Analysis Manual", AFFDL-TR-69-42, Air Force Flight Dynamics Laboratory, August 1969

251. Bruhn, E. F., Analysis and Design of Flight Vehicle Structures, Tri-State Offset Company, 1973

252. Flabel, J. C., Practical Stress Analysis for Design Engineers, Lake City Publishing Company, 1997

253. Wanttaja, R. J., "Kit Airplane Construction, 3rd Edition", McGraw-Hill Companies, Inc., 2006

254. Spencer, R., "Aircraft Woodwork, 2nd Edition", TAB Books, Inc., 1982

255. Markwardt, L. J., Wilson, T. R. C., "Strength and Related Properties of Woods Grown in the United States", U. S. Department of Agriculture, Technical Bulletin No. 479, September 1935

256. Wood, L. W., "Variation of Strength Properties in Woods used for Structural Purposes", U.S. Department of Agriculture, Forest Products Laboratory No. 1780, April 1960

257. Tiemann, H. D., "The Effect of the Speed of Testing Upon the Strength of Wood and the Standardization of Tests for Speed", Proceedings of the American Society for Testing Materials, Vol 8, 1908

258. Liska, J. A., "Effect of Rapid Loading on the Compressive and Flexural Strength of Wood", U. S. Department of Agriculture, Forest Products Laboratory No. R1767, June 1950

259. Anon, "Wood Handbook, Basic Information on Wood as a Material of Construction with Data for Its Use in Design and Specification", Agricultural Handbook No. 72, U.S. Department of Agriculture, 1955

260. Brokaw, M. P., Foster, G. W., "Effect of Rapid Loading and Duration of Stress on the Strength Properties of Wood Tested in Compression and Flexure", U.S. Department of Agriculture, Forest Products Laboratory No. 1518, 1958

261. American Institute of Timber Construction, “Timber Construction Manual, First Edition”, John Wiley and Sons, Inc., 1966

262. Wood, L. W., “Behavior of Wood Under Continued Loading”, Engineering News-Record, Vol 139, Issue 24, 1947

263. Raithby, K. D., “Effects of Rate and Duration of Loading on the Strength of Aircraft Structures”, Aeronautical Research Council, Reports and Memoranda No. 2736, May, 1949

264. Newlin, J. A., “Bearing Strength of Wood at Angle to the Grain”, U.S. Department of Agriculture, Forest Products Laboratory No. 1203, 1956

265. Goodell, H. R., Phillips, R. S., “Bolt-Bearing Strength of Wood and Modified Wood: Effects of Different Methods of Drilling Bolt Holes in Wood and Plywood”, FPL-1523, December 1944

266. Scholten, J. A., “Strength of Bolted Timber Joints”, U.S. Department of Agriculture, Forest Products Laboratory No. R1202, 1946

267. Sandborn, W. A., Goodell, H. R., Ely, A. W., Phillips, R. S., “Bolt-Bearing Strength of Wood and Modified Wood: Bearing Strength of Wood Members Reinforced with Plywood and Cross-Banded Compreg Under Single and Multiple Aircraft Bolts”, FPL-1523-D, September 1946

268. Grinter, L. E., *Theory of Modern Steel Structures, Volume 1, Statically Determinant Structures*, The Macmillian Company, 1936

269. Laurson, P. G., Cox, W. J., *Mechanics of Materials*, John Wiley & Sons, Inc, 1938

270. Sutherland, H., Bowman, H. L., *Structural Design*, John Wiley & Sons, Inc., 1938

271. Higdon, A., Ohlsen, E. H., Stiles, W. B., Weese, J. A., Riley, W. F., *Mechanics of Materials, 4th Edition*, John Wiley & Sons, 1985

272. Talbot, A. N., Moore, H. F., “Tests of Nickel-Steel Riveted Joints”, University of Illinois Bulletin No. 49. 27 February 1911

273. Batho, C., “The Partion of the Load in Riveted Joints”, Journal of the Franklin Institute, Volumen 182, Number 5, November 1916

274. Wolff, E. B., “The Failure of Boiler Plates in Service, and Investigation of the Stresses that Occur in Riveted Joints”, Engineering London, Volume 104, September 1917

275. Hrennikoff, A., “Work of Rivets in Riveted Joints”, Transactions, American Society of Civil Engineers, Volume 99, 1934

276. Moisseiff, L. S., Hartmann, E. C., Moore, R. L., “Riveted and Pin-Connected Joints of Steel and Aluminum Alloys”, Transactions of the American Society of Civil Engineers, Volume 109, 1944

277. Lantos, G., “Load Distribution in a Row of Fasteners Subjected to Lateral Load”, Wood Science, Volume 1, No. 3, 1969

278. Zahn, J. J., “Design Equation for Multiple-Fastener Wood Connections”, Journal of Structural Engineering, Volume 117, No. 11, November 1991

279. Bucci, R. J., Warren, C. J., Starke, E. A. Jr., “The Need for New Materials in Aging Aircraft Structures”, RTO AVT Workshop on “New Metallic Materials for the Structure of Aging Aircraft”, held in Corfu, Greece, 19-20 April 1999, RTO MP-25-01, 1999

280. Owen, C. R., Bucci, R. J., Kegarise, R. J., “An Aluminum Quality Breakthrough for Aircraft Structural Reliability”, AFWAL TR-88-4128, Proceedings of the 1987 Aircraft-Engine Structural Integrity Program Conference, 1988

281. Burns, J. G., Rudd, J. L., Harter, J. A., Magnusen, P. E., Hinkle, A. J., Bucci, R. J., “Probabilistic Durability Evaluation of ALCOA 7050 Aluminum”, WL-TR-92-4045, Proceedings of the 1991 USAF Structural Integrity Program Conference, July 1992

282. Grandt, A. F., Jr., Hinkle, A., J., Zezula, C. E., Elsner, J. H., “The Influence of Initial Quality on the Durability of 7050-T7451 Aluminum Plate”, WL TR-94-4079, Proceedings of the 1993 USAF Structural Integrity Program Conference, August 1994

283. Rice, R. C., Goode, R. J., Bakuckas, J. G. Jr., Thomson, S. R., “Development of MMPDS Handbook Aircraft Design Allowables”, Presented at the 7th Joint DoD/FAA/NASA Conference on Aging Aircraft, New Orleans, LA, September 10, 2003

284. DoD, “Airplane Strength and Rigidity, General Specification for”, Military Specification MIL-A-8860, 18 May 1960

285. FAA, “Part 25 Airworthiness Standards: Transport Category Airplanes, Subpart D—Design and Construction”, FAR 25.619 , 8 March 1970

286. DoD, “Aircraft Structures”, Joint Service Specification Guide JSSG-2006, 30 October 1998

287. Grenoble, H. S., “Bearing Strength of Bolts in Wood”, Navy Department, Bureau of Aeronatuics, Technical Note No. 147, 1925

288. Niles, A. S., Newell, J. S., Airplane Structures, Volume I, John Wiley & Sons, Inc., 1938

289. Freudenthal, A. M., “The Statistical Aspect of Fatigue of Materials”, Proceedings of the Royal Society of London. Series A, Mathematical and Physical Sciences, Volume 187, No. 1011, 13 December 1943

290. Freudenthal, A. M., “Planning and Interpretation of Fatigue Tests”, *Symposium on Statistical Aspects of Fatigue, ASTM STP 121*, 1952

291. Epremian, E., Mehl, R. F., “Investigation of Statistical Nature of Fatigue Properties”, NACA TN-2719, National Advisory Committee for Aeronautics, June 1952

292. Freudenthal, A. M., Gumbel, E. J., “Physical and Statistical Aspects of Fatigue”, Advances in Applied Mechanics, Volume IV, 1956

293. Weibull, W., *Fatigue Testing and Analysis of Results*, Pergamon Press, 1961

294. Finney, J. M., Mann, J. Y., “Fatigue SN Data in Relation to Variability in Predicted Life, ARL Structures Report 363, Aircraft Structural Fatigue, Proceedings of a Symposium held in Melbourne 19-20 October, 1976

295. Maney, G. A., Wyly, L. T., “Fatigue Strength of Flush-Riveted Joints for Aircraft Manufactured by Various Riveting Methods”, NACA ARR-No. 5H28, National Advisory Committee for Aeronautics, December 1945

296. Russell, H. W., Jackson, L. R., Grover, H. J., Beaver, W. W., “Fatigue Strength and Related Characteristics of Aircraft Joints I – Comparison of Spot-Weld and Rivet Patterns in 24S-T Alclad Sheet – Comparison of 24S-T Alclad and 75S-T Alclad”, NACA ARR No. 4F01, National Advisory Committee for Aeronautics, December 1944

297. Moore, R. L., Hill, H. N., “Comparative Fatigue Tests of Riveted Joints of Alclad 24S-T Alclad24S-T81, Alclad 24S-RT, Alclad 24S-T86 and Alclad 75S-T Sheet”, NACA RB No. 5F11, National Advisory Committee for Aeronautics, August 1945

298. Hartmann, E. C., Holt, M., Eaton, I. D., “Static and Fatigue Strengths of High-Strength Aluminum-Alloy Bolted Joints”, NACA TN-2276, National Advisory Committee for Aeronautics, February 1951

299. Hartmann, E. C., Holt, M., Eaton, I. D., “Additional Static and Fatigue Tests of High-Strength Aluminum Alloy Bolted Joints”, NACA TN-3269, National Advisory Committee for Aeronautics, July 1954

300. Kaechele, L., “Review and Analysis of Cumulative-Fatigue-Damage Theories”, Rand Corporation, August 1963

301. Schijve, J., “The Accumulation of Fatigue Damage in Aircraft Materials and Structures”, AGARD No. 157, North Atlantic Treaty Organization, January 1972

302. Hoeppner, D. W., Krupp, W. E., “Prediction of Component Life by Application of Fatigue-Crack Growth Knowledge”, LR 25123, Lockheed Aircraft Corporation, September 1972

303. Rice, R. C., Leis, B. N., Nelson, D. V., Eds., *Fatigue Design Handbook, Second Edition*, Society of Automotive Engineers, 1988

304. Anon, “Standard Practices for Cycle Counting in Fatigue Analysis”, ASTM E1049-85, 2005

305. Goodman, J., *Mechanics Applied to Engineering*, Volume 1, Longmans Gree, 1930

306. Gerber, W., “Bestimmung der zulossigen spannungen in eisen constructionen, Z. Bayer Arch. Ing. Ver., Volume 6 1974

307. Osgood, C. C., *Fatigue Design*, Wiley-Interscience, 1970

308. DoD, “Metallic Materials and Elements for Aerospace Vehicle Structures”, MIL-HDBK-5C, 15 September 1976

309. SAE, “Technical Report on Low Cycle Fatigue Properties Ferrous and Non-Ferrous Materials”, SAE J1099, Society of Automotive Engineers, August 2002

310. Wallbrink, C., Hu, W., “A Strain-Life Module for CGAP: Theory, User Guide and Examples”, DSTO-TR-2392, March 2010

311. Dowling, N. E., *Mechanical Behavior of Materials: Engineering Methods for Deformation, Fracture, and Fatigue*, Second Edition, Prentice Hall, 1999

312. Wilkins, E. W. C., Jessop, H. T., “A Photoelastic-Fatigue Programme of Experimental Research in Connection with Bolted Joints”, Journal of the Royal Aeronautical Society, Volume 58, Issue 522, June 1954

313. Jessop, H. T., Snell, C., Holister, G. S., “Photoelastic Investigation in Connection with the Fatigue Strength of Bolted Joints”, Aeronautical Quarterly, Volume 6 Issue 3, August 1955

314. Pilkey, W. D., *Peterson’s Stress Concentration Factors, Second Edition*, John Wiley & Sons, Inc., 1997

315. Spaulding, E. H., Book chapter “Detail Design for Fatigue in Aircraft Wing Structures”, *Metal Fatigue*, G. Sines, and J. L. Waisman, Ed., Mc-Graw Hill Book Company, Inc., 1959

316. Wei, R. P., Wei, W., Miller, G. A., “Effect of Measurement Precision and Data Processing Procedures on Variability in Fatigue Crack Growth Rate Data”, Journal of Testing and Evaluation, Volume 7, Issue 2, March 1979

317. Clark, W. G., Hudak, S. J., "Variability in Fatigue Crack Growth Rate Testing", Journal of Testing and Evaluation, Volume 3, Issue 6, November 1975

318. Clark, W. G., Hudak, S. J., "The Analysis of Fatigue Crack Growth Rate Data", *Application of Fracture Mechanics to Design; Sagamore Army Materials Research Conference Proceedings, Volume 22*, Plenum Press, 1979

319. Newman, J. C., Raju, I. S., Stress-Intensity Factor Equations for Cracks in Three-Dimensional Finite Bodies Subjected to Tension and Bending Loads", NASA TM-85793, April 1984

320. Fawaz, S. A., Andersson, B., "Accurate Stress Intensity Factor Solutions for Unsymmetric Corner Cracks at a Hole, Presented at the Joint DoD/FAA/NASA Conference on Aging Aircraft, May 2000

321. Fawaz, S., A., "Using the World's Largest Stress Intensity Factor Database for Fatigue Life Predictions", Presented at the First International Conference on Damage Tolerance of Aircraft Structures, 2007

322. Shah, R. C., "Stress Intensity Factors for Through and Part-Through Cracks Originating at Fastener Holes", *Mechanics of Crack Growth, ASTM STP 590*, American Society for Testing and Materials, 1976

323. Isida, M., "Laurent Series Expansion for Internal Crack Problems", *Methods of Analysis and Solutions of Crack Problems*, Noordhoff International Publishing, 1973

324. Harter, J. A., "An Alternative Closed-Form Stress Intensity Solution for Single Part-Through and Through-the-Thickness Cracks at Offset Holes", AFRL-VA-WP-TR-1999-3001, December 1998

325. Kobayashi, A. S., ed., *Experimental Techniques in Fracture Mechanics, 2*, SESA Monograph No. 2, Society for Experimental Stress Analysis, 1975

326. Blinn, M. P., McReaken, J., "L/ESS is More", Proceedings of the 2009 Aircraft Structural Integrity Program (ASIP) Conference, Jacksonville, FL, 2 December 2009

327. Hi-Shear Corporation, "Product Specification, Hi-Lok®/Hi-Tigue® and Hi-Lok® Fastening Systems, Hi-Lok®/Hi-Tigue® and Hi-Lok® Pin", Specification No. 342, Revision AG, 1 July 2003

328. Hi-Shear Corporation, "Hi-Lok® and Hi-Lok®/Hi-Tigue® Fastening Systems Installation Instructions", 1991

329. Hi-Shear Corporation, "Product Specification, Hi-Lok®/Hi-Tigue® and Hi-Lok® Fastening Systems, Hi-Lok®/Hi-Tigue® and Hi-Lok® Collars", Specification No. 345, Revision N, 8 July 2004

330. AIA/NAS, “Nut, Self-Locking, 450°F, Reduced Hexagon, Reduced Height, Ring Base, Non-Corrosion Resistant Steel”, NASM21042, October 1998

331. Department of Defense, “Screw Threads, Controlled Radius Root with Increased Minor Diameter, General Specification for”, MIL-S-8879C, 25 July 1991

332. Siemens, NX 7.5.0.32, Computer Modeling Software, 2009

333. Siemens, NX Nastran 7.0 64-bit ILP, Computer Finite Element Solver Software, 1 October 2009

334. Ramberg, W., Osgood, W. R., “Description of Stress-Strain Curves by Three Parameters,” NACA-TN-902, 1943

335. DoD, “Metallic Materials and Elements for Aerospace Vehicle Structures,” Department of Defense Handbook, MIL-HDBK-5J, 2003

336. Frocht, M. M., *Photoelasticity, Volume I*, John Wiley & Sons, Inc., 1941

337. Harter, J. A., “Lessons Learned While Developing K-Solutions for Pin Loaded Holes”, Presented at the AFGROW Workshop 2010, Layton, UT, 31 August 2010

338. Harter, J. A., “Closed-Form K-Solution for Cracks at Offset Holes Under Bearing Load”, Presented at the 2011 Aircraft Airworthiness and Sustainment Conference, San Diego, CA, 2011

339. Poe, C. C., “Stress-Intensity Factor for a Cracked Sheet With Riveted and Uniformly Spaces Stringers”, NASA TR R-358, May 1971

340. StressCheck® Finite Element Software, Version 9.2, Engineering Software Research & Development, Inc., 2011

341. Engineering Software Research & Development, Inc., “StressCheck® Master Guide”, Release 7, August 2005

342. Crack Growth Analysis Software, AFGROW, Version 5.1.5.16, Copyright LexTech, Inc., 26 July, 2010

343. Brooks, C., Honeycutt, K., Domasky, S. P., “Crack Growth and Stress Intensity Prediction Techniques”, AFRL-VA-WP-TR-2006-3043, Air Force Research Laboratory, March 2006

344. Pilarczyk, R. T., “Experimentally Derived Beta Corrections to Predict Fatigue Crack Growth at Cold Expanded Holes in 7075-T651 Aluminum Alloy”, Masters of Science Thesis, University of Utah, August 2008

345. ASTM, “Standard Test Method for Measurement of Fatigue Crack Growth Rates (E647)”, American Society for Testing and Materials, Committee E08, 2000

346. Private communication with Robert Pilarczyk including tabular data

347. Parker, A. P., *The Mechanics of Fracture and Fatigue, An Introductio*n, E. & F. N. Spon Ltd. 1981

348. Bowie, O. L., “Analysis of an Infinite Plate Containing Radial Cracks Originating from the Boundary of an Internal Circular Hole”, Journal of Mathematics and Physics, Volume 35, 1956

349. Newman, J. C., “An Improved Method of Collocation for the Stress Analysis of Cracked Plates With Various Shaped Boundaries”, NASA TN D-6376, August 1971

350. Broek, D., Vlieger, H., “Cracks Emanating from Holes in Plane Stress”, International Journal of Fracture Mechanics, Volume 8, Number 3, September 1972

351. Tweed, J., Rooke, D. P., “The Distribution of Stress Near the Tip of a Radial Crack at the Edge of a Circular Hole”, International Journal of Engineering Science, Volume 11, Issue 11, November 1973

352. Schijve, J., “Stress Intensity Factors of Hole Edge Cracks. Comparison between One Crack and Two Symmetric Cracks”, International Journal of Fracture, Volume 23, Number 3, November 1983

353. Tada, H., Paris, P. C., Irwin, G. R., *The Stress Analysis of Cracks Handbook*, Third Edition, ASME Press, 2000

354. Wilson, C. D., “Linear Elastic Fracture Mechanics Primer”, NASA TM-103591, July 1992

355. Pilarczyk, R., Allred, T., Clark, P., “Damage Tolerance Analysis Ground Rules for A-10A Reconfigured Post Desert Storm”, Revision W, OO-ALC/GHAEJ Document for DTA/FSMP Update, 22 September, 2010

356. Timoshenko, S., *Theory of Elasticity*, Engineering Societies Monograph, McGraw-Hill Book Company, Inc., 1934

APPENDIX A TEST SPECIMEN INFORMATION

A.1 Specimen Dimensional Data

This section contains dimensional data regarding the specimens. The first table contains information regarding the gap between the fastener head and the upper splice plate. A gap indicates that the fastener was not fully seated in the hole which is due to a lack of relief in the top plates to accommodate the shank to head radius of the Hi-Lok. All measurement were taken using a feeler gauge set with 0.001" increments. The number given in Table A-1 represents the largest thickness gauge that was able to slip fully under the main portion of the head.

Table A-1 Gap between Fastener Head and Upper Splice Plate

Hole	Specimen 1	Specimen 2	Specimen 3	Specimen 4
1	0.007	0.006	0.008	0.008
2	0.008	0.006	0.01	0.009
3	0.003	0.005	0.009	0.009
4	0.008	0.004	0.009	0.01
5	0.009	0.006	0.01	0.008
6	0.007	0.006	0.008	0.009
7	0.008	0.006	0.01	0.011
8	0.01	0.006	0.008	0.008
9	0.005	0.004	0.006	0.007
10	0.007	0.007	0.008	0.009
11	0.008	0.006	0.008	0.007
12	0.008	0.005	0.01	0.01
13	0.007	0.005	0.008	0.01
14	0.009	0.004	0.009	0.009
15	0.011	0.004	0.008	0.008
16	0.012	0.006	0.011	0.009
17	0.009	0.004	0.008	0.009
18	0.008	0.005	0.009	0.011

Offsets were measured by performing a step measurement from the edge of each plate to a neat fit pin (Hi-Lok) inserted into the hole. One-half the diameter was added to the step measurement to get the hole offset. Table A-2, Table A-3, and Table A-4 present the offsets for the top plate, main plates, and bottom plate respectively for each specimen.

Table A-2 Hole Offsets on the Top Plate

Measurement	Specimen 1	Specimen 2	Specimen 3	Specimen 4
End distance (A)	0.298	0.296	0.300	0.301
Offset Hole 1	0.380	0.392	0.380	0.379
Offset Hole 2	0.381	0.370	0.382	0.380
Offset Hole 3	0.380	0.390	0.378	0.379
Offset Hole 4	0.384	0.369	0.383	0.381
Offset Hole 5	0.378	0.390	0.378	0.378
Offset Hole 6	0.385	0.373	0.385	0.384
Offset Hole 7	0.380	0.389	0.376	0.377
Offset Hole 8	0.388	0.372	0.386	0.385
Offset Hole 9	0.378	0.389	0.375	0.375
Offset Hole 10	0.387	0.375	0.388	0.387
Offset Hole 11	0.375	0.386	0.374	0.373
Offset Hole 12	0.390	0.377	0.389	0.389
Offset Hole 13	0.373	0.384	0.373	0.369
Offset Hole 14	0.392	0.377	0.392	0.391
Offset Hole 15	0.371	0.383	0.372	0.369
Offset Hole 16	0.389	0.378	0.393	0.392
Offset Hole 17	0.369	0.381	0.370	0.367
Offset Hole 18	0.389	0.381	0.394	0.393
End distance (A)	0.305	0.300	0.301	0.297

Table A-3 Hole Offsets on the Main Plates

Measurement	Specimen 1	Specimen 2	Specimen 3	Specimen 4
Offset Hole 1	0.380	0.378	0.375	0.376
Offset Hole 2	0.384	0.386	0.386	0.386
Offset Hole 3	0.375	0.377	0.377	0.377
Offset Hole 4	0.383	0.385	0.385	0.384

Measurement	Specimen 1	Specimen 2	Specimen 3	Specimen 4
Offset Hole 5	0.378	0.378	0.379	0.379
Offset Hole 6	0.381	0.384	0.384	0.382
Offset Hole 7	0.380	0.380	0.381	0.380
Offset Hole 8	0.381	0.382	0.384	0.381
Offset Hole 9	0.382	0.381	0.381	0.382
End distance (B)	0.251	0.249	0.250	0.246
End distance (B)	0.250	0.250	0.253	0.247
Offset Hole 10	0.383	0.381	0.381	0.381
Offset Hole 11	0.383	0.382	0.381	0.381
Offset Hole 12	0.382	0.380	0.379	0.380
Offset Hole 13	0.383	0.383	0.383	0.383
Offset Hole 14	0.378	0.377	0.378	0.379
Offset Hole 15	0.385	0.384	0.385	0.385
Offset Hole 16	0.379	0.377	0.377	0.378
Offset Hole 17	0.390	0.385	0.386	0.386
Offset Hole 18	0.376	0.373	0.375	0.376

Table A-4 Hole Offsets for the Bottom Plate

Measurement	Specimen 1	Specimen 2	Specimen 3	Specimen 4
End distance (A)	0.300	0.299	0.300	0.300
Offset Hole 1	0.380	0.381	0.380	0.392
Offset Hole 2	0.380	0.382	0.382	0.368
Offset Hole 3	0.377	0.380	0.379	0.391
Offset Hole 4	0.383	0.384	0.383	0.371
Offset Hole 5	0.378	0.379	0.378	0.390
Offset Hole 6	0.385	0.384	0.386	0.372
Offset Hole 7	0.378	0.378	0.377	0.388
Offset Hole 8	0.386	0.386	0.386	0.373
Offset Hole 9	0.378	0.376	0.376	0.387
Offset Hole 10	0.385	0.387	0.388	0.375
Offset Hole 11	0.373	0.374	0.374	0.384
Offset Hole 12	0.388	0.389	0.390	0.376
Offset Hole 13	0.372	0.372	0.373	0.384
Offset Hole 14	0.389	0.391	0.393	0.377
Offset Hole 15	0.370	0.371	0.372	0.383
Offset Hole 16	0.391	0.393	0.393	0.378
Offset Hole 17	0.370	0.370	0.371	0.381

Measurement	Specimen 1	Specimen 2	Specimen 3	Specimen 4
Offset Hole 18	0.393	0.394	0.395	0.379
End distance (A)	0.298	0.302	0.297	0.299

A.2 Specimen Images of the Crack Starter Notch and Fracture Surface

This section contains images taken of the fracture surface and starter EDM notch using a microscope. Four different images are given for each specimen: the first is of the short ligament which is the primary fracture surface, the second is across the hole which shows the continuing damage that nucleated on the far side of the hole and grew, the third shows a close-up of the EDM notch near the hole, and the fourth shows the far side of the ligament where final fracture of the ligament occurred. Note on the fourth what appears black is a shadow cast by shear lip caused by the ring light of the microscope. Figure A-1 provides a map of where these images are taken relative to the ligament. Figure A-2 through Figure A-5 contain the images of specimen one, Figure A-6 through Figure A-9 contain the images of specimen two, Figure A-10 through Figure A-13 contain the images of specimen three, Figure A-14 through Figure A-17 contain the images of specimen four.

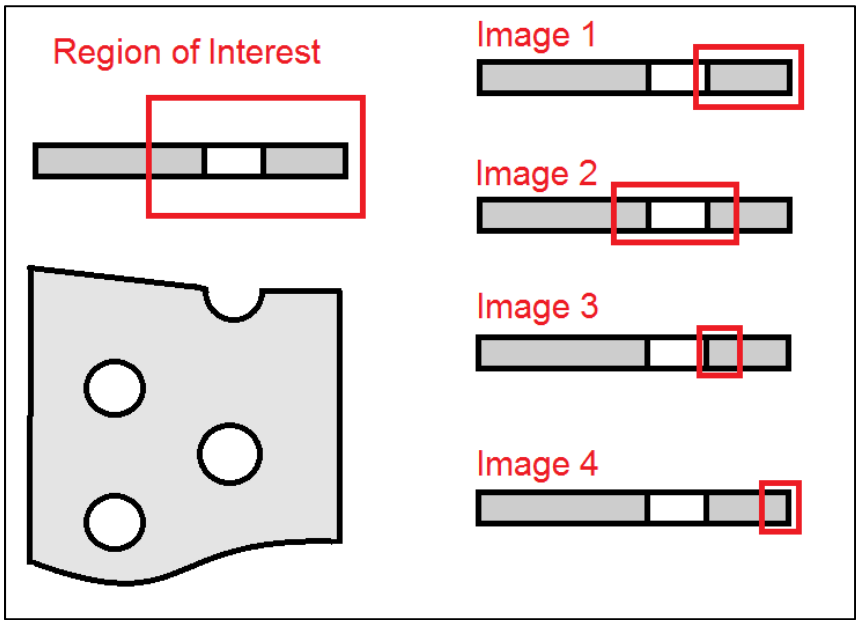

Figure A-1 Map of Microscope Images of Specimens

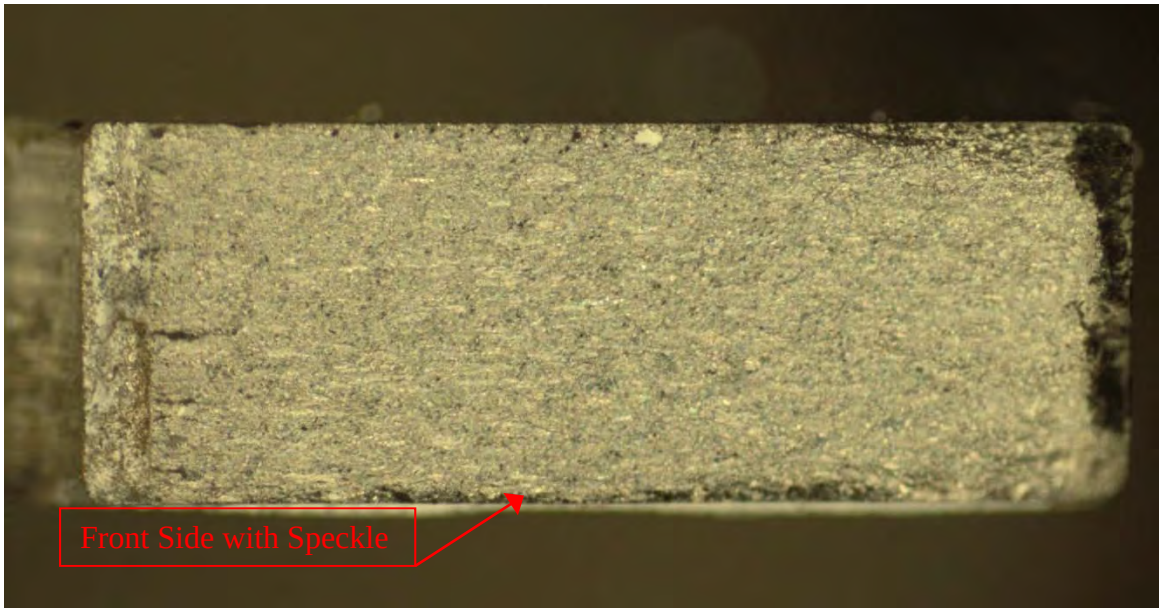

Figure A-2 Overall View of the Primary Fracture Surface of Specimen 1

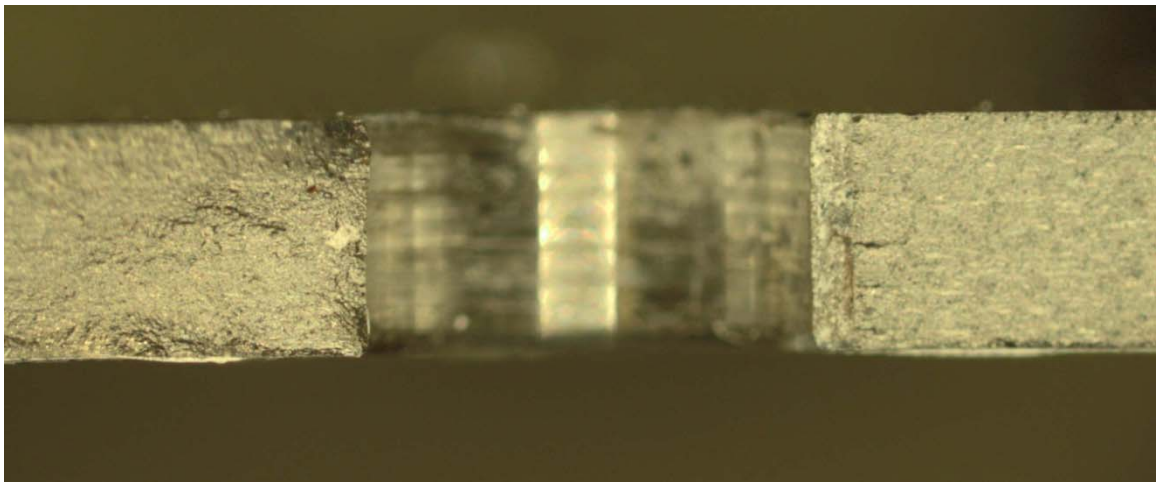

Figure A-3 View of the Fracture Surface on Both Sides of the Hole, Specimen 1

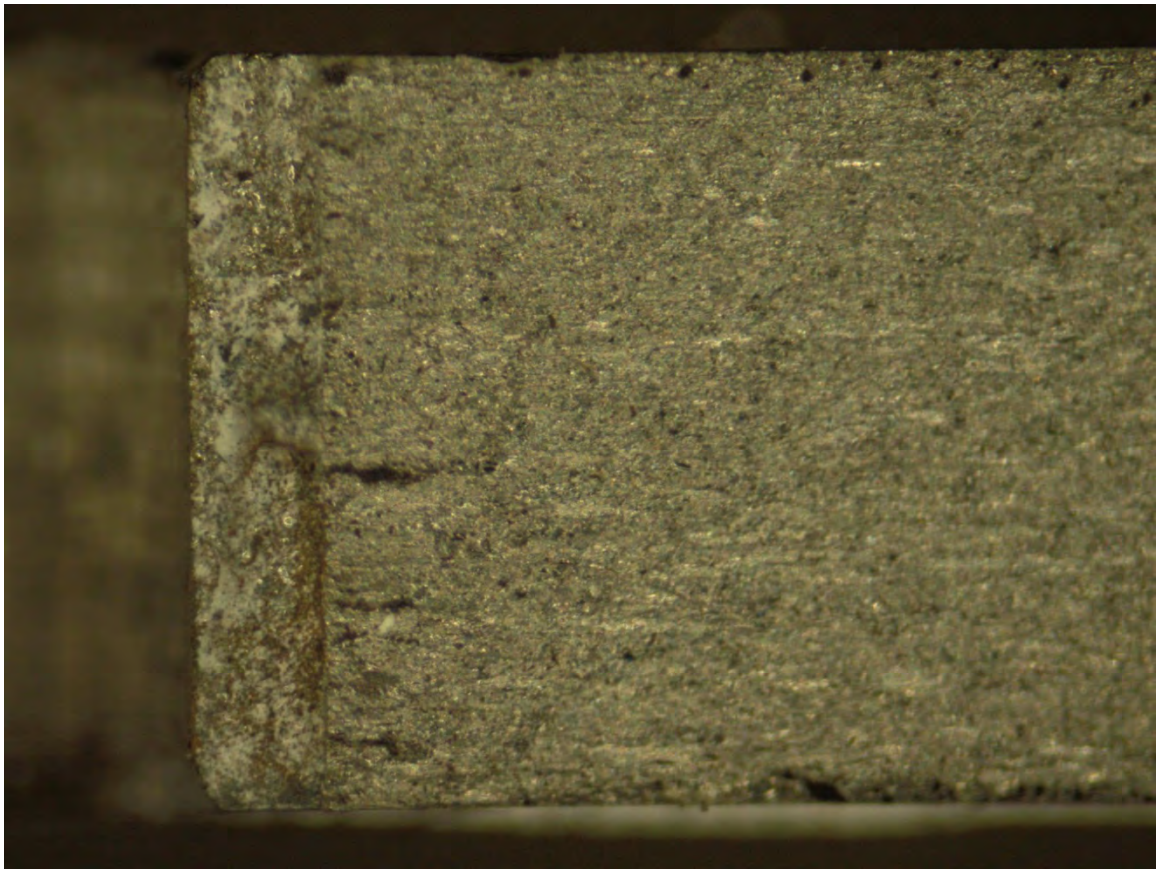

Figure A-4 Close-up of the EDM Notch and Fracture Surface Near the Hole, Specimen 1

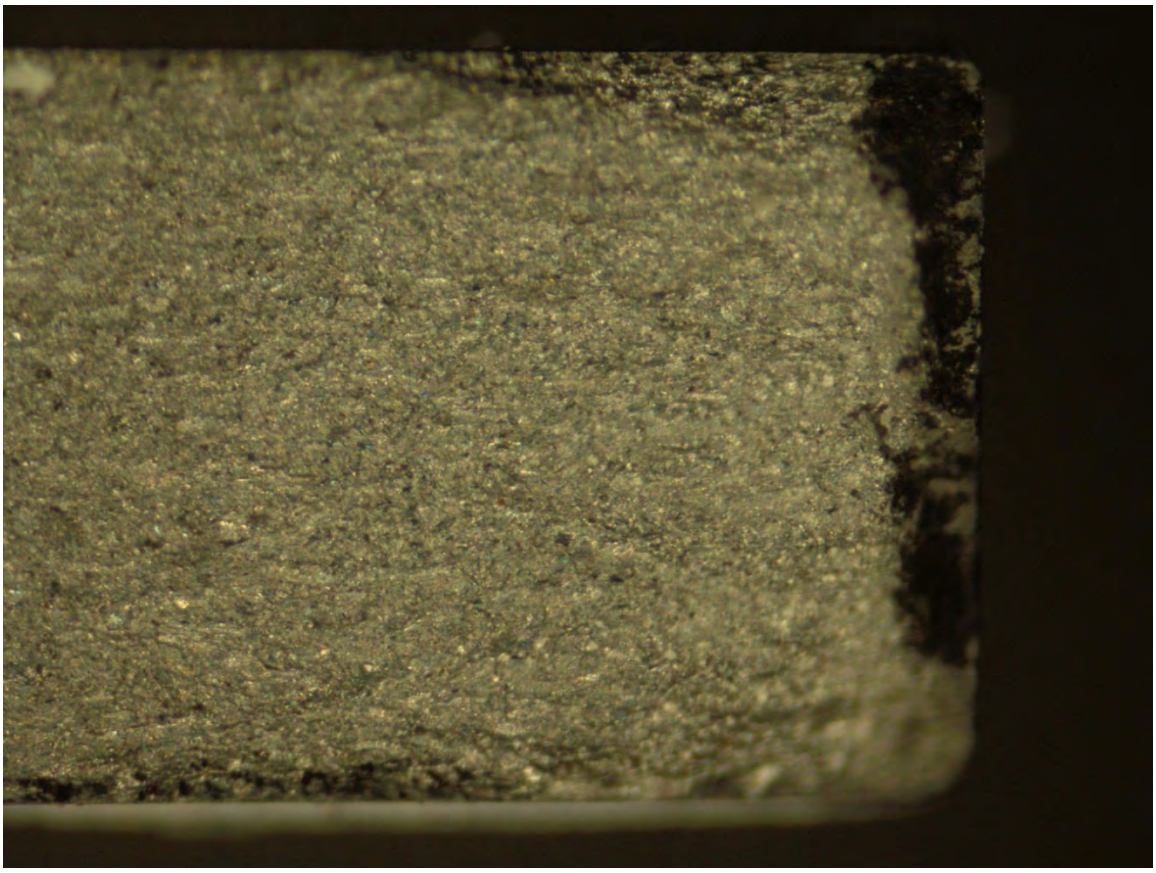

Figure A-5 Close-up of the End of the Broken Primary Crack Ligament, Specimen 1

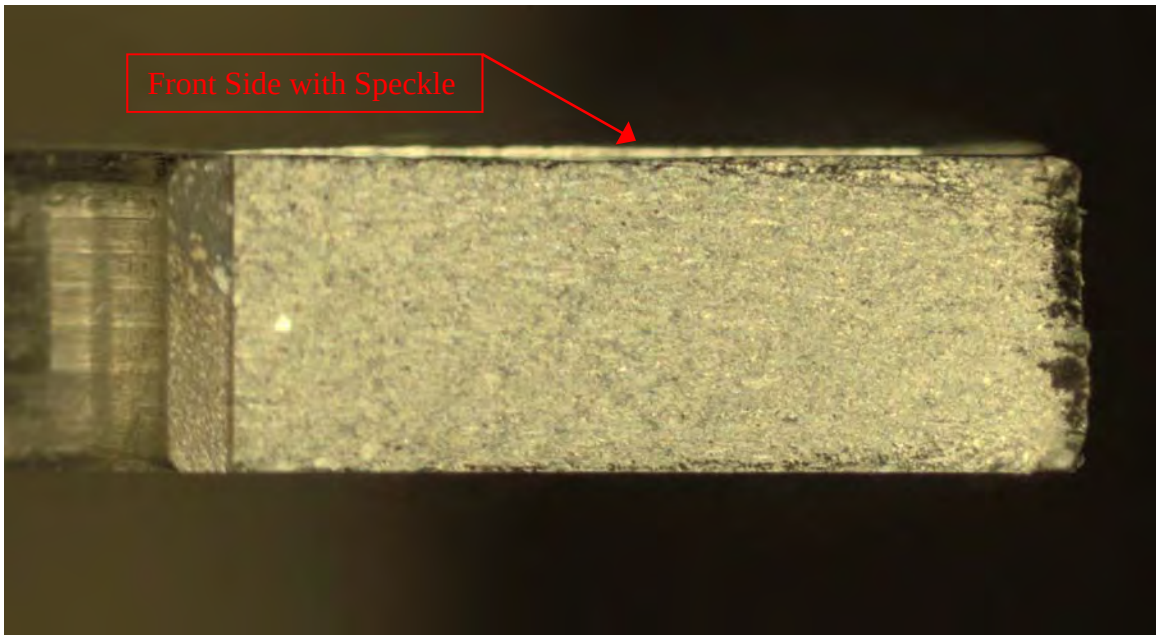

Figure A-6 Overall View of the Primary Fracture Surface of Specimen 2

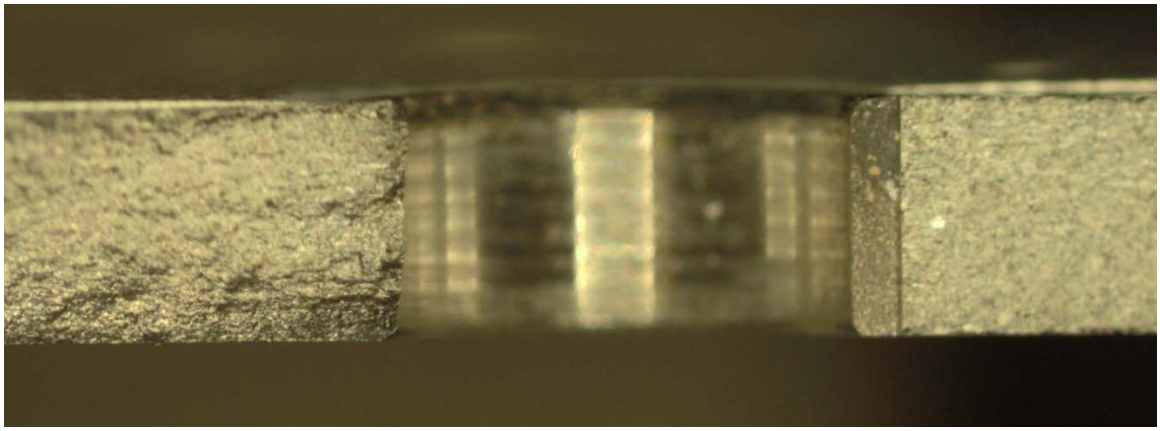

Figure A-7 View of the Fracture Surface on Both Sides of the Hole, Specimen 2

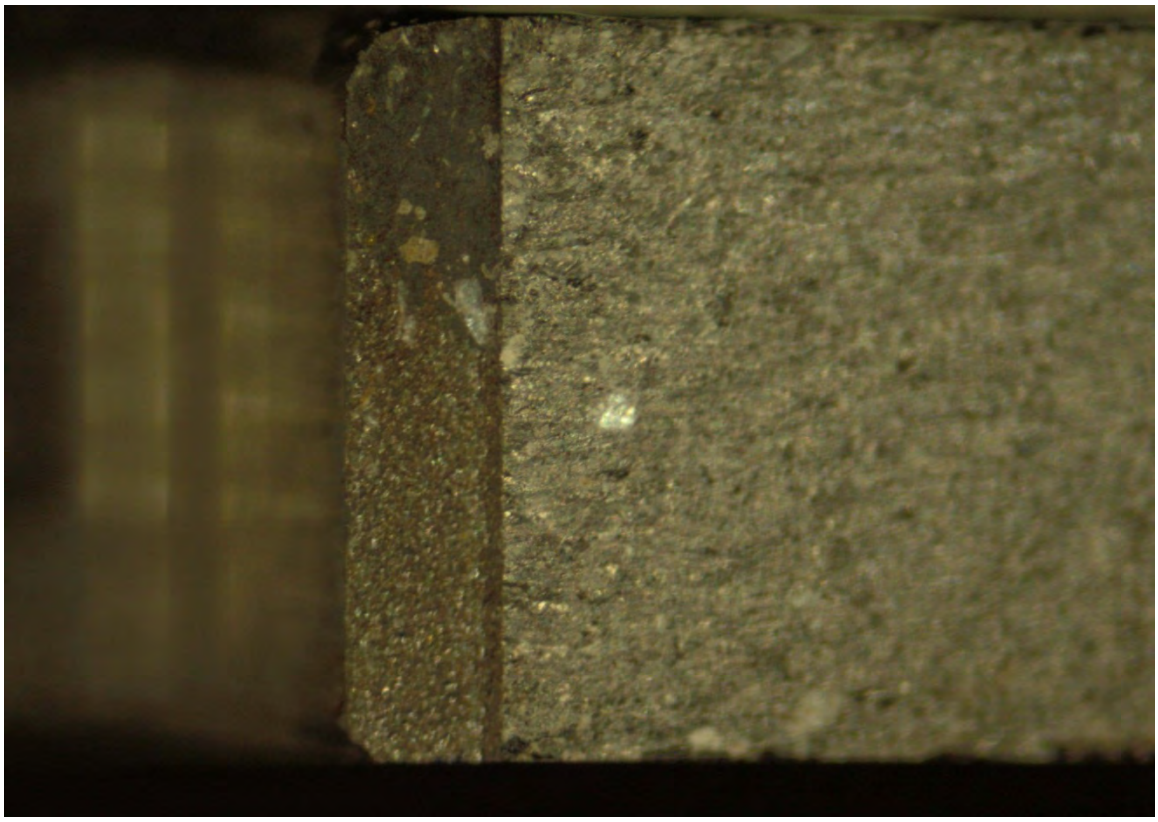

Figure A-8 Close-up of the EDM Notch and Fracture Surface Near the Hole, Specimen 2

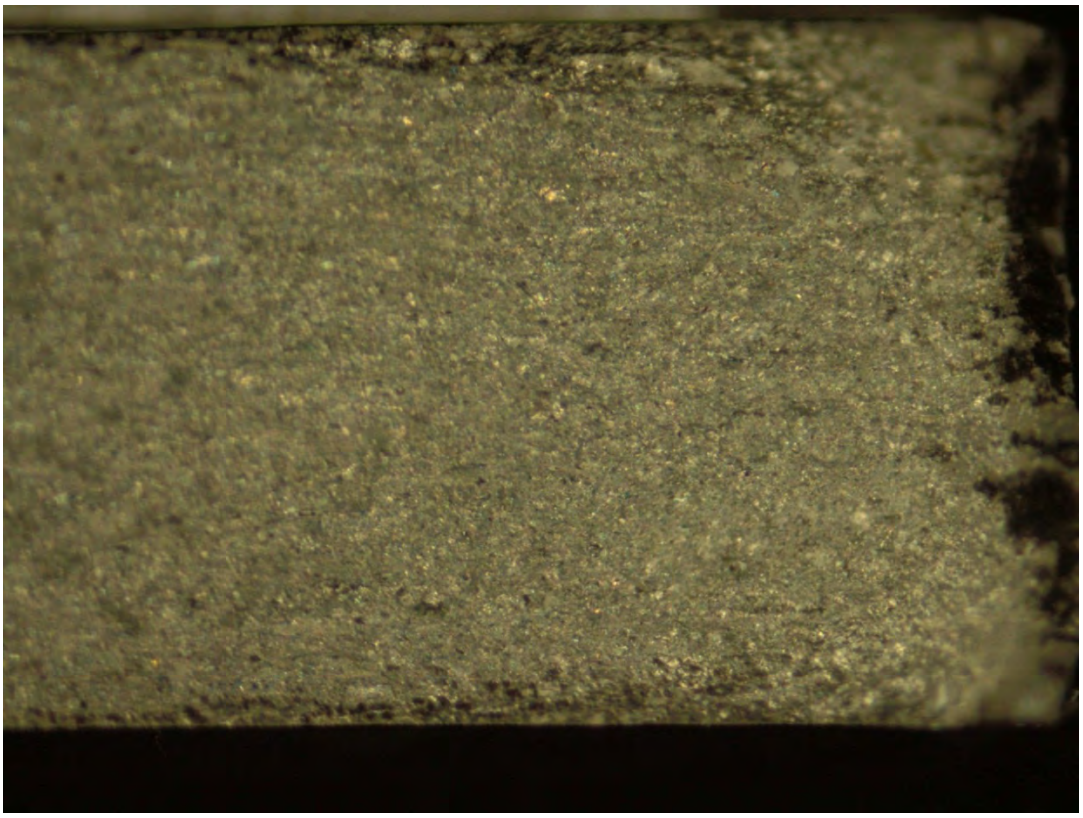

Figure A-9 Close-up of the End of the Broken Primary Crack Ligament, Specimen 2

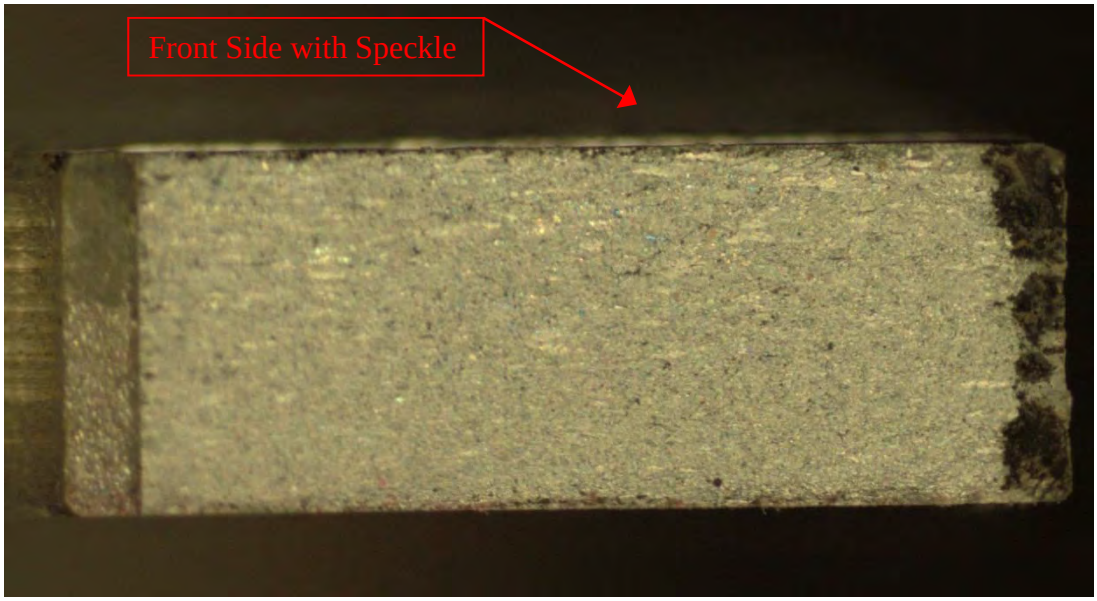

Figure A-10 Overall View of the Primary Fracture Surface of Specimen 3

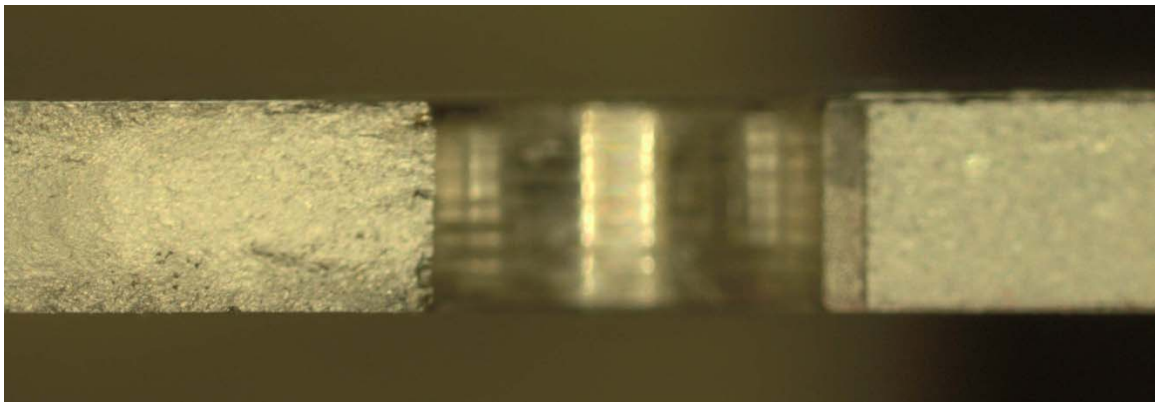

Figure A-11 View of the Fracture Surface on Both Sides of the Hole, Specimen 3

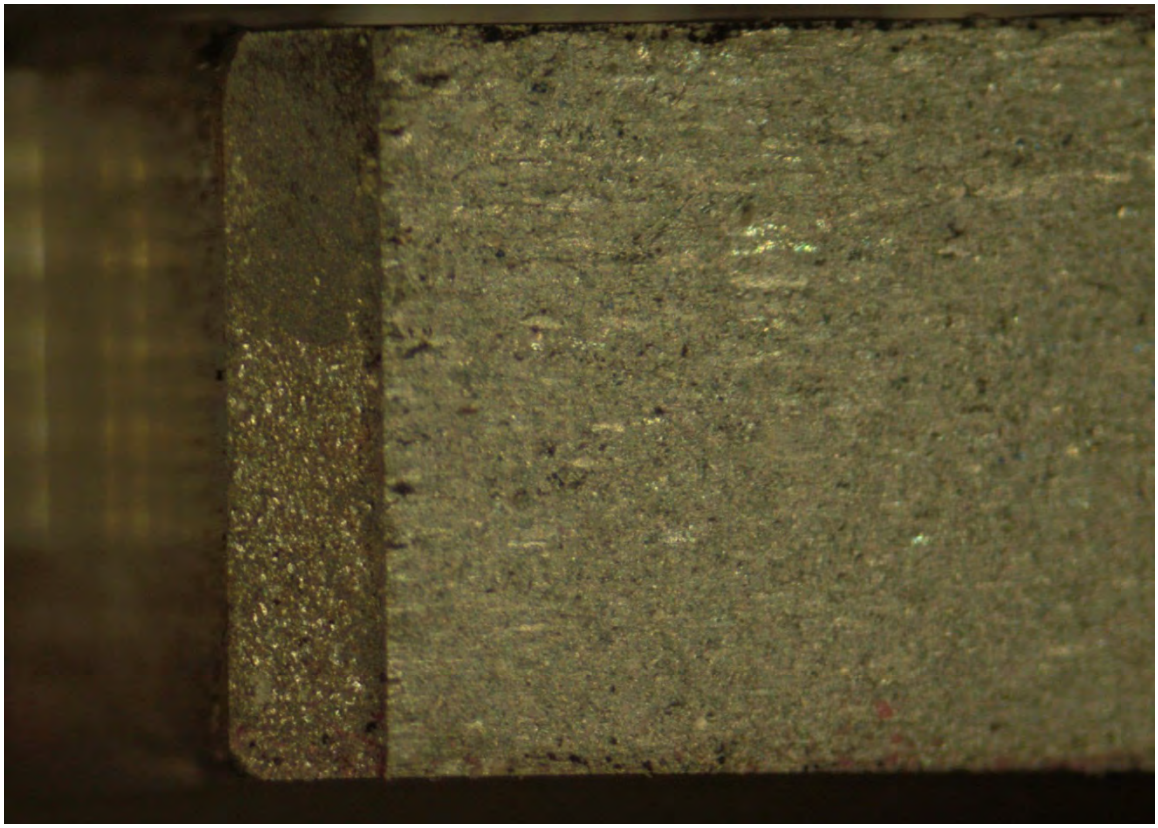

Figure A-12 Close-up of the EDM Notch and Fracture Surface Near the Hole, Specimen 3

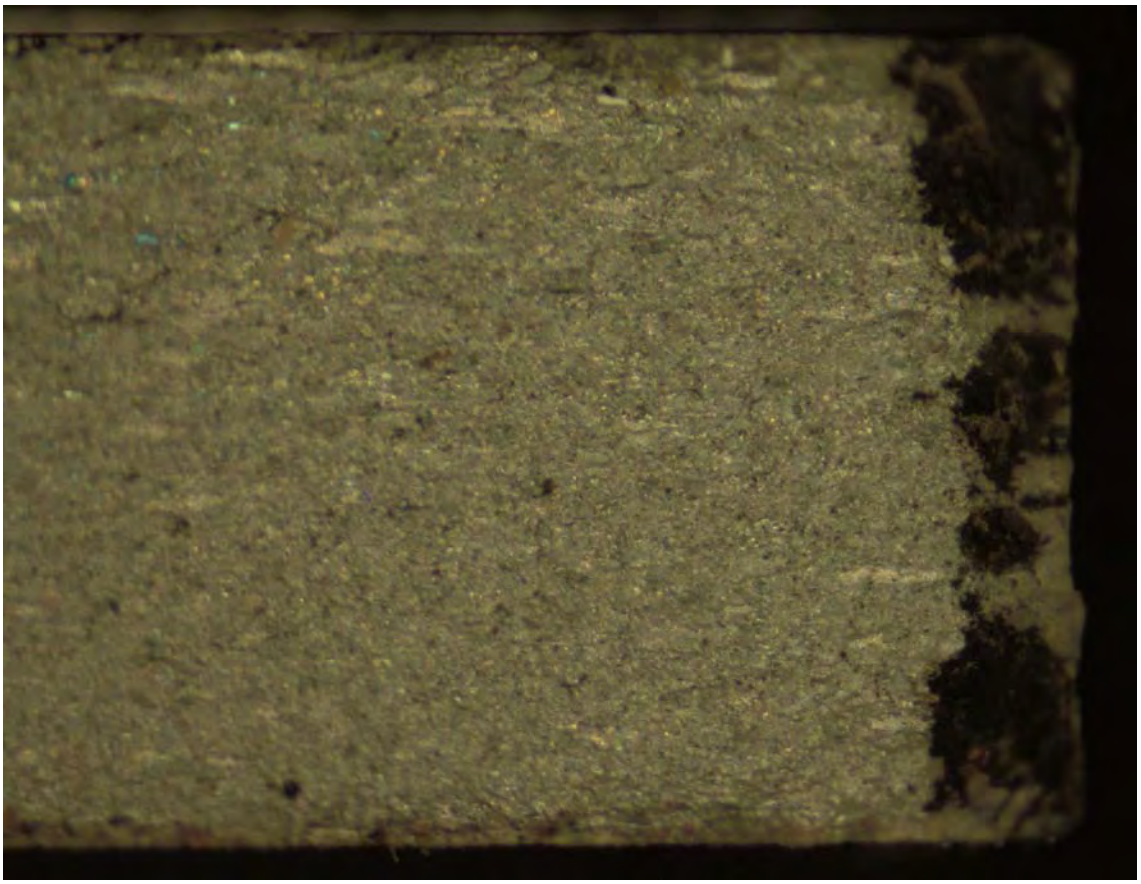

Figure A-13 Close-up of the End of the Broken Primary Crack Ligament, Specimen 3

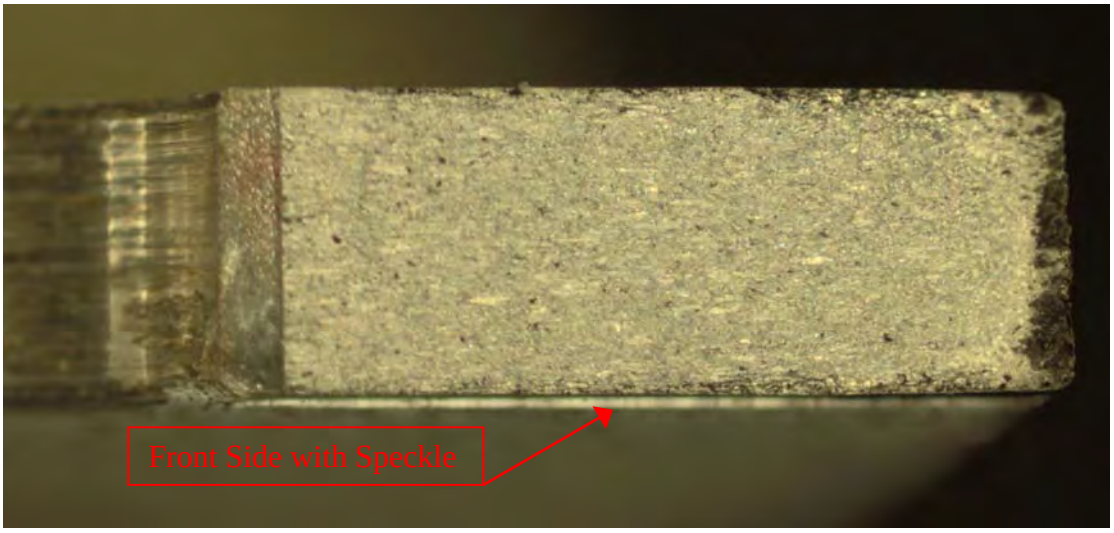

Figure A-14 Overall View of the Primary Fracture Surface of Specimen 4

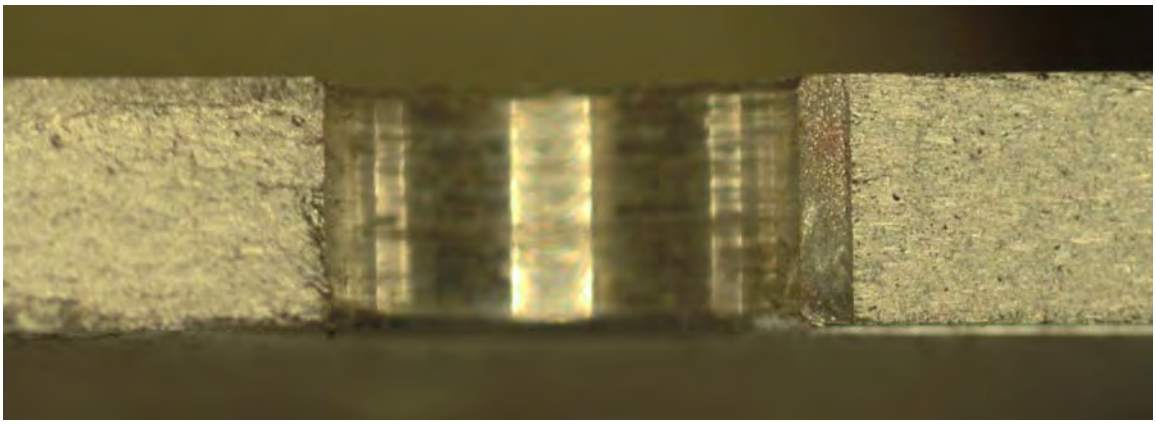

Figure A-15 View of the Fracture Surface on Both Sides of the Hole, Specimen 4

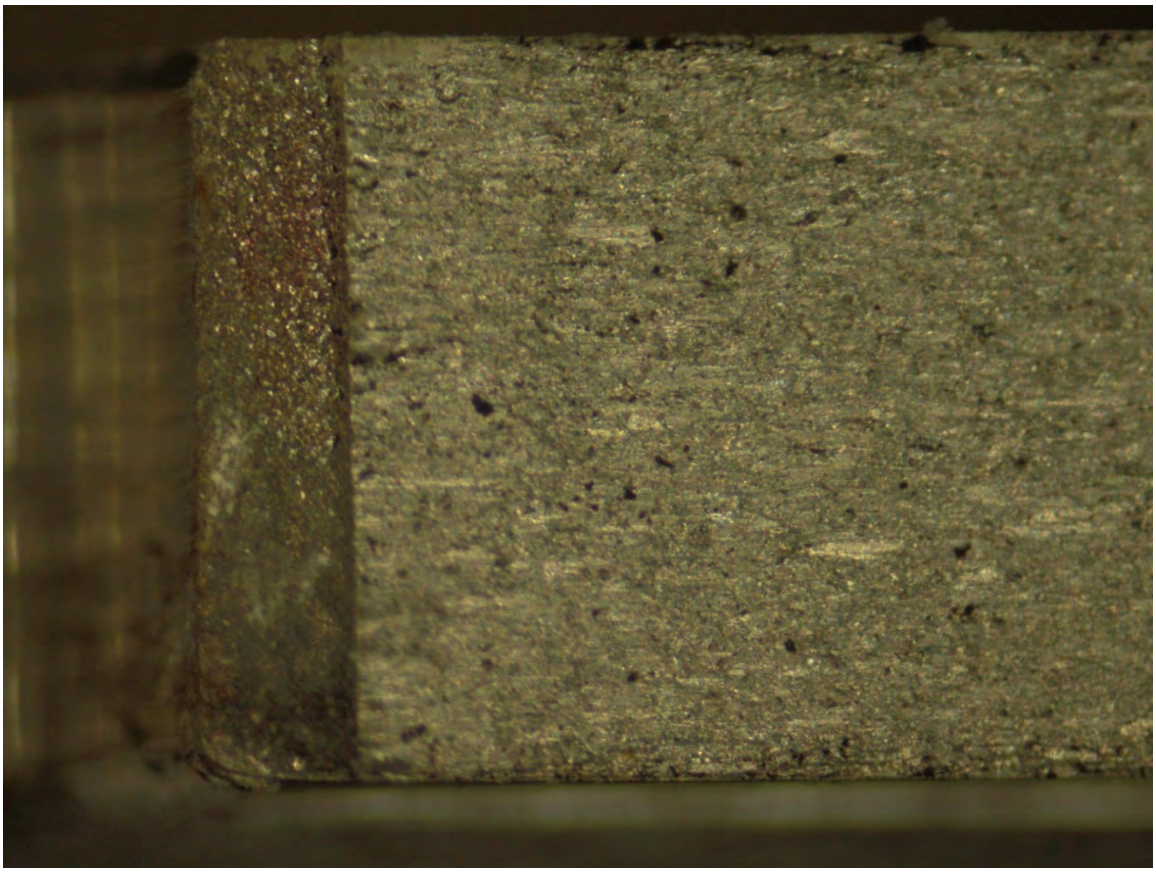

Figure A-16 Close-up of the EDM Notch and Fracture Surface Near the Hole, Specimen 4

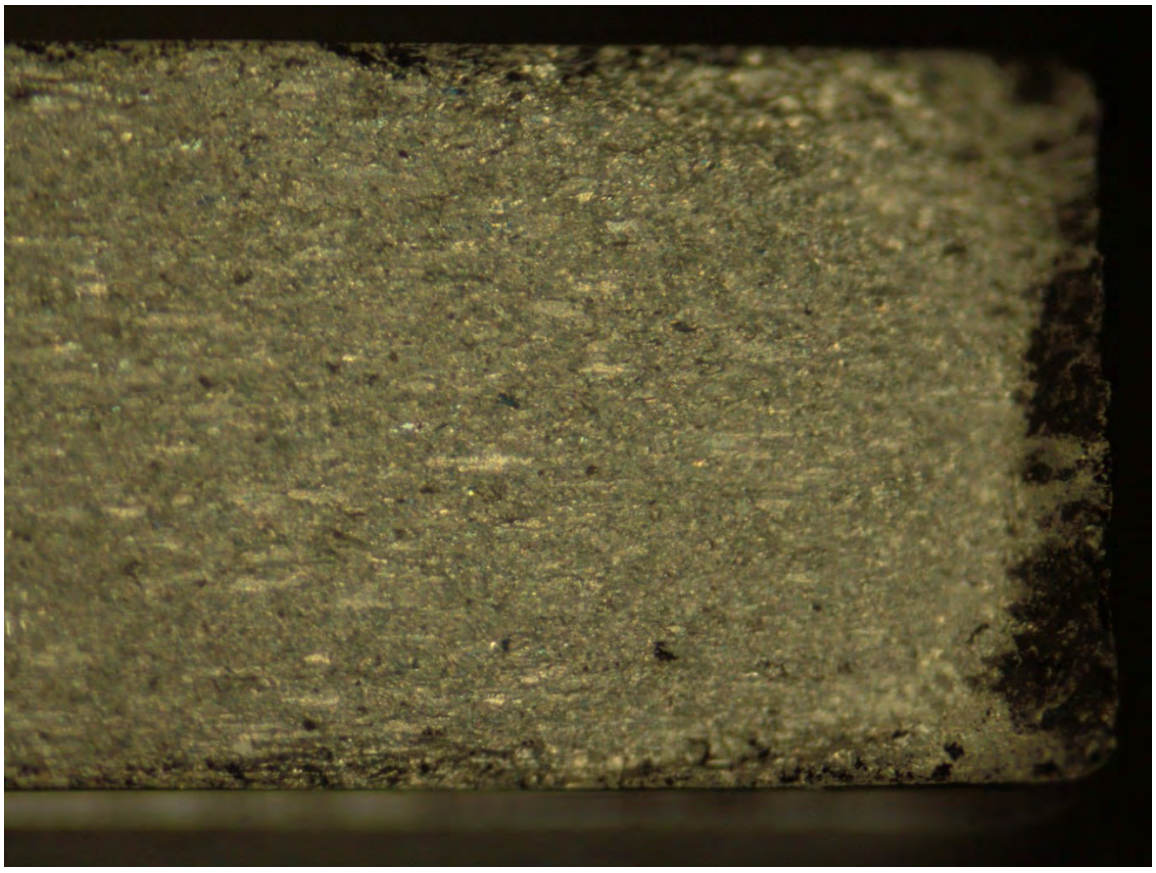

Figure A-17 Close-up of the End of the Broken Primary Crack Ligament, Specimen 4

A.3 Strain Gage Locations

The strain gages were not located in the same spot on specimen one and specimen three. The differences are not just related to the fact that it is difficult to place gages in a repeatable way but the relative locations of gages 1 through 6 were reversed between the specimens. The location of strain gage #1 is shown in Figure A-18 while the locations of gages #2 through #6 are shown in Figure A-19. Note that gages #1 and #3 are on opposite sides clear of the specimen. This provides an independent check of the load and will indicate if there is any out of plane deflections by way of differing strain from front to back. Gage # 2 is on the side of the specimen, on the main plate which has fastener #9

which is cracked in the top plate for specimen three, and on the opposite main plate for specimen one. Gage #5 is roughly in the middle of the bottom plate but the differences highlight the difficulty in precision laying of strain gages since they do not quite overlay from specimen one to specimen three. Gages #4 and #6 are in the field region of the bottom plate.

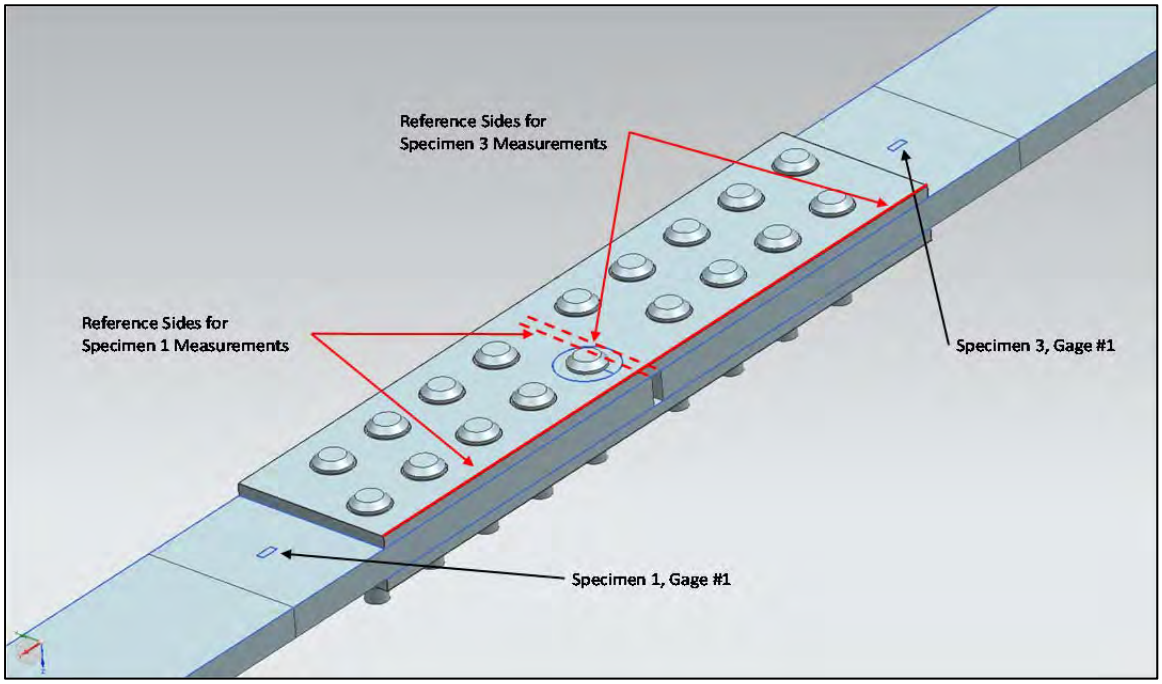

Figure A-18 Location of Strain Gage #1 on Specimens 1 and 3

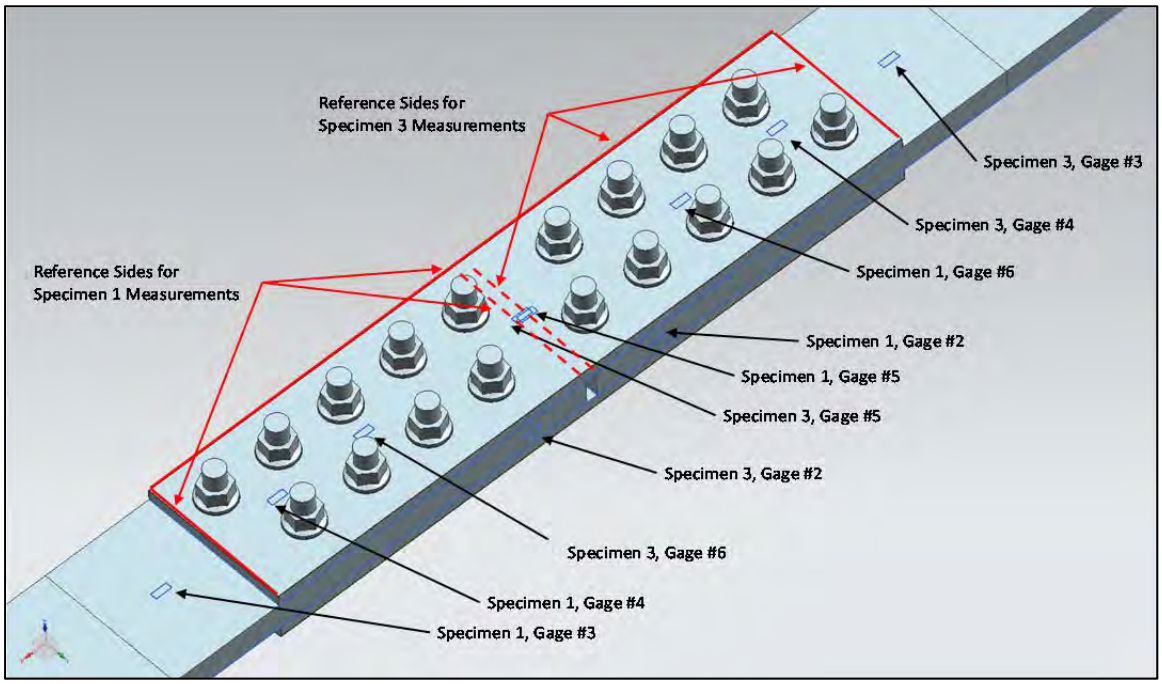

Figure A-19 Location of Strain Gages #2 through #6 on Specimens 1 and 3

Measurements were made from the edges indicated in Figure A-18 and Figure A-19 using the front step measurement function of a digital caliper with a resolution of ~0.001. Table A-5 contains those measurements for each gage on both specimens. Pictures of the strain gage locations for specimen one and specimen three are in Figure A-20 and Figure A-21 respectively.

Table A-5 Strain Gage Locations, Measured to Gage Center

Gage	Measurement	Specimen 1 (in inches)	Specimen 3 (in inches)
Strain Gage 1 Center	From Side	3.458	3.398
	From End	0.670	0.672
Strain Gage 2 Center	From Side	0.003 off of plate center	0.001 off of plate center
	From End	0.592	0.519
Strain Gage 3 Center	From Side	0.678	0.698
	From End	3.456	3.426
Strain Gage 4	From Side	0.684	0.668

Center	From End	0.611	0.568
Strain Gage 5 Center	From Side	0.687	0.677
	From End	3.010	3.023
Strain Gage 6 Center	From Side	0.684	0.675
	From End	4.493	4.550

Figure A-20 Pictures of Specimen 1 and Strain Gage Locations

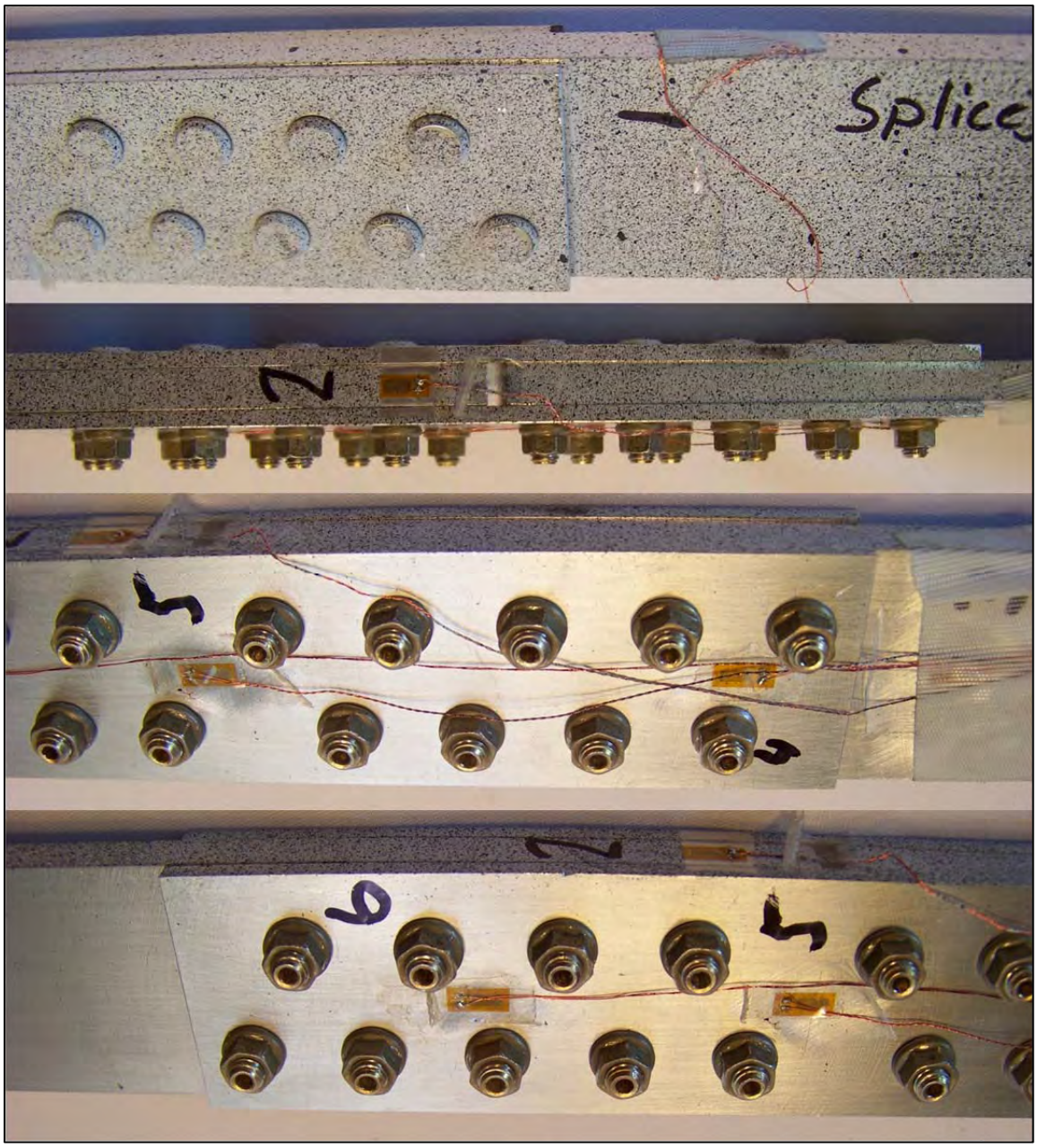

Figure A-21 Pictures of Specimen 3 and Strain Gage Locations

A.4 Non-Strain Gage Specimens

This section contains series of pictures of specimens two and four which did not have strain gages. As such, the pictures are not especially revealing but are included for the

sake of complete documentation. Figure A-22 contains a series of four images that show the top, bottom and two sides of specimen two. Figure A-23 contains a series of five images that show the top, bottom in two images, and the two sides of specimen four.

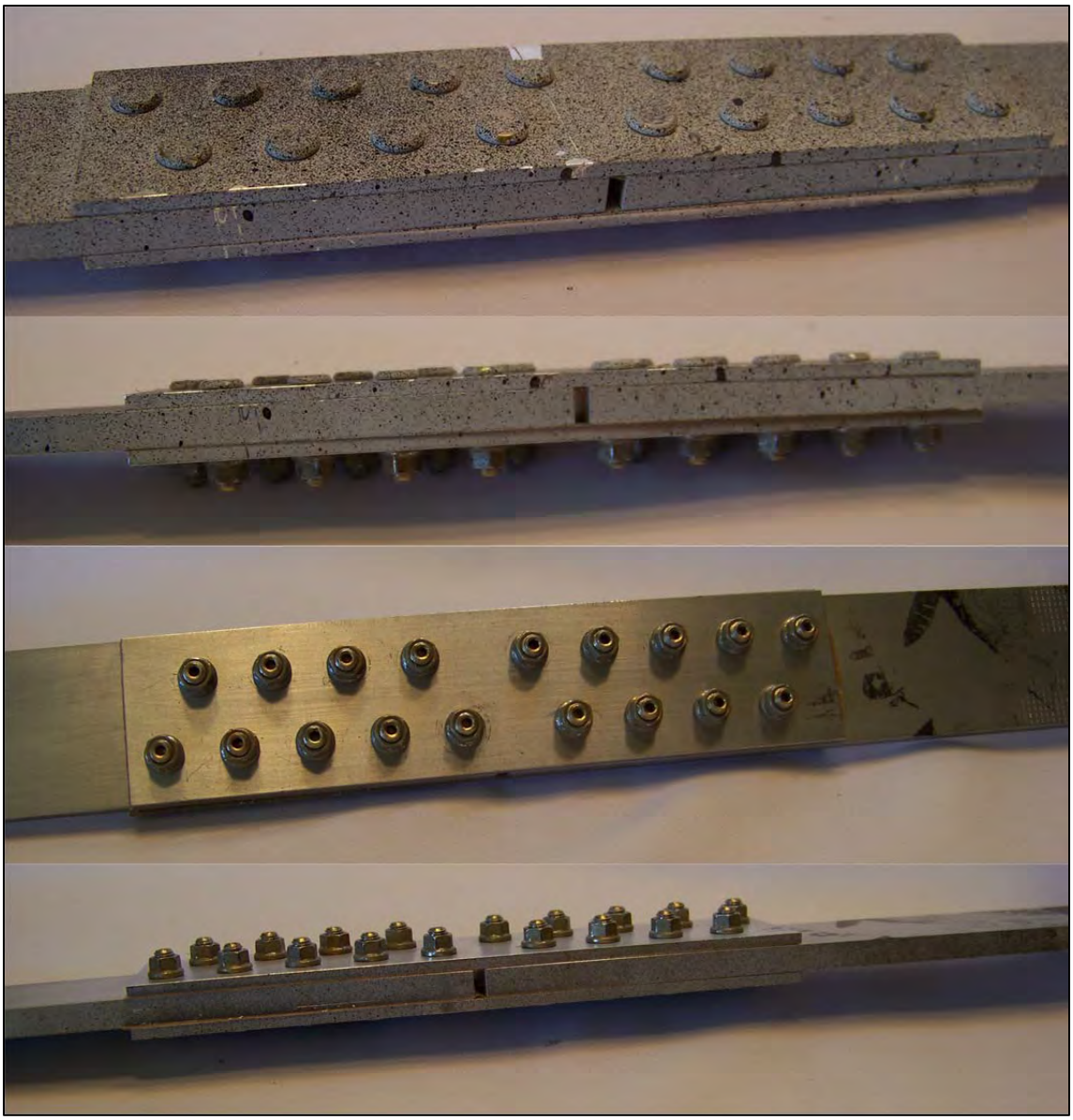

Figure A-22 Pictures of Specimen 2

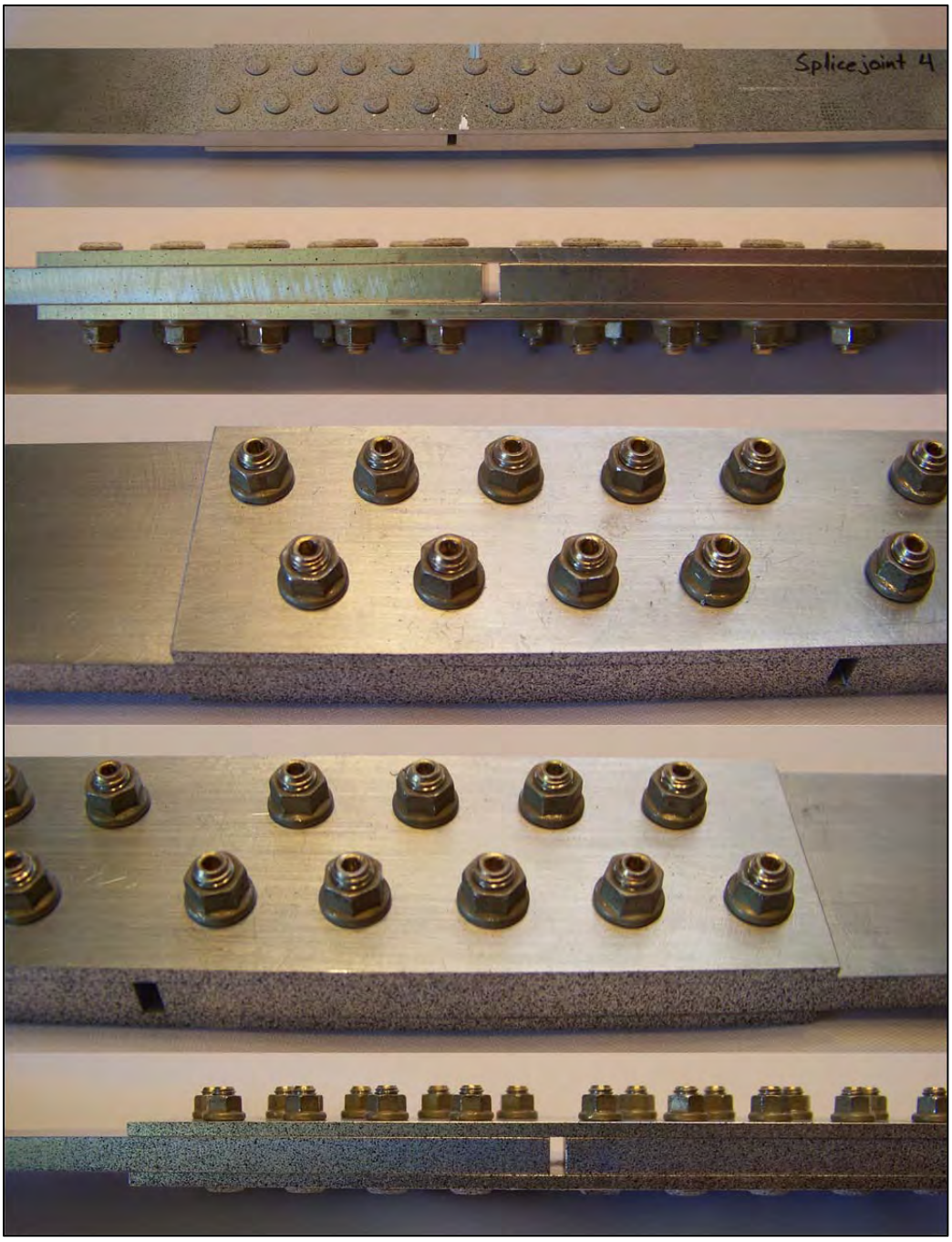

Figure A-23 Pictures of Specimen 4

A.5 Specimen Crack Growth Data

Specimen crack growth data is given in the following tables. Table A-6 contains the raw a-N data as collected by technicians at SwRI in the laboratory. Table A-7 contains the same curves with the cycles interpolated to a starting crack length of 0.034 inch which corresponds to the first recorded crack growth increment of specimen one which was the largest first crack length recorded.

Table A-6 Raw Crack Growth Data as Measured in the Laboratory

Specimen 1		Specimen 2		Specimen 3		Specimen 4	
Cycle Count	Crack Length	Cycle Count	Crack Length	Cycle Count	Crack Length	Cycle Count	Crack Length
0	0.02	0	0.02	0	0.02	0	0.02
5000	0.034	6000	0.024	3000	0.032	3000	0.027
6000	0.048	7000	0.033	4000	0.044	4000	0.038
7000	0.055	8000	0.052	5000	0.061	5000	0.053
8000	0.066	9000	0.065	6000	0.082	6000	0.067
9000	0.075	10000	0.082	7000	0.099	7000	0.081
10000	0.089	11000	0.101	8000	0.119	8000	0.096
11000	0.106	12000	0.123	9000	0.14	9000	0.113
12000	0.119	13000	0.146	10000	0.172	10000	0.134
13000	0.132	14000	0.171	11000	0.211	11000	0.155
14000	0.153	15000	0.211	12000	Through	12000	0.182
15000	0.167	16000	Through	20434	Through	13000	0.209
16000	0.196	17000	Through	20534	Through	14000	Through
17000	0.228	18000	Through	20634	Through	21000	Through
17661	Through	19000	Through	20734	Through	21100	Through
				20819	Through	21200	Through
						21300	Through
						21400	Through
						21500	Through
						21600	Through
						21700	Through
						21800	Through

Table A-7 Crack Growth Data Adjusted to a 0.034 Inch Starting Point

Specimen 1		Specimen 2		Specimen 3		Specimen 4	
Cycle Count	Crack Length	Cycle Count	Crack Length	Cycle Count	Crack Length	Cycle Count	Crack Length
0	0.034	947	0.052	833	0.044	364	0.038
1000	0.048	1947	0.065	1833	0.061	1364	0.053
2000	0.055	2947	0.082	2833	0.082	2364	0.067
3000	0.066	3947	0.101	3833	0.099	3364	0.081
4000	0.075	4947	0.123	4833	0.119	4364	0.096
5000	0.089	5947	0.146	5833	0.14	5364	0.113
6000	0.106	6947	0.171	6833	0.172	6364	0.134
7000	0.119	7947	0.211	7833	0.211	7364	0.155
8000	0.132	8947	Through	8833	Through	8364	0.182
9000	0.153	9947	Through	17267	Through	9364	0.209
10000	0.167	10947	Through	17367	Through	10364	Through
11000	0.196	11947	Through	17467	Through	17364	Through
12000	0.228			17567	Through	17464	Through
12661	Through			17652	Through	17564	Through
						17664	Through
						17764	Through
						17864	Through
						17964	Through
						18064	Through
						18164	Through

A.6 Strain Survey Data and Strain Gage Correlation

This section contains strain survey data from specimens one and three. Gage locations are indicated in Section A.3. Strain data for gage five is suspect for all points of specimen one and the first reading on specimen three. It appears that the gage factor programmed in was incorrect; in fact, all gage factors received for specimen 3 were off by a factor of 10 and the gage factor for gage three of specimen two was off by a factor of two. Table A-8 and Table A-9 contain the maximum strains from the strain surveys

taken during testing. The strains are ratioed by the load from the load cell at that strain divided by the target load of 4,000 lbs.

Table A-8 Strain Readings from the Strain Surveys in Micro Strain from Specimen One

Cycle Count	Crack Length	Strain Gage 1	Strain Gage 2	Strain Gage 3	Strain Gage 4	Strain Gage 5	Strain Gage 6
0	0.02	1150	472	1092	364	1954	804
5000	0.034	1129	460	1176	351	1933	788
6000	0.048	1127	466	1194	358	1922	770
7000	0.055	1127	469	1197	361	1937	774
8000	0.066	1129	470	1194	363	1934	777
9000	0.075	1128	471	1194	365	1928	774
10000	0.089	1124	468	1190	360	1914	771
11000	0.106	1127	472	1189	365	1913	775
12000	0.119	1128	476	1192	365	1912	779
13000	0.132	1122	474	1184	366	1907	778
14000	0.153	1118	473	1182	367	1901	777
15000	0.167	1121	475	1193	369	1895	781
16000	0.196	1116	477	1187	368	1888	784
17000	0.228	1107	475	1185	366	1871	780
17661	Through	1080	498	1211	373	1797	802

Table A-9 Strain Readings from the Strain Surveys in Micro Strain from Specimen Three

Cycle Count	Crack Length	Strain Gage 1	Strain Gage 2	Strain Gage 3	Strain Gage 4	Strain Gage 5	Strain Gage 6
0	0.02	1149	127	1082	330	1920	765
3000	0.032	1120	90	1115	311	1458	718
4000	0.044	1124	91	1116	310	1465	720
5000	0.061	1123	93	1114	312	1454	723
6000	0.082	1124	90	1117	309	1448	719
7000	0.099	1128	92	1120	312	1441	716
8000	0.119	1125	91	1119	311	1427	717
9000	0.14	1129	102	1124	322	1434	723
10000	0.172	1122	101	1125	320	1419	722
11000	0.211	1116	100	1128	322	1393	725
12000	Through	1090	109	1144	330	1346	738
20434	Through	1047	109	1184	345	1189	761

20534	Through	1037	113	1201	355	1201	788
20634	Through	1018	119	1224	378	1189	820
20734	Through	978	132	1282	409	1128	871
20819	Through	860	127	1380	450	1032	975

Figure A-24 and Figure A-25 contain plots of the measured strains as a function of crack size compared with the strains from the 3-D FEM. The specimen strains are also ratioed by the load at the measured strain by the target load.

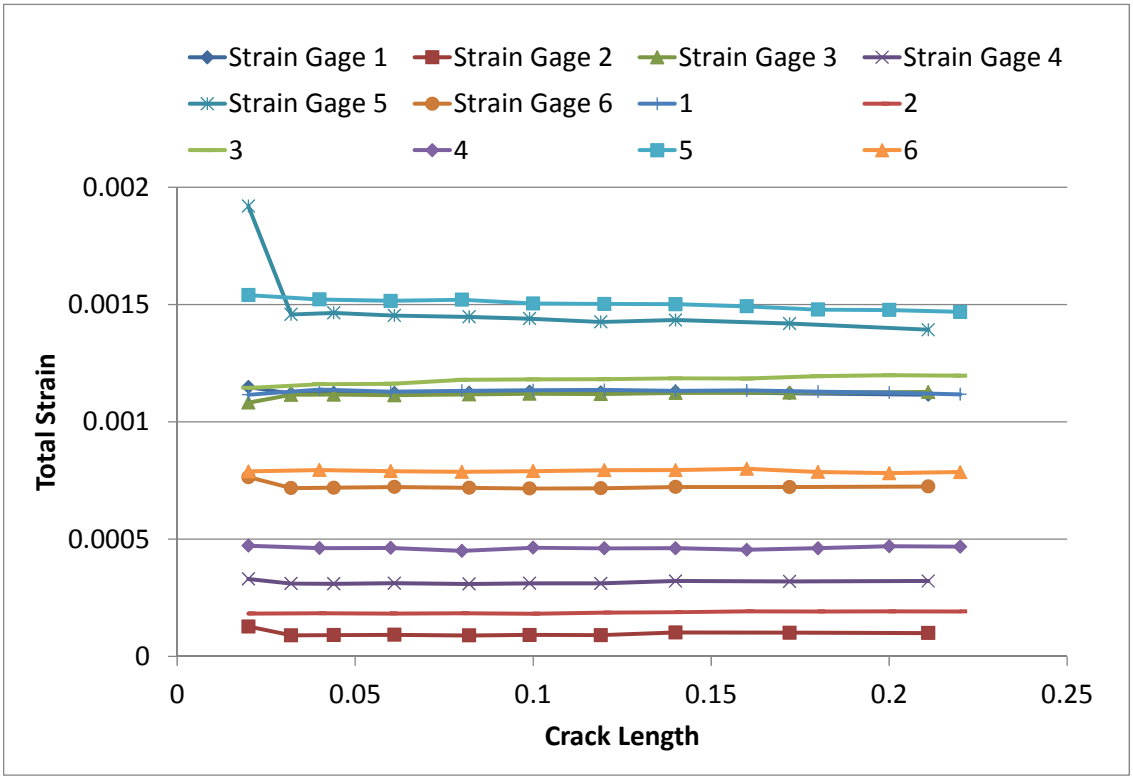

Figure A-24 Strains From FEM versus Strains from Specimen One

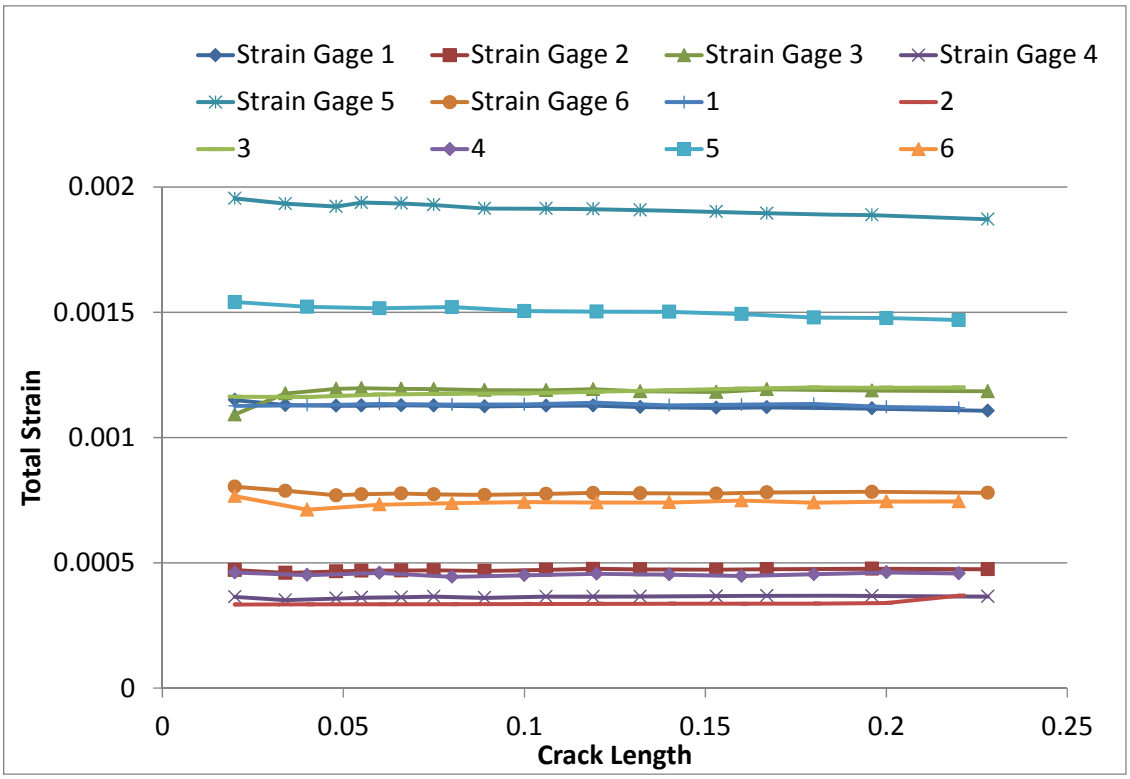

Figure A-25 Strains From FEM versus Strains from Specimen Three

A.7 Digital Image Correlation Data and Strain Correlation

The DIC system can be used to compute strains based on the total relative movement of the different speckles painted on the surface of the specimens. The calculations are done automatically by the VIC-3D 2010 software based on a number of inputs. The most significant input is the number of points to cluster to come up with the solution. This is important since too small of a group will cause point estimates to vary wildly while too large of a group will hide local peaks and average away strain gradients.

Point-wise comparison of every location on the surface is not possible due to the lack of closeness that the DIC is able to get to areas of interest such as near holes. These locations are obscured by both the fastener heads as well as the need to average larger

areas. Figure A-26 shows a representative map of strains in the x-direction from the 3-D FEM above the same map from the DIC analysis software. Note that scales are set equal and that some strains predicted by the FEM are beyond the maximum described by the DIC analysis. Figure A-27 repeats the same plot but with the regions unanalyzable from the DIC blacked out on the FEM. Notice how many of the high strain regions suddenly disappear. Also visual comparisons are hampered by the inability to change color gradients to match from one software to another.

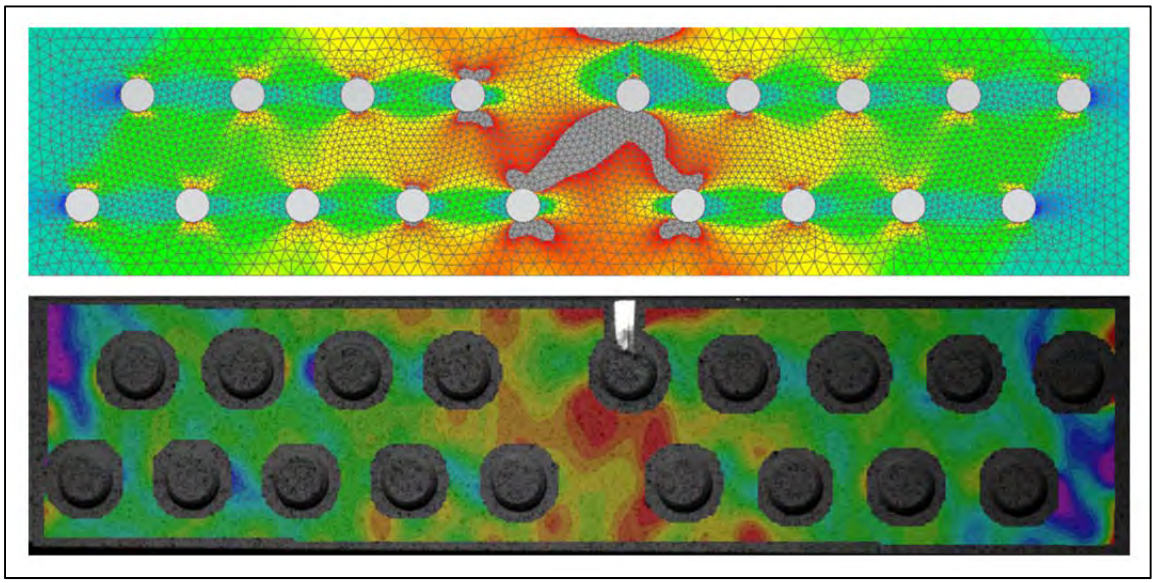

Figure A-26 Strain Map from the 3-D FEM and the DIC Analysis of Joint 1, Both Scales Set Equal

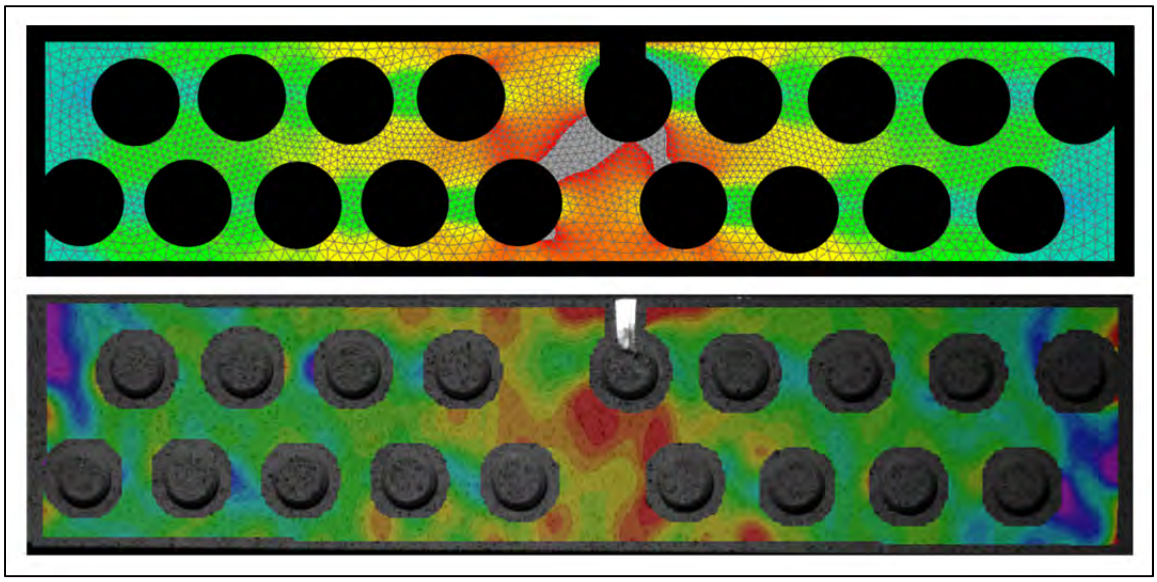

Figure A-27 Repeat of Figure A-26 but with the Unanalyzed Regions from the DIC Image Blacked Out on the FEM Strain Map

Because of these issues, the method used for correlating the FEM with the DIC analysis was one using faux strain gages that average the point results over identical rectangular areas. The value of a faux gage location increases as the strain increases and the strain gradient captured within the area decreases.

An analogy would be averaging a sine wave over different regions of varying length. Averaging the sine wave over an interval of 2π would give zero no matter where the interval was centered. Using a smaller interval and including the peak of interest may come closer but the most accurate estimate would be infinitesimally small and centered on the peak. Using the DIC trying to get infinitesimally small averages into complications including speckle quality and refinement, lighting for the images, stereo camera correlation pattern size, etc. The same problem exists for the FEM since nodal results for the FEM are also discrete locations with minimum distances between nodes.

A study was undertaken to determine the best filter size to use to extract data from the DIC images. Specimen two was used because it had Teflon inserts which reduced the hysteresis which may complicate the determination. Also, it had the most even stresslines, or strainlines in this case, at the tightest sampling set allowed by the software (smallest filter is 5). Figure A-28 displays the more even strain lines (0.0005 inch/inch gradients) versus joint specimens one through four shown in Figure A-29 through Figure A-32 respectively.

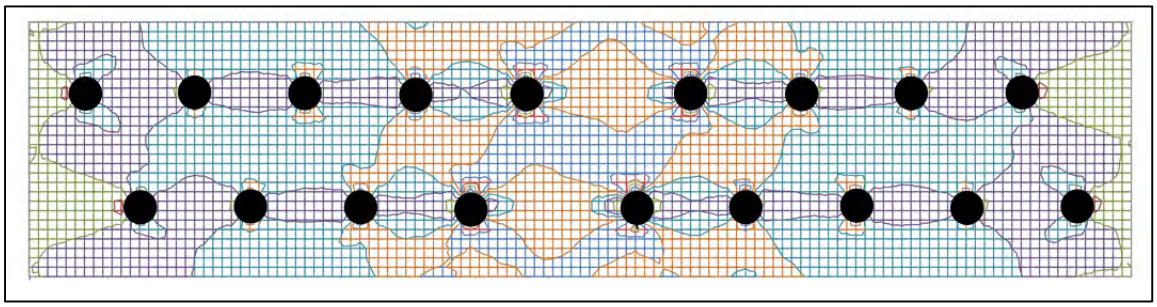

Figure A-28 Strainlines from 3-D FEM

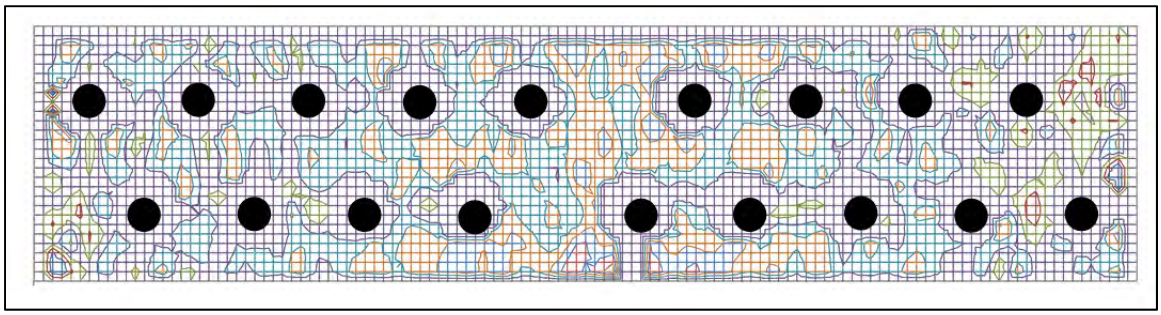

Figure A-29 Strainlines on Joint Specimen 1

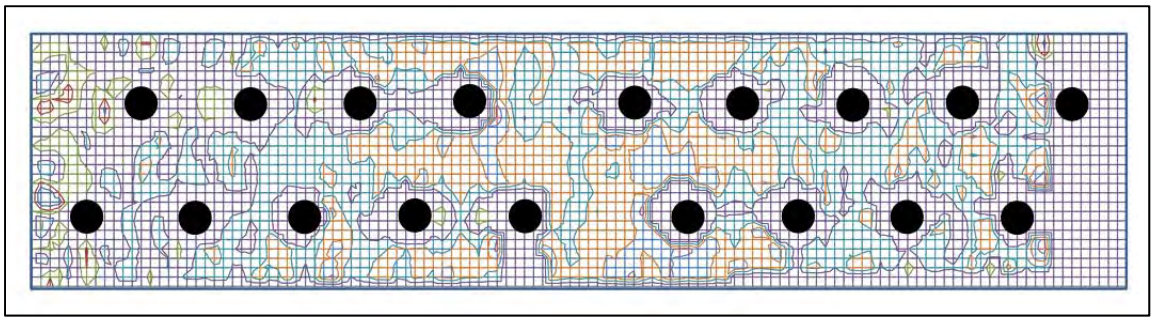

Figure A-30 Strainlines on Joint Specimen 2

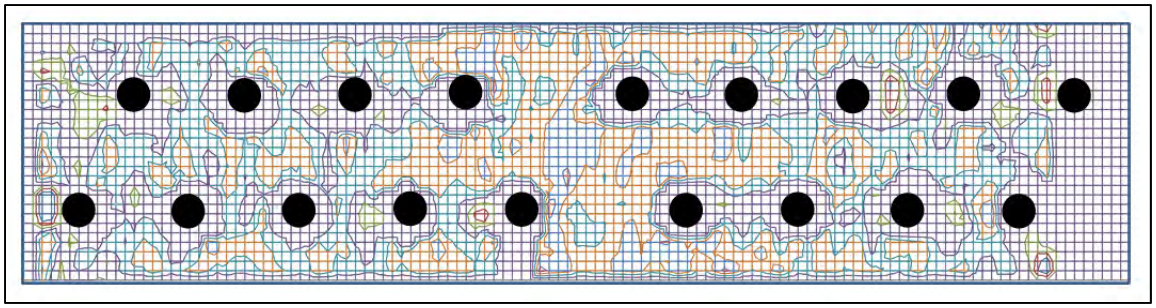

Figure A-31 Strainlines on Joint Specimen 3

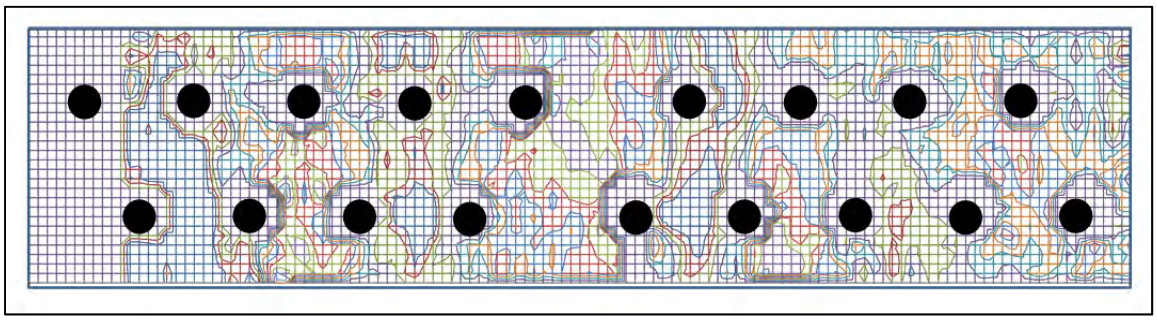

Figure A-32 Strainlines on Joint Specimen 4

Since some of the joint specimen images were slightly oblique or skewed the resulting mapping may not put the exact location in the right place. Every attempt was made to map the relative placement of the pixels to the correct location on the splice plate but some variation may exist. Thus different faux gage sizes were tested and the results appeared to be more stable with a slightly larger gage. The chosen gage size of 0.3 inch

in the x-direction and 0.15 inch in the y-direction was somewhat arbitrarily chosen; but is exactly double the micro gage size that was used on specimens one and three.

A number of different locations were considered for locating the faux gages to determine the optimum filter size. Based on the ideal gradient from the 3-D FEM it is more or less down the centerline. Variation from this is evident in the specimens as hole-to-hole variation causes some fasteners to be more effective due to a closer tolerance than other holes. Seventeen faux gages were evaluated; eight on each side down the centerline in-line with fasteners two through seventeen, faux gage nine was centered between fasteners nine and ten. Figure A-33 shows the results for joint specimen two initially with the 0.020 inch notch. Filter size is required to be an odd number and results are displayed for filter sizes: 5, 9, 11, 13, 15, 17, 21, 31, 41, and 61. Based on the figure it appears the best compromise for filter size is 13. Note that based on Figure A-28 through Figure A-32 that faux gages 1 through 17 progress from right to left for the FEM, joint one and joint four, but left to right for joint two and joint three.

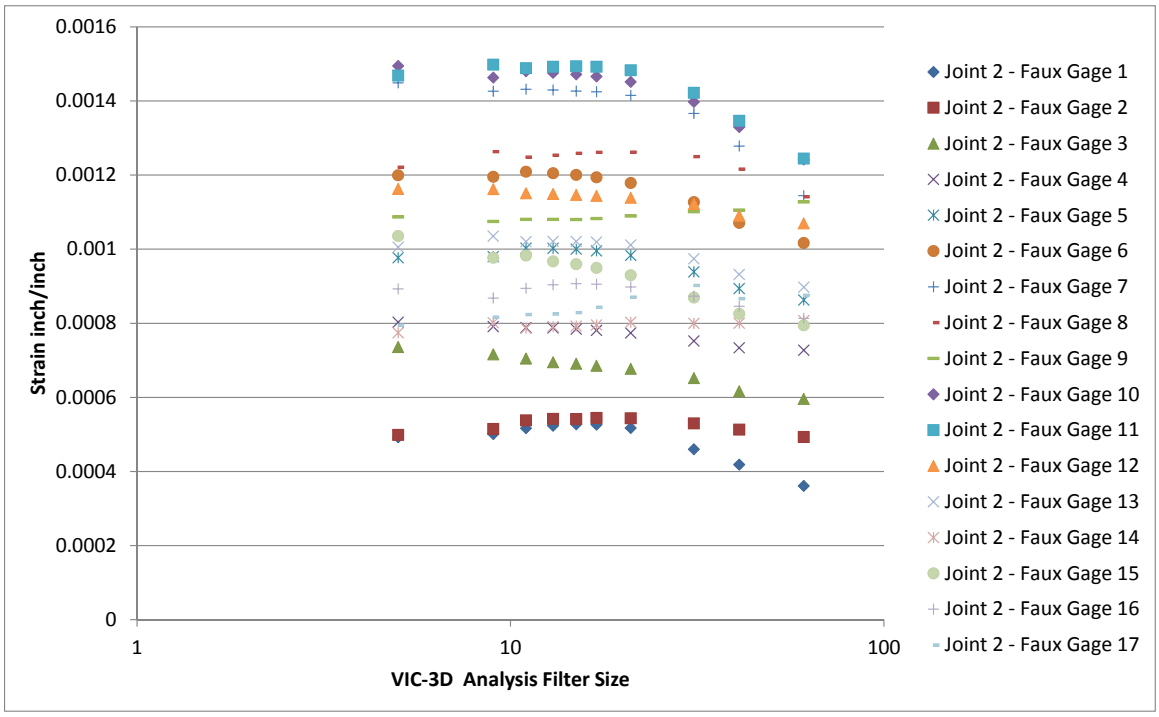

Figure A-33 Strain Calculated by Faux Gages on Joint 2 for Various Filter Sizes

One advantage of this method is that additional faux gages are 'free' and can be placed post-experiment. To evaluate the strains from the FEM both down the centerline as well as on the fringes to the side outside of the fastener pattern additional faux gages were added numbers 18 to 34. Note that gages 24 and 26 are opposing gages on opposite sides of the crack. They are placed on a line halfway to the holes centerline or 0.19 inch as shown in Figure A-34. Comparisons of the 34 faux gages are presented in order in Figure A-35 and Figure A-68. Faux gages are not placed inline with holes one or seventeen because of issues with the image region captured during testing for joint specimens two, three, and four.

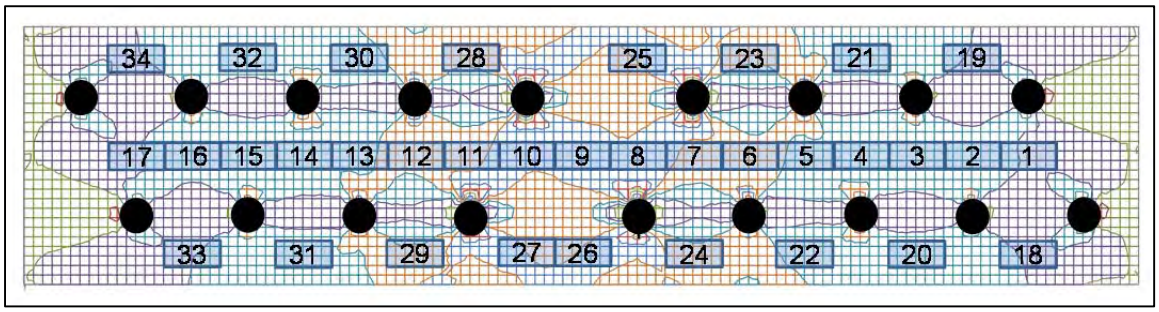

Figure A-34 Location of Faux Gages for 3-D FEM Correlation

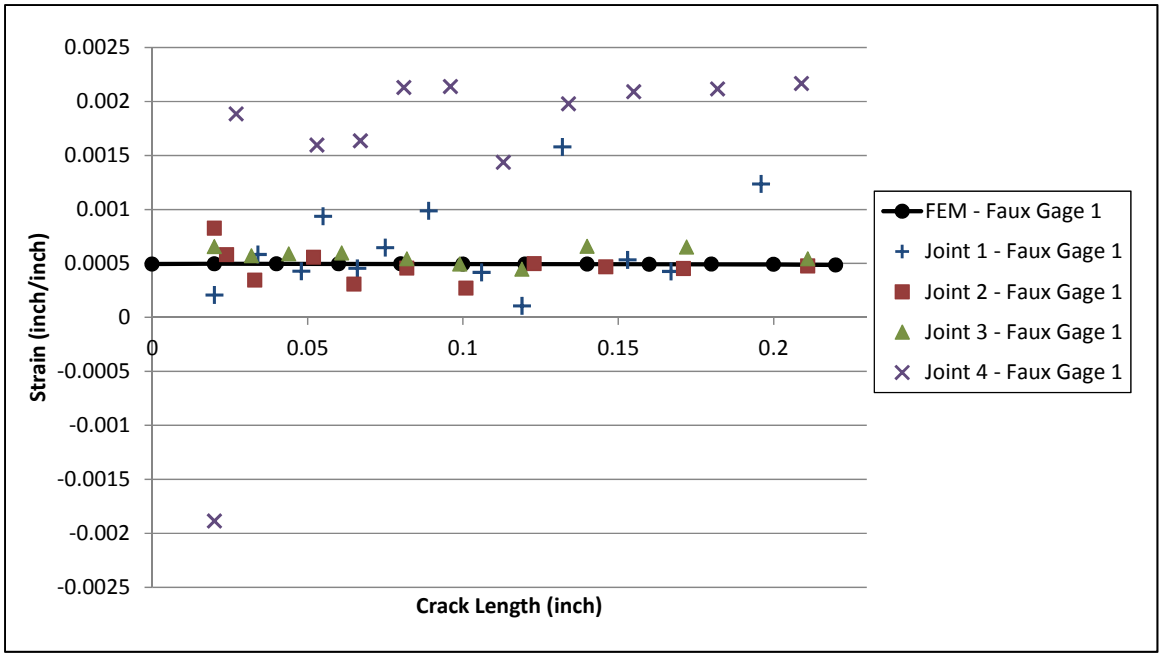

Figure A-35 Faux Gage 1 Response

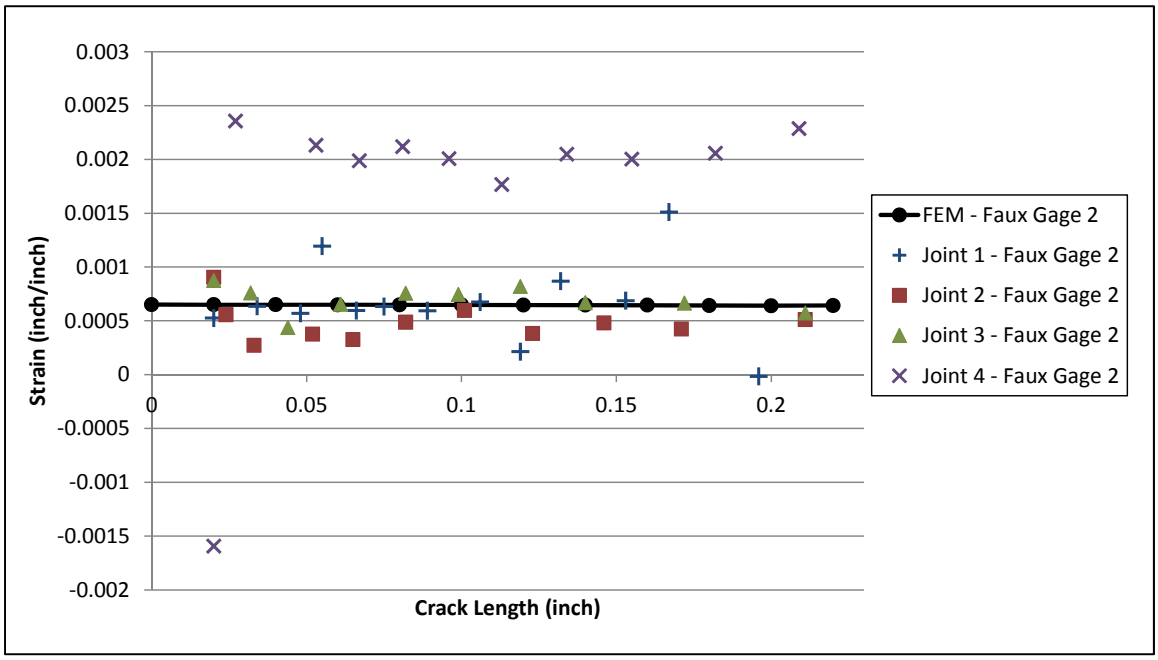

Figure A-36 Faux Gage 2 Response

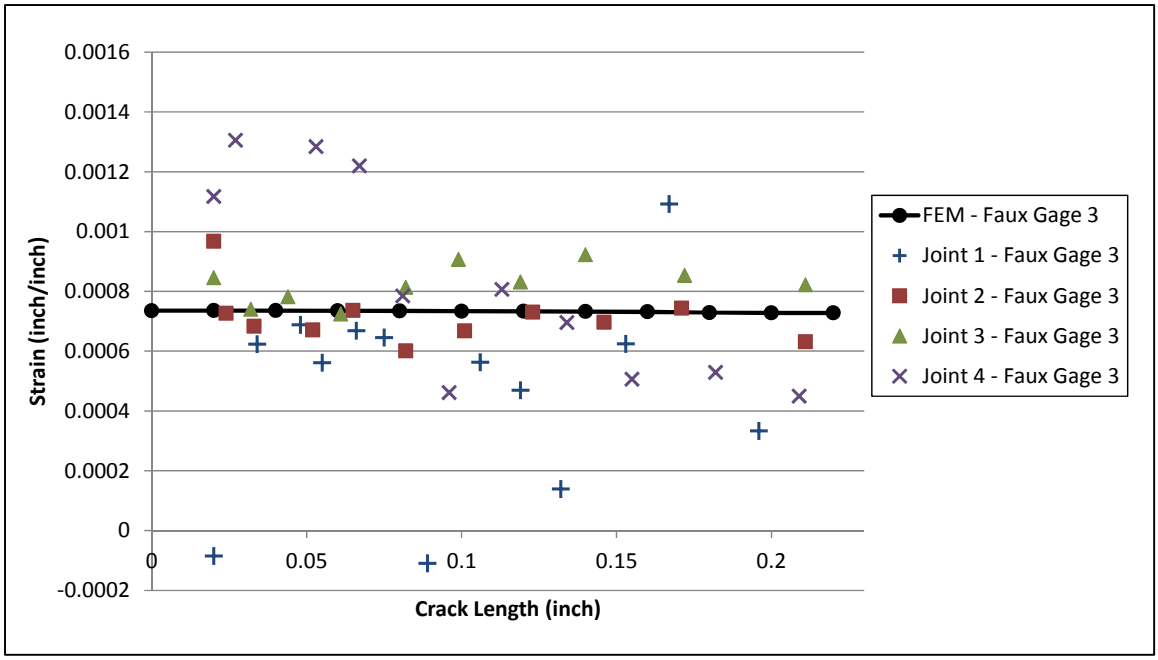

Figure A-37 Faux Gage 3 Response

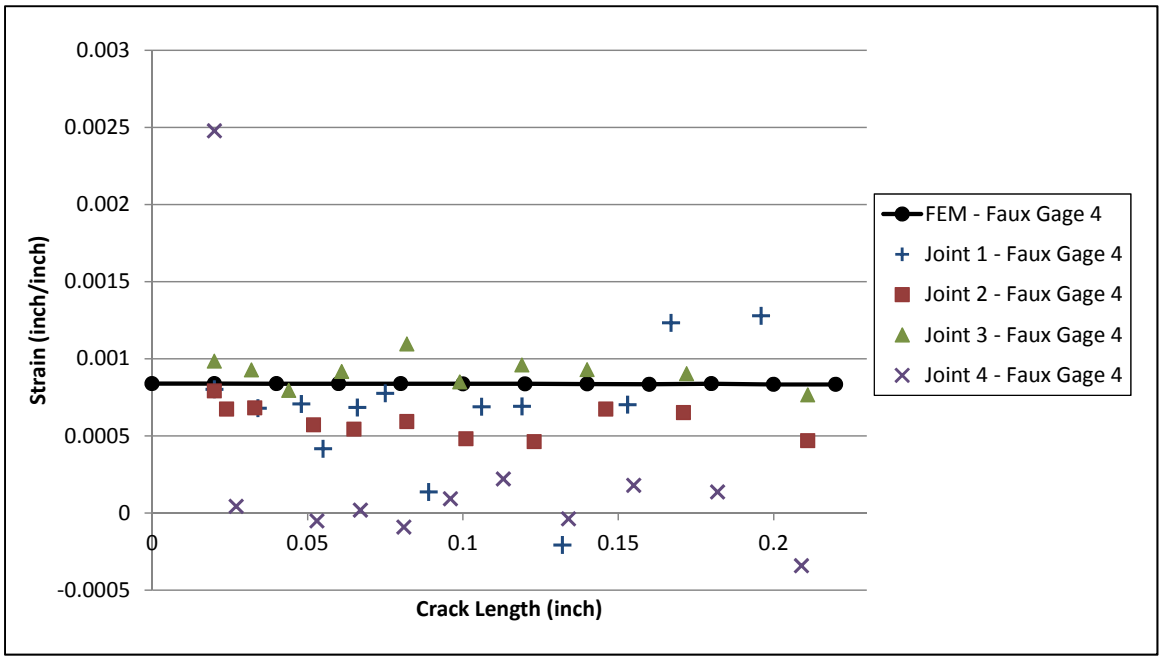

Figure A-38 Faux Gage 4 Response

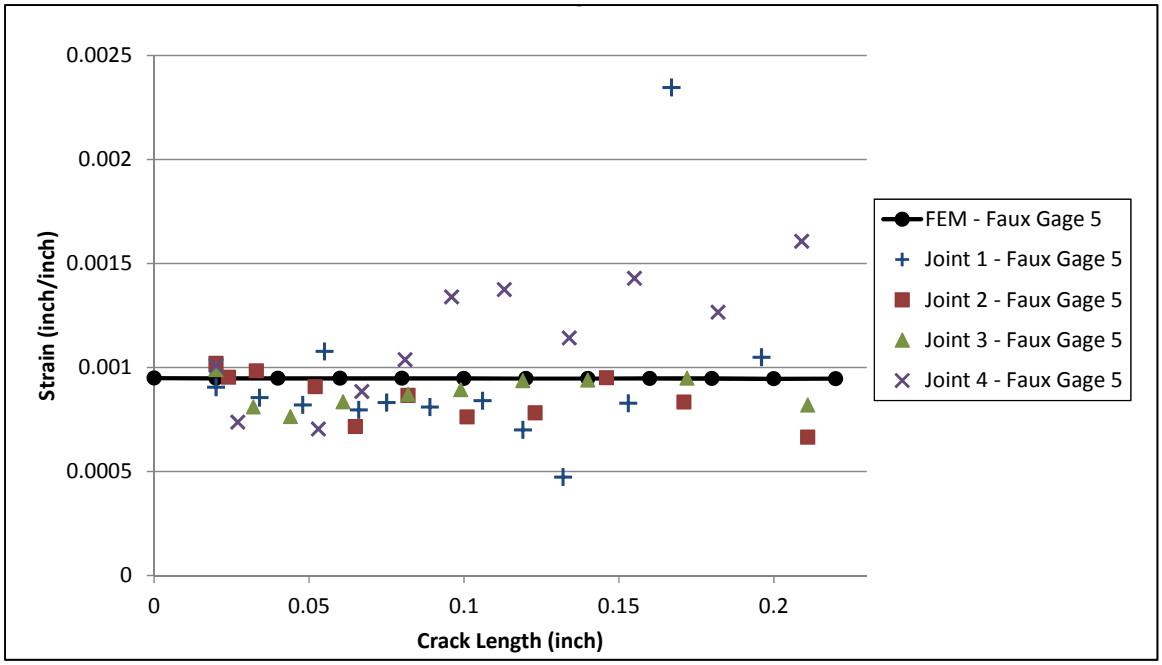

Figure A-39 Faux Gage 5 Response

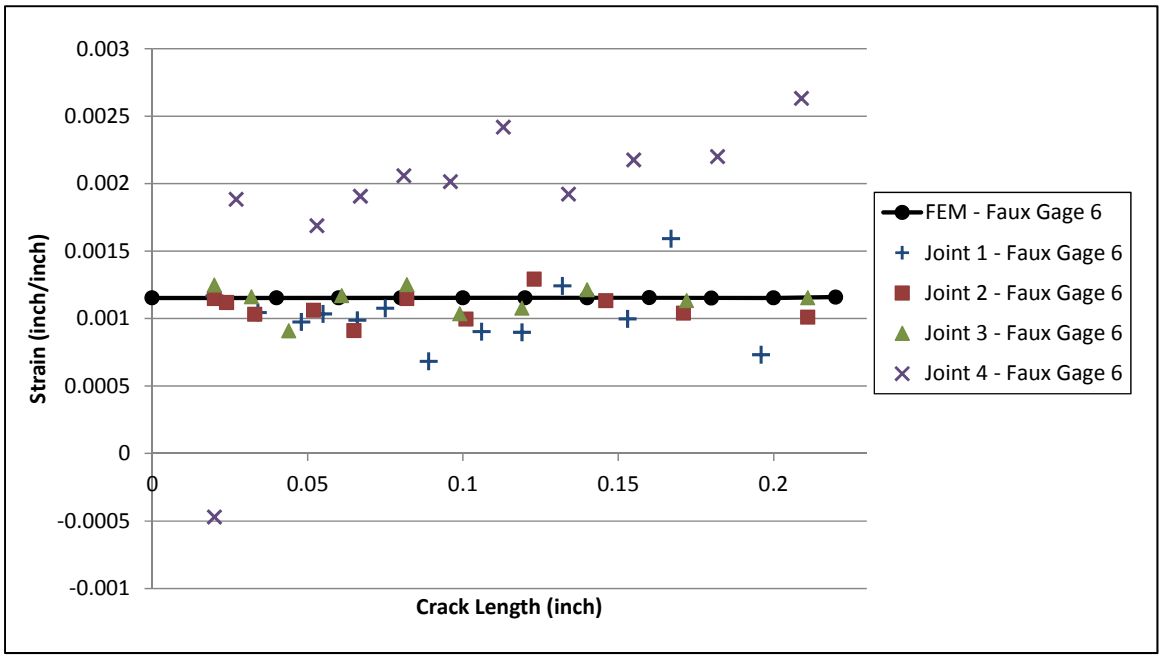

Figure A-40 Faux Gage 6 Response

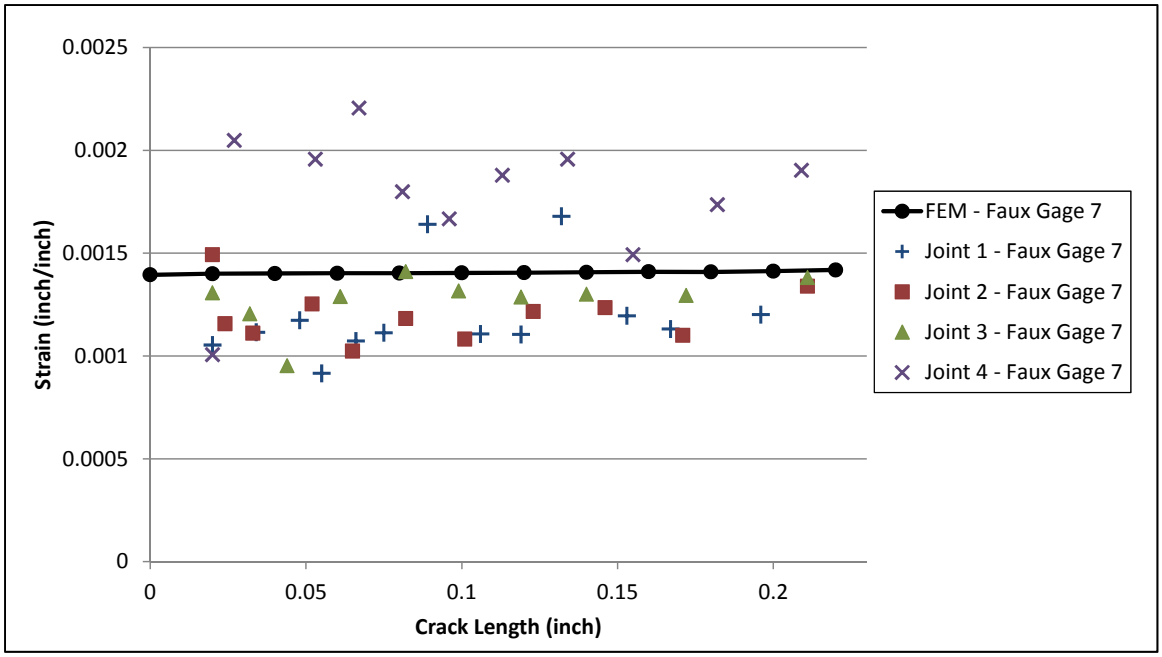

Figure A-41 Faux Gage 7 Response

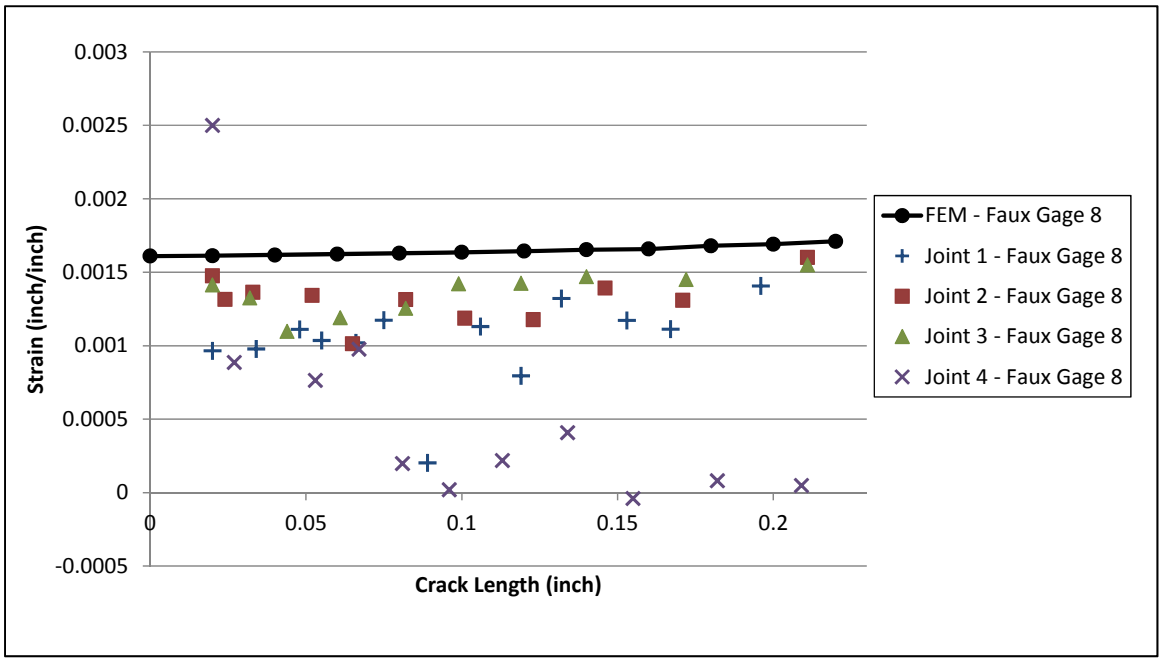

Figure A-42 Faux Gage 8 Response

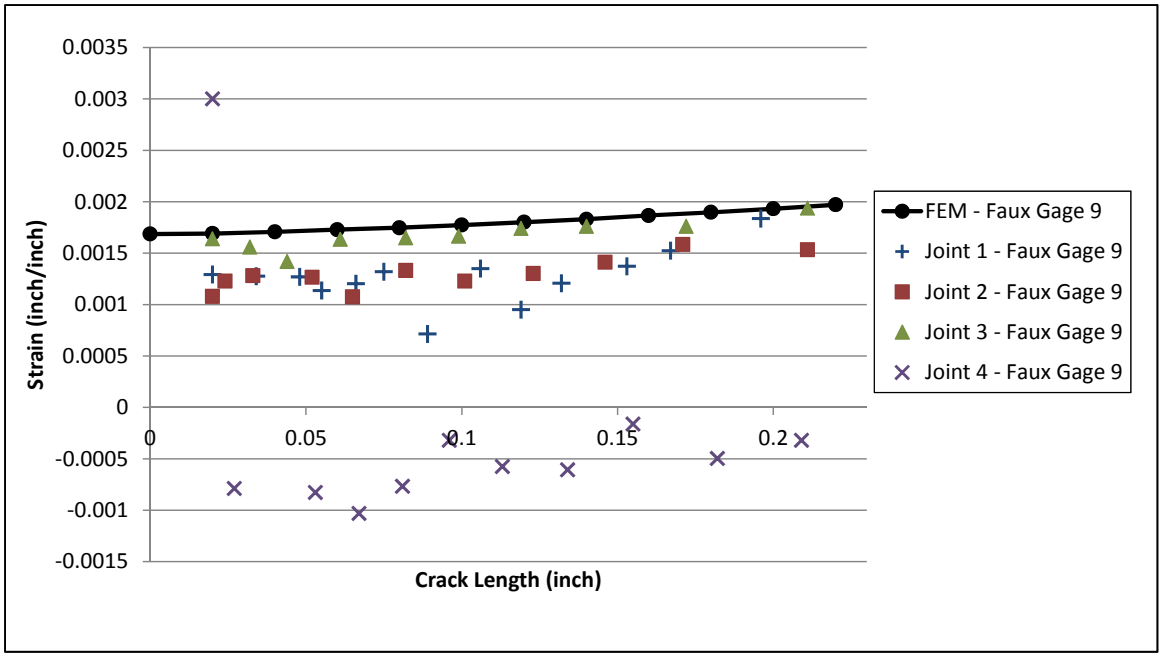

Figure A-43 Faux Gage 9 Response

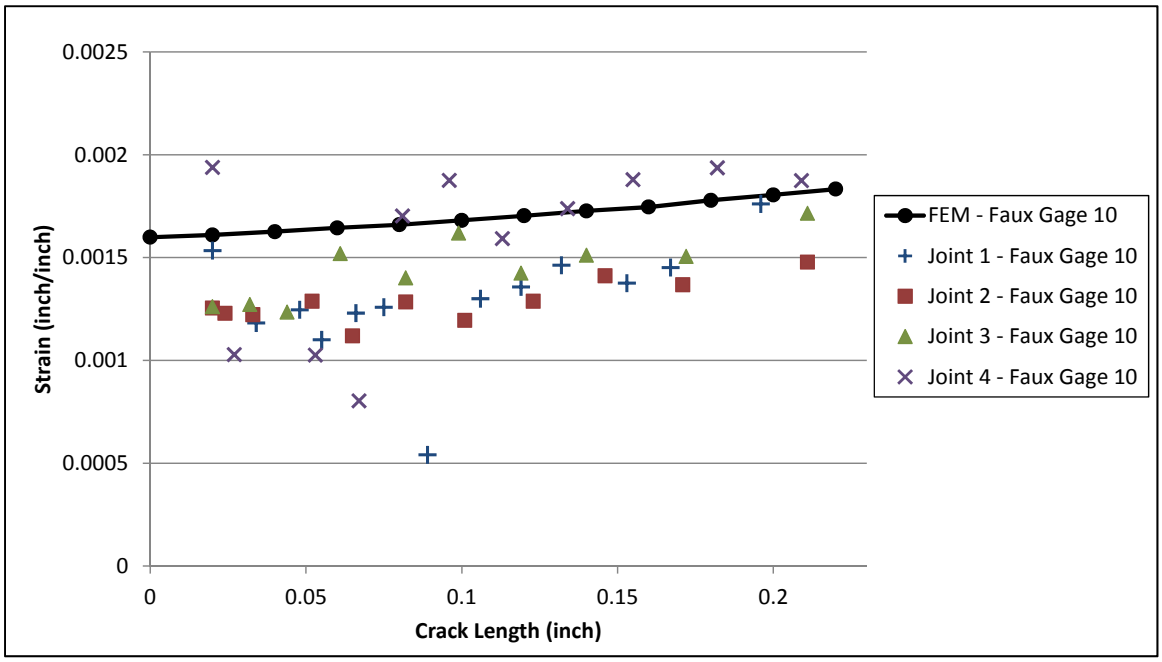

Figure A-44 Faux Gage 10 Response

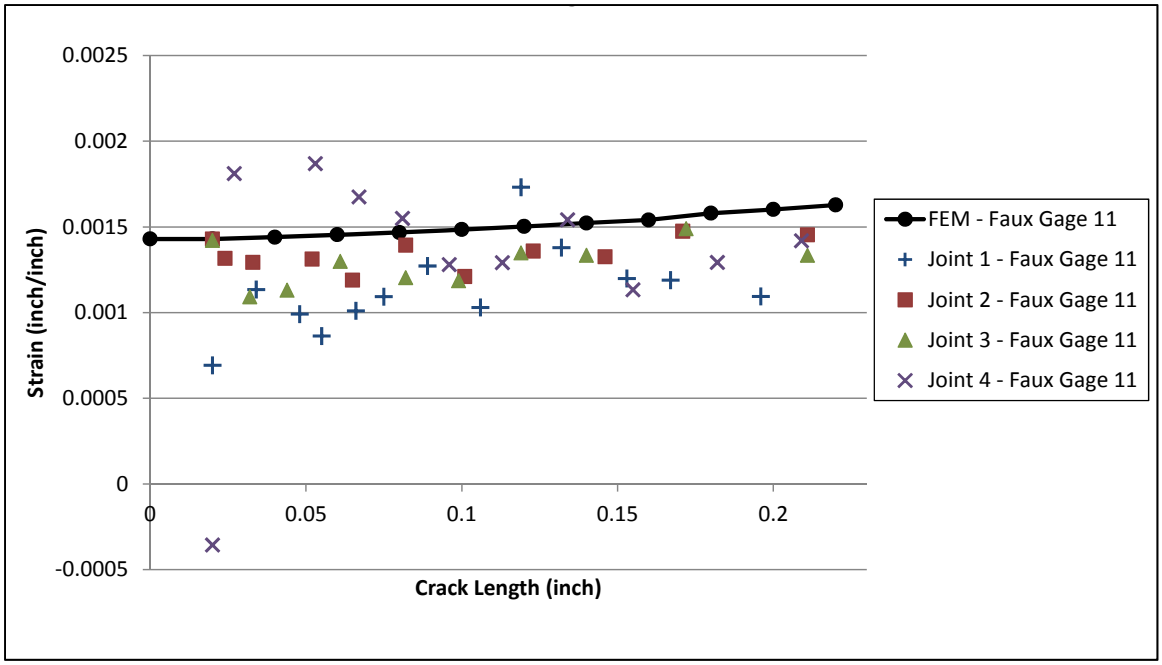

Figure A-45 Faux Gage 11 Response

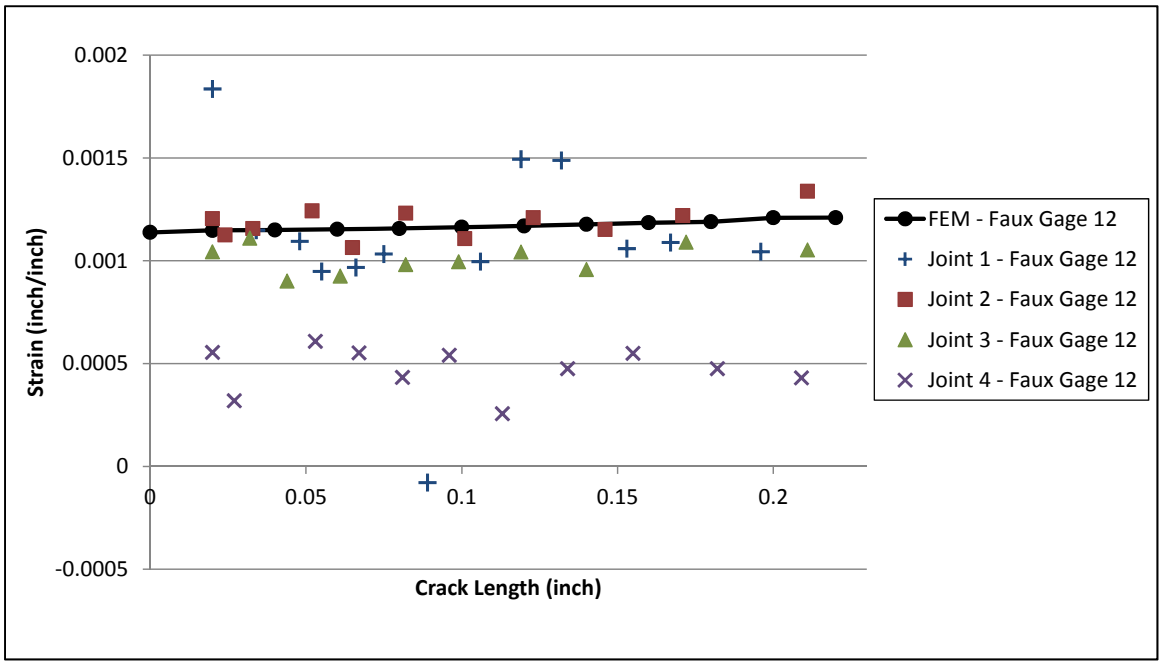

Figure A-46 Faux Gage 12 Response

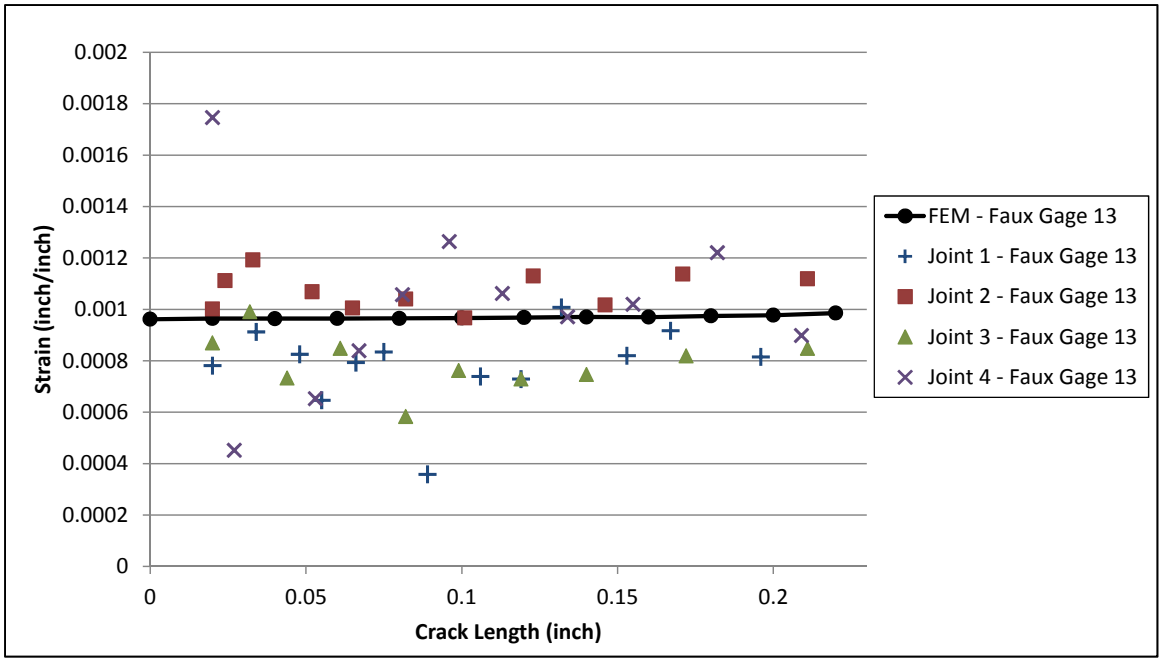

Figure A-47 Faux Gage 13 Response

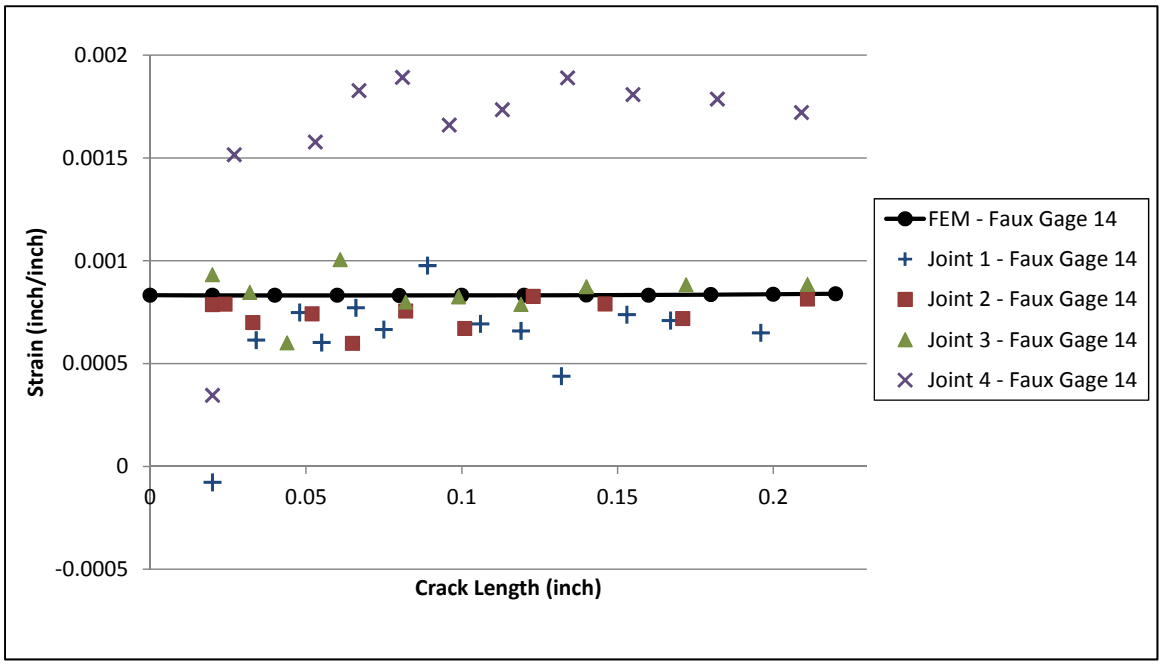

Figure A-48 Faux Gage 14 Response

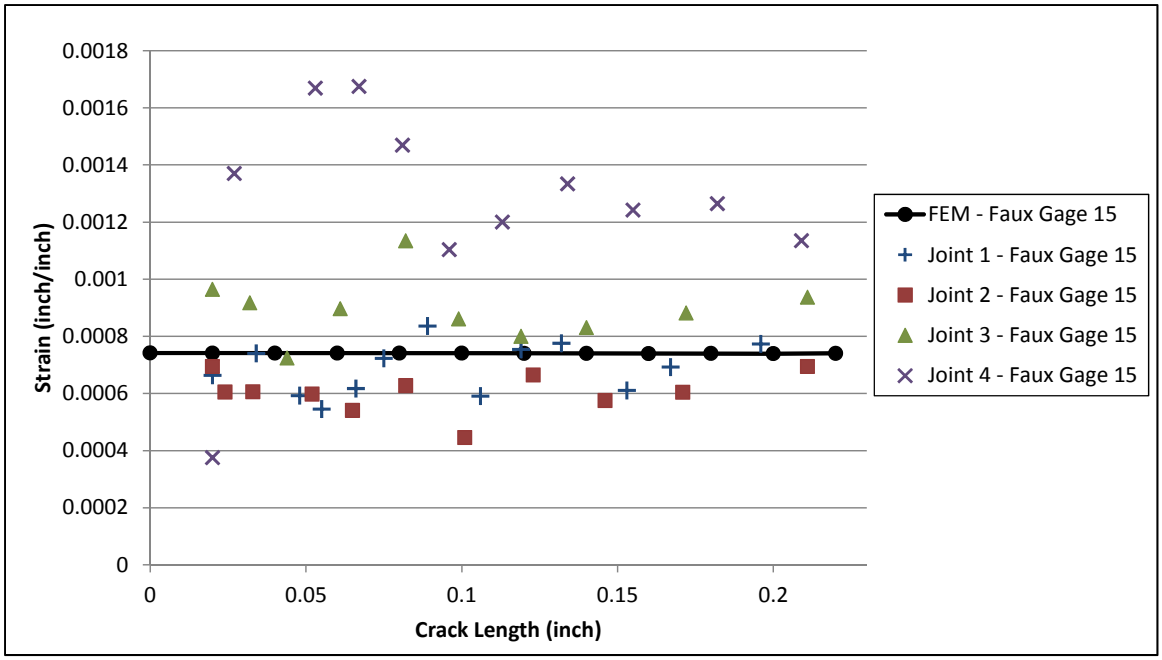

Figure A-49 Faux Gage 15 Response

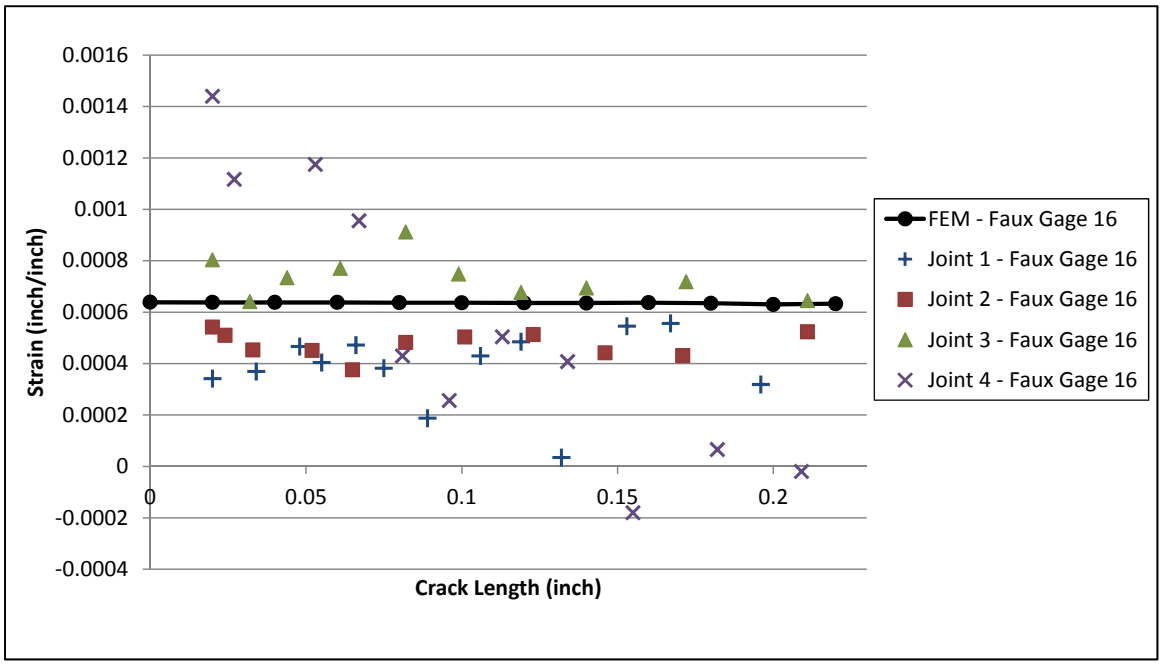

Figure A-50 Faux Gage 16 Response

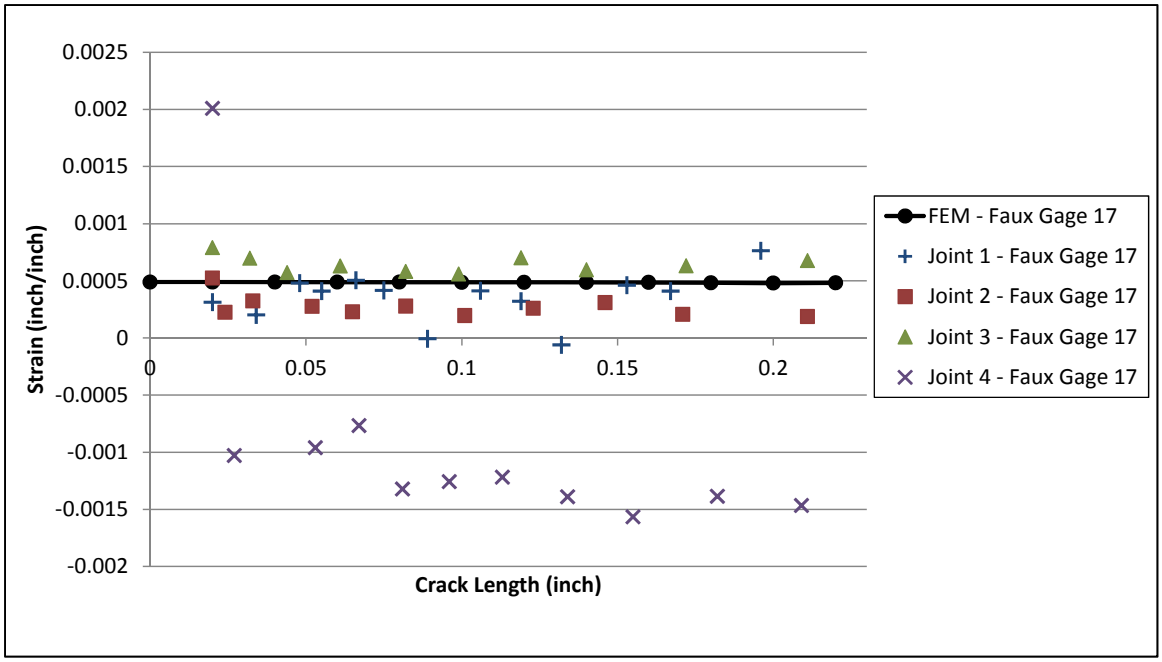

Figure A-51 Faux Gage 17 Response

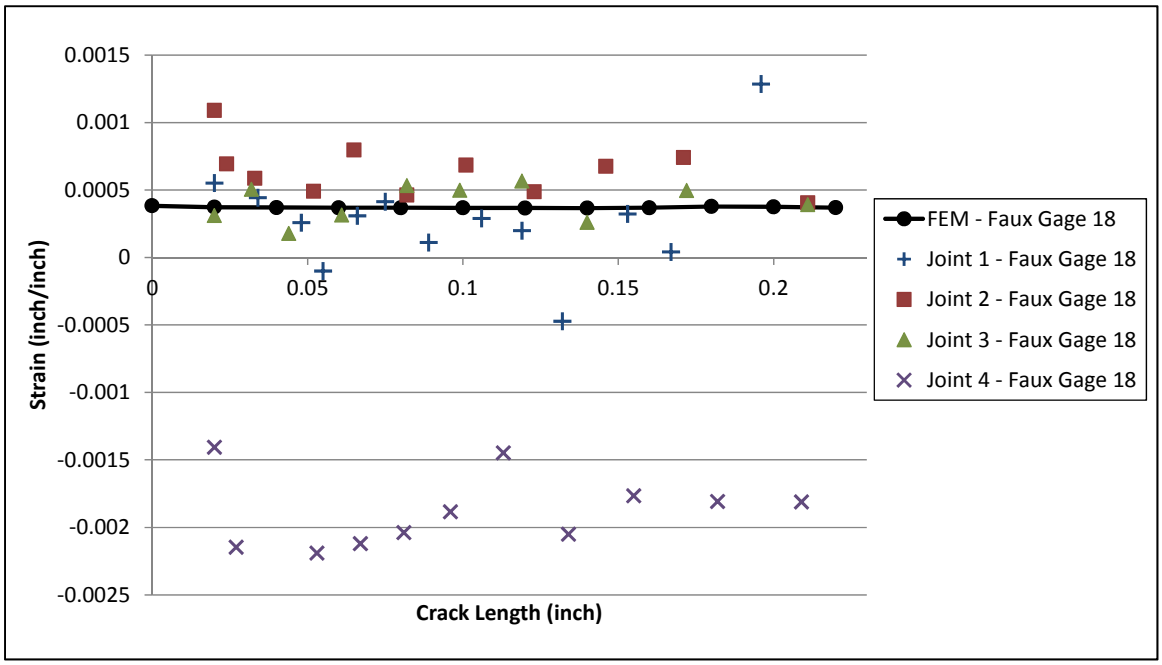

Figure A-52 Faux Gage 18 Response

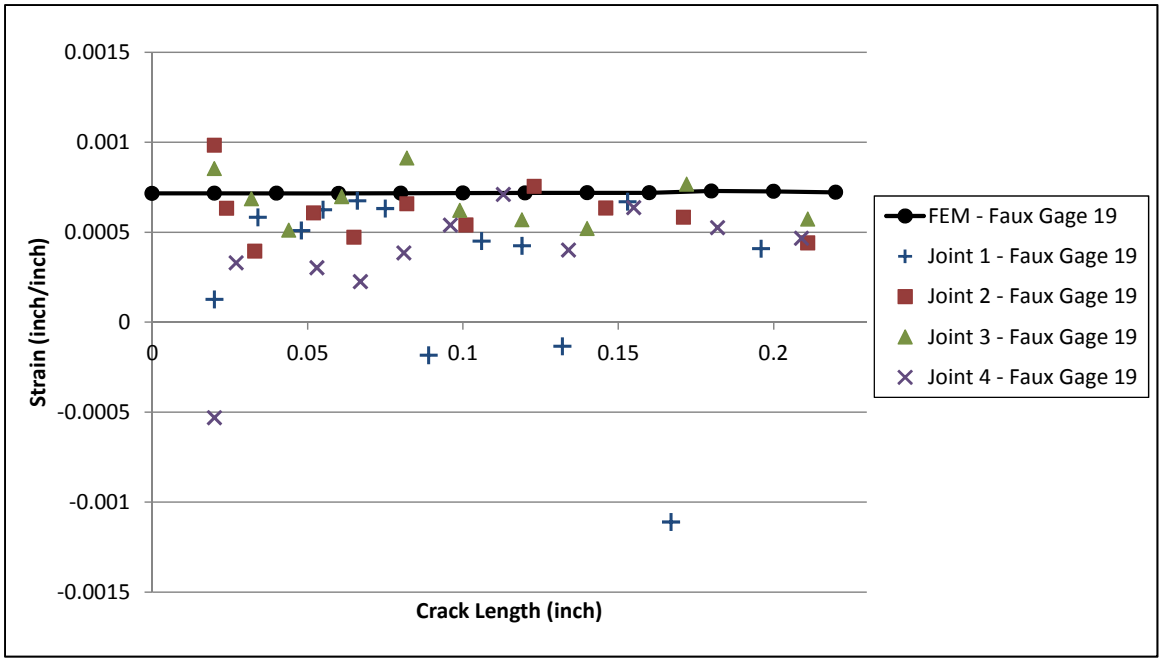

Figure A-53 Faux Gage 19 Response

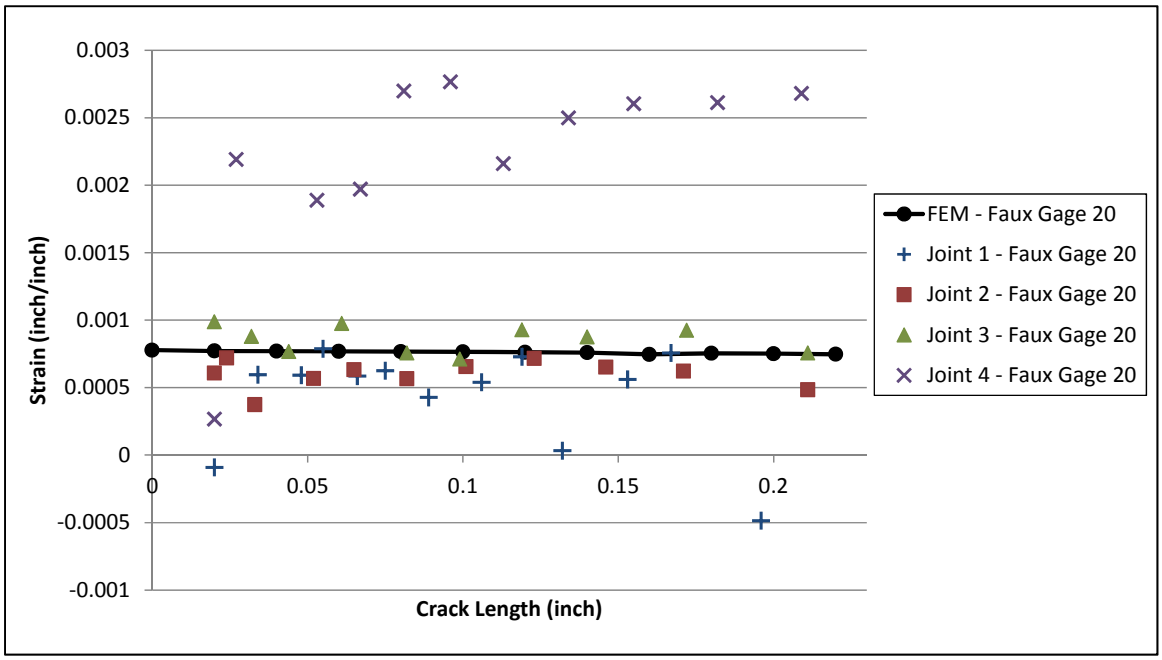

Figure A-54 Faux Gage 20 Response

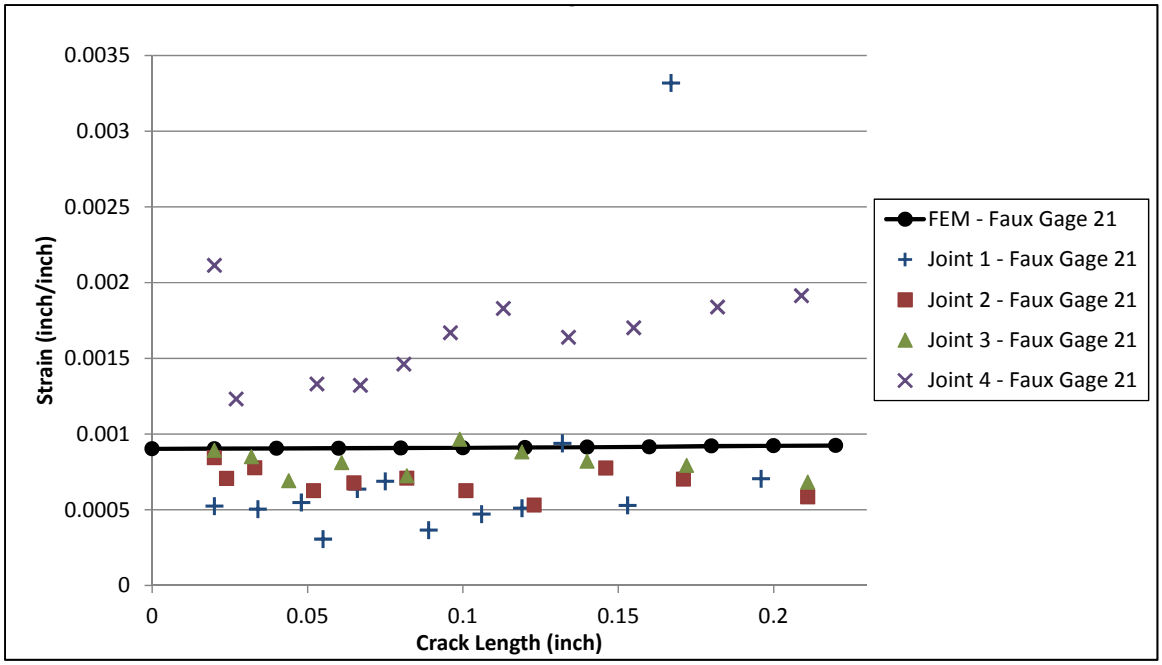

Figure A-55 Faux Gage 21 Response

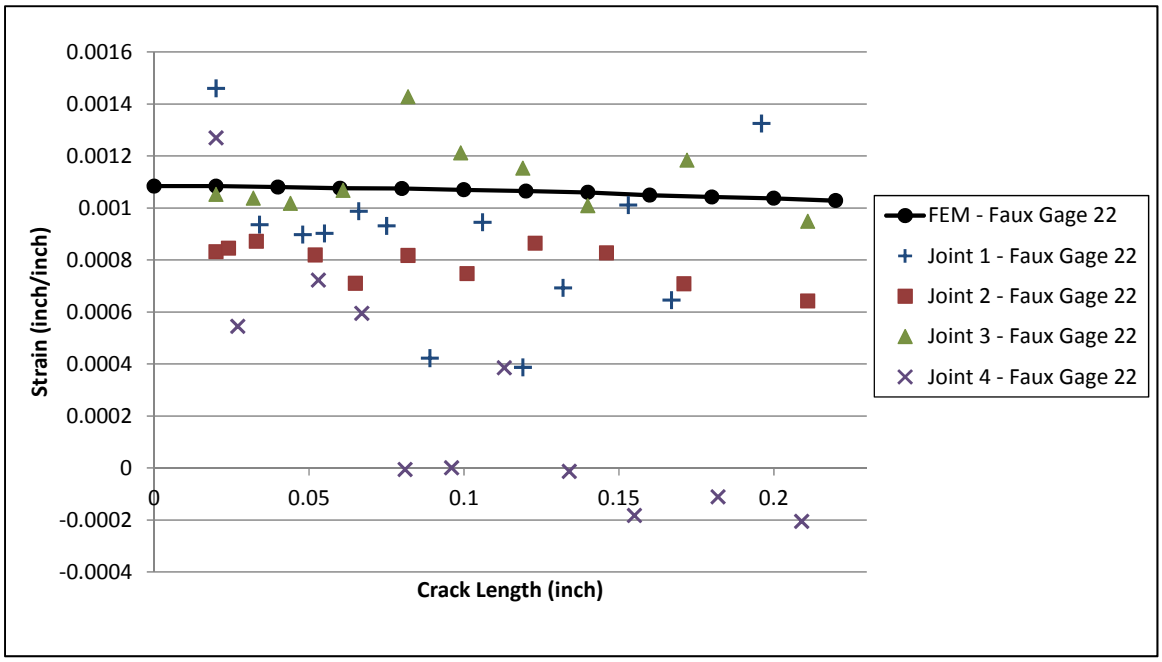

Figure A-56 Faux Gage 22 Response

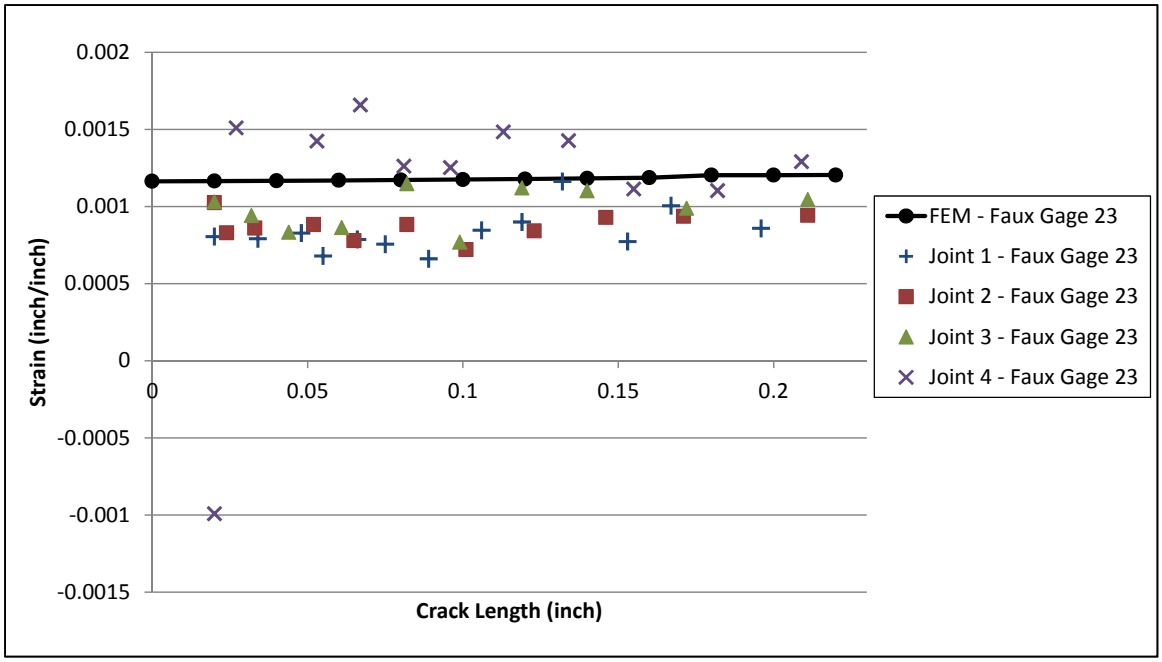

Figure A-57 Faux Gage 23 Response

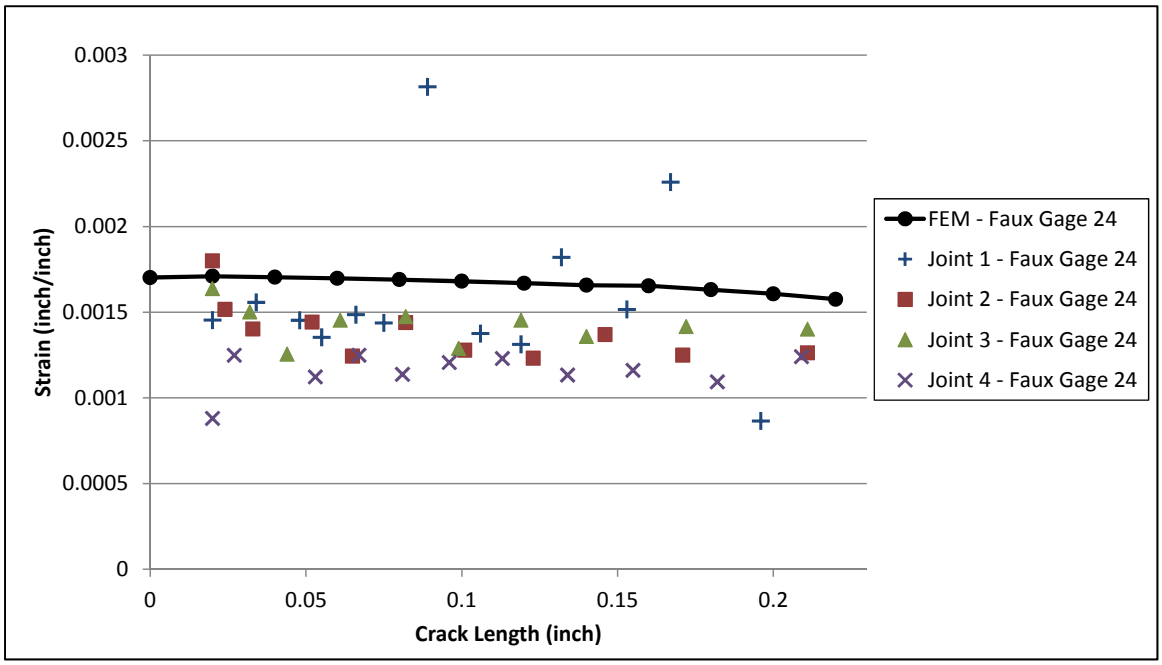

Figure A-58 Faux Gage 24 Response

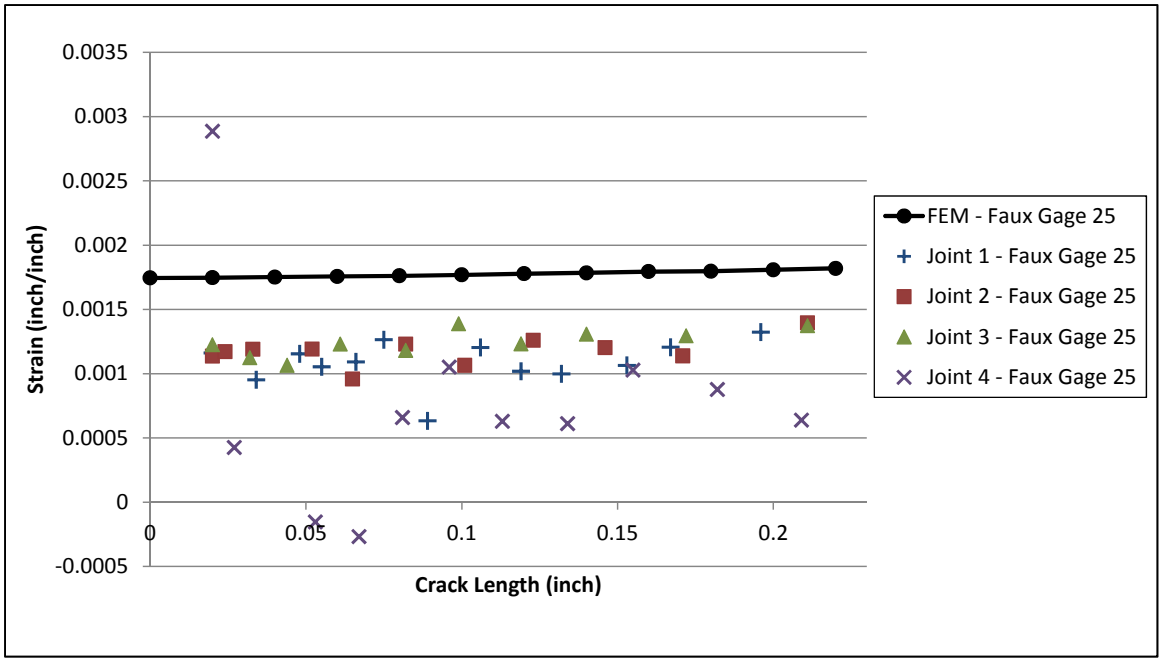

Figure A-59 Faux Gage 25 Response

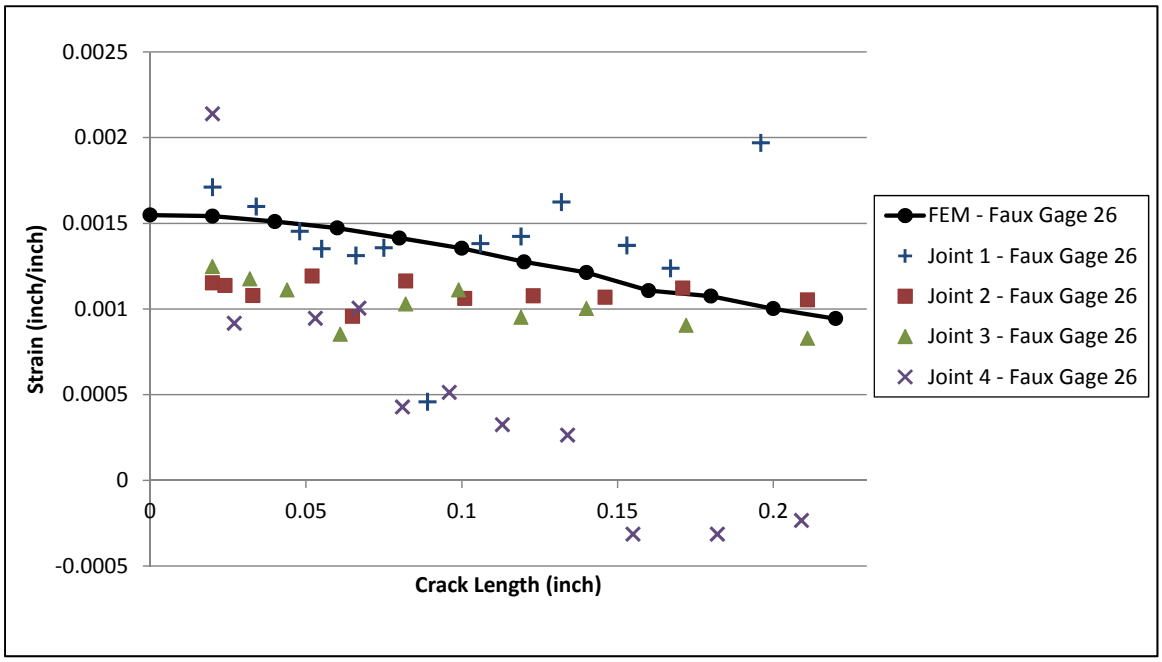

Figure A-60 Faux Gage 26 Response

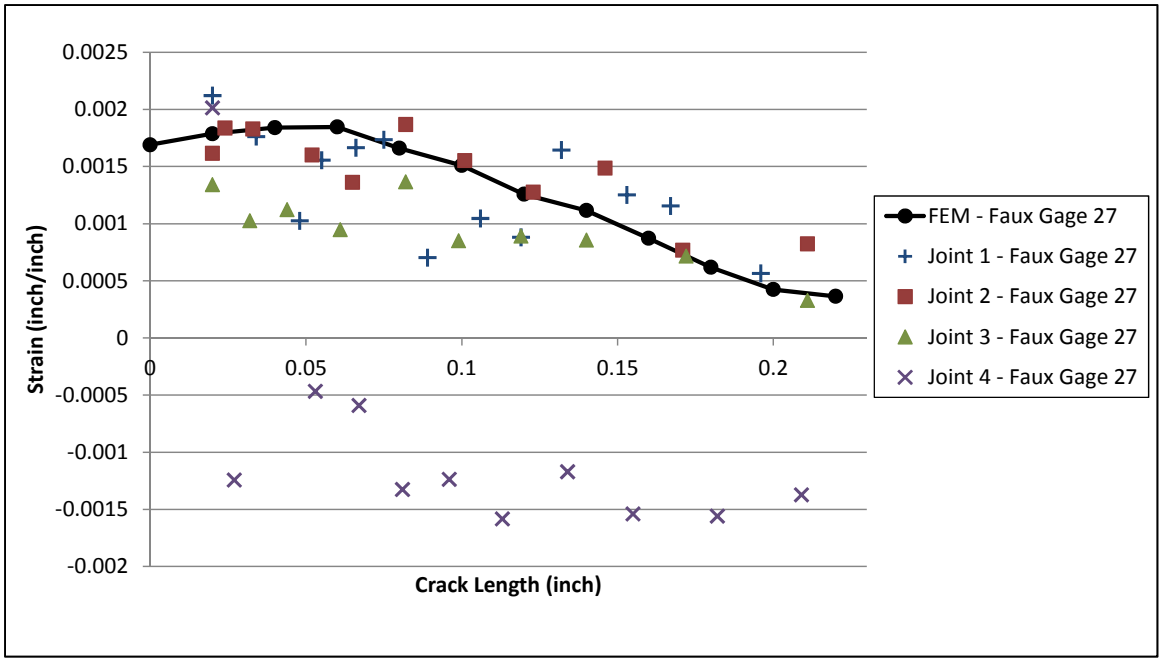

Figure A-61 Faux Gage 27 Response

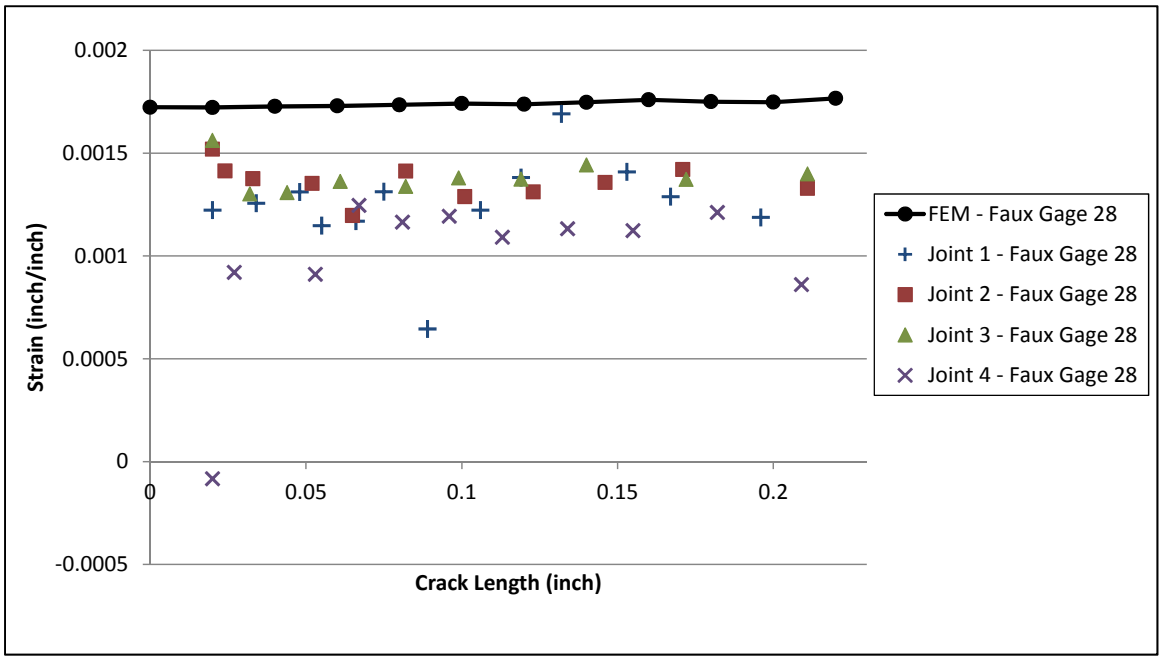

Figure A-62 Faux Gage 28 Response

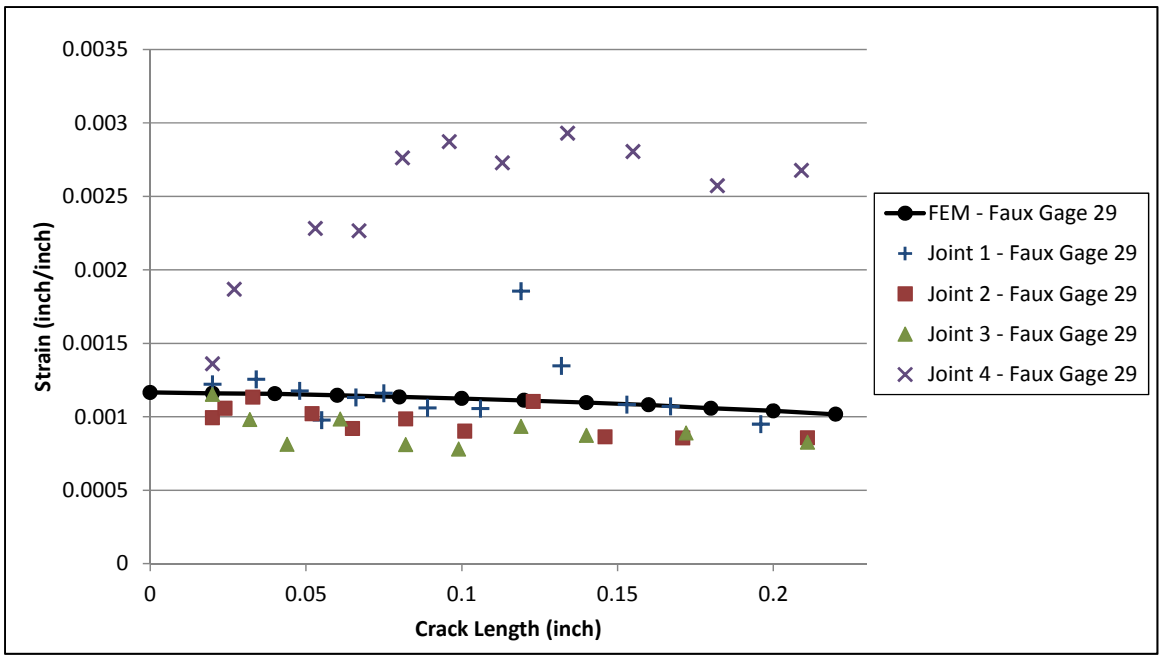

Figure A-63 Faux Gage 29 Response

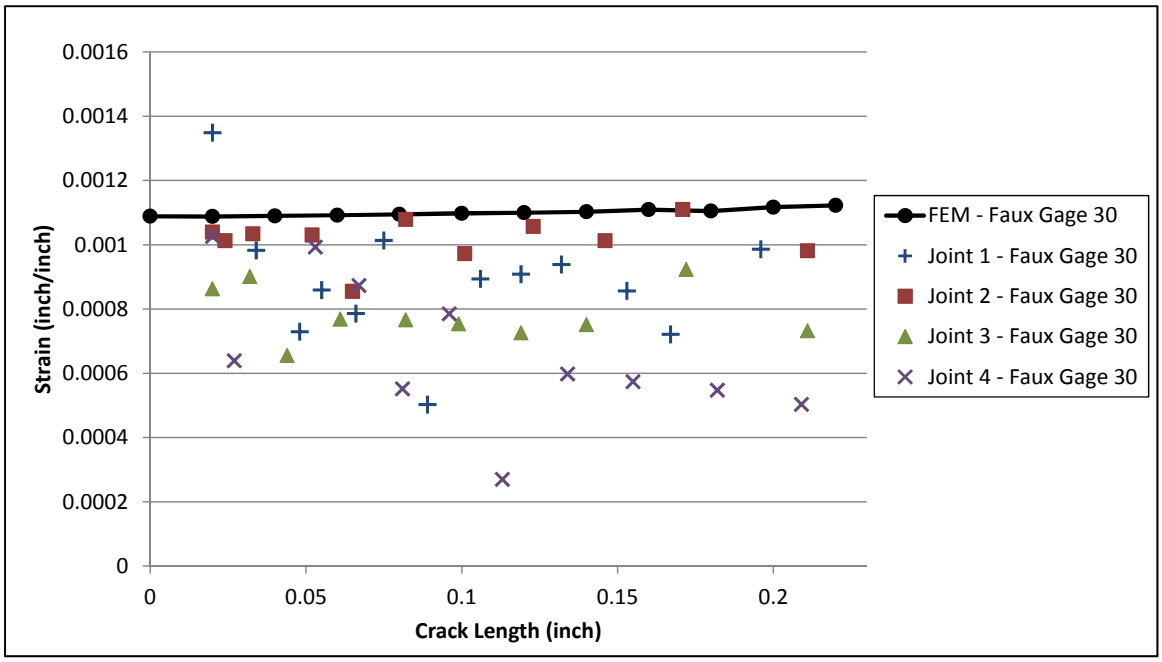

Figure A-64 Faux Gage 30 Response

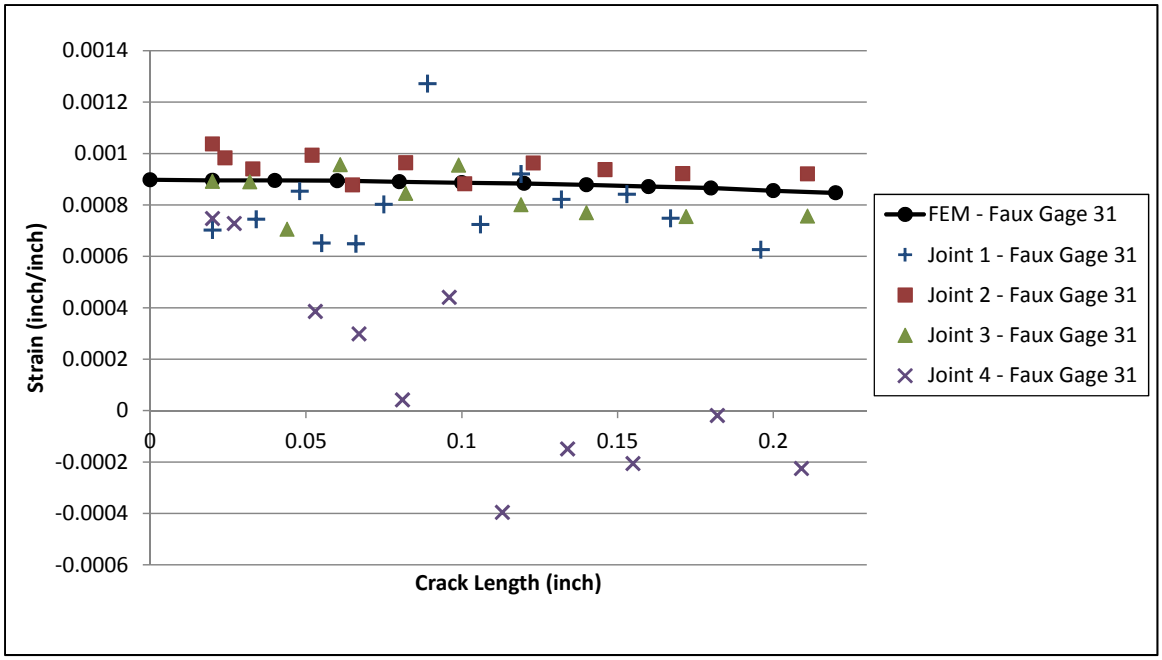

Figure A-65 Faux Gage 31 Response

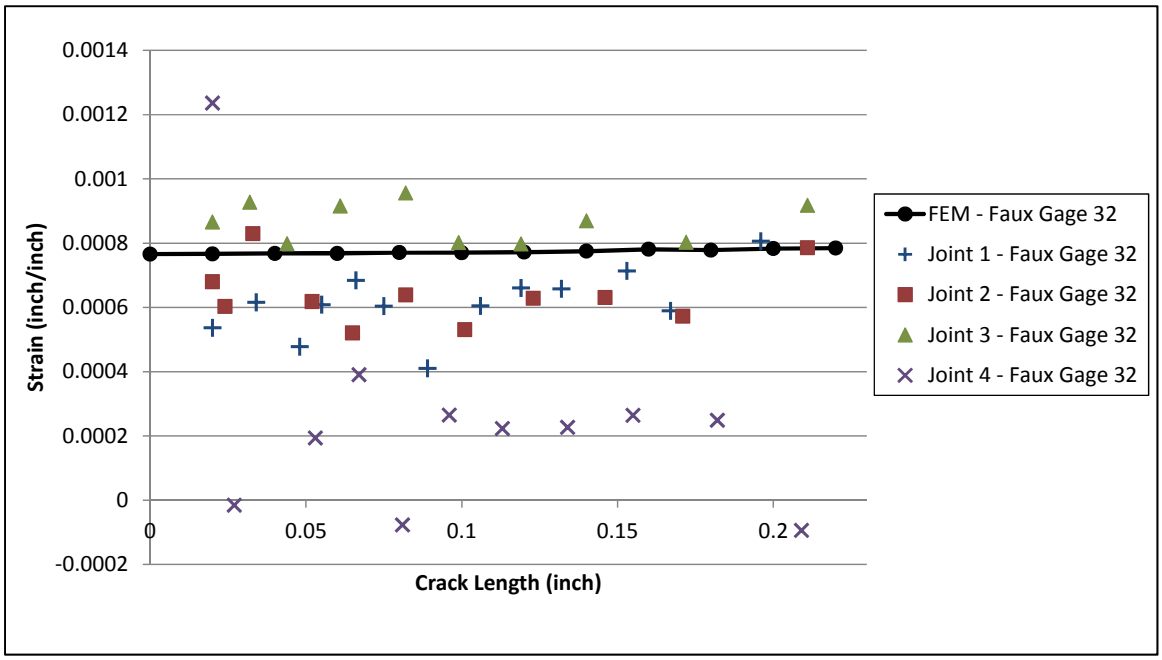

Figure A-66 Faux Gage 32 Response

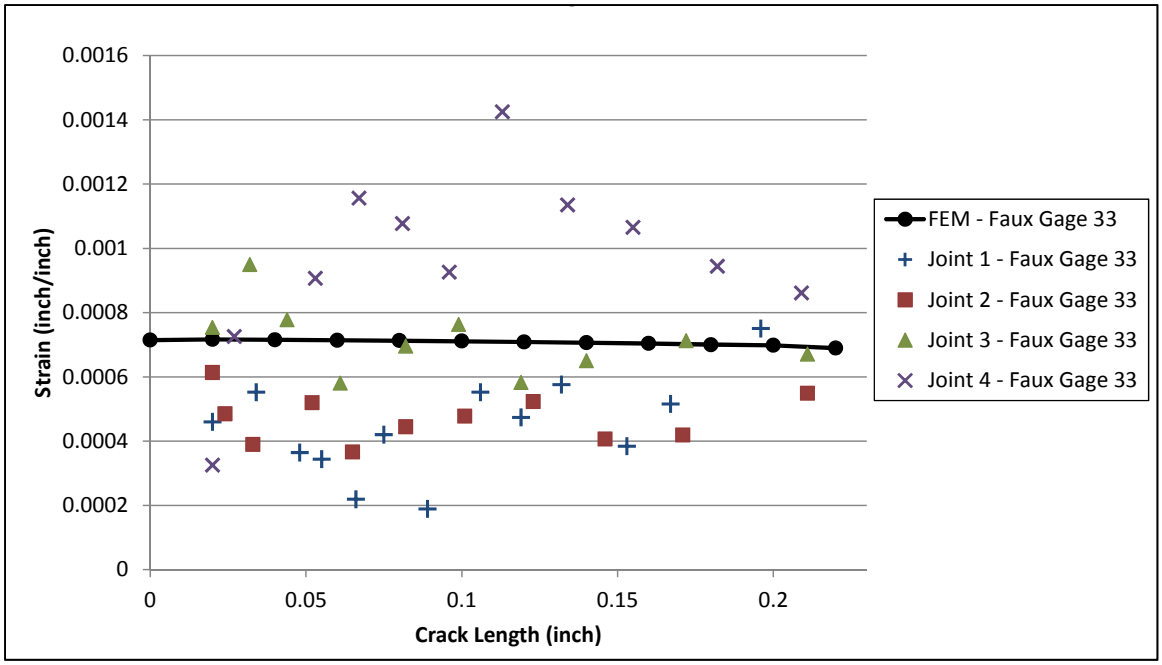

Figure A-67 Faux Gage 33 Response

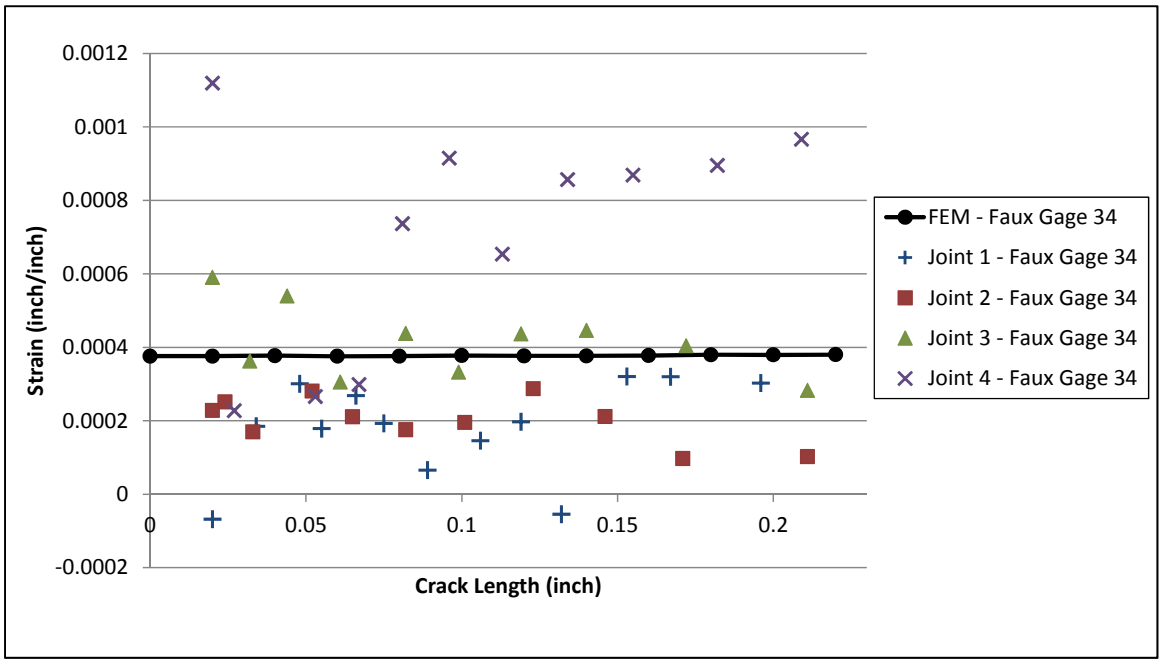

Figure A-68 Faux Gage 34 Response

APPENDIX B JOINT ANALYSIS-CLASSICAL METHODS

B.1 INTRODUCTION

The first method presented is the static strength approach to bolt loads presented in Equation 4-1 through Equation 4-6 for the model analyzed in this dissertation. Following that is a section presenting the calculation of 284 Splice fastener loads using load transfer methods discussed in Section 4.3 and Section 4.4. Next are two sections that present analyses using two dimensional planar models to calculate fastener loads.

In all of these methods, the models calculate the load transfer of the whole, uncracked joint. None of the methods are conducive to embedding or accounting for the additional compliance created by the crack at the fastener hole.

B.2 STATIC STRENGTH APPROACH

This section contains images from the static strength approach done in spreadsheet format. Figure B-1 and Figure B-2 contain the images of the two pages of analysis.

Fastener	X-position	Y-position
1	0.3	0.98
2	0.6	0.38
3	0.9	0.98
4	1.2	0.38
5	1.5	0.98
6	1.8	0.38
7	2.1	0.98
8	2.4	0.38
9	2.7	0.98

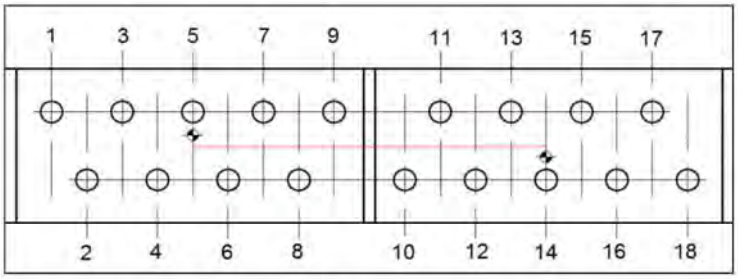

Simplification: since Pb is the same for all fasteners, assume that it is equal to 1

Assumption: Load passes through the center line of the splice, midway between patterns

$$\bar{y} = \frac{\sum_{i=1}^{n} P_{Bi} y_i}{\sum_{i=1}^{n} P_{Bi}} \qquad \bar{x} = \frac{\sum_{i=1}^{n} P_{Bi} x_i}{\sum_{i=1}^{n} P_{Bi}}$$

ybar= 0.7133 inch xbar= 1.5 inch

$$I_p = \sum_{i=1}^{n} P_{Bi} * r_i^2$$

Ip= 6.2 in^2

$$P_{Mi} = \frac{M * P_{Bi} * r_i}{I_p}$$

Pjoint = 4000 lbs

ejoint= 0.0333 inch

M= 133.33 inch*lbs

Fastener	Radial distance from Centroid (r)	r^2
1	1.229	1.511
2	0.960	0.921
3	0.657	0.431
4	0.448	0.201
5	0.267	0.071
6	0.448	0.201
7	0.657	0.431
8	0.960	0.921
9	1.229	1.511

Fastener	Pmi	Units
1	26.44	lbs
2	20.64	lbs
3	14.12	lbs
4	9.64	lbs
5	5.73	lbs
6	9.64	lbs
7	14.12	lbs
8	20.64	lbs
9	26.44	lbs

Check calculation:	Pmi*ri	Units	
	32.50	inch*lbs	
	19.81	inch*lbs	
	9.27	inch*lbs	
	4.32	inch*lbs	
	1.53	inch*lbs	
	4.32	inch*lbs	
	9.27	inch*lbs	
	19.81	inch*lbs	
	32.50	inch*lbs	
Total=	133.33	=M	<-Check

Figure B-1 Page One of Two of the Static Strength Bolt Load Analysis

Px (all fasteners)= 444.4444 lbs

$$P_{BoltTotal} = P_{bolt} + P_{\Delta M}$$

Fastener	Ptotal	Units
1	470.9	lbs
2	465.1	lbs
3	458.6	lbs
4	454.1	lbs
5	450.2	lbs
6	454.1	lbs
7	458.6	lbs
8	465.1	lbs
9	470.9	lbs

Resolve Fastener Moment Loads to X and Y Portions

Fastener	Xdist to Centroid	Ydist to Centroid	ATAN(X/Y) Degrees	Px	Py	
1	-1.2	-0.267	167.5	5.73	25.81	
2	-0.9	0.333	200.3	-7.17	19.35	
3	-0.6	-0.267	156.0	5.73	12.90	
4	-0.3	0.333	228.0	-7.17	6.45	
5	0	-0.267	90.0	5.73	0.00	
6	0.3	0.333	312.0	-7.17	-6.45	
7	0.6	-0.267	24.0	5.73	-12.90	
8	0.9	0.333	-20.3	-7.17	-19.35	
9	1.2	-0.267	12.5	5.73	-25.81	
Check by summing and see if it goes to zero->				0.00	0.00	<-Check

Fastener	PxTotal	PyTotal	Units
1	450.2	25.8	lbs
2	437.3	19.4	lbs
3	450.2	12.9	lbs
4	437.3	6.5	lbs
5	450.2	0.0	lbs
6	437.3	-6.5	lbs
7	450.2	-12.9	lbs
8	437.3	-19.4	lbs
9	450.2	-25.8	lbs

Figure B-2 Page Two of Two of the Static Strength Bolt Load Analysis

B.3 FASTENER FLEXIBILITY METHODS

Two different double shear fastener flexibility methods were discussed in Section 4.3: Tate and Rosenfeld, and Huth. Both these equations develop different fastener flexibilities that are then solved using the same technique developed by Tate and Rosenfeld discussed in Section 4.4. These two equations are used to produce total fastener loads in two different analyses. One where the plates are split down the line into two separate sections, one with four rows of fasteners and one with five rows of fasteners. The other analysis pairs fasteners starting at either end leaving a single fastener in the middle row. These two different assumptions are solved using the Tate and Rosenfeld fastener flexibility equation in Figure B-3 through Figure B-8, while the Huth method is used in Figure B-9 through Figure B-14.

Another set of calculations is presented that are for the optimized fastener flexibility that minimizes the error between the resulting fastener loads and the results for P_X from the 3-D FEM. The pages of calculations are presented in Figure B-15 through Figure B-17.

Parameter	Value	Units
Strap t	0.1	inches
Main Plate t	0.25	inches
Diameter	0.189	inches
Width	1.36	inches
Offset	0.38	inches
Pitch	0.6	inches
Estrap	10,450,000	psi
Eplate	10,300,000	psi
Efastener	29,000,000	psi
PoissonStrap	0.33	---
PoissonPlate	0.33	---
PoissonFastener	0.32	---

Tate and Rosenfeld Fastener Flexiblity Equation

$$f = \frac{2t_s + t_p}{3G_b A_b} + \frac{8t_s^3 + 16t_s^2 t_p + 8t_s t_p^2 + t_p^3}{192\,E_{bb} I_b} + \frac{2t_s + t_p}{t_s t_p E_{bbr}} + \frac{1}{t_s E_{sbr}} + \frac{2}{t_p E_{pbr}}$$

G_b = Shear modulus of the bolt or $E_{bb} / 2 * (1 + \nu_b)$

Gb= 10,984,848 psi

A_b = area of the bolt cross-section or π * bolt diameter^2 / 4

Ab= 0.0281 in^2

I_b = moment of inertia of the bolt cross-section or π * bolt diameter^4 / 64

Ib= 6.264E-05 in^4

f= 3.196E-06 in/lbs

$$P_{i+1} = \frac{f_i}{f_{i+1}} P_i + \frac{2K_p + K_s}{f_{i+1}} P_i - \frac{2K_p}{f_{i+1}} P_{Total} + \frac{2K_p + K_s}{f_{i+1}} \sum_{1}^{i-1} P$$

where $K = \frac{p}{btE}$

Note: pitch is the same for all rows so Kp and Ks will be the same

Kp= 3.427E-07 in/lbs

Ks= 8.444E-07 in/lbs

Figure B-3 Page One of Three of the Tate and Rosenfeld Fastener Flexibility Calculations with Split Rows

In this approach the two different lines of fasteners will be considered seperately
Each side will take a portion of Ptotal equivalent to its number of fasteners

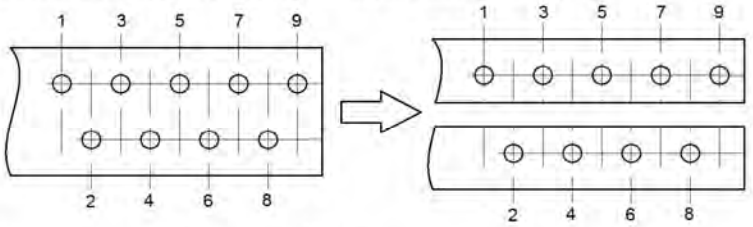

A) Ptotal = 4000 lbs
(2kp+ks)/f= 0.479
2kp/f= 0.214

Side 1 Pside1 = 4000*5/9 Side 2 Pside2=4000*4/5
Pside1= 2222 lbs Pside2= 1778 lbs

Side 1 Calculations

P1= P1
P2= P1+0.479P1-0.214P
1.479P1-0.214P
P3= P2+0.479P2-0.214P+0.479P1
1.479P2-0.214P+0.479P1
1.479(1.479P1-0.214P)-0.214P+0.479P1
2.666P1-0.531P
P4= P3+0.479P3-0.214P+0.479(P1+P2)
1.479P3-0.214P+0.479(P1+P2)
1.479(2.666P1-0.531P)-0.214P+0.479(P1+(1.479P1-0.214P))
5.131P1-1.101P
P5= P4+0.479P4-0.214P+0.479(P1+P2+P3)
1.479P4-0.214P+0.479(P1+P2+P3)
1.479(5.131P1-1.101P)-0.214P+0.479(P1+(1.479P1-0.214P)+(2.666P1-0.531P))
10.054P1-2.199P

$$P_{Total} = \sum P_i$$

P= P1+1.479P1-0.214P+2.666P1-0.531P+5.131P1-1.101P+10.054P1-2.199P
5.045P=20.33P1

Fastener	Ptotal	Units
P1=	551.4	lbs
P2=	340	lbs
P3=	291.4	lbs
P4=	382.3	lbs
P5=	656.5	lbs
Check->	2221.6	lbs

Figure B-4 Page Two of Three of the Tate and Rosenfeld Fastener Flexibility Calculations with Split Rows

Side 2 Calculation

P1= P1

P2= P1+0.479P1-0.214P

1.479P1-0.214P

P3= P2+0.479P2-0.214P+0.479P1

1.479P2-0.214P+0.479P1

1.479(1.479P1-0.214P)-0.214P+0.479P1

2.666P1-0.531P

P4= P3+0.479P3-0.214P+0.479(P1+P2)

1.479P3-0.214P+0.479(P1+P2)

1.479(2.666P1-0.531P)-0.214P+0.479(P1+(1.479P1-0.214P))

5.131P1-1.101P

$$P_{Total} = \sum P_i$$

P=P1+1.479P1-0.214P+2.666P1-0.531P+5.131P1-1.101P

2.846P=10.277P1

Fastener	Ptotal	Units
P1=	492.3	lbs
P2=	347.7	lbs
P3=	369.6	lbs
P4=	568.5	lbs
Check ->	1778.1	lbs

Thus:

Fastener	Ptotal	Units
1	551.4	lbs
2	492.3	lbs
3	340	lbs
4	347.7	lbs
5	291.4	lbs
6	369.6	lbs
7	382.3	lbs
8	568.5	lbs
9	656.5	lbs

Figure B-5 Page Three of Three of the Tate and Rosenfeld Fastener Flexibility Calculations with Split Rows

Parameter	Value	Units
Strap t	0.1	inches
Main Plate t	0.25	inches
Diameter	0.189	inches
Width	1.36	inches
Offset	0.38	inches
Pitch	0.6	inches
Estrap	10,450,000	psi
Eplate	10,300,000	psi
Efastener	29,000,000	psi
PoissonStrap	0.33	---
PoissonPlate	0.33	---
PoissonFastener	0.32	---

Tate and Rosenfeld Fastener Flexiblity Equation

$$f = \frac{2t_s + t_p}{3G_b A_b} + \frac{8t_s^3 + 16t_s^2 t_p + 8t_s t_p^2 + t_p^3}{192\, E_{bb} I_b} + \frac{2t_s + t_p}{t_s t_p E_{bbr}} + \frac{1}{t_s E_{sbr}} + \frac{2}{t_p E_{pbr}}$$

G_b = Shear modulus of the bolt or $E_{bb} / 2 * (1 + \nu_b)$

Gb= 10,984,848 psi

A_b = area of the bolt cross-section or π * bolt diameter^2 / 4

Ab= 0.0281 in^2

I_b = moment of inertia of the bolt cross-section or π * bolt diameter^4 / 64

Ib= 6.264E-05 in^4

f= 3.196E-06 in/lbs

$$P_{i+1} = \frac{f_i}{f_{i+1}} P_i + \frac{2K_p + K_s}{f_{i+1}} P_i - \frac{2K_p}{f_{i+1}} P_{Total} + \frac{2K_p + K_s}{f_{i+1}} \sum_{1}^{i-1} P$$

where $K = \frac{p}{btE}$

Note: pitch is the same for all rows so Kp and Ks will be the same

Kp= 1.713E-07 in/lbs

Ks= 4.222E-07 in/lbs

Figure B-6 Page One of Three of the Tate and Rosenfeld Fastener Flexibility Calculations with Paired Fastener Rows

In this approach fasteners will be paired except for the middle row

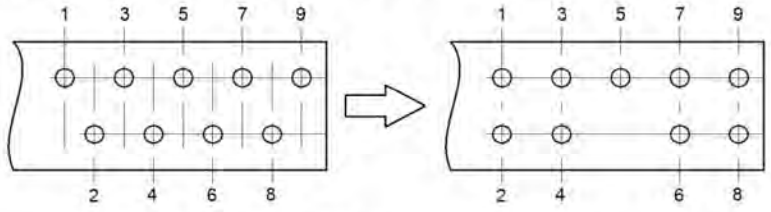

Ptotal = 4000 lbs

Rows 1, 2, 4, and 5

f= 1.598E-06
(2kp+ks)/2f= 0.479
2kp/2f= 0.214

Row 3

f= 3.196E-06
(2kp+ks)/f= 0.239
2kp/f= 0.107

P1= P1
P2= P1+0.479P1-0.214P
1.479P1-0.214P
P3= 2P2+0.239P2-0.107P+0.239P1
0.739P2-0.107P+0.239P1
0.739(1.479P1-0.214P)-0.107P+0.239P1
3.55P1-0.586P
P4= 0.5P3+0.479P3-0.214P+0.479(P1+P2)
2.479P3-0.214P+0.479(P1+P2)
2.479(3.55P1-0.586P)-0.214P+0.479(P1+(1.479P1-0.214P))
5.023P1-0.89P
P5= P4+0.239P4-0.107P+0.239(P1+P2+P3)
1.479P4-0.214P+0.479(P1+P2+P3)
1.479(5.023P1-0.89P)-0.214P+0.479(P1+(1.479P1-0.214P)+(3.55P1-0.586P))
8.465P1-1.884P

$$P_{Total} = \sum P_i$$

P= P1+1.479P1-0.214P+3.55P1-0.586P+5.023P1-0.89P+8.465P1-1.884P
4.337P=16.766P1

Figure B-7 Page Two of Three of the Tate and Rosenfeld Fastener Flexibility Calculations with Paired Fastener Rows

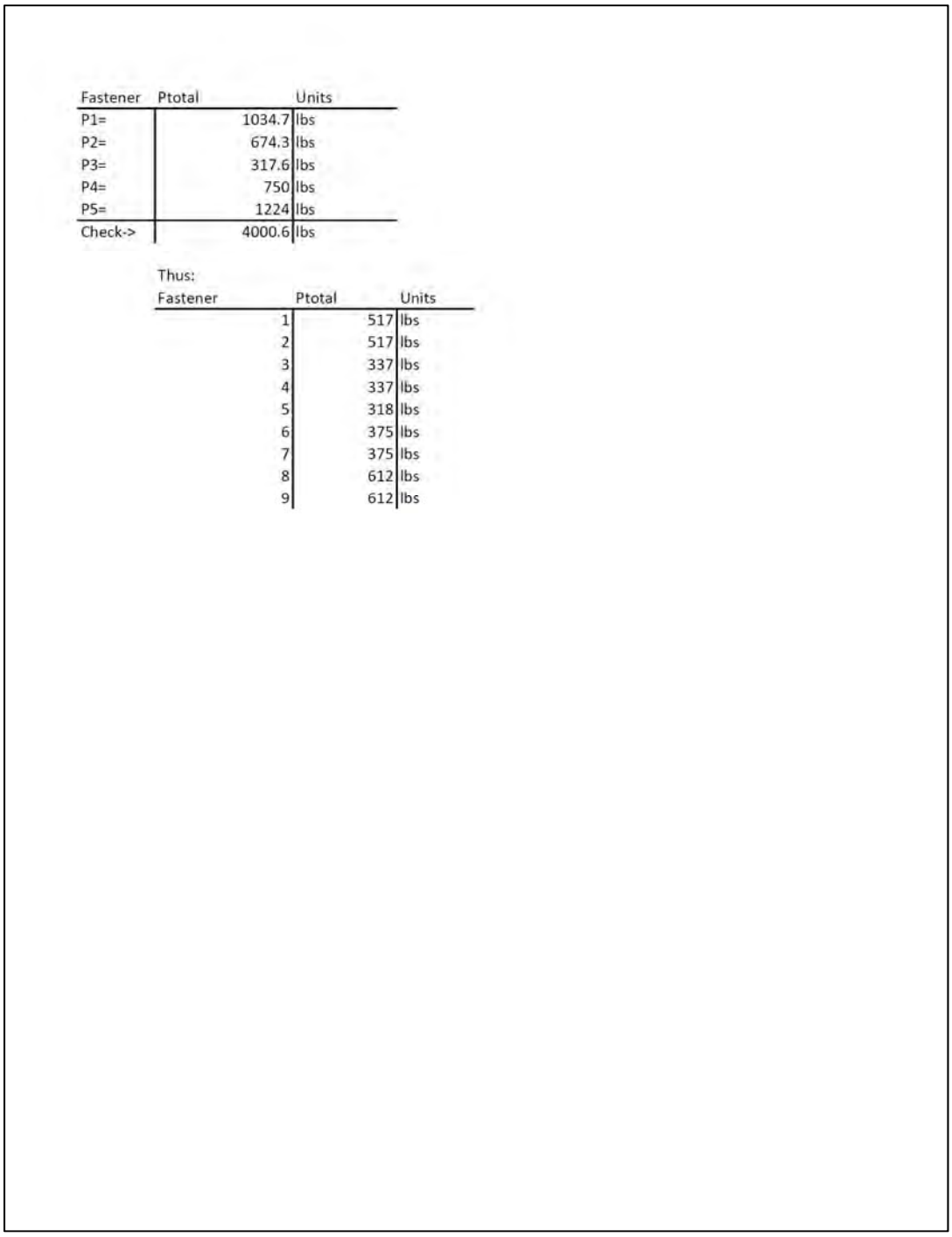

Fastener	Ptotal	Units
P1=	1034.7	lbs
P2=	674.3	lbs
P3=	317.6	lbs
P4=	750	lbs
P5=	1224	lbs
Check->	4000.6	lbs

Thus:

Fastener	Ptotal	Units
1	517	lbs
2	517	lbs
3	337	lbs
4	337	lbs
5	318	lbs
6	375	lbs
7	375	lbs
8	612	lbs
9	612	lbs

Figure B-8 Page Three of Three of the Tate and Rosenfeld Fastener Flexibility Calculations with Paired Fastener Rows

Parameter	Value	Units
Strap t	0.1	inches
Main Plate t	0.25	inches
Diameter	0.189	inches
Width	1.36	inches
Offset	0.38	inches
Pitch	0.6	inches
Estrap	10,450,000	psi
Eplate	10,300,000	psi
Efastener	29,000,000	psi
PoissonStrap	0.33	---
PoissonPlate	0.33	---
PoissonFastener	0.32	---

Huth Fastener Flexiblity Equation

$$f_i = \left(\frac{t_1 + t_2}{2d}\right)^n * \frac{b}{n}\left(\frac{1}{t_1 E_1} + \frac{1}{nt_2 E_2} + \frac{1}{2t_1 E_3} + \frac{1}{2nt_2 E_3}\right)$$

Parameter	Value	Reason
n	2	Double Shear
a	0.6667	For Bolted Joints
b	3	For Bolted Joints

f= 1.456E-06 in/lbs

$$P_{i+1} = \frac{f_i}{f_{i+1}} P_i + \frac{2K_p + K_s}{f_{i+1}} P_i - \frac{2K_p}{f_{i+1}} P_{Total} + \frac{2K_p + K_s}{f_{i+1}} \sum_{1}^{i-1} P$$

where $K = \frac{p}{btE}$

Note: pitch is the same for all rows so Kp and Ks will be the same

Kp=	3.427E-07	in/lbs
Ks=	8.444E-07	in/lbs

In this approach the two different lines of fasteners will be considered seperately
Each side will take a portion of Ptotal equivalent to its number of fasteners

Figure B-9 Page One of Three of the Huth Fastener Flexibility Calculations with Split Rows

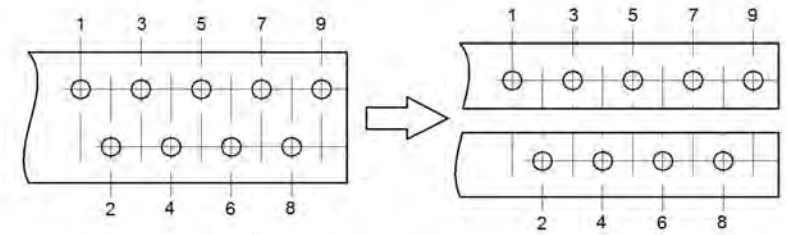

A)

	Ptotal =	4000 lbs
	(2kp+ks)/f=	1.05
	2kp/f=	0.471

Side 1 Pside1 = 4000*5/9 Side 2 Pside2=4000*4/5

Pside1= 2222 lbs Pside2= 1778 lbs

Side 1 Calculations

P1= P1

P2= P1+1.05P1-0.471P

2.05P1-0.471P

P3= P2+1.05P2-0.471P+1.05P1

2.05P2-0.471P+1.05P1

2.05(2.05P1-0.471P)-0.471P+1.05P1

5.253P1-1.437P

P4= P3+1.05P3-0.471P+1.05(P1+P2)

2.05P3-0.471P+1.05(P1+P2)

2.05(5.253P1-1.437P)-0.471P+1.05(P1+(2.05P1-0.471P))

13.97P1-3.91P

P5= P4+1.05P4-0.471P+1.05(P1+P2+P3)

2.05P4-0.471P+1.05(P1+P2+P3)

2.05(13.97P1-3.91P)-0.471P+1.05(P1+(2.05P1-0.471P)+(5.253P1-1.437P))

37.356P1-10.49P

$$P_{Total} = \sum P_i$$

P= P1+2.05P1-0.471P+5.253P1-1.437P+13.97P1-3.91P+37.356P1-10.49P

17.308P=59.629P1

Fastener	Ptotal	Units
P1=	645	lbs
P2=	275.6	lbs
P3=	195.5	lbs
P4=	320.8	lbs
P5=	782.9	lbs
Check->	2219.8	lbs

Figure B-10 Page Two of Three of the Huth Fastener Flexibility Calculations with Split Rows

Side 2 Calculation

P1= P1
P2= P1+1.05P1-0.471P
2.05P1-0.471P
P3= P2+1.05P2-0.471P+1.05P1
2.05P2-0.471P+1.05P1
2.05(2.05P1-0.471P)-0.471P+1.05P1
5.253P1-1.437P
P4= P3+1.05P3-0.471P+1.05(P1+P2)
2.05P3-0.471P+1.05(P1+P2)
2.05(5.253P1-1.437P)-0.471P+1.05(P1+(2.05P1-0.471P))
13.97P1-3.91P

$$P_{Total} = \sum P_i$$

P=P1+2.05P1-0.471P+5.253P1-1.437P+13.97P1-3.91P
6.818P=22.273P1

Fastener	Ptotal	Units
P1=	544.2	lbs
P2=	278.3	lbs
P3=	304.5	lbs
P4=	650.6	lbs
Check ->	1777.6	lbs

Thus:

Fastener	Ptotal	Units
1	645	lbs
2	544.2	lbs
3	275.6	lbs
4	278.3	lbs
5	195.5	lbs
6	304.5	lbs
7	320.8	lbs
8	650.6	lbs
9	782.9	lbs

Figure B-11 Page Three of Three of the Huth Fastener Flexibility Calculations with Split Rows

Parameter	Value	Units
Strap t	0.1	inches
Main Plate t	0.25	inches
Diameter	0.189	inches
Width	1.36	inches
Offset	0.38	inches
Pitch	0.6	inches
Estrap	10,450,000	psi
Eplate	10,300,000	psi
Efastener	29,000,000	psi
PoissonStrap	0.33	---
PoissonPlate	0.33	---
PoissonFastener	0.32	---

Huth Fastener Flexiblity Equation

$$f_1 = \left(\frac{t_1 + t_2}{2d}\right)^a * \frac{b}{n}\left(\frac{1}{t_1 E_1} + \frac{1}{nt_2 E_2} + \frac{1}{2t_1 E_3} + \frac{1}{2nt_2 E_3}\right)$$

Parameter	Value	Reason
n	2	Double Shear
a	0.6667	For Bolted Joints
b	3	For Bolted Joints

f= 1.184E-06 in/lbs

$$P_{i+1} = \frac{f_i}{f_{i+1}} P_i + \frac{2K_p + K_s}{f_{i+1}} P_i - \frac{2K_p}{f_{i+1}} P_{Total} + \frac{2K_p + K_s}{f_{i+1}} \sum_{1}^{i-1} P$$

where $K = \frac{p}{btE}$

Note: pitch is the same for all rows so Kp and Ks will be the same

Kp=	1.713E-07	in/lbs
Ks=	4.222E-07	in/lbs

Figure B-12 Page One of Three of the Huth Flexibility Calculations with Paired Fastener Rows

In this approach fasteners will be paired except for the middle row

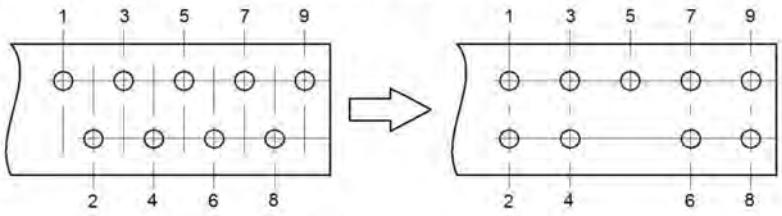

Ptotal = 4000 lbs

Rows 1, 2, 4, and 5

f= 5.919E-07
(2kp+ks)/2f= 1.292
2kp/2f= 0.579

Row 3

f= 1.184E-06
(2kp+ks)/f= 0.646
2kp/f= 0.289

P1= P1
P2= P1+1.292P1-0.579P
2.292P1-0.579P
P3= 2P2+0.646P2-0.289P+0.646P1
1.146P2-0.289P+0.646P1
1.146(2.292P1-0.579P)-0.289P+0.646P1
6.711P1-1.821P
P4= 0.5P3+1.292P3-0.579P+1.292(P1+P2)
3.292P3-0.579P+1.292(P1+P2)
3.292(6.711P1-1.821P)-0.579P+1.292(P1+(2.292P1-0.579P))
17.25P1-4.591P
P5= P4+0.646P4-0.289P+0.646(P1+P2+P3)
2.292P4-0.579P+1.292(P1+P2+P3)
2.292(17.25P1-4.591P)-0.579P+1.292(P1+(2.292P1-0.579P)+(6.711P1-1.821P))
42.931P1-12.79P

$$P_{Total} = \sum P_i$$

P= P1+2.292P1-0.579P+6.711P1-1.821P+17.25P1-4.591P+42.931P1-12.79P
19.786P=64.525P1

Figure B-13 Page Two of Three of the Huth Flexibility Calculations with Paired Fastener Rows

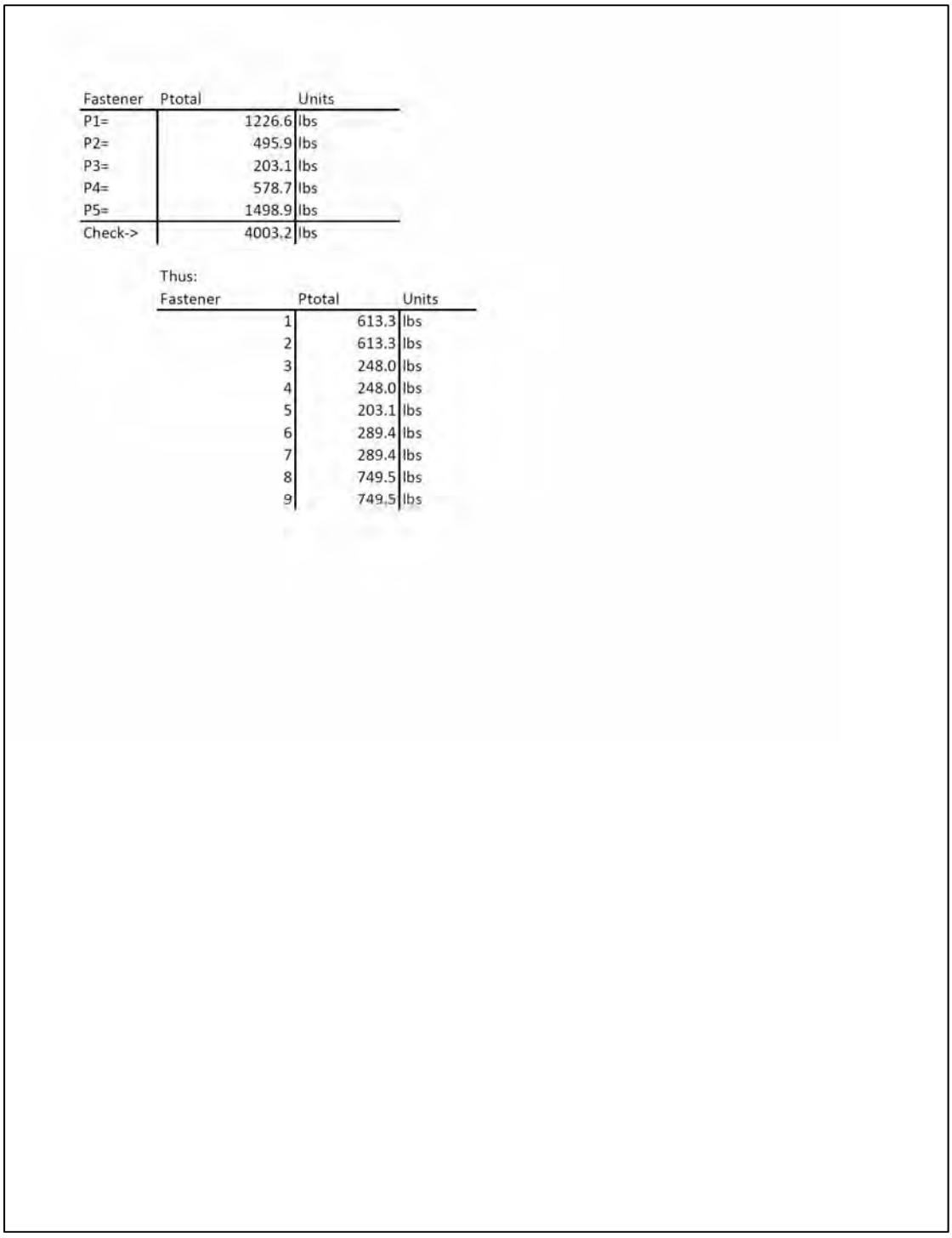

Fastener	Ptotal	Units
P1=	1226.6	lbs
P2=	495.9	lbs
P3=	203.1	lbs
P4=	578.7	lbs
P5=	1498.9	lbs
Check->	4003.2	lbs

Thus:

Fastener	Ptotal	Units
1	613.3	lbs
2	613.3	lbs
3	248.0	lbs
4	248.0	lbs
5	203.1	lbs
6	289.4	lbs
7	289.4	lbs
8	749.5	lbs
9	749.5	lbs

Figure B-14 Page Three of Three of the Huth Flexibility Calculations with Paired Fastener Rows

Parameter	Value	Units
Strap t	0.1	inches
Main Plate t	0.25	inches
Diameter	0.189	inches
Width	1.36	inches
Offset	0.38	inches
Pitch	0.6	inches
Estrap	10,450,000	psi
Eplate	10,300,000	psi
Efastener	29,000,000	psi
PoissonStrap	0.33	---
PoissonPlate	0.33	---
PoissonFastener	0.32	---

The Fastener Flexibility was developed to minimize the resulting error between these loads and the 3-D FEM

f= 1.941E-06 in/lbs

$$P_{i+1} = \frac{f_i}{f_{i+1}} P_i + \frac{2K_p + K_s}{f_{i+1}} P_i - \frac{2K_p}{f_{i+1}} P_{Total} + \frac{2K_p + K_s}{f_{i+1}} \sum_{1}^{i-1} P$$

where $K = \frac{p}{btE}$

Note: pitch is the same for all rows so Kp and Ks will be the same

Kp=	3.427E-07	in/lbs
Ks=	8.444E-07	in/lbs

In this approach the two different lines of fasteners will be considered seperately
Each side will take a portion of Ptotal equivalent to its number of fasteners

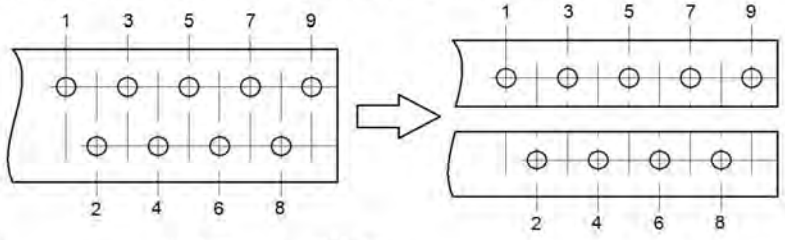

A)

Ptotal =	4000 lbs
(2kp+ks)/f=	0.788
2kp/f=	0.353

Figure B-15 Page One of Three of the Optimized Fastener Flexibility Calculations with Split Rows

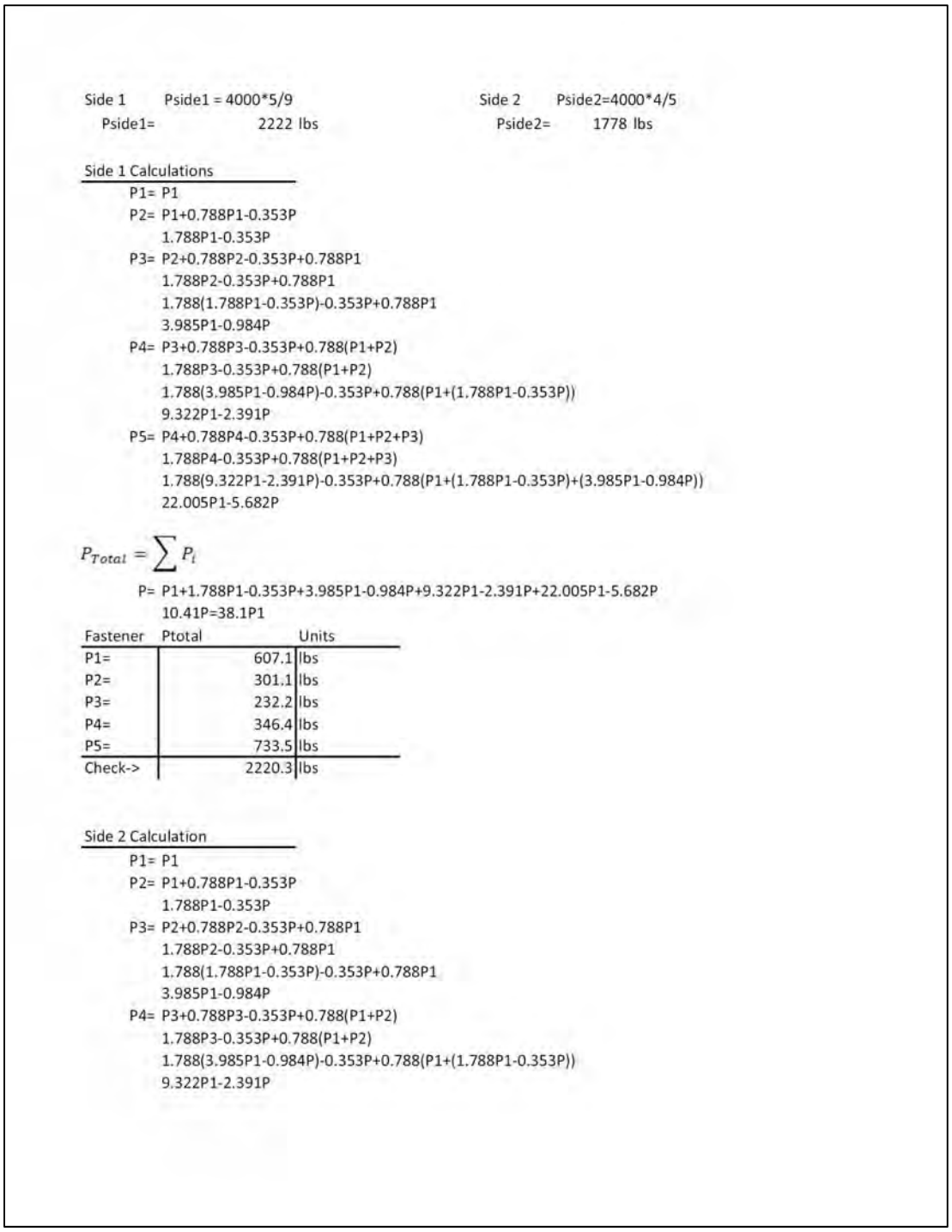

Side 1 Pside1 = 4000*5/9 Side 2 Pside2=4000*4/5

Pside1= 2222 lbs Pside2= 1778 lbs

Side 1 Calculations

P1= P1

P2= P1+0.788P1-0.353P

1.788P1-0.353P

P3= P2+0.788P2-0.353P+0.788P1

1.788P2-0.353P+0.788P1

1.788(1.788P1-0.353P)-0.353P+0.788P1

3.985P1-0.984P

P4= P3+0.788P3-0.353P+0.788(P1+P2)

1.788P3-0.353P+0.788(P1+P2)

1.788(3.985P1-0.984P)-0.353P+0.788(P1+(1.788P1-0.353P))

9.322P1-2.391P

P5= P4+0.788P4-0.353P+0.788(P1+P2+P3)

1.788P4-0.353P+0.788(P1+P2+P3)

1.788(9.322P1-2.391P)-0.353P+0.788(P1+(1.788P1-0.353P)+(3.985P1-0.984P))

22.005P1-5.682P

$$P_{Total} = \sum P_i$$

P= P1+1.788P1-0.353P+3.985P1-0.984P+9.322P1-2.391P+22.005P1-5.682P

10.41P=38.1P1

Fastener	Ptotal	Units
P1=	607.1	lbs
P2=	301.1	lbs
P3=	232.2	lbs
P4=	346.4	lbs
P5=	733.5	lbs
Check->	2220.3	lbs

Side 2 Calculation

P1= P1

P2= P1+0.788P1-0.353P

1.788P1-0.353P

P3= P2+0.788P2-0.353P+0.788P1

1.788P2-0.353P+0.788P1

1.788(1.788P1-0.353P)-0.353P+0.788P1

3.985P1-0.984P

P4= P3+0.788P3-0.353P+0.788(P1+P2)

1.788P3-0.353P+0.788(P1+P2)

1.788(3.985P1-0.984P)-0.353P+0.788(P1+(1.788P1-0.353P))

9.322P1-2.391P

Figure B-16 Page Two of Three of the Optimized Fastener Flexibility Calculations with Split Rows

$$P_{Total} = \sum P_i$$

P=P1+1.788P1-0.353P+3.985P1-0.984P+9.322P1-2.391P
4.728P=16.095P1

Fastener	Ptotal	Units
P1=	522.2	lbs
P2=	306.1	lbs
P3=	331.3	lbs
P4=	617.6	lbs
Check ->	1777.2	lbs

Thus:

Fastener	Ptotal	Units
1	607.1	lbs
2	522.2	lbs
3	301.1	lbs
4	306.1	lbs
5	232.2	lbs
6	331.3	lbs
7	346.4	lbs
8	617.6	lbs
9	733.5	lbs

Figure B-17 Page Three of Three of the Optimized Fastener Flexibility Calculations with Split Rows

Parameter	Value	Units
Strap t	0.1	inches
Main Plate t	0.25	inches
Diameter	0.189	inches
Width	1.36	inches
Offset	0.38	inches
Pitch	0.6	inches
Estrap	10,450,000	psi
Eplate	10,300,000	psi
Efastener	29,000,000	psi
PoissonStrap	0.33	---
PoissonPlate	0.33	---
PoissonFastener	0.32	---

The Fastener Flexibility was developed to minimize the resulting error between these loads and the 3-D FEM

f=	1.953E-06	in/lbs

where $K = \frac{p}{btE}$

Note: pitch is the same for all rows so Kp and Ks will be the same

Kp=	1.713E-07	in/lbs
Ks=	4.222E-07	in/lbs

$$P_{i+1} = \frac{f_i}{f_{i+1}} P_i + \frac{2K_p + K_s}{f_{i+1}} P_i - \frac{2K_p}{f_{i+1}} P_{Total} + \frac{2K_p + K_s}{f_{i+1}} \sum_{1}^{i-1} P$$

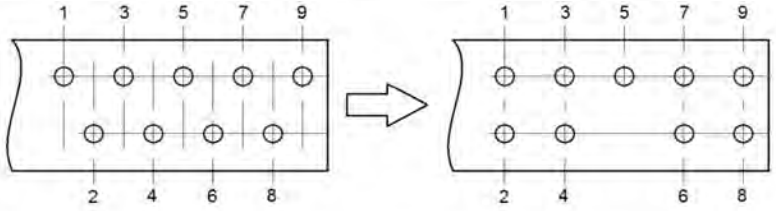

In this approach fasteners will be paired except for the middle row

	Ptotal =	4000 lbs
Rows 1, 2,	f=	9.766E-07
	(2kp+ks)/2f=	0.783
	2kp/2f=	0.351
Row 3	f=	1.953E-06
	(2kp+ks)/f=	0.392
	2kp/f=	0.175

Figure B-18 Page One of Two of the Optimized Fastener Flexibility Calculations with Paired Rows

P1= P1

P2= P1+0.783P1-0.351P

1.783P1-0.351P

P3= 2P2+0.392P2-0.175P+0.392P1

0.892P2-0.175P+0.392P1

0.892(1.783P1-0.351P)-0.175P+0.392P1

4.656P1-1.015P

P4= 0.5P3+0.783P3-0.351P+0.783(P1+P2)

2.783P3-0.351P+0.783(P1+P2)

2.783(4.656P1-1.015P)-0.351P+0.783(P1+(1.783P1-0.351P))

8.742P1-1.928P

P5= P4+0.392P4-0.175P+0.392(P1+P2+P3)

1.783P4-0.351P+0.783(P1+P2+P3)

1.783(8.742P1-1.928P)-0.351P+0.783(P1+(1.783P1-0.351P)+(4.656P1-1.015P))

17.453P1-4.547P

P= P1+1.783P1-0.351P+4.656P1-1.015P+8.742P1-1.928P+17.453P1-4.547P

8.371P=29.912P1

$$P_{Total} = \sum P_i$$

Fastener	Ptotal	Units
P1=	1119.4	lbs
P2=	592.6	lbs
P3=	264.9	lbs
P4=	674.6	lbs
P5=	1347.7	lbs
Check->	3999.2	lbs

Thus:

Fastener	Ptotal	Units
1	559.7	lbs
2	559.7	lbs
3	296.3	lbs
4	296.3	lbs
5	264.9	lbs
6	337.3	lbs
7	337.3	lbs
8	673.9	lbs
9	673.9	lbs

Figure B-19 Page Two of Two of the Optimized Fastener Flexibility Calculations with Paired Rows

Parameter	Value	Units
Strap t	0.1	inches
Main Plate t	0.25	inches
Diameter	0.189	inches
Width	1.36	inches
Offset	0.38	inches
Pitch	0.6	inches
Estrap	10,450,000	psi
Eplate	10,300,000	psi
Efastener	29,000,000	psi
PoissonStrap	0.33	---
PoissonPlate	0.33	---
PoissonFastener	0.32	---

The Fastener Flexibility was developed from the 3-D FEM

f=	1.599E-06	in/lbs

$$P_{i+1} = \frac{f_i}{f_{i+1}} P_i + \frac{2K_p + K_s}{f_{i+1}} P_i - \frac{2K_p}{f_{i+1}} P_{Total} + \frac{2K_p + K_s}{f_{i+1}} \sum_{1}^{i-1} P$$

where $K = \frac{p}{btE}$

Note: pitch is the same for all rows so Kp and Ks will be the same

Kp=	3.427E-07	in/lbs
Ks=	8.444E-07	in/lbs

In this approach the two different lines of fasteners will be considered seperately
Each side will take a portion of Ptotal equivalent to its number of fasteners

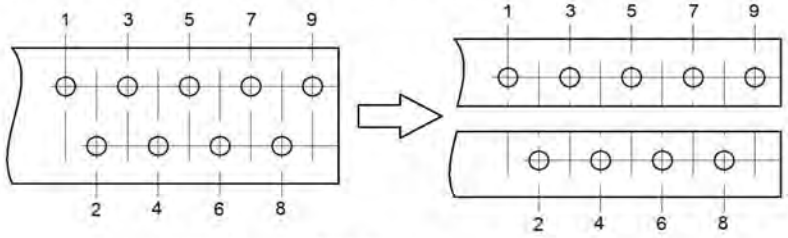

Ptotal =	4000 lbs
(2kp+ks)/f=	0.956
2kp/f=	0.429

Figure B-20 Page One of Three of the 3-D FEM Based Fastener Flexibility Calculations with Split Rows

Side 1 Pside1 = 4000*5/9 Side 2 Pside2=4000*4/5

Pside1= 2222 lbs Pside2= 1778 lbs

Side 1 Calculations

P1= P1

P2= P1+0.956P1-0.429P

1.956P1-0.429P

P3= P2+0.956P2-0.429P+0.956P1

1.956P2-0.429P+0.956P1

1.956(1.956P1-0.429P)-0.429P+0.956P1

4.782P1-1.268P

P4= P3+0.956P3-0.429P+0.956(P1+P2)

1.956P3-0.429P+0.956(P1+P2)

1.956(4.782P1-1.268P)-0.429P+0.956(P1+(1.956P1-0.429P))

12.179P1-3.32P

P5= P4+0.956P4-0.429P+0.956(P1+P2+P3)

1.956P4-0.429P+0.956(P1+P2+P3)

1.956(12.179P1-3.32P)-0.429P+0.956(P1+(1.956P1-0.429P)+(4.782P1-1.268P))

31.22P1-8.545P

$$P_{Total} = \sum P_i$$

P= P1+1.956P1-0.429P+4.782P1-1.268P+12.179P1-3.32P+31.22P1-8.545P

14.561P=51.138P1

Fastener	Ptotal	Units
P1=	632.8	lbs
P2=	284.4	lbs
P3=	208	lbs
P4=	330.3	lbs
P5=	768.4	lbs
Check->	2223.9	lbs

Side 2 Calculation

P1= P1

P2= P1+0.956P1-0.429P

1.956P1-0.429P

P3= P2+0.956P2-0.429P+0.956P1

1.956P2-0.429P+0.956P1

1.956(1.956P1-0.429P)-0.429P+0.956P1

4.782P1-1.268P

P4= P3+0.956P3-0.429P+0.956(P1+P2)

1.956P3-0.429P+0.956(P1+P2)

1.956(4.782P1-1.268P)-0.429P+0.956(P1+(1.956P1-0.429P))

12.179P1-3.32P

Figure B-21 Page Two of Three of the 3-D FEM Based Fastener Flexibility Calculations with Split Rows

$$P_{Total} = \sum P_i$$

P=P1+1.956P1-0.429P+4.782P1-1.268P+12.179P1-3.32P
6.017P=19.917P1

Fastener	Ptotal	Units
P1=	537	lbs
P2=	287.7	lbs
P3=	313.5	lbs
P4=	638.9	lbs
Check ->	1777.1	lbs

Thus:

Fastener	Ptotal	Units
1	632.8	lbs
2	537	lbs
3	284.4	lbs
4	287.7	lbs
5	208	lbs
6	313.5	lbs
7	330.3	lbs
8	638.9	lbs
9	768.4	lbs

Figure B-22 Page Three of Three of the 3-D FEM Based Fastener Flexibility Calculations with Split Rows

B.4 PLANAR FEM, SPLICE SPLIT

This analysis uses a two dimensional planar simplification of the model using the finite element software StressCheck®. A tool was developed ASIP engineers at Hill AFB to take the dimensions of a joint and automatically build a FEM, solve the FEM, and extract fastener loads. The common approach is to model half the joint with the split between halves. If the halves are different then two different models are produced but they are still split with symmetry boundary conditions on the edges of the straps as shown in Figure B-23.

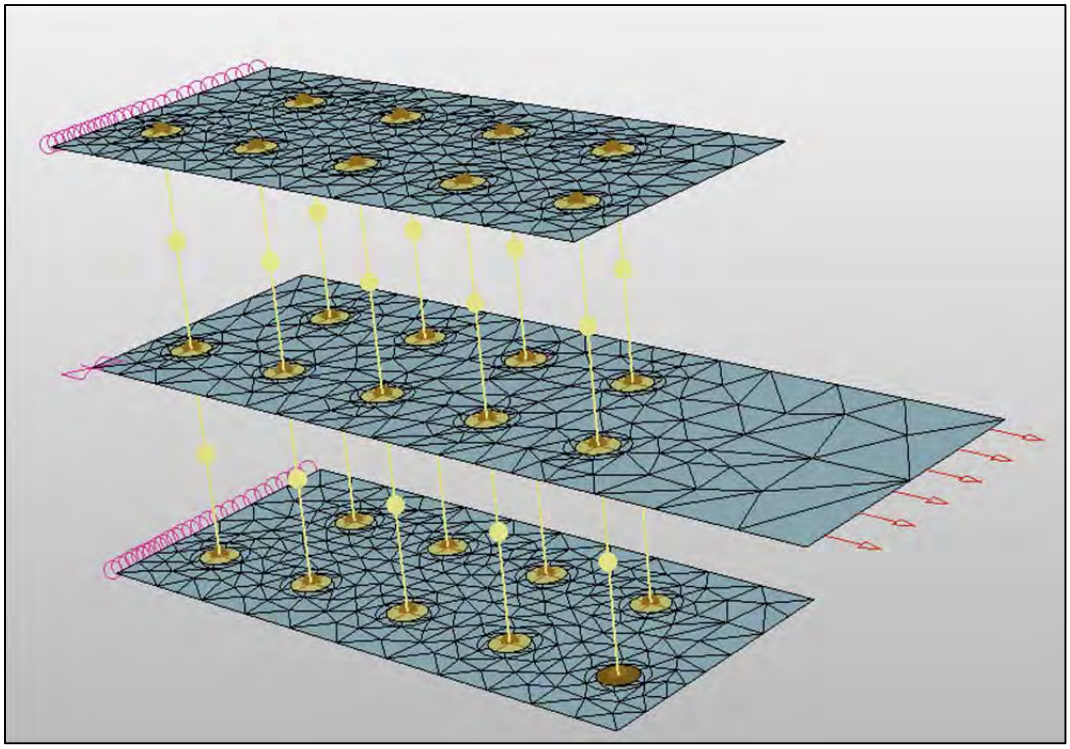

Figure B-23 Planar Half FEM of the 284 Joint

This model uses the fastener and link elements internal to StressCheck to simulate the fasteners. The fastener element automatically 'wagon wheels' a central node to the surrounding elements with a stiffness calculated by material parameters from the material model assigned. This provides the displacement due to bearing in the fastener material. The link element connects the center nodes of the fastener elements with a stiffness representative of the bending and shear of the fastener. This is a user defined input and was based on the shear and bending components of the Tate and Rosenfeld equation given in Reference [220].

The symmetry boundary condition is obviously not applicable here since the midpoint in between the main plates is not a plane of symmetry. The staggered fastener pattern is primarily to blame. None the less, it is an approximation whose validity is worth exploration. Figure B-24 below shows a deformed plot of the von Mises stress with the original geometry displayed as dashed lines. Note that the main plate racks in the y-direction due to in plane bending from the fastener pattern eccentricity to the load path. Another drawback of the planar model is the idealization of the fastener itself. First, with the symmetric model there is not a reasonable means of definition to capture the true asymmetry from fastener head to collar or nut side, not necessarily in the shank section but in the restraint provided at either end. Secondly, because two different links are used to connect the three layers there is no continuity of rotation through the middle plate. This can cause a theoretical 'kink' in the center of the fastener.

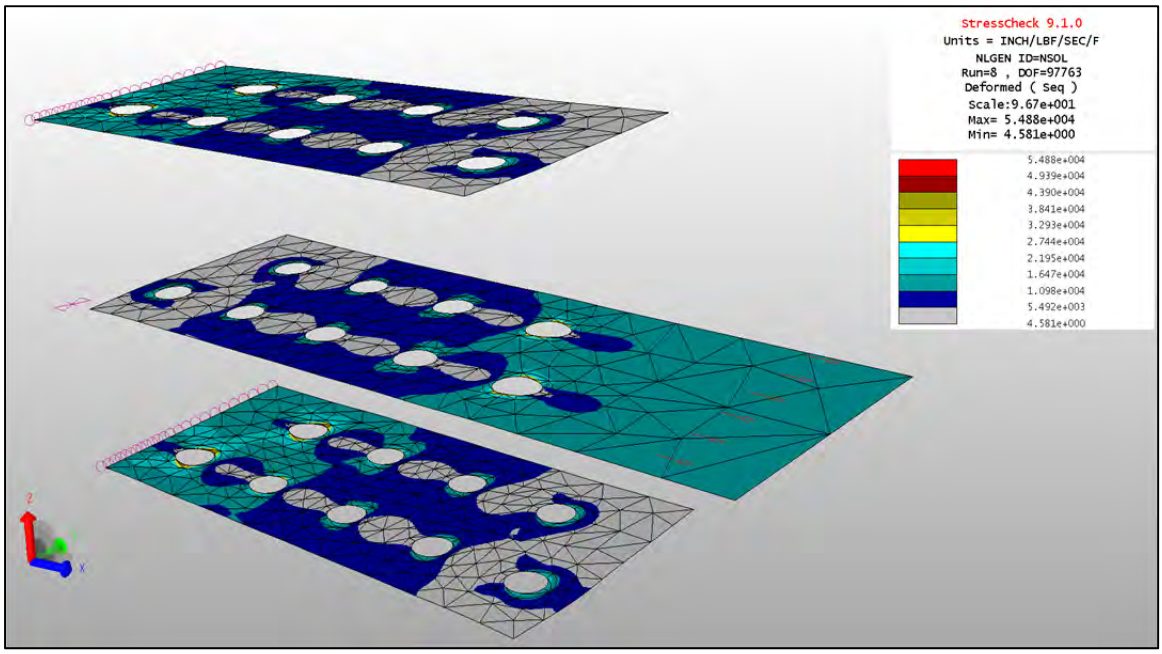

Figure B-24 von Mises Stress Profile with Exaggerated Deformation

The FEM builder tool has a number of pre-defined materials. The 7075-T76511 data was used for the plates, and the 7075-T6 data was used for the straps. Both models were of the Ramberg-Osgood type but the definition was slight different than that used in the three dimensional FEM described in Section 6.2. The Ramberg-Osgood model in Stress-Check uses a 70% yield parameter to begin the non-linearity. The bolt material model is linear elastic since the maximum bearing stress in the fastener is far below the material yield strength.

Table B-1 Material Parameters for the StressCheck Model Builder Tool

Material Name	7075-T651	7075-T7351	HL18
Modulus of Elasticity	10.45E6	10.3E6	29.0E6
Poisson's Ratio	0.33	0.33	0.32
Material	Aluminum	Aluminum	Steel 4340
S70E (R-O Parameter)	69,777	57,314	N/A
n (R-O Parameter)	32	32	N/A

The stiffness of the link was developed by using the shear and bending components of the Tate and Rosenfeld equation only. The calculated value for link stiffness was 1,188,773 lbs/in.

All solutions were solved for p-levels one through eight to capture convergence data. The bolt load transfer values extracted all come from the maximum p-level of eight. Overall magnitude of each bolt's load for the elastic solution is given in Table B-2 in pounds. The non-linear elastic solution results are given in Table B-3.

Table B-2 Total Bolt Loads from the Planar Half FEM, Elastic Solution

Fastener Number	Top/Bottom Strap	Middle Plate
1	304	608
2	286	572
3	140	280
4	141	283
5	103	207
6	155	310
7	162	324
8	345	689
9	371	742

Table B-3 Total Bolt Loads from the Planar Half FEM, Non-Linear Elastic Solution

Fastener Number	Top/Bottom Strap	Middle Plate
1	283	565
2	273	546
3	157	312
4	156	311
5	124	247
6	169	337
7	182	361
8	326	648

Fastener Number	Top/Bottom Strap	Middle Plate
9	338	672

B.5 PLANAR FEM OF THE COMPLETE 284 JOINT

This analysis uses a two dimensional planar simplification of the model using the finite element software StressCheck®. Unlike the model from the previous section it models the entire joint and has parameters optimized to closely mimic the three dimensional analysis of Section 6.2. The same material parameters shown in Table B-1 are used in this model as well. All other modeling methods are the same other than it was built by hand instead of using the automated tool.

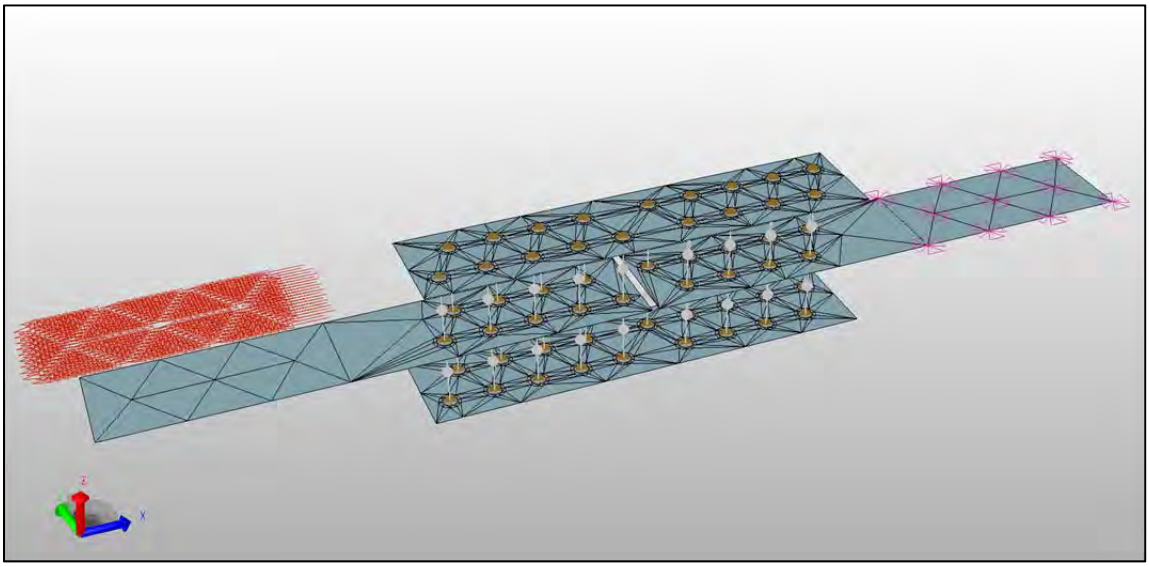

Figure B-25 Planar Full FEM of the 284 Joint

Table B-4 Total Bolt Loads from the Planar Full FEM, Elastic Solution

Fastener Number	Top/Bottom Strap	Middle Plate

Fastener Number	Top/Bottom Strap	Middle Plate
1	308	615
2	283	566
3	142	283
4	141	281
5	105	209
6	155	310
7	164	327
8	345	690
9	368	736
10	370	739
11	344	688
12	164	327
13	155	309
14	105	209
15	140	280
16	142	284
17	282	564
18	309	617

Table B-5 Total Bolt Loads from the Planar Full FEM, Non-Linear Elastic Solution

Fastener Number	Top/Bottom Strap	Middle Plate
1	283	566
2	274	548
3	157	314
4	156	311
5	124	248
6	169	338
7	181	362
8	326	652
9	336	672
10	338	675
11	326	651
12	181	361
13	169	337
14	124	248
15	156	311
16	157	314

17	274	547
18	284	567

APPENDIX C FEM VERIFICATION AND VALIDATION TESTING

C.1 StressCheck Triangle Single Element Tests

This section provides an overview of the single element testing that was done on the triangular element in StressCheck. This element is a basic building block of the auto-mesher provided by StressCheck thus is commonly used. It is a two dimensional planar element and can have a polynomial level up to eight. A basic triangle was built with symmetry boundary conditions on one side with a corner pinned in the y-direction to prevent translation. Loading in the x-direction was applied to the sloped side as shown in Figure C-1. Note that the automesh feature of StressCheck builds a six-node triangular element with mid-nodes on each side but that geometric mapping of an automesh deletes mid-nodes at contact regions thus both three-node (Figure C-1) and six-node (Figure C-2) triangular elements are being tested.

There are many different steps to the verification testing done for this report. First and foremost is the verification of the strain law used by the code. To verify that strain is defined as $\varepsilon = (L - L_0) / L_0$ Hooke's law for uniaxial stress, $\sigma = E\varepsilon$, is used. Stretch, given by the Greek letter λ, is defined as L / L_0. Therefore, Hooke's law can be transformed to the form $F = EA(\lambda - 1)$ so strain is equal to $(\lambda - 1)$. Displacements and strains in the x-direction were extracted for a number of different applied stresses from 1psi to 10 psi. The displacements were converted into stretch and it was verified that after subtracting one were equal to the strains in all cases.

The Ramberg-Osgood non-linear material model was used in StressCheck as well so it was tested using the single element to verify the response was as described by the equation given in the handbook [341]. The modulus and S_{70E} parameters were both set to unity and the (n) parameter was set to 2 and the Poisson's Ratio was 0.33. The non-linear solution was given a convergence criterion of 0.05% with respect to changes in stress. Figure C-3 shows the expected response and the actual response of the single element for stresses from 1 psi to 10 psi. Responses of the three-node and six-node elements were identical up to three decimal places. The average error for all ten points was six one-hundredths of a percent.

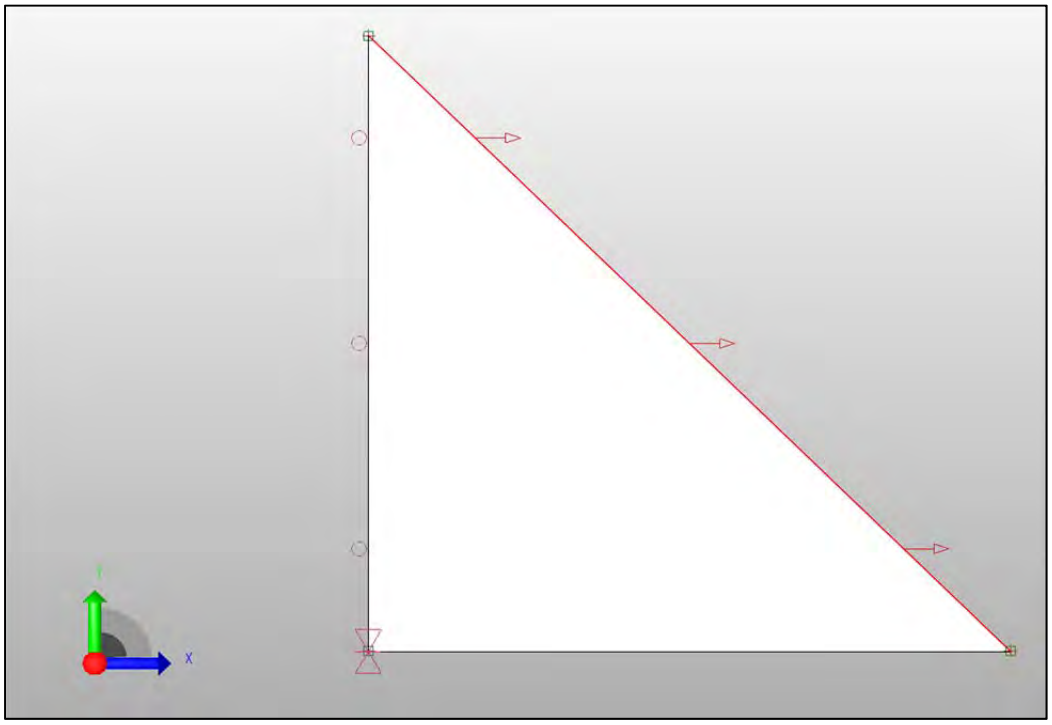

Figure C-1 View of the Single Three-Node Triangular Element Test

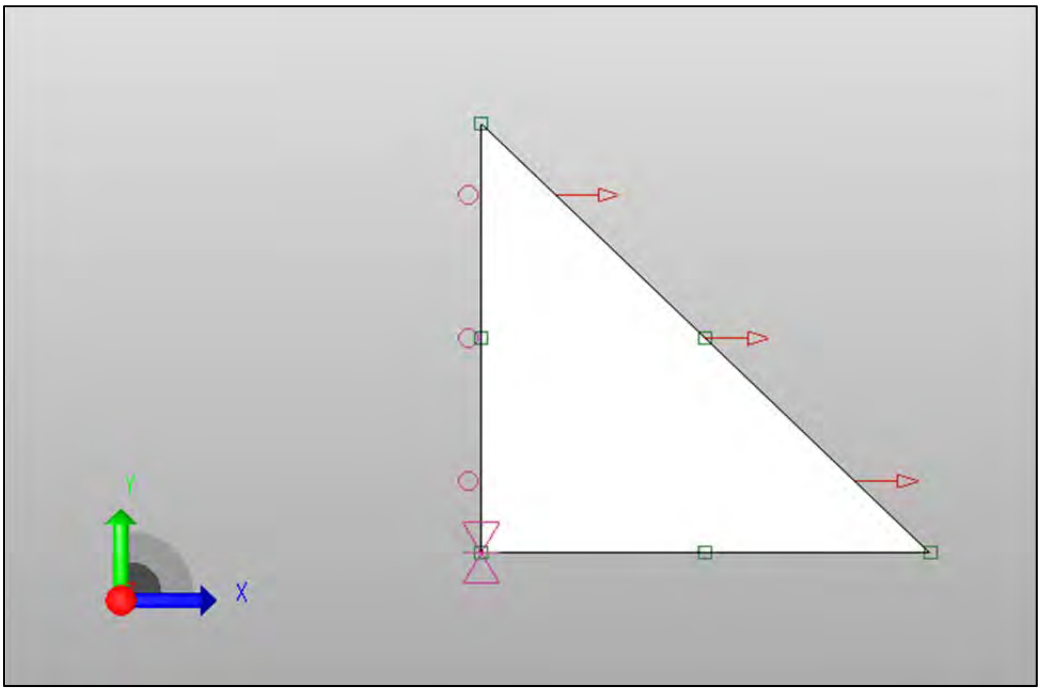

Figure C-2 View of the Single Six-Node Triangular Element Test

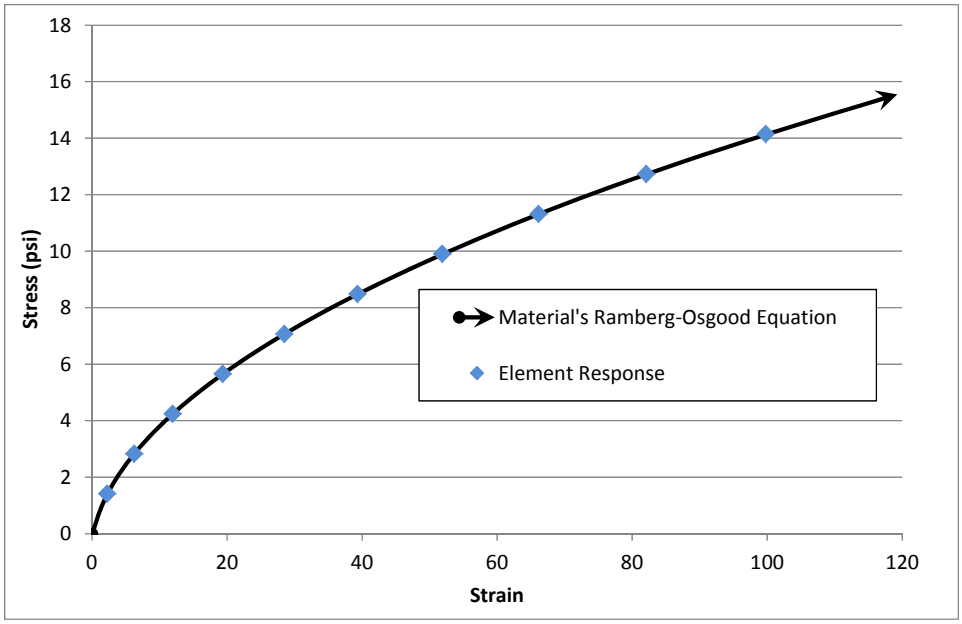

Figure C-3 Stress versus Strain Response of the Single Triangle Element with a Ramberg-Osgood Material Model

C.2 StressCheck Fastener Single Element Tests

This test contains two fastener elements but only one is the focus of the test. The upper plate and fastener are given a modulus of 1E10 as is the link connecting the two fasteners and the plate surrounding the lower fastener as shown in Figure C-4. The lower fastener is assigned a material with a modulus of unity. This ensures that the surrounding structure is so stiff that the deflections due to them will be several orders of magnitude less. Note that this is a planar model and thus the separation of the upper and lower plate is for visualization only. The link that connects the two fasteners may appear to be a beam but really is a spring connecting the two center nodes of the fastener elements which can only move within the plane.

The fastener element receives a material assignment just like any other part with typical elastic parameters and StressCheck performs an internal calculation to determine the stiffness of the wagon wheel spokes surrounding it. The overall stiffness from Reference [340] for the fastener is:

$$Stiffness = \frac{2E\pi}{D(1+\nu)(1-2\nu)}$$

Equation 9-1 Equation for Fastener Element Stiffness

This equation was used as the closed-form solution for the element and the response was evaluated at ten different steps from three to thirty pounds. Figure C-5 shows the resulting deflection versus applied load along with a plot of a line of expected response with the slope equal to the fastener stiffness. All points were within 0.05% of the expected value.

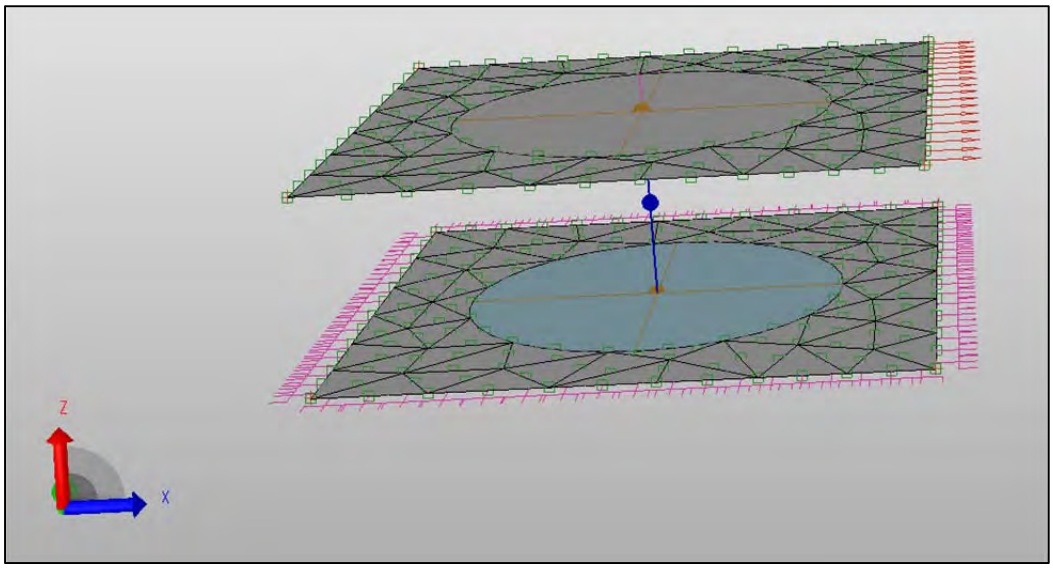

Figure C-4 View of the Single Fastener Test

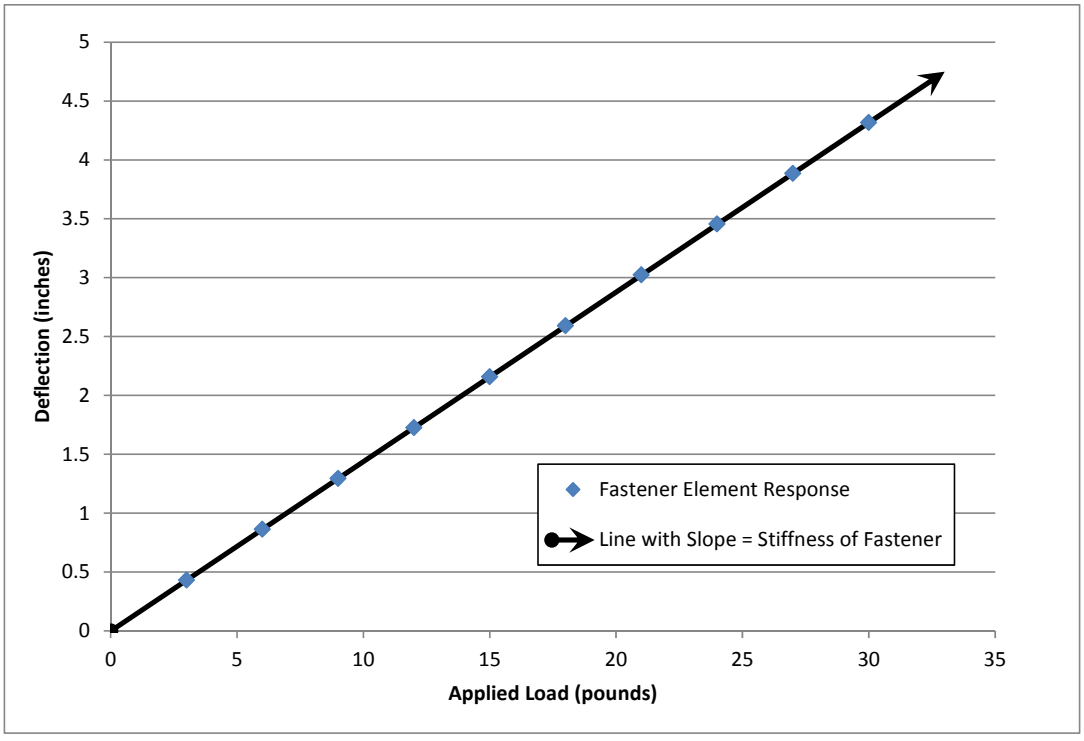

Figure C-5 Plot of Fastener Response and Defined Stiffness

C.3 StressCheck Link Single Element Tests

The link element is one of several different elements utilized in the StressCheck Software. To verify the response of the link to the defined stiffness a model was created that used two rigid planar sections connected by a single link as depicted in Figure C-6. The triangle and fastener elements making up the planar regions had a modulus of 1E10 and the single link had a stiffness of unity. The lower plate was built in on all corners and step loading in three pound increments was applied to the top plate in the x-direction.

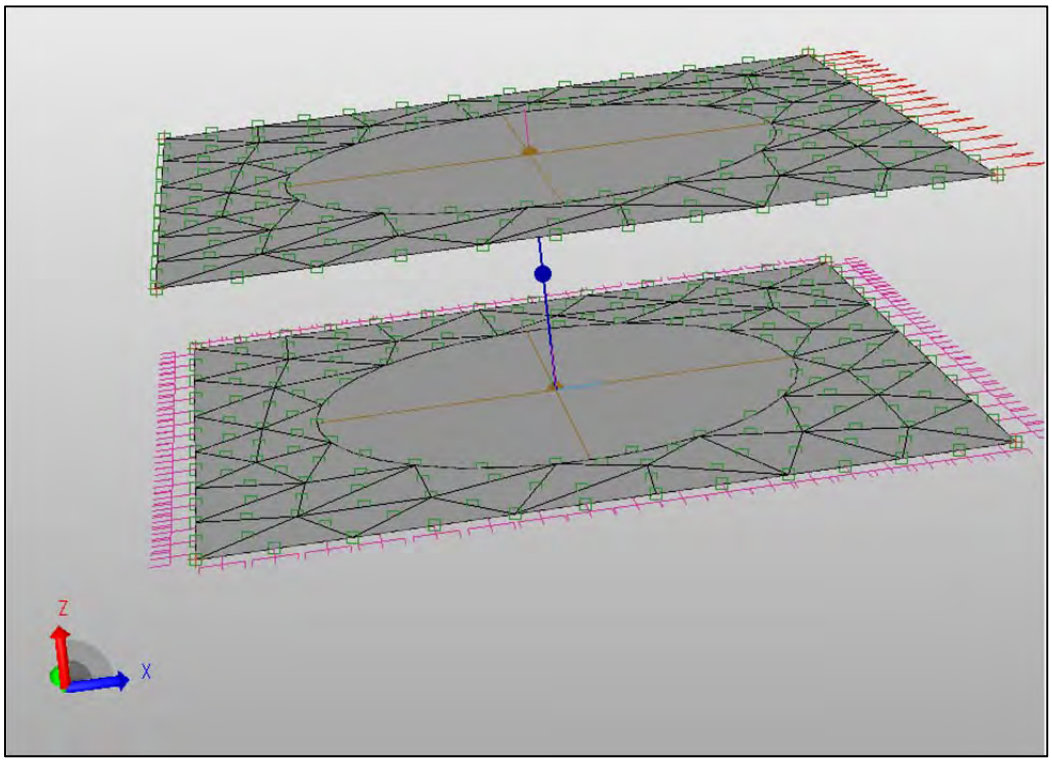

Figure C-6 View of Single Link Element Test

Since the stiffness of the link (force per unit length in pounds/inch) was unity, then a three pound applied load should displace the upper plate three inches, a six pound applied load would displace it six inches, and so on and so forth. Deflections were taken at five points around the circumference of the fastener and compared to the applied load. Figure C-7 shows the response of the upper plate against a 1 to 1 line which represents the stiffness of the fastener and note the response is as expected.

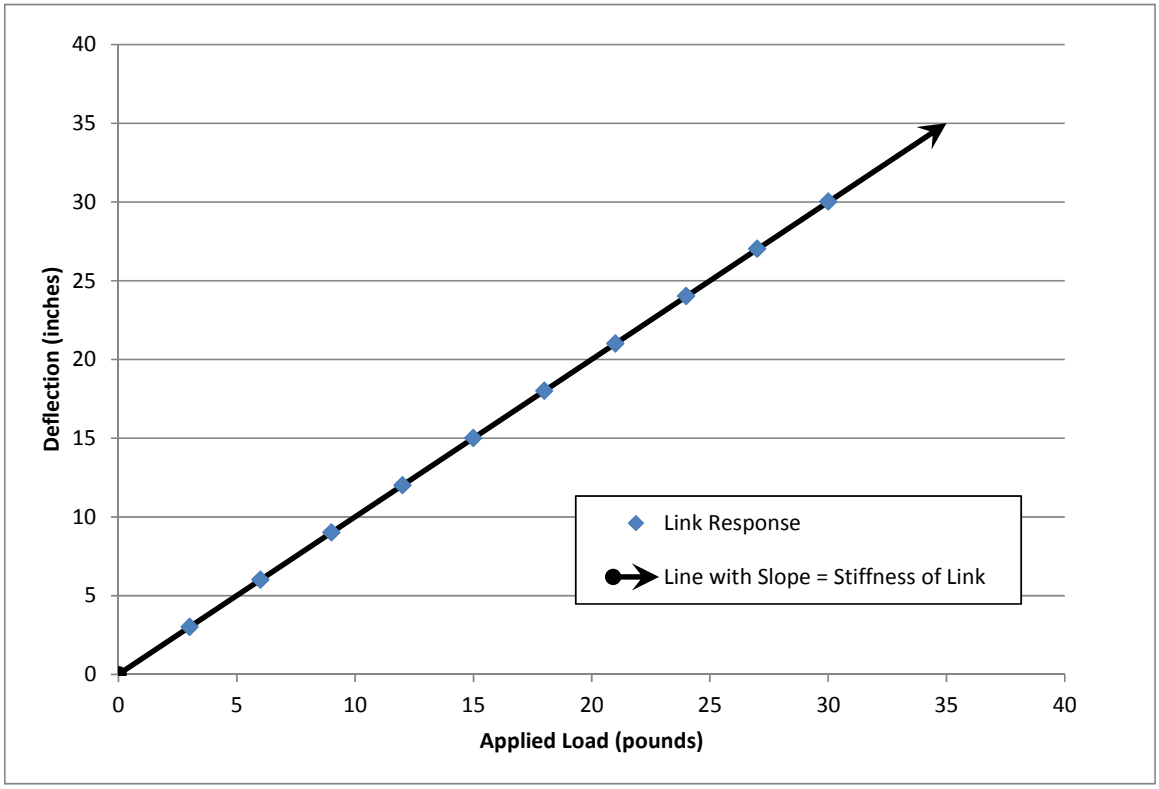

Figure C-7 Plot of Link Response and the Defined Stiffness

C.4 NASTRAN Tetrahedron Single Element Tests

This section provides an overview of the single element testing that was done on the tetrahedron element in NX NASTRAN. This element is a basic building block of the auto-mesh used for the 3-D joint modeling. It has four sides and has ten nodes. The single element test was built of three legs each one inch long in the x, y, and z-axes. Symmetry conditions were applied to the sides common to each of the origin planes thus fully constraining the element. Loading in the x-direction was applied to the sloped side as shown in Figure C-8.

Displacements and strains in the x-direction were extracted for a number of different applied stresses from 1psi to 10 psi. The displacements were converted into stretch and it was verified that after subtracting one were equal to the strains in all cases thus the strain law is the same as was shown earlier in Section C.1.

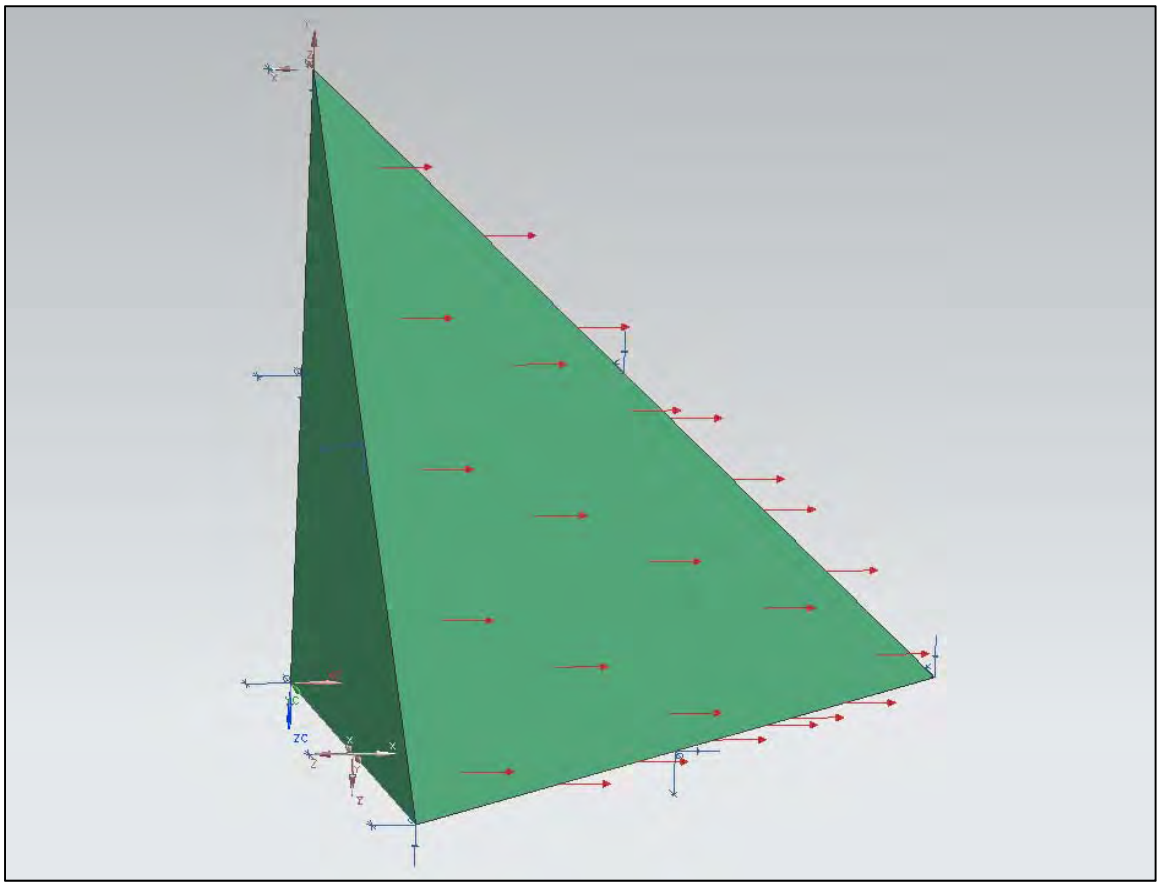

Figure C-8 NASTRAN Single Tetrahedron Element Test

C.5 Small Model Validation Testing of StressCheck and NASTRAN

Several different small models were built to test certain aspects of StressCheck against classical solutions. One common solution is the plain-stress elasticity solution for the Kt at an open hole in an infinite plate. A square planar model was built with a central hole and width and length dimensions 100 times greater than the hole diameter (see Figure C-9). Using a mesh refinement convention of imprinting a circle 1.5 times the diameter of the hole on the surface with common centers will help discretization when using the auto-mesh feature. The strategy of imprinting a circle 1.5 times the open hole is the same as

the general refinement techniques used in other StressCheck models depicted in this dissertation. The edge opposite the loading was assigned a symmetry boundary condition and the lower corner was pinned from translation in the y-direction.

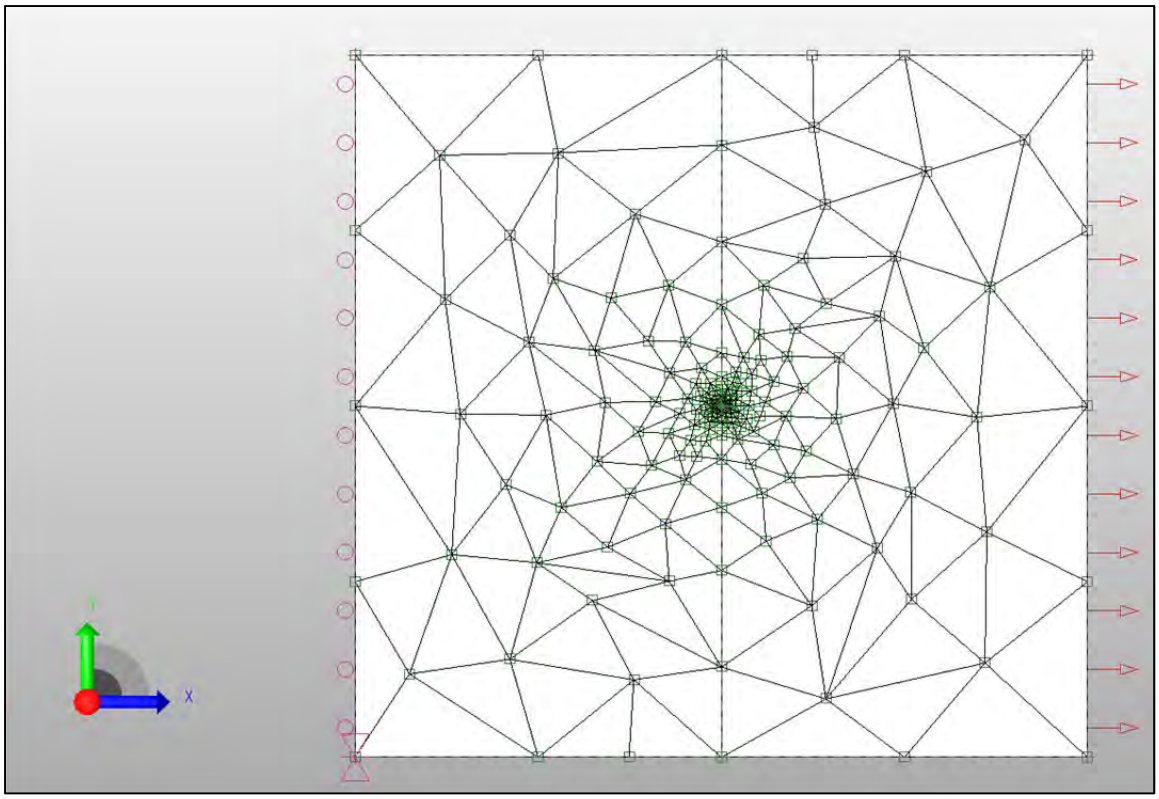

Figure C-9 View of Model for Verification Test of Open Hole Kt

The stress concentration at the edge of the hole is the tangential stress divided by the applied stress assuming that the relationship between hole radius (r) and the distance from the hole center to the edge of the plate (a) is, $r << a$ such that $r / a \approx 0$. The classic plane stress equation from Reference [356] is:

$$\sigma_\theta = \frac{S}{2}\left(1+\frac{r^2}{a^2}\right) - \frac{S}{2}\left(1+\frac{3r^4}{a^4}\right)cos2\theta$$

Equation 9-2 Tangential Stress at an Open Hole in an Infinite Plate

where:

θ is the angle off of the loading axis

S is the applied stress

Thus Kt is defined as σ_θ / S which reaches a maximum of three at the edge of the hole normal to the loading direction. Figure C-10 shows the results for different polynomial levels up to the maximum element polynomial level of eight. Note it approaches the closed-form solution of three as the polynomial level increases and converges at level eight.

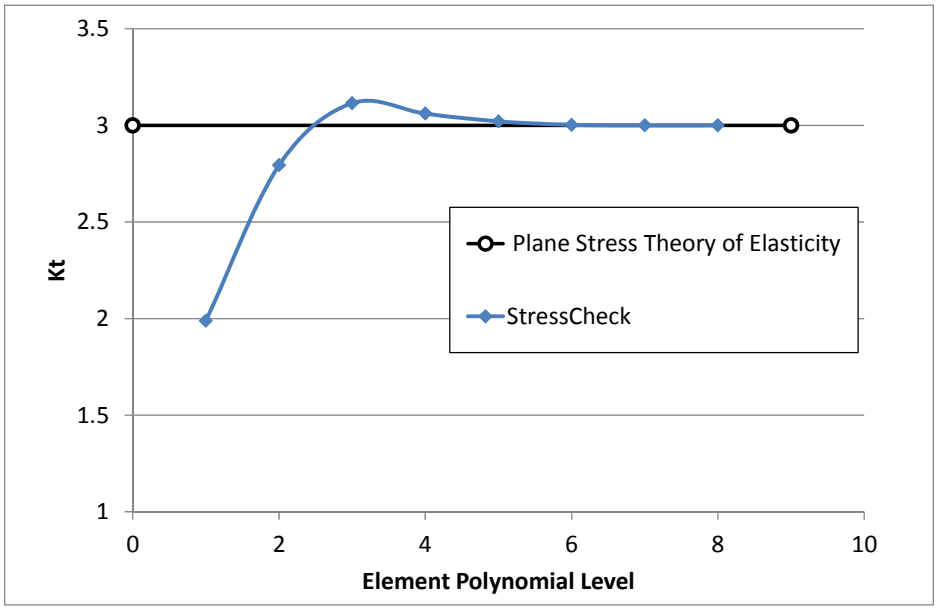

Figure C-10 Convergence of the StressCheck Calculated Kt at the Edge of the Hole

Figure C-11 presents the StressCheck results and the closed-form solution for Kt in a line normal to the applied load both at the hole edge and further away for a polynomial level of 8 along with the magnitude of the error as a percentage. With the local refinement there is a reasonable match with some divergence at the junction of elements, especially at the mesh transition region defined by the 1.5D refinement circle. Figure C-12 shows the same error depicted in Figure C-11 along with two other error calculations for two additional models with increased mesh density. Note as mesh density increases the solution is converging to a steady error that is a fraction of a percent.

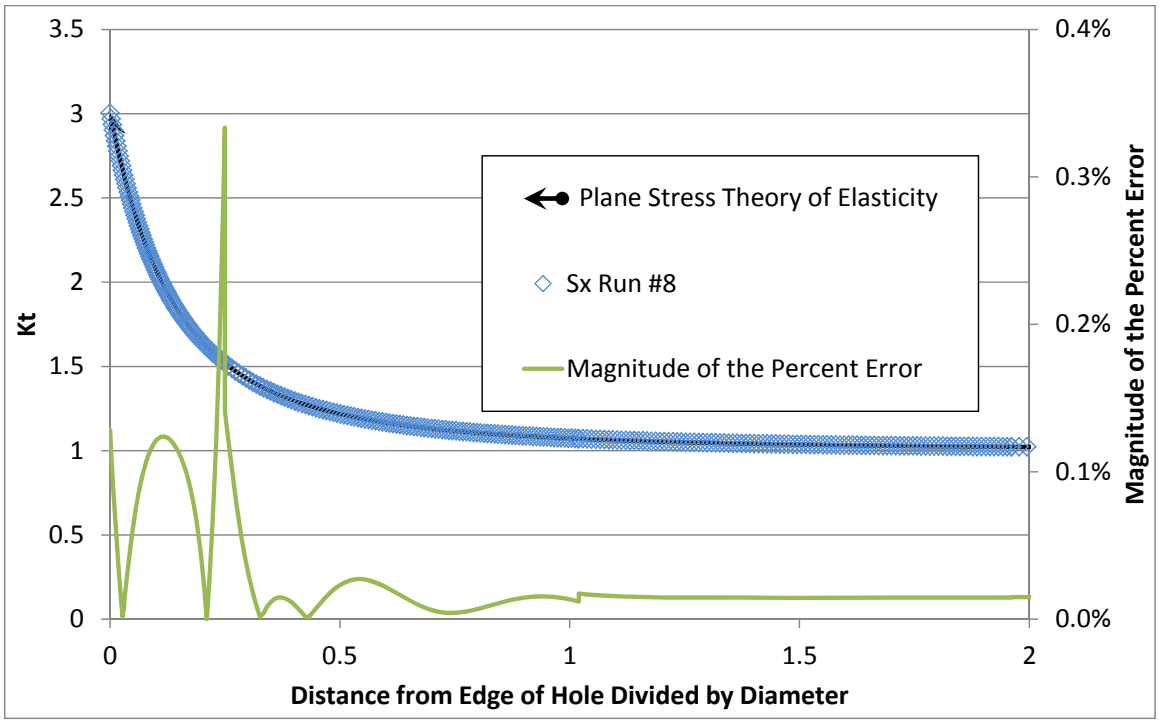

Figure C-11 Stresses in the X-direction from StressCheck versus the Closed-Form Solution

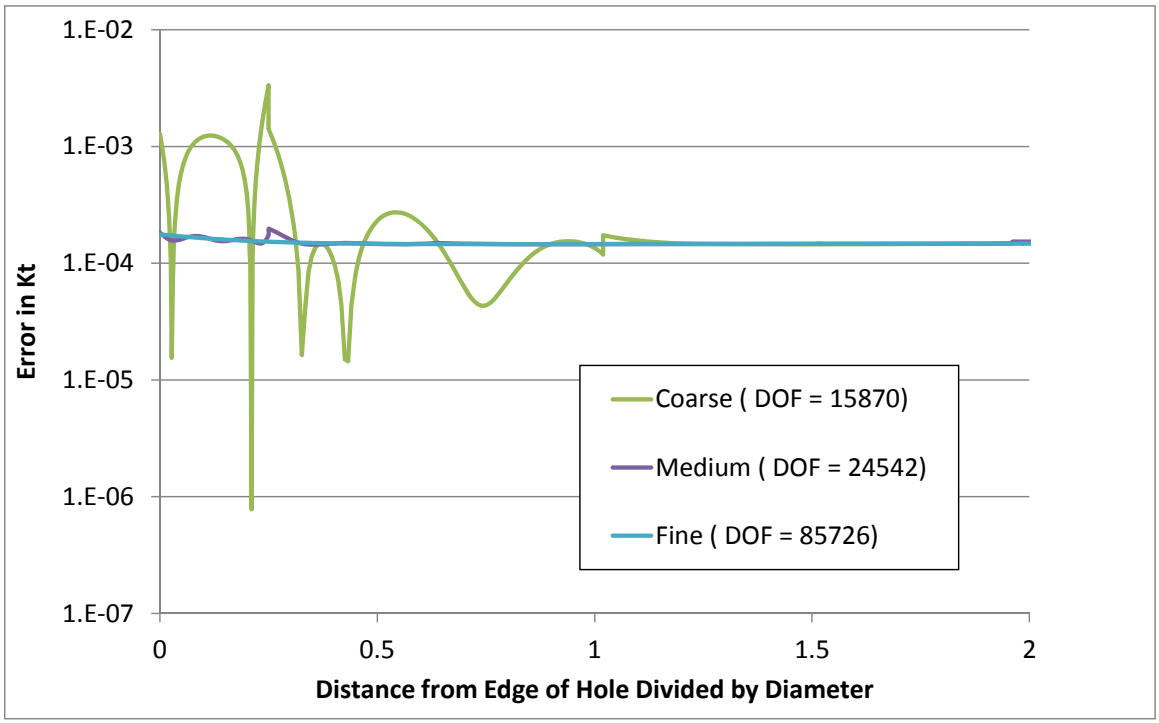

Figure C-12 Error in Kt with Increasing Mesh Density at a P-Level of Eight

The same set of tests were performed with NASTRAN but with slightly different meshing methods. The model had three planes of symmetry, one mid-way through the thickness, and two splitting the hole center at right angles. Symmetry constraints were applied to the symmetry sides. The overall plate had the same general dimensions as the StressCheck test but the thickness was set to unity. It had a refinement circle with a diameter of seven placed around the hole to localize the mesh refinement as shown in Figure C-13. The refinement region size was chosen because the Kt at that radius is ~ 1% so the low gradient will not be significantly affected by the much larger elements away from the hole.

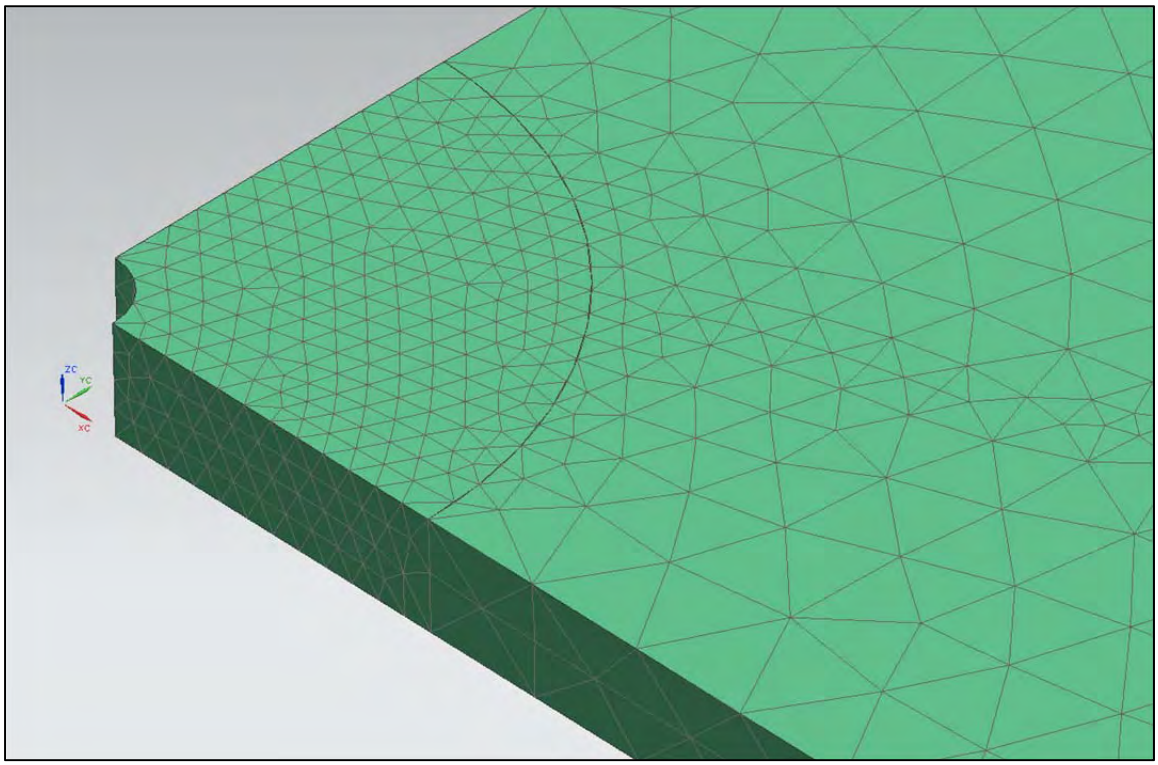

Figure C-13 View of the Local Mesh Refinement Region

Mesh density in the refinement region was set to the diameter of the hole or unity, 1/4th the diameter of the hole, and 1/16th the diameter of the hole however at the lowest density the auto-mesh produced a density of approximately one-half the diameter at the hole. Differences in stress were apparent through the thickness with slightly lower stresses on the surface relative to the middle of the thickness. For the sake of plotting the data it was necessary to average through the thickness. Nodal stresses were averaged to the nearest one-hundreth of the hole diameter in the y-direction and completely through the thickness and are presented in Figure C-14. The absolute value of the percent error in Kt is presented in Figure C-15.

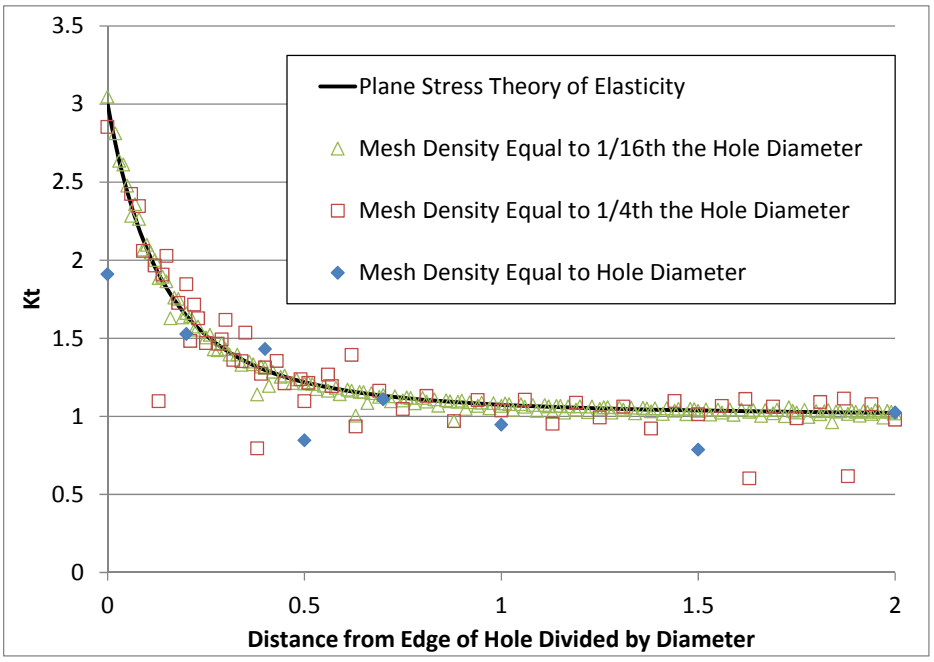

Figure C-14 Stresses in the X-direction Averaged Through the Thickness from NASTRAN versus the Closed-Form Solution

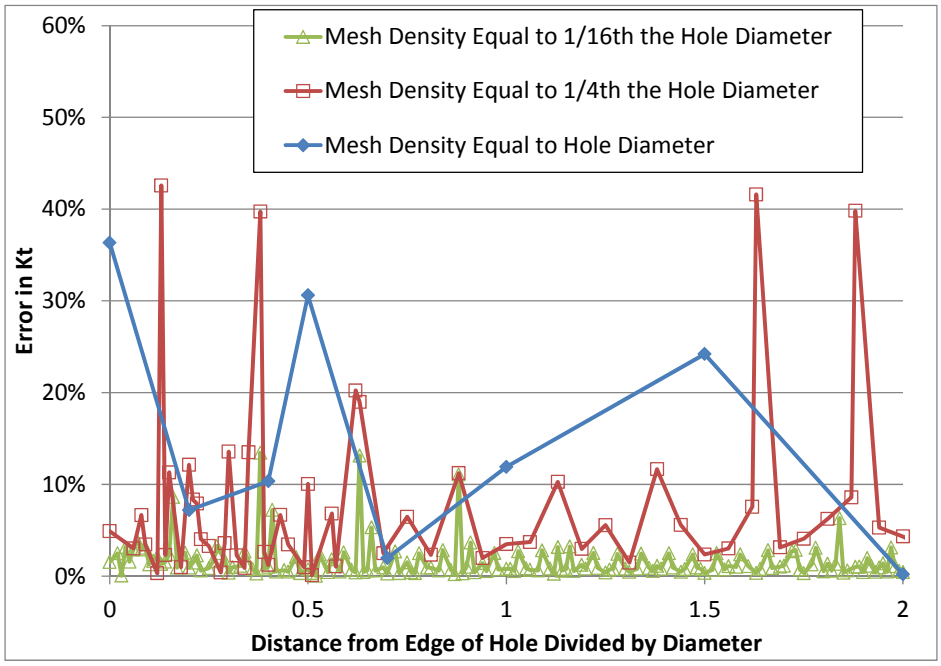

Figure C-15 Error in Kt with Increasing Mesh Density

The next test was for the necessary mesh density to obtain suitable convergence of the loads from the 3-D NASTRAN FEM. A single fastener model was built using the general geometry that was used in the splice joint except the fastener was centered. The plate and splice straps were 1.5 inches wide and the plates were 2 inches long with the fastener in the center. The upper and lower straps were given a fully fixed boundary condition on one of the short sides while the center plate was loaded on the other short side with a constraint against side-to-side motion to prevent rotation. The material models used were the same as in the 3-D FEM of the 284 Splice as were the fastener and nut models. Frictionless contact constraints were placed between all faying surfaces resulting in the model depicted in Figure C-16.

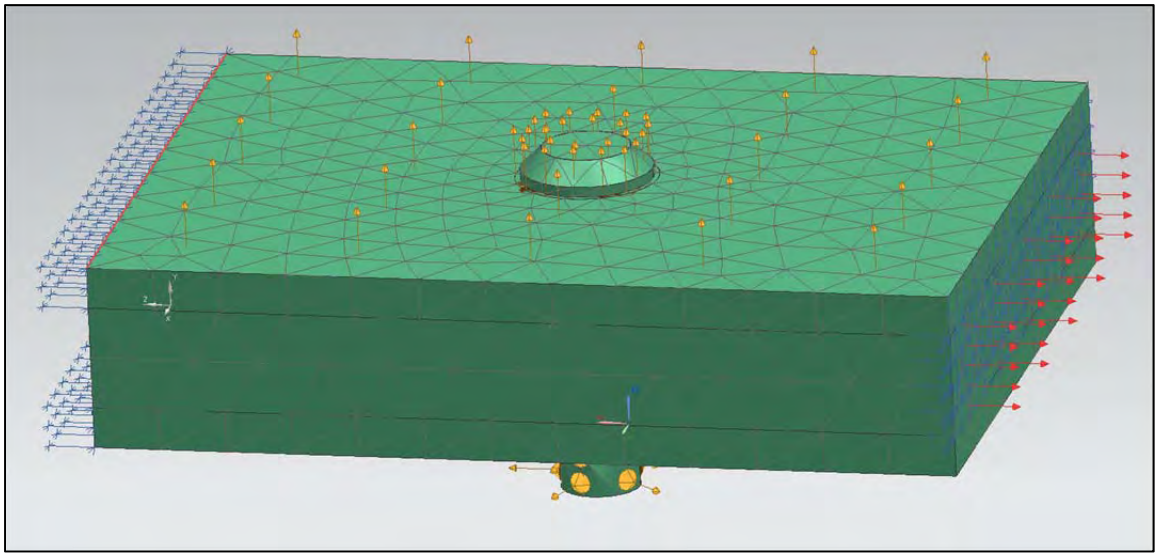

Figure C-16 View of the Single Fastener Model for Mesh Density Convergence

Circular surfaces were defined slightly larger than the faying size of the fastener head and nut to give the ability to apply a higher mesh density in those regions. While different

mesh densities were tried, all faying surfaces of the fastener and nut, as well as the bores of the plate and splice straps and faying surfaces under the fastener head and nut had densities twice that of the general FEM. The first step was rather coarse with densities of 0.16 inch throughout the model and 0.08 at the mesh refinement regions as shown in Figure C-16. Next reduction was to 0.12 and 0.06 inch but convergence not obtained in the first load step at 100 iterations. It was further reduced to 0.08 and 0.04 inch and, finally, was reduced to 0.04 and 0.02 inch. The goal was to produce convergence of the displacement which affects the fastener load distribution in the joint, not necessarily convergence in the stress. Table C-1 presents the results of the convergence study for mesh density. Loads in the upper and lower plates were pulled from nodes in contact with the fastener. Note that at the most coarse mesh density the nodal loads do not sum to 700 pounds due to lateral forces due to an over-rotated fastener head. The reactions at the fixed ends of the strap are correct however. The end displacements between the 0.08 and 0.04 mesh and the most fine mesh are only 0.15% while the loads differ by approximately 0.7%. The increase in solution time for a fraction of a percent increase in accuracy suggests that little practical benefit exists for further mesh refinement. Additionally, these models are very simple relative to the final 3-D FEM of the entire 284 Splice; thus the 0.08 and 0.04 mesh density combination will be used. Note that the maximum stress in the x-direction at the holes in the straps are presented in Table C-2 and as mentioned, are not converging nearly as quick as the loads which are the point of the 3-D FEM.

Table C-1 Mesh Density Convergence Study Results

Mesh Density	Average End Displacement (inch)	Upper Plate Load (lbs)	Lower Plate Load (lbs)	Solution Time (HH:MM:SS)
0.16 and 0.08	-1.3021E-03	341.6	356.3	0:03:53
0.12 and 0.06	N/A	N/A	N/A	N/A
0.08 and 0.04	-1.2960E-03	344.0	356.0	2:00:50
0.04 and 0.02	-1.2948E-03	346.4	353.6	27:17:58

Table C-2 Stresses from the Mesh Density Convergence Study

Mesh Density	Max Nodal Stress, X-Direction Upper Strap (ksi)	Max Nodal Stress, X-Direction Lower Strap (ksi)	Max Elemental Stress, X-Direction Upper Strap (ksi)	Max Elemental Stress, X-Direction Lower Strap (ksi)
0.16 and 0.08	22.64	17.23	13.53	16.43
0.12 and 0.06	N/A	N/A	N/A	N/A
0.08 and 0.04	22.71	22.69	18.3	18.07
0.04 and 0.02	25.24	24.82	20.24	19.9

The next verification test comes from Reference [336] for a cylindrical contact condition with a small gap between the faying surfaces. The same test is not performed for a 3-D NASTRAN model since a clearance contact model is not used, rather all fasteners are assumed to be neat-fit.

The comparison is made for a 2-D planar StressCheck model against a photoelasticity solution for a ‘rivet’ bearing upon a plate with an initial clearance of 0.0005”. The specimen is made of Bakelite BT-61-893 with a Young’s Modulus of 620,000 psi and a Poisson’s ratio of 0.37. These elastic parameters were used in the FEM for the verification test. The ‘rivet’ was a Bakelite bushing with a steel core for loading which had a diameter of 0.4455 inch. Based on a figure, the steel core was estimated to be 0.175 inch in diameter. The plate was 2.922 inches wide and 0.1925 inch thick with a

centered hole. The overall length is not given but the hole is 1.718 inches from the end of the plate in the direction of loading. Based on a figure showing the general set up the other length from the hole to the loaded end was taken as three times the length edge distance of 1.718 inch for a total plate length of 6.872 inches. The StressCheck model of this photoelastic experiment is shown in Figure C-17.

The photoelasticity result is subject to some error given how graphical techniques required. The radial stress due to fastener bearing around the hole is presented and used for this verification test. It was noted in Reference [336] that some error in the result existed of about seven percent. The data points were numerically integrated using a trapezoidal method and it was found the resulting load was 419.4 pounds which is 7.55% too high. Thus the data points given in the table were reduced by this percentage for the comparison. Results are presented in Figure C-18. The average error magnitude from 10 degrees to 90 degrees is 2.3%. Even though there are numerous potential error sources in the photoelasticity solution that are not quantified such as the judgment of isocline locations, manual measurements, etcetera; the exact value is not known thus no error range can be presented.

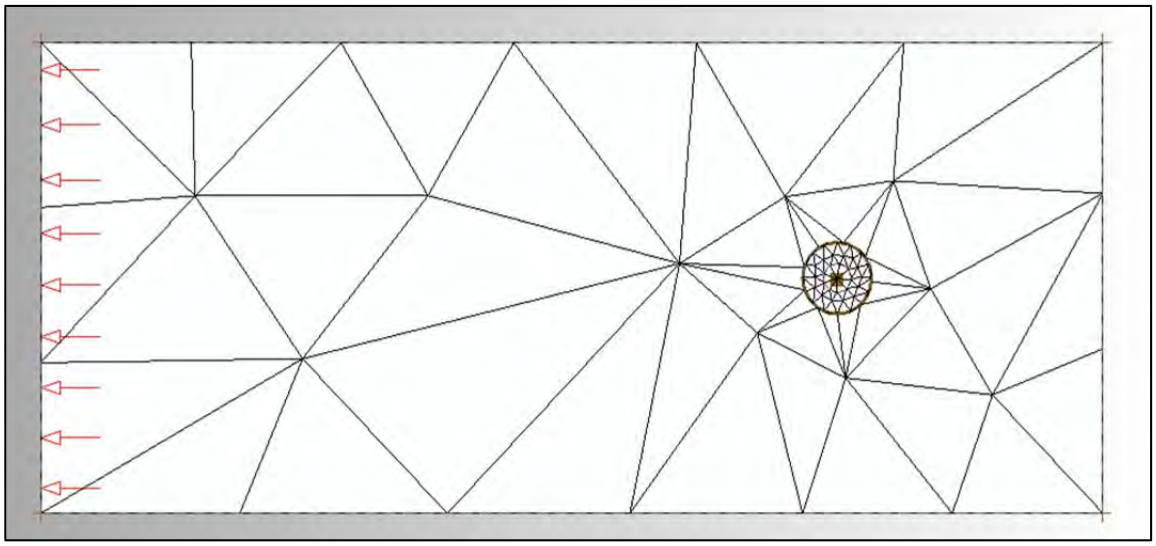

Figure C-17 Image of the Basic Contact Correlation Model

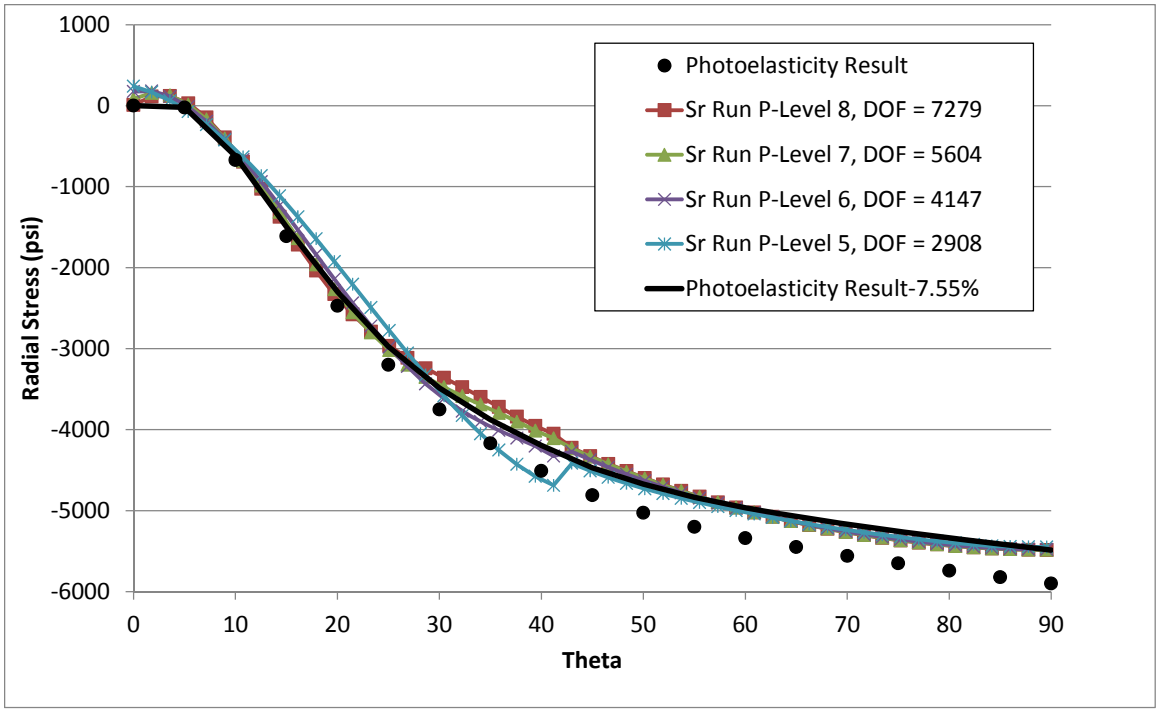

Figure C-18 Photoelasticity Solution for Radial Stress with StressCheck Results for P-Levels 5 through 8 as a Function of Angle around the hole.

The next sets of tests verify both the stress intensity factor solution for StressCheck as well as attempt to define standard refinement techniques for stress intensity extraction. One method is to apply three circles to define areas of refinement of the mesh at the crack tip. Use here is a circle with two inner circles, each layer being five times smaller than the next outer. Solutions are then extracted midway between the inner most two circles. The basic solution evaluated here is the classic solution of a single through crack at the edge of a plate. The first has a crack length (a) to width (W) ratio of 1/100 and 1/2. The extracted solutions are explored for a range of p-levels and radii of integration and compared with the Brown solution which has a stated accuracy of 0.5% for a/W ≤ 0.6 [184]. The following equation gives a K_I of 1.9864 psi√in with upper and lower 0.5% bounds of {1.9825, 1.9904} psi√in. StressCheck results are given in Table C-3.

$$K_I = C\sigma\sqrt{\pi a}$$

$$C = 1.122 - 0.231\left(\frac{a}{W}\right) + 10.550\left(\frac{a}{W}\right)^2 - 21.710\left(\frac{a}{W}\right)^3 + 30.382\left(\frac{a}{W}\right)^4$$

Equation 9-3 Single Edge Notch Plate Solution from Brown [184]

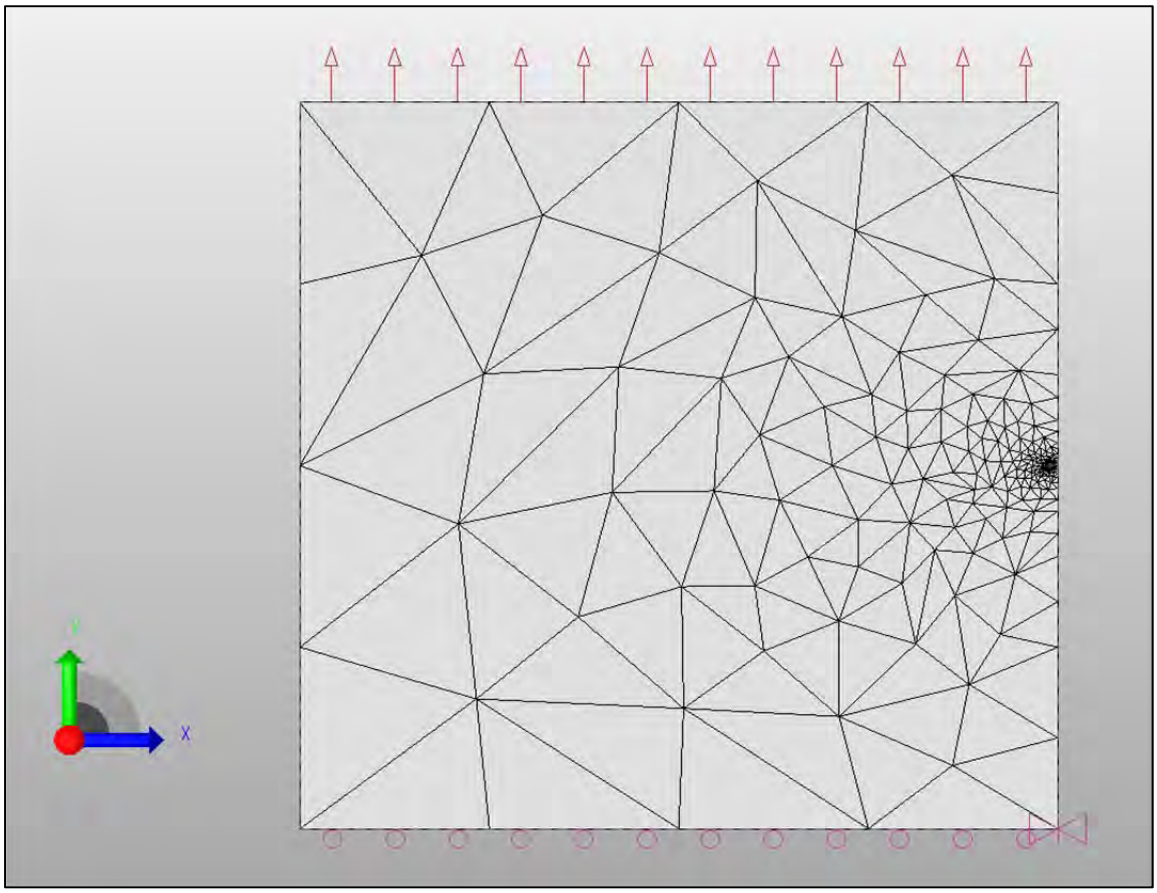

Figure C-19 View of Edge Crack Validation Test

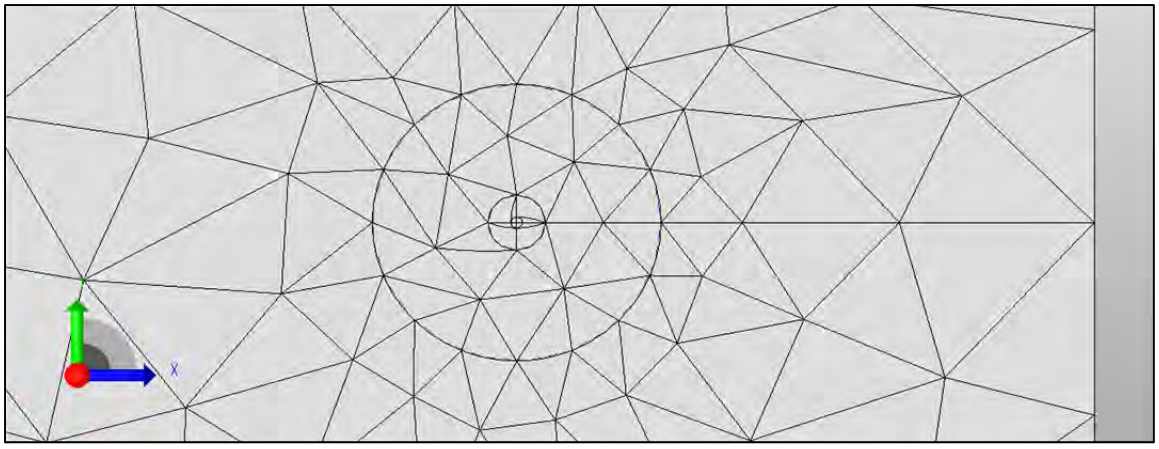

Figure C-20 Close-Up of Mesh Refinement around the Crack Tip

Table C-3 StressCheck Stress Intensity Results

	Radius of Integration, 0.3 is Centered Between Refinement Circles								
P-Level	0.011	0.02	0.25	0.275	0.3	0.325	0.35	0.4	0.49
1	1.3369	1.6072	1.7293	1.7822	1.8179	1.8616	1.8923	1.9548	2.0453
2	1.8017	2.0113	2.0486	2.0534	2.0393	2.0326	2.0104	1.9667	1.8612
3	1.9062	2.0095	2.0027	1.9940	1.9809	1.9738	1.9688	1.9714	2.0262
4	1.9551	1.9959	1.9881	1.9839	1.9858	1.9842	1.9887	1.9932	1.9846
5	1.9724	1.9954	1.9878	1.9856	1.9868	1.9871	1.9891	1.9917	1.9876
6	1.9817	1.9897	1.9869	1.9873	1.9895	1.9909	1.9917	1.9904	1.9939
7	1.9869	1.9887	1.9892	1.9903	1.9907	1.9908	1.9898	1.9895	1.9895
8	1.9889	1.9895	1.9900	1.9901	1.9897	1.9897	1.9897	1.9905	1.9914

As table Table C-3 shows, near the center between the rings the results are well within the +/- 0.5% range with values outside that range shaded. Thus it appears that the current method of extracting between the two inner most circles will produce valid results. Another a/W aspect ratio was chosen at the other end of the spectrum for comparison at 1/2. Brown's equation produces a K_I of 5.0145 psi√in with a +/- 0.5% of {4.9895, 5.0396} psi√in. It was found that with the same outer refinement diameter as the previous example the solution did not match Brown's nearly as close. The effect of the diameter was explored by reducing it from 1/2 of the crack length to 1/5 and then 1/20. Resulting K_I values extracted from the midpoint between the two inner most circles are shown in Figure C-21.

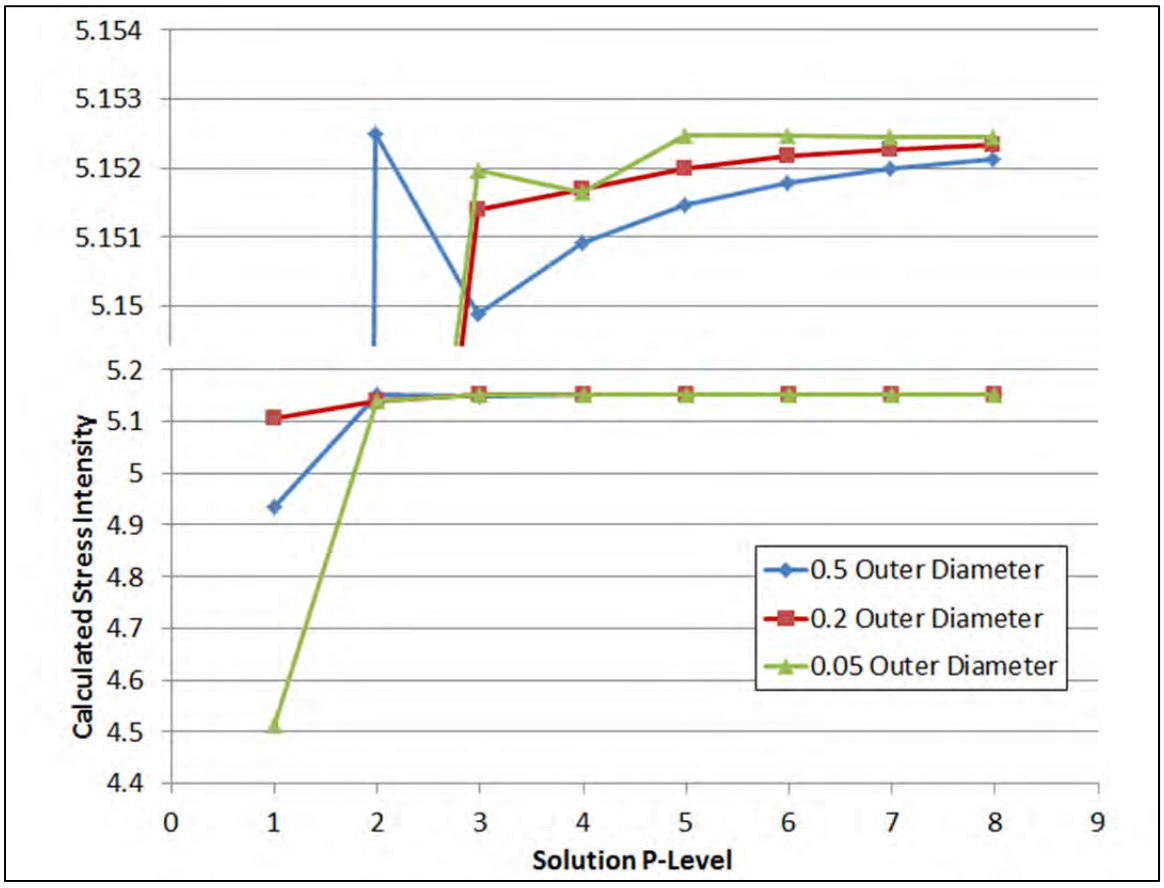

Figure C-21 StressCheck Stress Intensity Solutions with Different Outer Diameter Refinement Circles

Note that all of the curves appear to be converging on the same value of 5.1524 psi√in with increasing p-level with the smaller outer diameter refinement circle converging much faster than the others. This value of stress intensity is 2.7% higher than that predicted by the Brown equation. Note that the graph is split with the same curves on a much tighter scale presented above to highlight the shape.

On aspect that can cause problems is that figures of these solutions are drawn as shown in Figure C-22. No real value is given for the length from the crack that the far-field tension is being applied. The example given above has a width to length ratio of 1 and with a/W

of 1/2, the ratio of crack length to the edge of plate where the load is applied (a/L) is unity. A second model was constructed with a/W equal to 1/2 but with a/L of 1/10. Three different boundary conditions were explored to demonstrate the differences as shown in Figure C-23. Two images are portrayed for each condition: one of just the model, and another of the model deflected showing deflection in the horizontal direction. The left most of the three has the same boundary conditions as the previous models, the center has a symmetry condition applied to the edge opposite the crack and the third has lateral restraint the loaded end not unlike a specimen in a load-frame being tested. Results are presented for eight p-levels for each of the three boundary conditions and compared with Brown's solution with a percent error next to each individual value in Table C-4. This demonstrates that the 'far-field stress' must stay 'far' way to match the analytical solution though 'far' is not defined anywhere to the author's knowledge beyond 'rules of thumb' from different analysts. However, this does verify that StressCheck can obtain results within the bounds of accuracy for Brown's solution.

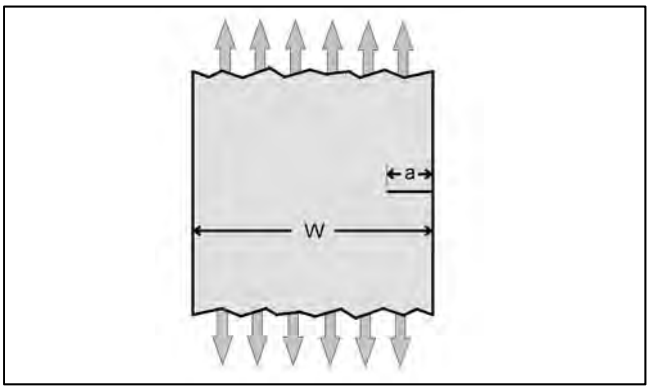

Figure C-22 Typical Depiction of a Finite Width Edge Crack

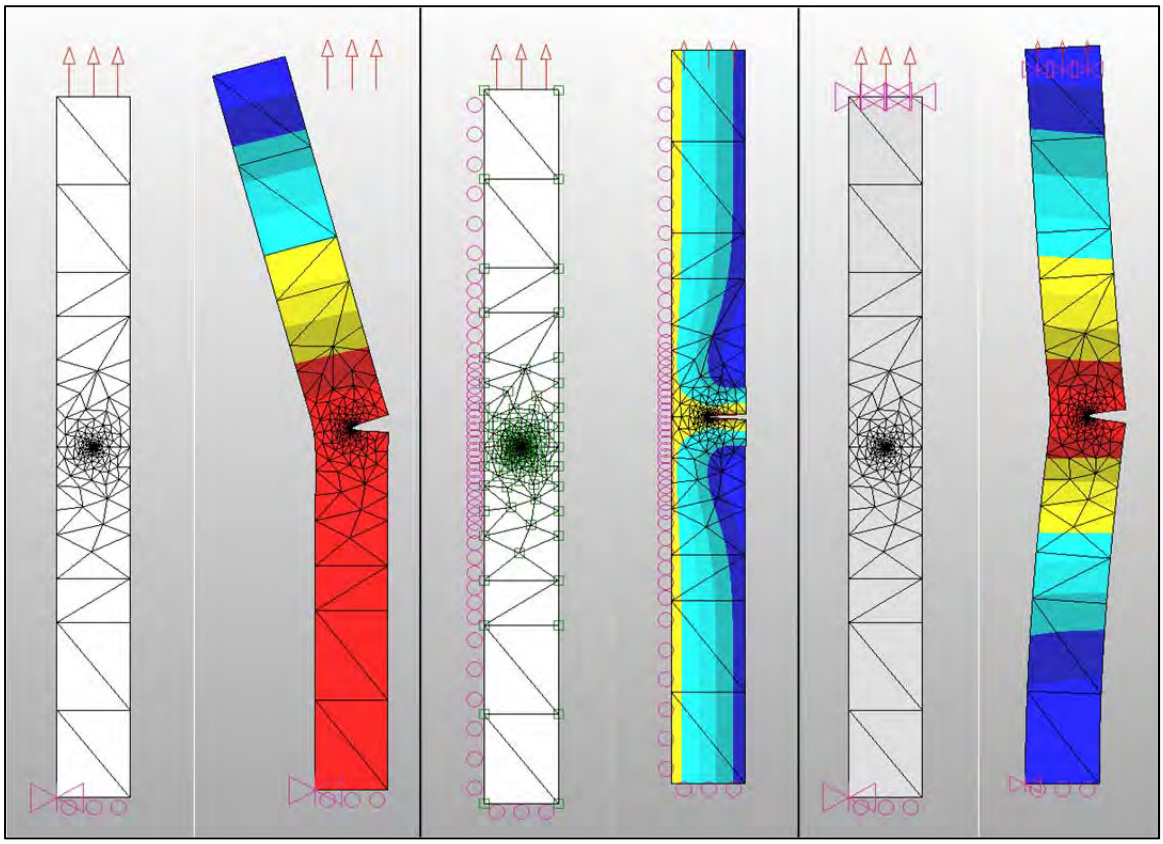

Figure C-23 Views of Three Different Boundary Conditions Applied to the Longer a/W Equals 1/2 Stress Intensity Model

Table C-4 StressCheck Stress Intensity Results Compared with Brown's Solution

P-Level	No Restraint, Loaded End		Back-Side Symmetry		Lateral Restraint, Loaded End	
	K_I (psi√in)	Percent Difference	K_I (psi√in)	Percent Difference	K_I (psi√in)	Percent Difference
1	4.2883	-14.48%	1.9037	-62.04%	3.0198	-39.78%
2	5.0968	1.64%	2.1134	-57.85%	4.1994	-16.26%
3	4.9724	-0.84%	2.0589	-58.94%	4.0960	-18.32%
4	4.9951	-0.39%	2.0679	-58.76%	4.1146	-17.95%
5	4.9988	-0.31%	2.0694	-58.73%	4.1178	-17.88%
6	5.0058	-0.17%	2.0723	-58.67%	4.1236	-17.77%
7	5.0086	-0.12%	2.0734	-58.65%	4.1259	-17.72%
8	5.0063	-0.16%	2.0724	-58.67%	4.1241	-17.76%

The same issues exist for the through stress around a hole in a plate. However additional considerations need to be made to compare solutions with holes similar to the oft seen depiction in Figure C-24. As shown previously, the gage length is important since the further away from the hole the load is applied, the greater the chance that at a nearby cross section the stress distribution is no longer even as it 'flows' around the discontinuity created by the hole and the crack. Another complication is whether or not the hole is filled, the level of hole fill, and the ratio of the elastic moduli between the plate and the fastener or bushing filling the hole. All of these factors should be known for a given solution for an adequate comparison.

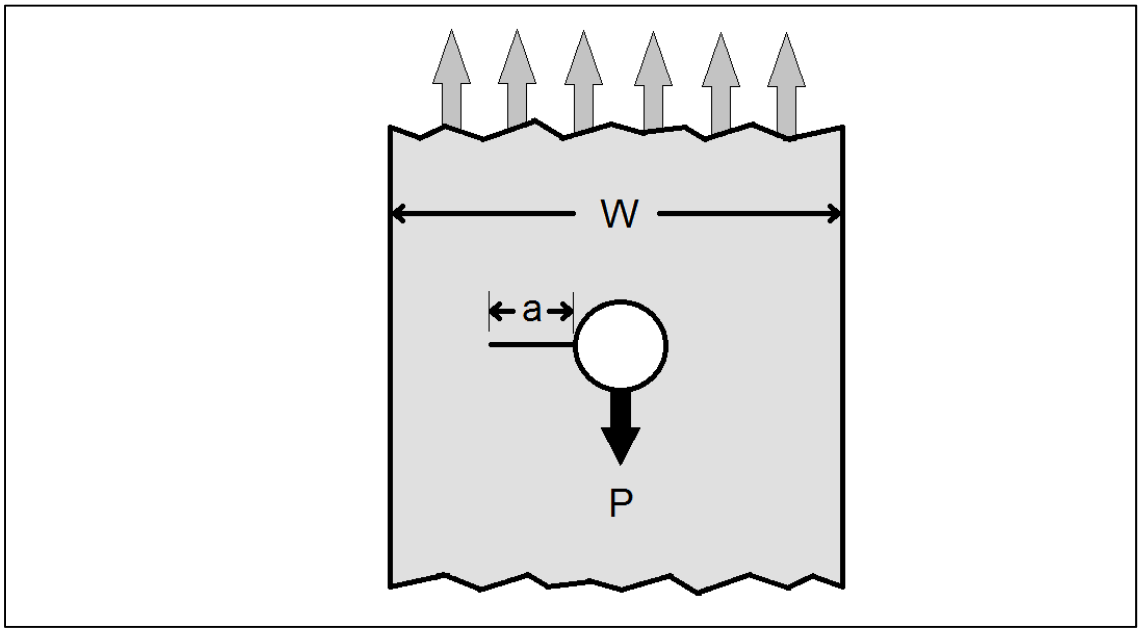

Figure C-24 Finite Width Plate with a Centered Cracked Hole

A final validation test that would be applicable to the full splice model used to calculate stress intensities is that of an infinite plate with a filled, loaded hole. A solution by Shah

exists and is reproduced below from Reference [322] for a through crack at a hole due to bearing stress with a neat fit. The equation is presented in Section 6.5.1.

For an infinite plate with a one inch diameter hole with a half inch crack, the correction factor, F_1, is 0.281 when a/R equals unity. A model was built with a width to diameter ratio of 100 with a/R equal to unity as well. A neat fit plug representing a pin was inserted in the hole with a contact condition all around. The plug had a center circle with all nodes pinned to fix the fastener. Two different methods of loading the fastener by affecting the plate were tried however; it was not possible to match this solution at all.

One loading method tried was to apply a constant stress on the end of the plate and the other assigned a translation to the deflection to the plate which creates an uneven load at the side deflected. The far-field stress method converged to a correction factor of 0.193 while the model with the deflected end converged to a correction factor of 0.198. The modulus of both the pin and the plate were unity. To see if the difference was due to similarity in moduli another model was built with a modulus for the pin of three. The far-field stress method then converged to a correction factor of 0.198 which is less than a 3% difference for moduli differences of 1:1 and 3:1. An AFGROW model was built of the plate and the correction factor extracted was 0.195. This solution was developed from finite element models with a cosine load distribution inside the hole representing the load from the pin. Given the similarity between the AFGROW and StressCheck results it is concluded that the StressCheck method with a filled hole with contact produces an acceptable stress intensity solution and that the Shah equation for a filled hole, as published, is in error.

While working on validating this solution some strange behavior was noted in StressCheck that bears mentioning. During the construction of the first model for validation there was a lack of separation of the crack mesh at the hole; cause of this is unknown. This caused a ‘bridge’ that resisted crack opening and resulted in a correction factor of 0.169 with a modulus ratio of 1:1. Figure C-25 shows this model with exaggerated deflection and note the bridge at the edge of the hole. A second model was created that had an even more strange anomaly where at the edge of the pin, in-line with the crack, the model showed a extremely massive point load causing the edge to collapse inward as shown in Figure C-26. Radial stresses around the pin were extracted which showed a point stress that was 30 times the expected maximum bearing stress at a point located 90° counter-clockwise away. This was corrected by imprinting a line on the surface of the pin breaking the outer boundary at the same point as the crack. Compare these two figures to the expected deflection pattern shown in Figure C-27.

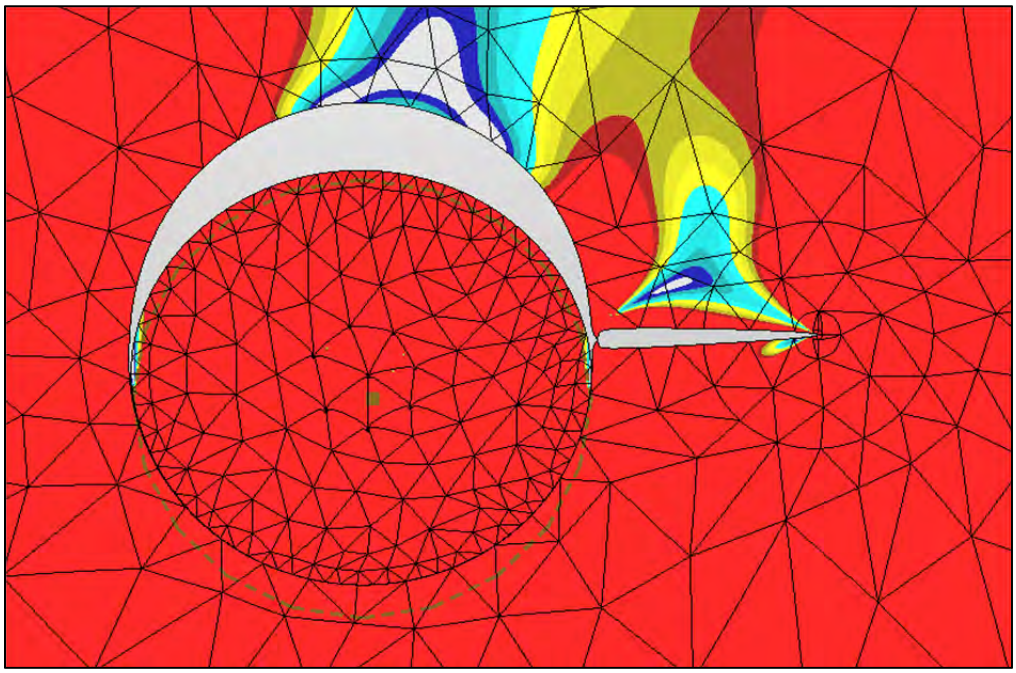

Figure C-25 Crack Mesh without Proper Separation at the Hole

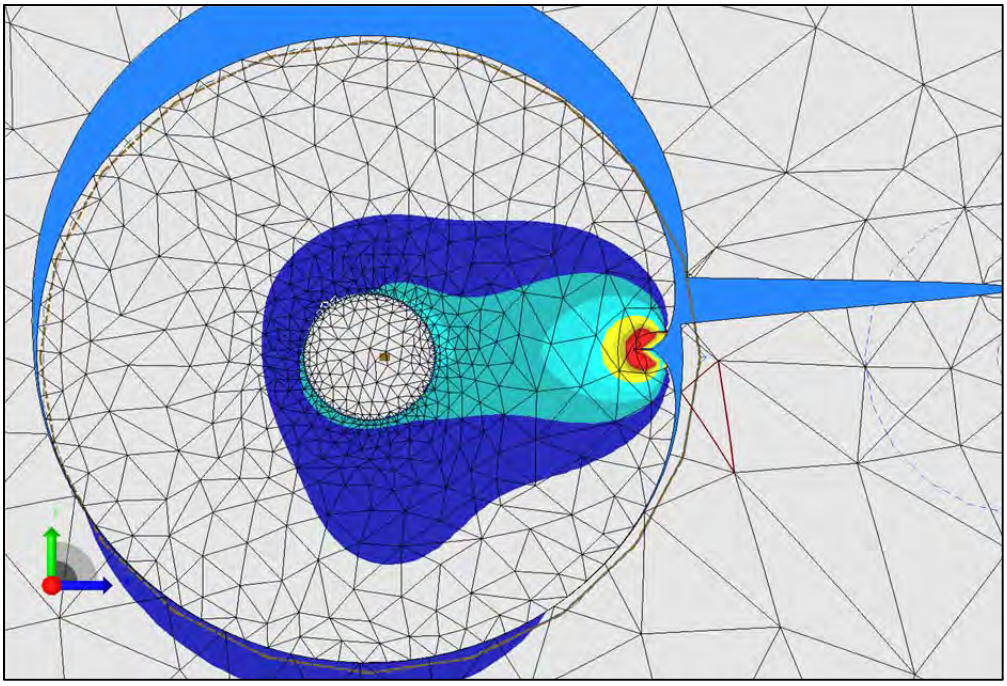

Figure C-26 Unknown Singularity at the Pin In-line with the Crack

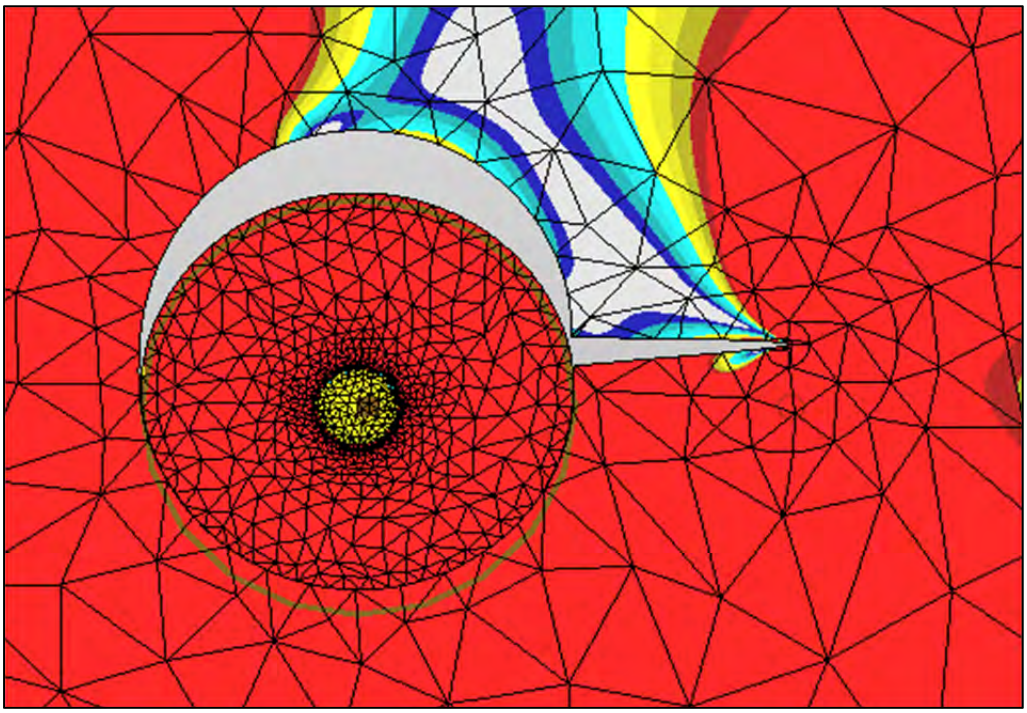

Figure C-27 Example of Proper Deflection for the Crack at a Filled Hole